



NATIONAL TECHNICAL UNIVERSITY OF
ATHENS

SCHOOL OF ELECTRICAL AND COMPUTER
ENGINEERING

PHYSICS DEPARTMENT OF SCHOOL OF
APPLIED MATHEMATICS AND PHYSICS

**Photoinjector study of a novel XFEL in the
CompactLight Collaboration**

DIPLOMA THESIS

by

Eirini C. Telali

Supervisor : Evangelos Gazis
Professor N.T.U.A.

Athens, September 2019



ΕΘΝΙΚΟ ΜΕΤΣΟΒΙΟ ΠΟΛΥΤΕΧΝΕΙΟ
ΣΧΟΛΗ ΗΛΕΚΤΡΟΛΟΓΩΝ ΜΗΧΑΝΙΚΩΝ ΚΑΙ
ΜΗΧΑΝΙΚΩΝ ΗΛΕΚΤΡΟΝΙΚΩΝ ΥΠΟΛΟΓΙΣΤΩΝ
ΤΟΜΕΑΣ ΦΥΣΙΚΗΣ ΣΧΟΛΗΣ ΕΦΑΡΜΟΣΜΕΝΩΝ
ΜΑΘΗΜΑΤΙΚΩΝ ΚΑΙ ΦΥΣΙΚΩΝ ΕΠΙΣΤΗΜΩΝ

**Μελέτη διάταξης φωτοεγχυτή για επιταχυντή
υψηλής ενέργειας Ακτίνων-Χ Ελεύθερων
Ηλεκτρονίων της Συνεργασίας CompactLight**

ΔΙΠΛΩΜΑΤΙΚΗ ΕΡΓΑΣΙΑ

της

Ειρήνη Χ. Τελάλη

Επιβλέπων : Ευάγγελος Γαζής
Καθηγητής Ε.Μ.Π.

Αθήνα, Σεπτέμβριος 2019



ΕΘΝΙΚΟ ΜΕΤΣΟΒΙΟ ΠΟΛΥΤΕΧΝΕΙΟ
ΣΧΟΛΗ ΗΛΕΚΤΡΟΛΟΓΩΝ ΜΗΧΑΝΙΚΩΝ ΚΑΙ
ΜΗΧΑΝΙΚΩΝ ΗΛΕΚΤΡΟΝΙΚΩΝ ΥΠΟΛΟΓΙΣΤΩΝ
ΤΟΜΕΑΣ ΦΥΣΙΚΗΣ ΣΧΟΛΗΣ ΕΦΑΡΜΟΣΜΕΝΩΝ
ΜΑΘΗΜΑΤΙΚΩΝ ΚΑΙ ΦΥΣΙΚΩΝ ΕΠΙΣΤΗΜΩΝ

**Μελέτη διάταξης φωτοεγχυτή για επιταχυντή
υψηλής ενέργειας Ακτίνων-Χ Ελεύθερων
Ηλεκτρονίων της Συνεργασίας CompactLight**

ΔΙΠΛΩΜΑΤΙΚΗ ΕΡΓΑΣΙΑ

της

Ειρήνη Χ. Τελάλη

Επιβλέπων : Ευάγγελος Γαζής
Καθηγητής Ε.Μ.Π.

Εγκρίθηκε από την τριμελή εξεταστική επιτροπή την 21η Οκτωβρίου 2019

.....
Ε. Γαζής
Καθηγητής Ε.Μ.Π.

.....
Η. Γλύτσης
Καθηγητής Ε.Μ.Π.

.....
Ι. Ξανθάκης
Καθηγητής Ε.Μ.Π.

Αθήνα, Σεπτέμβριος 2019

.....
Ειρήνη Χ. Τελάλη

Διπλωματούχος Ηλεκτρολόγος Μηχανικός και Μηχανικός Υπολογιστών Ε.Μ.Π.

Copyright © Ειρήνη Τελάλη

Με επιφύλαξη παντός δικαιώματος. All rights reserved.

Απαγορεύεται η αντιγραφή, αποθήκευση και διανομή της παρούσας εργασίας, εξ ολοκλήρου ή τμήματος αυτής, για εμπορικό σκοπό. Επιτρέπεται η ανατύπωση, αποθήκευση και διανομή για σκοπό μη κερδοσκοπικό, εκπαιδευτικής ή ερευνητικής φύσης, υπό την προϋπόθεση να αναφέρεται η πηγή προέλευσης και να διατηρείται το παρόν μήνυμα. Ερωτήματα που αφορούν τη χρήση της εργασίας για κερδοσκοπικό σκοπό πρέπει να απευθύνονται προς τον συγγραφέα.

Οι απόψεις και τα συμπεράσματα που περιέχονται σε αυτό το έγγραφο εκφράζουν τον συγγραφέα και δεν πρέπει να ερμηνευθεί ότι αντιπροσωπεύουν τις επίσημες θέσεις του Εθνικού Μετσόβιου Πολυτεχνείου.

ΠΕΡΙΛΗΨΗ

Το H2020 CompactLight Project είναι ένα διεθνές έργο 24 ινστιτούτων (21 Ευρωπαϊκά και 3 εκτός Ευρώπης) με σκοπό τη σχεδίαση μίας συμπαγούς επιταχυντικής διάταξης, νέας γενιάς, επιταχυντή υψηλής ενέργειας Ακτίνων-X Ελεύθερων Ηλεκτρονίων (hard X-Rays Free-Electron Lasers-FEL). Οι εν λειτουργία επιταχυντές X-FEL στην Ευρώπη χρησιμοποιούν επιταχυντικές διατάξεις στο φάσμα συχνοτήτων 2-4 GHz (S-band) . Σκοπός του έργου είναι να παραδοθεί μία καινοτόμος και συμπαγής σχεδίαση ενός επιταχυντή υψηλής ενέργειας Ακτίνων-X Ελεύθερων Ηλεκτρονίων, χαμηλότερης ενεργειακής κατανάλωσης και χαμηλότερης ενέργειας δέσμης. Η σχεδίαση βασίζεται σε επιταχυντικές διατάξεις υψηλής βαθμίδας (100 MV/m) μέχρι τις συχνότητες X-band (12GHz), σε υπεραγωγίμο ή μη undulator (μονάδα κυματισμού της δέσμης για την εκπομπή ακτίνων X) μικρής περιόδου, και photoinjector (Φωτοεγχυτής: μονάδα παραγωγής δέσμης ηλεκτρονίων από φωτοκάθοδο και εισαγωγή στον επιταχυντή) υψηλής φωτεινότητας. Η ποιότητα της δέσμης ηλεκτρονίων στον γραμμικό επιταχυντή είναι καίριας σημασίας για την τελική επίδοση του X-FEL, εξαρτώμενη από πληθώρα παραμέτρων. Μια καλής ποιότητας δέσμη έχει μικρή εκπεψιμότητα (emittance), υψηλή φωτεινότητα και τη δυνατότητα υψηλού ρυθμού επανάληψης. Τα υλικά από τα οποία εξάγονται τα ηλεκτρόνια, όταν φωτίζονται από δέσμη Laser, μπορεί να είναι είτε μέταλλα είτε ημιαγωγοί. Μελετήθηκαν ως υποψήφιος φωτοκάθοδοι ο Χαλκός και το Καίσιο-Τελλούριο. Για το σχεδιασμό του Φωτοεγχυτή, προτάθηκαν διάφορες διατάξεις συμπεριλαμβανομένων διατάξεων στις συχνότητες S-band, C-band and X-band. Στην παρούσα διπλωματική εργασία μελετήθηκαν συνολικές διατάξεις παραγωγής και προεπιτάχυνσης ηλεκτρονίων (Electron-Gun) που περιέχουν τρεις διαφορετικές δομές με υλικό συμβατικής αγωγιμότητας. Οι δομές αυτές διέφεραν ως προς τη σύνθεση της μικροκυματικής κοιλότητας (RF cavity) με δομή 1.5 κελιών (S-band), με 2.5 κελιών (S-band) και με 4.6 κελιών (X-band).

Η διπλωματική εργασία απαρτίζεται από τρία μέρη, το πρώτο αποτελείται από τον προσδιορισμό των κατάλληλων παραμέτρων για την προσομοίωση των φωτοκαθόδων. Το δεύτερο μέρος πραγματεύεται την εφαρμογή διάφορων αρχών της δυναμικής της δέσμης στις διατάξεις προσομοίωσης, καθώς και τη σύγκριση της επίδοσης των δύο προαναφερθέντων υλικών των φωτοκαθόδων σε όλες τις δομές. Για τις προσομοιώσεις χρησιμοποιήθηκε το πρόγραμμα ASTRA, που υλοποιεί έναν αλγόριθμο ανίχνευσης χωρικού φορτίου. Το τρίτο και τελευταίο μέρος ασχολείται με τη βελτιστοποίηση δύο από τους πιθανούς Φωτοεγχυτές, ένα για το φάσμα S-band με 1.5 κελιά και έναν για το φάσμα X-band με 4.6 κελιά, τροφοδοτούμενα από δέσμη παραγόμενη από φωτοκάθοδο με Χαλκό. Η διαδικασία βελτιστοποίησης περιείχε ένα κομμάτι χειροκίνητης βελτιστοποίησης και ένα κομμάτι αλγοριθμικής βελτιστοποίησης με χρήση γενετικού αλγορίθμου, υλοποιημένου στο πρόγραμμα GIOTTO. Πρόκειται για ένα πρόγραμμα βελτιστοποίησης επιταχυντικών διατάξεων που συνάδει με το πρόγραμμα ASTRA. Εν κατακλείδι, το τελευταίο μέρος, παραθέτει τη σύγκριση των αποτελεσμάτων της βελτιστοποιημένης διάταξης συναρτήσει της φωτοκάθοδου από Καίσιο-Τελλούριο. Τελικός στόχος, η παρουσίαση των πλεονεκτημάτων και μειονεκτημάτων κάθε είδους φωτοκάθοδου με βάση τα αποτελέσματα προσομοίωσής των χαρακτηριστικών της τελικής δέσμης στις διάφορες διατάξεις και η εξέταση των ορίων βελτιστοποίησής τους.

Λέξεις-Κλειδιά: Δυναμική δέσμης, Laser Ελεύθερων Ηλεκτρονίων, Γραμμικοί Επιταχυντές, Φωτοκάθοδος, Χαλκός, Καίσιο-Τελλούριο, S-band, X-band, Electron Gun, CompactLight, Γενετικοί Αλγόριθμοι, ASTRA, GIOTTO.

ABSTRACT

The H2020 CompactLight Collaboration Project is an international project of 24 institutes (21 European + 3 extra Europeans), that aims at designing the next generation of compact hard X-Rays Free-Electron Lasers. Currently operating FELs in Europe use S-band (3GHz) accelerating structures. The aim of the project is to produce an innovative compact design with less power demand and of smaller beam energy hard X-Ray FEL in frequencies in the X-band. The conceptual, yet, design relies on high-gradient X-band (12 GHz) accelerating fields, short-period superconductive undulators and bright photoinjectors. The quality of the electron beam injected to the linear accelerator is crucial for the final performance of the X-Ray FEL and depends on a numerous set of parameters. A high quality beam is a beam of a very low emittance, high brightness as well as having the capability of a high repetition rate. The material where the electrons are extracted from is one of these parameters and can either be a metal or a semiconductor. Two candidates were studied, Copper (Cu) and Cesium-Telluride (Cs_2Te). For the design of the photoinjector several layouts have been proposed for the project, including design proposals in the S-band, C-band and X-band frequencies. The present Diploma Thesis takes into account several photoinjector layouts and components proposed, including three different normal conducting electron-guns, an 1.5 cells S-band gun, a 2.5 cells S-band and a 4.6 cells X-band gun.

This work is divided in three parts. The first part is dedicated to the determination of the material parameters needed to perform the simulations. The second part presents several aspects of the beam dynamics theory applied to some of the proposed layouts and compares the performance of the two materials, Cu (Cu) and Cesium-Telluride (Cs_2Te), in all the guns. The simulations required were performed using the code ASTRA, a space charge tracking algorithm. The third part is concerned with the optimisation of two photoinjectors, one in the S-band, 1.5 cells gun, and one in the X-band, 4.6 cells gun, operating with a Cu photocathode. The optimisation has manual and algorithmic parts, with the latter being performed by the code GIOTTO, designed to perform ASTRA simulations through a genetic algorithm. Lastly, the last part compares these results with the performance of the optimised lattice operating with a Cs_2Te photocathode. The main goal of this thesis is to study possible layouts of the photoinjector in terms of the CompactLight project, to present the pros and cons of the different photocathode materials through their performance in the proposed lattices and examine the limits of their optimisation.

Keywords

Beam dynamics, Free Electron Laser, Linear accelerator, Photoinjector, Photocathode, Copper (Cu), Cesium-Telluride (Cs_2Te), S-band, X-band, Electron Gun, CompactLight, Genetic Algorithms, GIOTTO, ASTRA.

*Σε όλους όσους ήταν δίπλα μου σε αυτή την προσπάθεια, με
βοήθησαν να προχωρήσω, με προκάλεσαν να προσπαθήσω και
με ενέπνευσαν...*

Table of Contents

ΠΕΡΙΛΗΨΗ	8
ABSTRACT	11
ΕΚΤΕΤΑΜΕΝΗ ΠΕΡΙΛΗΨΗ	14
Table of Contents	15
1.Introduction to Accelerators and Photoinjectors	18
1.1 Particle Accelerators	18
1.1.1 Circular Accelerators	18
1.1.2 Linear Accelerators (LINACs)	18
1.1.3. X-Free Electron Lasers	18
1.2 Photoinjectors	19
1.2.1 Normal Conducting RF Gun	19
1.2.1 Travelling wave structure (TWS)	21
1.3 References	21
2.CompactLight Collaboration XLS	22
2.1 CompactLight XLS Goals	23
2.1 References	24
3. Basic Concepts of Beam Dynamics	25
3.1 Phase space	25
3.3 Brightness	27
3.4 Beam waist	27
3.5 References	28
4. Photocathode Theory	29
4.1 Transverse Emittance for Metals	29
4.2 Semiconductor Photocathodes	29
4.3 Semiconductors and Cu Photocathode Parameters	30
4.4 Laser Parameters	31
4.5 References	32
5. Ferrario Working Point	33
5.1 Working Point	33
5.2 Double emittance Minimum	33
5.3 References	34
6. ASTRA A Space Charge Tracking Algorithm	35
6.1 Introduction to ASTRA	35
6.1.1 The program Generator	35

6.1.2 The program Astra	36
6.1.3 Plotting programs	38
6.2 Parameters and Distributions Used	38
6.3 References	40
7. Genetic algorithms in Photoinjector optimisation	41
7.1 Algorithms Generally Used for optimisation	41
7.2 Genetic Algorithms	42
7.3 GIOTTO Algorithm for ASTRA	43
7.3.1 Running GIOTTO	45
7.4 References	46
8. Laser and Material Parameters Choice	48
8.1 Material Parameters	48
8.1.1 Space Charge Limit and Minimum Radius	48
8.1.1 Cu Photocathode	49
8.1.1 Cs ₂ Te Photocathode	51
8.2 Cu vs Cs ₂ Te	51
8.3 Laser Parameters	52
8.3 References	53
9. ASTRA Simulations	54
9.1 Space charge field simulation	55
9.2 Emittance evolution inside the gun	57
9.2 Beam drift	57
9.3 Beam Distributions and Comparison through Gun - Solenoid	59
9.3.1 1.5 cells gun S-band	59
9.3.2 2.5 cells gun S-band	72
9.3.3 4.6 cells gun X-band	74
9.3.4 Conclusions	83
9.4 Double emittance minimum	83
10. Photoinjector optimisation 1.5 cells S-band	85
10.1 Cavities	86
10.2 STEP 1. Solenoid choice	89
10.3 STEP 2. Optimal beam waist	95
10.3.1 Solenoid No 2	95
10.3.2 Solenoid No 3	99
10.4 STEP 3. GIOTTO optimisation of the Gun and TWS	104
10.4.1 Solenoid No 2	104
10.4.2 Solenoid No 3	109
10.4.3 Comments and conclusions	113
10.5 STEP 4. GIOTTO optimisation	113
10.5.1 Solenoid No 2	113

10.5.2 Solenoid No 3	118
10.6 Final Lattice with the second Booster	123
10.6.1 Solenoid No 2	124
10.6.2 Solenoid No 3	129
10.6.3 Conclusions	134
11. Photoinjector optimisation 4.6 cells X-band	135
11.1 Cavities	135
11.2 optimisation	137
11.6.3 Conclusions	148
12. Conclusions and Suggestions for further analysis	148
13. Bibliography	151
Appendix A. Particle Beam Dynamics	154
A.1 Single Particle Dynamics	154
A.2 RF fields and gun geometries	158
A.3 Particle Beams and Phase Space	158
A.3 Longitudinal Beam Dynamics and Phase Space	170
A.4 Beam Dynamics without space charge	173
A.5 Beam Dynamics with space charge	175
A.4 References	178
Appendix B. Photocathode Theory	179
B.1 Three-Step Model in Metals	179
B.2 Transverse Emittance and Quantum Efficiency in the Three-Step Model for Metals	182
B.3 The Schottky Effect	182
B.4 Semiconductor Photocathodes	183
B.5 Semiconductors and Cu Photocathode Parameters	184
B.6 Laser Parameters	185
B.8 The “Halo” Effect	187
B.7 References	187
Appendix C. Table of abbreviations	188

1.Introduction to Accelerators and Photoinjectors

1.1 Particle Accelerators

A particle accelerator is an accelerating machine that uses electromagnetic fields to propel charged particles to very high speeds and energies, and to contain them in well-focused beams.[1.4] The particle accelerators have a wide range of applications. Usually, larger and more powerful accelerators are used in physics experiments, like the LHC at CERN, Geneva. Smaller accelerators are used in industrial and medical applications.

1.1.1 Circular Accelerators

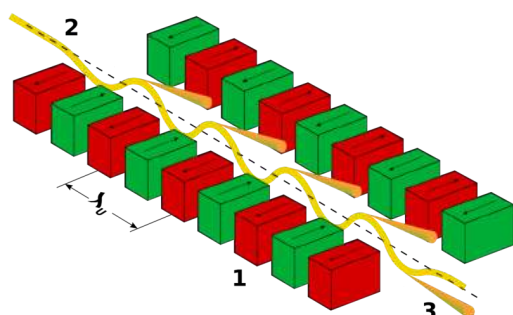
There are two categories of accelerators, the circular and the linear accelerators. The circular accelerators, the particles are accelerated in a circle-like trajectory, and they orbit until they reach a particular energy. The bending of the particle trajectory is done with strong electromagnets. The energy gain of the particles inside the accelerator has an upper limit dictated by synchrotron radiation, which occurs from the constant centrifugal acceleration that causes the particles to emit light (synchrotron radiation) losing energy.

1.1.2 Linear Accelerators (LINACs)

The other category is the linear accelerators. As the name indicates, the particles are accelerated in a straight line with a target of interest at one end. Their applications can be the generation of X-Rays in high-energy electrons, injection to higher energy particle accelerators and experiments with light particles (electrons and positrons) eg as colliders. In this thesis, the photoinjection part of an X-Ray Free Electron Laser (XFEL) Linear Accelerator (LiNAC) will be examined.

1.1.3. X-Free Electron Lasers

An X-Rays free-electron laser (X-FEL) is a kind of laser whose lasing medium consists of very-high-speed electrons moving freely through a magnetic structure, hence the term *free electron*. The free-electron laser is tunable and has the widest frequency range of any laser type, currently ranging in wavelength from microwaves, through terahertz radiation and infrared, to the visible spectrum, ultraviolet, and X-ray.



F.1.1 Undulator magnets and beam motion

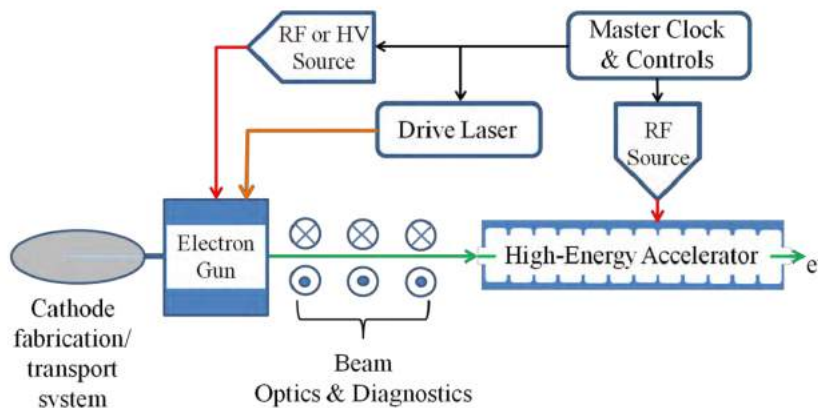
The main principle of an XFEL is that an electron beam is generated and accelerated in high energy and near to speed of light velocity and injected in a magnet called an undulator F.1.1. The undulator has a sinusoidal magnetic field and in this field one electron moves along a sinusoidal, oscillating trajectory, and emits an electromagnetic wave-train, with a number of periods equal to the number of undulator periods and a wavelength equal to the undulator period, reduced by a relativistic contraction factor inversely proportional to the square of its energy.[1.5] Practically, an FEL undulator produces synchrotron radiation in a directed way.

The thesis is concerned with the part of generation and the first acceleration of electrons in a conceptual X-Ray FEL in terms of the CompactLight XLS Collaboration project. This part is called the photoinjector.

1.2 Photoinjectors

A typical configuration of a photoinjector is shown below. The electron beam is generated from a conducting or semiconducting cathode that is illuminated by a drive laser, then, accelerated through an electron gun, properly focused by beam optic elements matching the beam to the high-energy accelerator, and assorted diagnostics. The electron gun can either be a high voltage DC gun, normal conducting RF gun or a superconducting RF gun. The beam optics can be performed by solenoids. The high-energy accelerator is often called a Booster and is in this thesis case a Travelling Wave Structure. All the accelerating RF cavities should operate in the same or multiple frequencies.

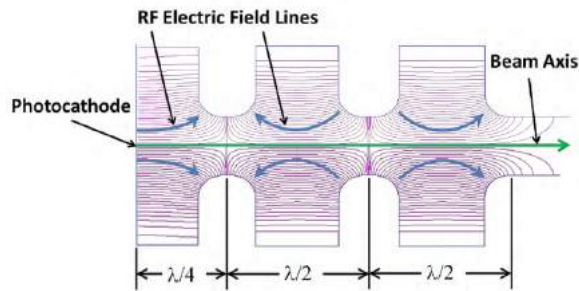
Equally important as the high field RF gun, cathode and laser is the optical matching of the beam size and divergence into the first linac section. The distance between the end of the gun and the entrance to the linac is determined by the bunch's plasma oscillation period.



F.1.2 Photoinjector configuration

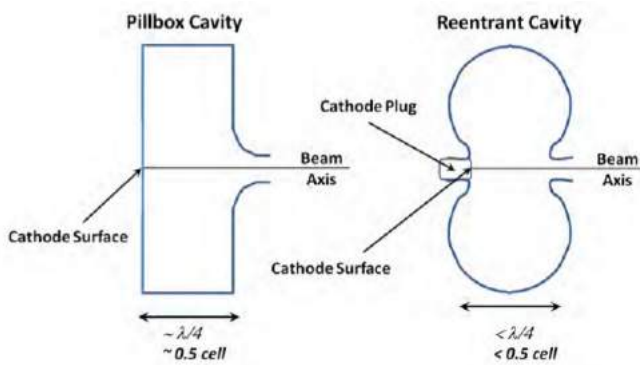
1.2.1 Normal Conducting RF Gun

The photocathode RF gun consists of a cathode in a half length cavity only, or the cathode 1/2-cell followed by one or more full length cavities. These cavities operate typically in a TM_{011} transverse magnetic mode. [1.1]



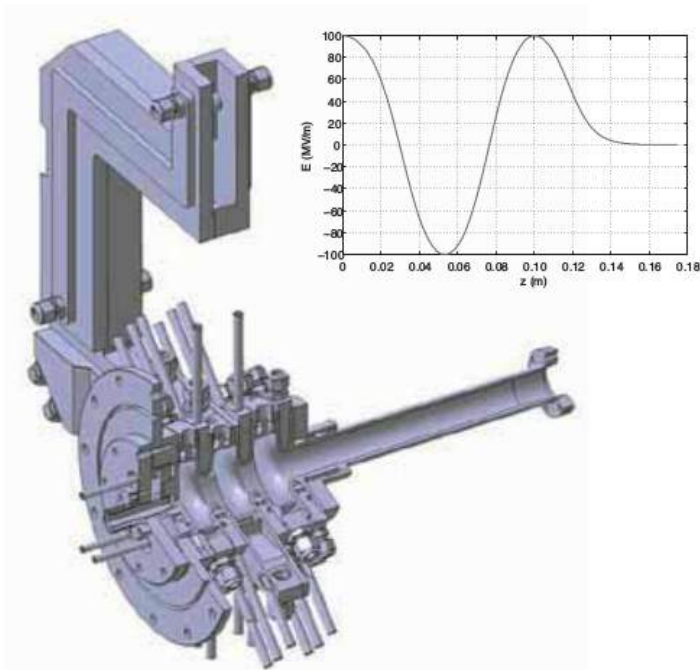
F.1.3a 2.5 cells RF gun

The two common geometries for the RF gun half cavity are the Pillbox (left) and the re-entrant (right) cavity [1.1]



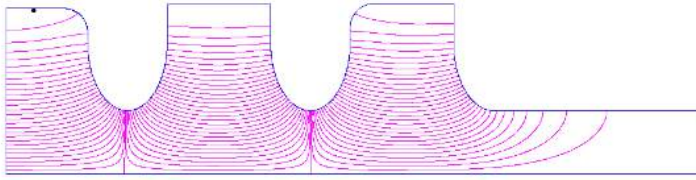
F.1.3b Common Geometries for the half cell

For example, the RF gun shown in F.1.4 is a 2.5 cells normal conducting RF gun from the SwissFEL project. This is the 2.5 cells gun simulated in Chapter 9.



F.1.3 Design and on-axis field distribution of the

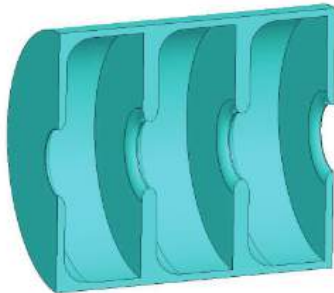
SwissFEL gun [1.9]



F.1.4 Electric field contour lines of the operating π mode. [1.8]

1.2.1 Travelling wave structure (TWS)

Travelling wave structure is a periodic accelerating structure of travelling electromagnetic waves. In electron accelerators, usually it consists of identical cells. For example, the S-Band TWS for the Swiss FEL consists of cells like the ones in F.1.5.



F.1.5 3D model of the S-band structure cells [1.10]

1.3 References

- [1.1] Rao, Triveni, and David H. Dowell. *An Engineering Guide to Photoinjectors*. CreateSpace Independent Publishing, 2013.
- [1.2] Wangler, Thomas P. *RF Linear Accelerators*. Wiley-VCH Verlag, 2017.
- [1.3] Wiedemann, Helmut. *Particle Accelerator Physics: with 264 Figures*. Springer, 2007
- [1.4] Livingston, Milton Stanley., and John Paul. Blewett. *Particle Accelerators*. McGraw-Hill, 1962.
- [1.5]<https://www-ssrl.slac.stanford.edu/stohr/xfels.pdf>
- [1.6] https://en.wikipedia.org/wiki/Particle_accelerator#Low-energy_machines_and_particle_therapy
- [1.7] <https://en.wikipedia.org/wiki/Undulator>
- [1.8] Raguin, Jean-Yves & Bopp, M & Citterio, A & Scherer, A. (2012). The Swiss FEL RF Gun: RF Design and Thermal Analysis.
- [1.9] Falone, Antonio & Adelman, A. & Raguin, Jean-Yves & Stingelin, Lukas. (2011). RF Gun Studies for the SwissFEL Injector.
- [1.10] J.-Y. Raguin, PSI, CH-5232 Villigen, Switzerland (2012). The Swiss FEL S-Band Accelerating Structure : RF Design. ISBN 978-3-95450-122-9

2.CompactLight Collaboration XLS

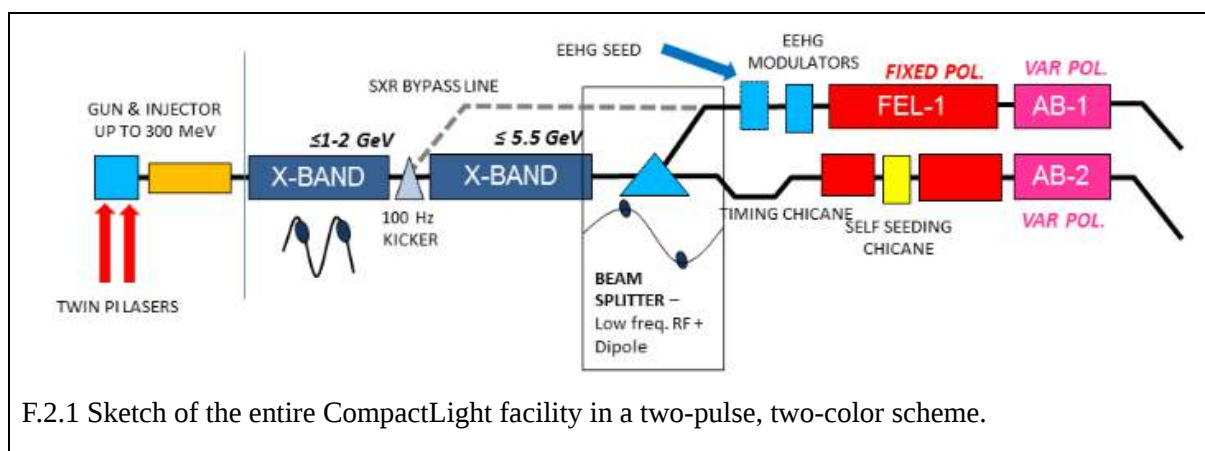
H2020 CompactLight Project aims at designing the next generation of compact hard X-Rays Free-Electron Lasers, relying on very high accelerating gradients and on novel undulator concepts. CompactLight intends to design a compact Hard X-ray FEL facility based on very high-gradient acceleration in the X-band of frequencies, on a very bright photoinjector, and on short-period/superconductive undulators in order to enable smaller electron beam energy. If compared to existing facilities, the proposed facility will benefit from a lower electron beam energy, due to the enhanced undulators performance, and will be significantly more compact, have lower electrical power demand and a smaller footprint, as a consequence both of the lower energy and of the high-gradient X-band structures. CompactLight is a consortium of 24 institutes (21 European + 3 extra Europeans), gathering the world-leading experts both in the domains of X-band acceleration and undulator design.[2.2]

Free Electron Lasers (FELs) produce synchrotron radiation, a fundamental tool on studying matter properties. The demand for FELs is increasing, while the cost of construction and operation is not always affordable. The main objective of the CompactLight XLS Collaboration is to facilitate the widespread development of X-ray FEL facilities across Europe and beyond, by making them more affordable to construct and operate, through an optimum combination of emerging and innovative accelerator technologies.[2.2]

The Collaboration intends to design an hard X-ray FEL facility beyond today's state of the art, using the latest concepts for bright electron photoinjectors, high-gradient X-band structures operating at 12 GHz, and innovative short-period undulators. Compared with existing facilities, the proposed facility will (i) benefit from a lower electron beam energy, due to the enhanced undulator performance, (ii) be significantly more compact, as a consequence of the lower beam energy and the high gradient of the X-band structures, (iii) be more efficient (less power consumption), as a consequence of the lower energy and the use of higher frequency structures. [2.2]

There will be two operation modes, one producing Soft X-Ray and one for Hard X-Rays. When running in hard X-ray mode the electron energy will be up to 5.5 GeV at 100Hz, in soft X-ray mode the energy will be up to 2 GeV and, since the linac gradient will be much reduced, the repetition rate will be able to be increased significantly. A repetition rate of 1000 Hz for the soft-X-ray FEL will be a unique and highly desirable feature of the facility.

Below, in F.2.1, is a concept of the design as published in [2.2]:



F.2.1 Sketch of the entire CompactLight facility in a two-pulse, two-color scheme.

2.1 CompactLight XLS Goals

The goals of CompactLight are the design of a full-fledged free-electron laser (FEL) based on the most advanced technologies for a compact electron injector gun, an X-band based linac, and a short-period/superconductive undulator to enable smaller electron beam energy. [8.2] Some of the technological advances the CompactLight XLS project plans to take advantage of are:

- Lower emittance and higher repetition-rate photo-injectors
- High-gradient linacs – Gradients in excess of 100 MV/m are now routinely achieved
- High-efficiency klystrons – Techniques to bring efficiencies above 60% at high frequency have been demonstrated
- Advanced concept undulators – Cryogenic permanent magnet undulators and superconducting undulators have both been demonstrated and since used operationally on 3rd generation light sources in recent years
- Improved diagnostics including X-band deflectors for longitudinal bunch dynamics
- Better beam dynamics and optimisation tools including those developed for linear colliders.

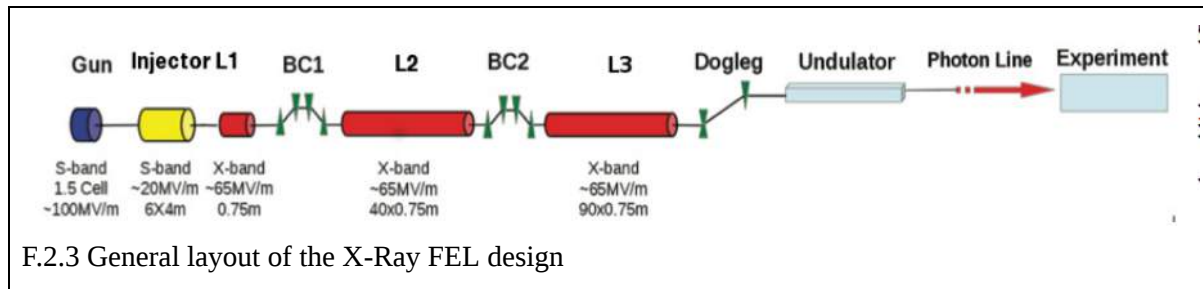
The final goal is to produce the design of a next-generation facility with significantly lower cost and size than existing facilities. The goal is to make XFELs feasible for smaller countries, regions and universities. [2.1]

The preliminary parameters published by the CompactLight community are presented below, in F.2.2:

Parameter	Units	Value
Linac frequency	GHz	12
Linac gradient	MV/m	70
Beam energy	GeV	< 4.6
Bunch Charge	pC	< 250
Normalized emittance	mm mrad	< 0.5
Bunch length	μm	< 8
Pulse duration	fs	< 1 to 50
Pulse repetition rate	Hz	100-1000
Number of bunches per pulse	#	1-3
FEL Parameters		
<i>K</i> value	#	1.13
Minimum wavelength	\AA	1
Number of photons per pulse	#	> 10^{12}
Pulse bandwidth	%	$\ll 0.1$

F.2.2 Preliminary Parameters of the Proposed Compact-Light Hard X-ray Facility

The general layout is shown in F.2.3.



2.1 References

[2.1] CompactLight, <http://www.compactlight.eu>.

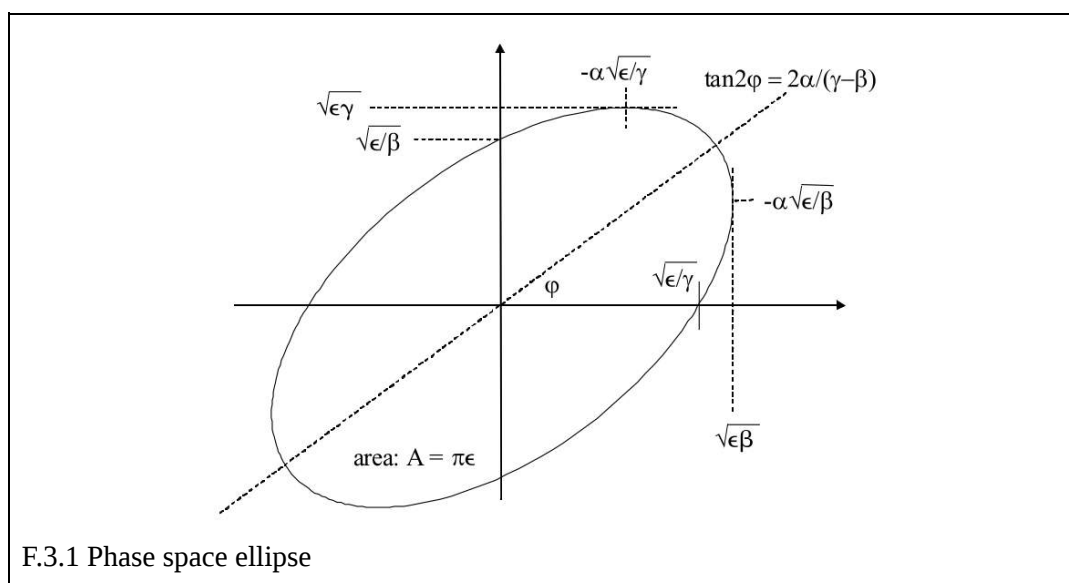
[2.2] D'auria, G & Di Mitri, S. & Rochow, Regina & Trieste, Sincrotrone & Latina, Italy & Liu, Xiongyi & Rossi, Carlo & Schulte, D & Cortes, H & Clarke, Jim & Dunning, David & Thompson, N & Goryashko, V & Jacewicz, M & Ruber, R & Dowd, R & Zhu, D & Aksoy, Australia & Negriz, Z & Zhang, L. (2019). CompactLight DESIGN STUDY. 10.18429/JACoW-IPAC2019-TUPRB032.

3. Basic Concepts of Beam Dynamics

In this chapter the aspects of Appendix A that are important for the cohesion of this thesis are presented. The enumeration of figures and relations in this chapter will not be taken into account in other chapters, the enumeration of Appendix A will be used instead.

3.1 Phase space

Customarily, the phase space of a beam is represented by an ellipse called the phase ellipse. Of course, the shape of the ellipse is not completely arbitrary but derives from the way the differential equation of motion is solved and will be presented later. The general form of the ellipse is presented in F.3.1.



The ellipse is described by:

$$\gamma x^2 + 2\alpha x x' + \beta x'^2 = \epsilon \quad (3.1)$$

The area enclosed by the ellipse is the emittance ϵ , defined as :

$$\int_{\text{ellipse}} dx dx' = \pi\epsilon \quad (3.2)$$

From this definition, the emittance is measured in meters-radians (usually pi mm mrad).

In practice the emittance is statistically defined as (see Appendix A):

$$\begin{cases} \sigma_x = \sqrt{\beta_x \epsilon_{x,\text{rms}}} \\ \sigma_{x'} = \sqrt{\gamma_x \epsilon_{x,\text{rms}}} \end{cases} \quad (3.3)$$

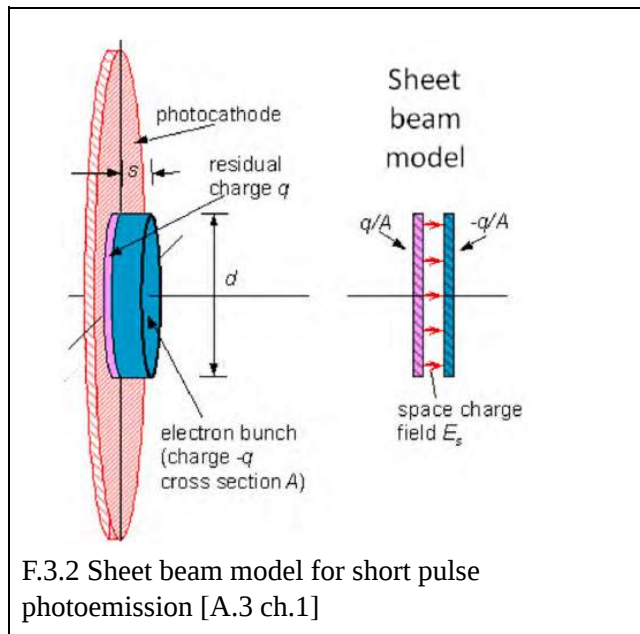
$$\epsilon_{\text{rms}} = \sqrt{\sigma_x^2 \sigma_{x'}^2 - \sigma_{xx'}^2} = \sqrt{(\langle x^2 \rangle \langle x'^2 \rangle - \langle xx' \rangle^2)} \quad (3.4)$$

3.2 Beam Dynamics with space charge

This part of the chapter corresponds to Appendix A.5 and its most crucial parts for the coherence of the thesis are also presented here.

Space Charge Limited Emission

In the case of photoemission, the bunch charge can be photon limited or space charge limited. The photon limited emission is given by the quantum efficiency (QE) [see Appendix B] times the number of incident photons, and space charge limited emission is given by a sheet beam model, as in F.3.2.



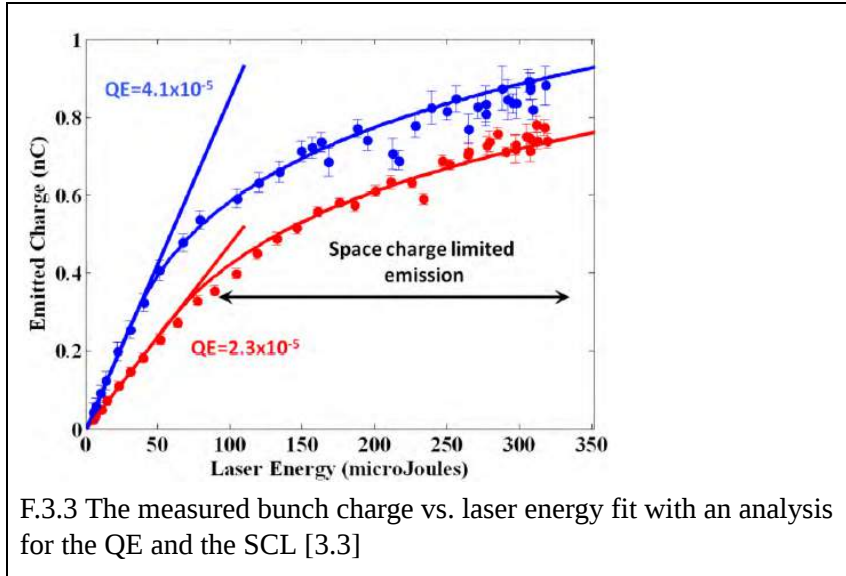
The field induced by the bunch is similar to a capacitor's electrical field. With this said:

$$E_{SCL} = \frac{q}{A\epsilon_0} = \frac{\sigma}{\epsilon_0} = E_{applied}$$

So, the space charge density limit is :

$$\sigma_{SCL} = \epsilon_0 E_0 \sin(\phi_0) \quad (3.5)$$

In the plot of F.3.3, the bunch charge is presented with respect to the laser energy. For small charges the relation is linear with the slope depending on the Quantum Efficiency QE and for greater charges, saturation is observed.



For low laser energies below the SCL, the curve is linear with a slope related to the quantum efficiency, QE :

$$q_{bunch} = \frac{eE_{laser}}{\hbar\omega} QE \quad (3.6)$$

QE is often obtained from the linear portion of the curve (see Fig.3.3)

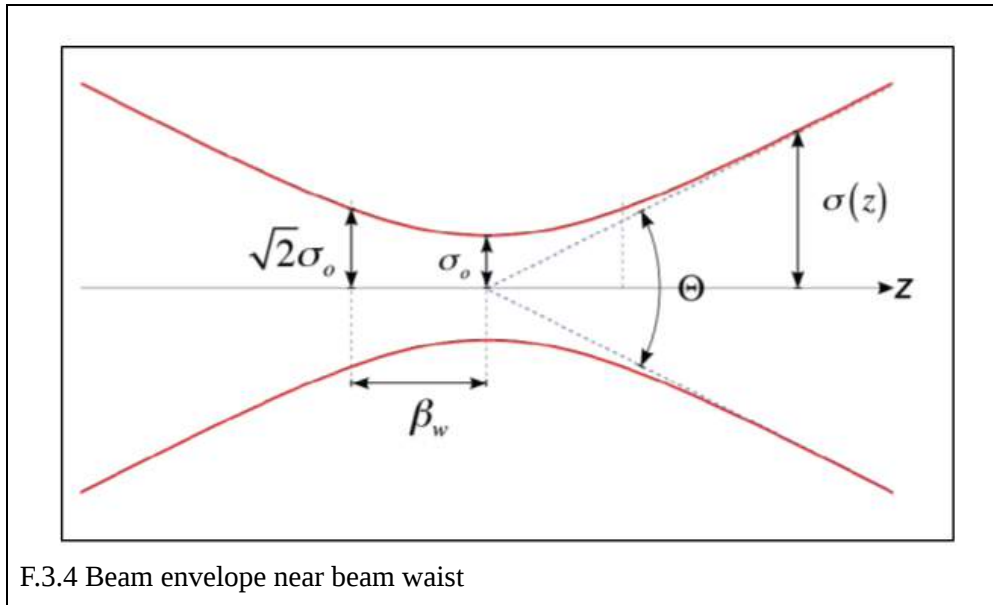
3.3 Brightness

The beam brightness combines the emittance and the peak current into a single parameter measuring the electron volume density. The most common practice is to define the transverse, normalized beam brightness, B_n :

$$B_n = \frac{2I}{\pi^2 \mathcal{E}_{n,x} \mathcal{E}_{n,y}} \quad (3.7)$$

3.4 Beam waist

Beam waist is defined as the longitudinal position where the transverse size of the beam becomes minimum. In F.3.4 the minimum transverse size is σ_0 and the red lines represent the premises of the beam. The beam waist is a very important phenomenon that defines the working point of the photoinjector (see Chapter 5).



3.5 References

- [3.1] Wiedemann, Helmut. *Particle Accelerator Physics: with 264 Figures*. Springer, 2007
- [3.2] Ferrario, Massimo. "Space Charge Mitigation." *CERN Yellow Reports: School Proceedings*, dx.doi.org/10.23730/CYRSP-2018-001.177.
- [3.3] Rao, Triveni, and David H. Dowell. *An Engineering Guide to Photoinjectors*. CreateSpace Independent Publishing, 201A.
- [3.4] Wangler, Thomas P. *RF Linear Accelerators*. Wiley-VCH Verlag, 2017.
- [3.5] Hernandez-Garcia, C., et al. "Charge Production Studies from Cs₂Te Photocathodes in a Normal Conducting RF Gun." *Nuclear Instruments and Methods in Physics Research Section A: Accelerators, Spectrometers, Detectors and Associated Equipment*, vol. 871, 2017, pp. 97–104., [doi:10.1016/j.nima.2017.06.051](https://doi.org/10.1016/j.nima.2017.06.051).
- [3.6] Maurizio. "Linear Accelerators." *CERN Document Server*, CERN, 29 Mar. 2013, arxiv.org/ct?url=https://dx.doi.org/10.5170/CERN-2013-001.225&v=e1312714.

4. Photocathode Theory

In this chapter, the main theory of photoemission are presented. The detailed theory of photocathodes and the definitions of the quantities used are described in Appendix B. The rest of the thesis will refer to the relations below through their respective ones in Appendix B.

4.1 Transverse Emittance for Metals

The emittance of an electron beam emitted from a metallic photocathode can be expressed as:

$$\varepsilon_n = \sigma_x \sqrt{\frac{h\nu - \phi_{eff}}{3mc^2}} \quad (4.1)$$

where , $h\nu$ the photon energy, ϕ_{eff} the effective work function, m the electron mass. The effective work function is the energy required to excite an electron to the vacuum without kinetic energy.

The average kinetic energy of the electrons extracted from the metallic cathode is given by

$$E_{kin} = \phi_{exc} / 2 = \frac{(h\nu - \phi_0)}{2} \quad (4.2)$$

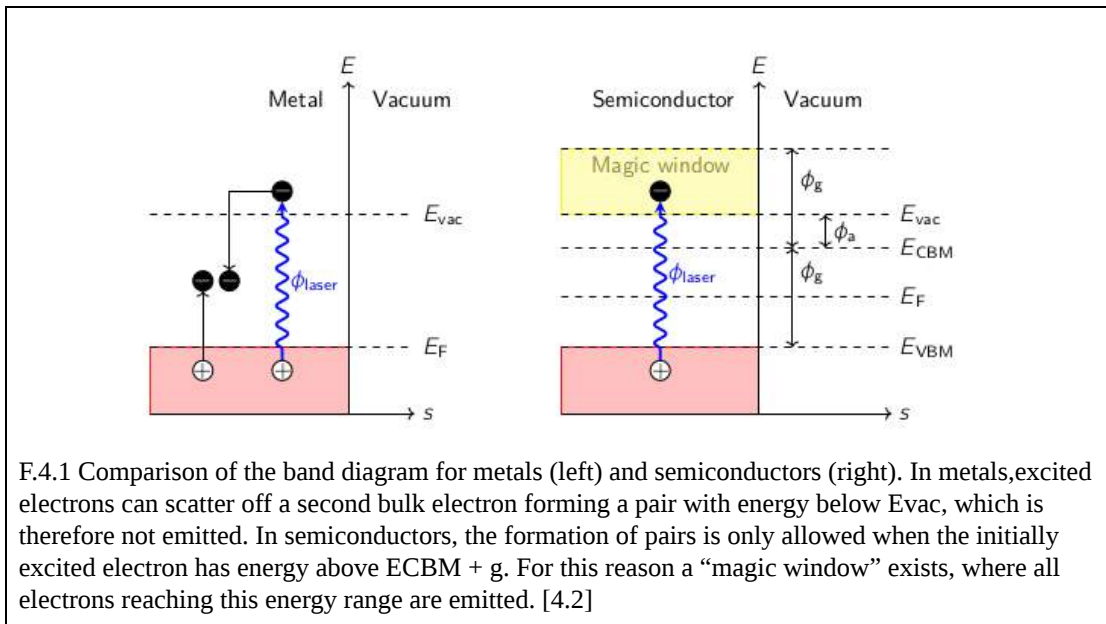
4.2 Semiconductor Photocathodes

In a semiconductor the relations introduced above differ at some points because of the effect of the “*magic window*” introduced in Appendix B. The first parameter is the much higher QE that enables greater charge production with less laser power.

The effective work function is defined by :

$$\phi_{eff} = \phi_g + \phi_a \quad (4.3),$$

where ϕ_a is denoted in F.4.1.



The next parameter is the kinetic energy. The kinetic energy in semiconductors equals to the excessive energy $E_{kin} = \varphi_{exc} = hv - \varphi_{eff}$, the alteration in the density of electron states. E_{kin} is often written as MTE, which is the mean transverse energy.

The normalised thermal emittance is estimated as:

$$\frac{\varepsilon_{n,th}}{\sigma_x} = \sqrt{\frac{MTE}{3m_0c^2}} \quad , \quad \text{where } MTE = hv - (\varphi_g - \varphi_\alpha) + \Delta\Phi_{Schottky} \quad (4.4)$$

and $m_0c^2 = 0.511$ MeV is the electron's rest energy, hv the photon energy and $\Delta\Phi_{Schottky}$ the Schottky energy.

Another parameter that cannot be ignored in semiconductors is the Emission Delay or Response Time (τ), which is the time between the electron excitation and its exit from the metallic surface. In metals it is very small, as shown in Table B.1 (Appendix B), thus, is ignored. For semiconductors like Cs_2Te the time delay is non-negligible and in the order of $\Delta t = 0.1\text{--}1$ ps. Specific Monte Carlo simulations for Cs_2Te predict a time response of $\Delta t = 0.4$ ps [4.2]

4.3 Semiconductors and Cu Photocathode Parameters

In the following tables [4.2][4.3], the most important parameters for Cs_2Te and Cu photocathodes.

TABLE 4.2 Cs_2Te Emission parameters					
Cathode Wavelength	λ [nm], E_{ph} [eV]	QE [%]	$E_a + E_{gap}$ [eV]	Thermal emittance $\left[\frac{\text{mm mrad}}{\text{mm rms}} \right]$	
				Theory (Equ. 7.6)	Experiment
Cs_2Te	262, 4.73	~10	3.5	0.9	1.2 ± 0.1

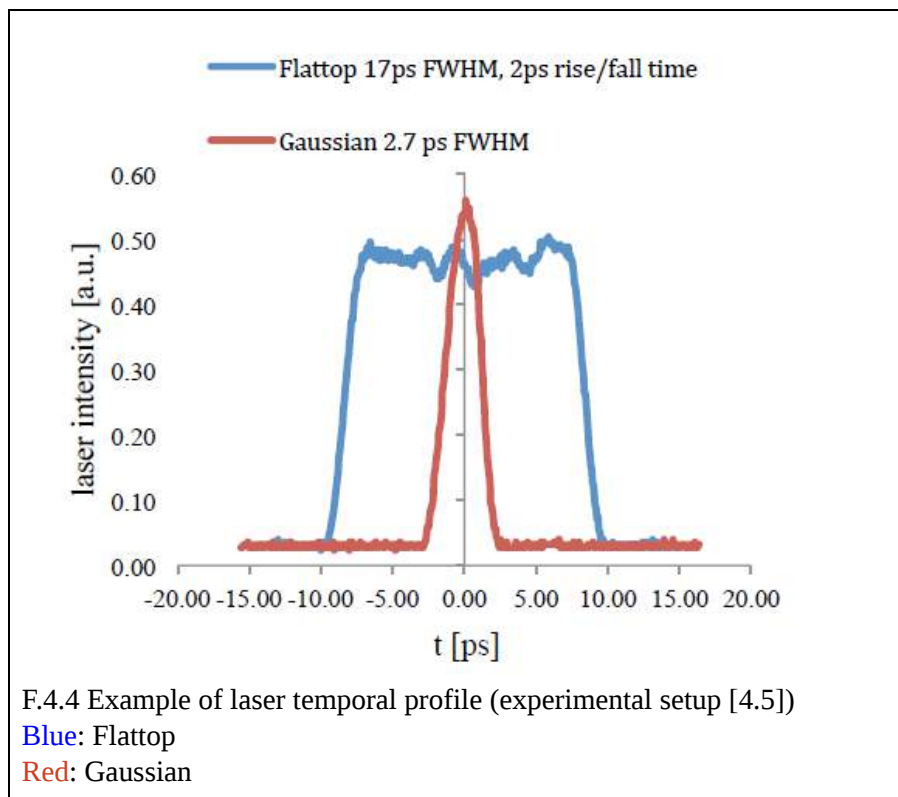
TABLE 4.3 Cu Emission parameters		
QE [%]	φ_{eff} [eV]	Normalized Thermal Emittance [mm mrad /mm]
$\sim 10^{-5}$	4.65	0.23

The laser parameters for Cu are not strict the ones chosen in each case are presented before the simulations. In general the laser must be adjusted so that the excessive energy is low, so that the thermal emittance is small.

4.4 Laser Parameters

The laser parameters that will concern the simulations of this thesis are the photon wavelength and energy, the transverse and the longitudinal profile of the laser pulse. The photon energy, as mentioned already, is chosen in such a way that the excess energy of the electrons is low, thus the emittance.

The longitudinal/temporal profile of a laser usually either a Gaussian or a Flattop one. The Flattop profile can be created by stacking Gaussian pulses, as done in SwissFEL [4.2]. Recently the case of an ellipsoidal profile is tested as it shows better performance.



The temporal profile of the laser translates to beam temporal profile. The temporal profile affects the stability of the beam and the transverse emittance and the transverse size [see 4.1 ch.9.6.1] as it affects the space charge fields and the stability of the beam. In [4.1] it is reported that in simulations an Ellipsoidal temporal distribution would result in the least emittance while a Flattop one gives smaller emittance than a Gaussian in simulations. In [4.7] specific simulations are also reported confirming the above. In the simulations below a Flattop profile was used as such a laser system is already in use in SwissFEL facilities.

The duration of the pulse can not be arbitrary, it is limited by the RF frequency. The bunch length, and hence the peak current from the injector depends upon the RF frequency of the main accelerator since the bunch length should be a small fraction of an RF period. A sensible guideline is less than 10° RF for the full bunch length.[4.1] The simulations of following Chapters will concern guns in the S-band and X-band of frequencies. The S-band frequencies that were used are 2.856 GHz (1.5 cells), 2.998GHz (2.5 cells) and in the X-band 11.992GHz (4.6 cells). The upper limits in these cases are approximately the one presented in Table 4.4.

TABLE 4.4 : Maximum laser pulse duration		
3GHz	<10 psec	The pulse duration can be computed by: $L_t = \frac{1}{f} \cdot \frac{10^9}{360^\circ}$
12GHz	<2.3 psec	

As for the laser transverse profile, the spot size needs to be determined. From equation (B.16)/(4.4) and the space charge limit (A.66) one can assume that the best choice is to choose the smaller size permitted. But, this does not work because the smaller the size, the greater the space charge forces and, as a result, the emittance increases. The transverse profile usually is Gaussian, Flattop or Uniform with the latter introducing the least non-linear space charge forces. The uniform distribution is often assumed, as well as in the simulations of Chapters 9-11.

4.5 References

- [4.1] Rao, Triveni, and David H. Dowell. *An Engineering Guide to Photoinjectors*. CreateSpace Independent Publishing, 2013.
- [4.2] Schaer, and Mattia. "RF Traveling-Wave Electron Gun for High Brightness Photoinjectors." *RF Traveling-Wave Electron Gun for High Brightness Photoinjectors - Research Collection*, ETH Zürich, 1 Jan. 1970, doi.org/10.3929/ethz-a-010749949.
- [4.3] Jensen, Kevin L., et al. "Delayed Photo-Emission Model for Beam Optics Codes." *Journal of Vacuum Science & Technology B, Nanotechnology and Microelectronics: Materials, Processing, Measurement, and Phenomena*, vol. 35, no. 2, 2017, doi:10.1116/1.4968511.
- [4.5] Hernandez-Garcia, C., et al. "Charge Production Studies from Cs2Te Photocathodes in a Normal Conducting RF Gun." *Nuclear Instruments and Methods in Physics Research Section A: Accelerators, Spectrometers, Detectors and Associated Equipment*, vol. 871, 2017, pp. 97–104., doi:10.1016/j.nima.2017.06.051.
- [4.6] Spicer, William E., and Alberto Herrera-Gomez. "Modern Theory and Applications of Photocathodes." *Photodetectors and Power Meters*, 1993, doi:10.1117/12.158575.
- [4.7]Bakr, Mahmoud & Vashchenko, Grygorii & Khojoyan, Martin & Krasilnikov, M. & Stephan, F.. (2015). BEAM DYNAMICS SIMULATION FOR THE UPGRADED PITZ PHOTO INJECTOR APPLYING VARIOUS PHOTOCATHODE LASER PULSES.

5. Ferrario Working Point

5.1 Working Point

The so called “*Ferrario working point*” is a matching condition that, if it is met, it leads to envelope oscillations damping when a beam enters a booster accelerator. The working point was formulated for the LCLS injector. [5.1] In order for the point to be met, **the beam must be a waist and the emittance a local maximum in the entrance of the booster** (TWS). In this scheme, the RF focusing of the linac is matched to the invariant envelope to damp the emittance to its final value at a relativistic energy.

The matched transverse size is

$$\sigma_{matched} = \frac{1}{\gamma'} \sqrt{\frac{I}{2I_A \gamma}} \quad (5.1), \text{ where}$$

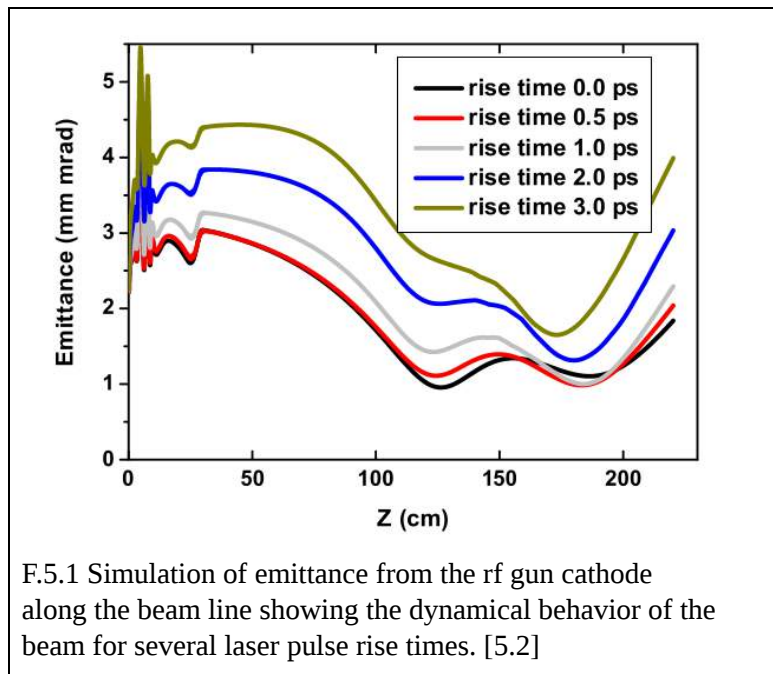
$$\gamma' = \frac{eE_{linac}}{mc^2}$$

as the waist size at injection into the linac. Once matched the beam emittance decreases along the accelerator due to the initial focus at the entrance and Landau damping. [5.1]

During the simulations, this was the condition that needed to be met to optimise the performance of the lattices. For example, if a beam reaches the entrance of a linac of 25 MV/m with an energy 8 MeV, assuming $I=10A$ (mean current) the resulting matched size is 0.089 mm. The optimisations below show that the beam sizes will not be far from that value.

5.2 Double emittance Minimum

In several setups the emittance can demonstrate a behaviour of double minimum. For example F.5.1 shows the emittance evolution with the typical SPARC parameters for different laser pulse rise times in the drift space downstream the gun. [5.2]



It is observed that a flattop distribution with a short rise time leads to a smaller emittance minimum since nonlinear space charge effects are smaller in this configuration.

In such cases, the booster can be located at the local maximum of the emittance and the second emittance minimum will be moved to the linac output [5.2] leading to further decrease of the final emittance.

5.3 References

[5.1] Ferrario, M., et al. "Homodyn Study For The Lcls Rf Photo-Injector." *The Physics of High Brightness Beams*, 2000, doi:10.1142/9789812792181_0037.

[5.2] Cianchi, A., et al. "High Brightness Electron Beam Emittance Evolution Measurements in an Rf Photoinjector." *Physical Review Special Topics - Accelerators and Beams*, vol. 11, no. 3, 2008, doi:10.1103/physrevstab.11.032801.

[5.3] Rao, Triveni, and David H. Dowell. *An Engineering Guide to Photoinjectors*. CreateSpace Independent Publishing, 2013.

6. ASTRA A Space Charge Tracking Algorithm

ASTRA is a space charge tracking algorithm, written in modern Fortran and functions with user-defined namelists. Namelist is a way of getting parameters as input, classified by kind. It is a commonly used code for simulations of linear accelerators.

6.1 Introduction to ASTRA

ASTRA is a space charge tracking algorithm developed at DESY, Hamburg. It uses the numerical method Runge-Kutta integration of 4th order with adjustable steps to solve the equations of motion of the particles. It produces data for all the important measures of the beam that were described above and detailed 2D phase spaces. The input parameters are the beam initial distribution and, of course, the lattice. A beam can be either given as a known distribution, or it can be “generated by a cathode” if the laser distribution and the material parameters are known, according to the relations presented in Appendix B.

The particle distribution is created by a program called ‘*generator*’. The number of particles can also be set, with the total charge ‘divided to the particles that are being tracked, meaning that the electrons have been assigned with greater charge than theirs. The particles are tracked through the beamline by the program ‘*Astra*’.

6.1.1 The program Generator

The program generator creates the beam distribution that is tracked through the lattice. The input parameters of the generator are read for a user-composed file. The parameters used for the simulations of the thesis are described in Table 6.1

TABLE 6.1 Parameters of generator used in the simulations		
Parameter	Utility	Simulation
FNAME	The name of the file the distribution is saved to . ASTRA uses the exit file of generator	-
IPart	The number of particles generated. It is not the number or electrons of the real beam. Each ‘particle’ has a charge of $Q_{total} / IPart$	1000 - 10000
Species	The species of particles	Electrons
Probe	If true, the trajectories of 6 of the particles are tracked and saved.	True

Cathode	If true the particles will be generated with a time spread rather than with a spread in the longitudinal position	True
Q_total	Total charge of the beam	0.075 / 0.100 nC
Dist_z	Longitudinal/Temporal distribution (Plateau is the Flattop profile)	Plateau
Lt	Laser pulse duration	0.0067 / 0.0036 / 0.0020 nsec
rt	Laser pulse rise/fall time	0.0005 nsec
Dist_pz	Longitudinal/Temporal momentum distribution. If assumed to be isotropic it requires only the Kinetic energy and is the same in all directions x,y,z	Isotropic
Dist_px / Dist_py	Transverse momentum distribution	Isotropic
LE	Kinetic energy of the particles	Parameter E_{kin} of Chapter 8
Dist_x / Dist_y	Transverse distribution Radial = Radially uniform	radial
sig_x, sig_y	Rms Transverse size	0.1 - 0.3 mm

6.1.2 The program Astra

The program Astra uses the distribution Generator produces and tracks it through the given lattice. The lattice is given to the program through files that contain the electric and magnetic fields on the z-axis the components produce. Astra uses these files as field longitudinal distributions rather than using the absolute values described, so that the user can adjust the peak field preferably.

For the calculation of the space charge field a cylindrical grid (r, φ, z coordinates), consisting of rings in the radial direction and slices in the longitudinal direction, is set up over the extension of the bunch. The grid is Lorentz transformed into the average rest system of the bunch, where the motion of the particles is to good approximation non relativistic and a static field calculation can be performed by integrating numerically over the rings thereby assuming a constant charge density inside a ring.

As long as the simulation of the thesis are concerned, the main parameters used are described in Table 6.2.

TABLE 6.2: ASTRA namelists

In this table the main parameters used for the simulations of the following chapters are presented.

Namelist NEWRUN	
This namelist contains the parameters that concern the running parameters, the Runge-Kutta method parameters, what data must be saved	
Distribution	The file from the beam distribution is taken
Q_bunch	If not zero the charge given from the Distribution file is rescaled
ZSTART / ZSTOP	Starting and Finishing point of the simulation
AUTO_PHASE	if true, the RF phases will be set relative to the phase with maximum energy gain.
Tau	Emission delay.
Namelist CHARGE	
This namelist contains the parameters that concern the space charge forces computation.	
Lmirror	If true, mirror charge effects on cathode are taken into account
Namelist CAVITY	
In this namelist the Electric fields are specified. For each cavity the user can specify parameters, some of the most important are :	
FILE_EFIELD()	Input field file
MaxE()	Peak of the field
Nue()	Frequency of the cavity operation
Phi()	Phase shift of the cavity
C_pos()	Longitudinal position of the field
C_Numb()	If a field needs to be repeated the number of cells/repetitions is defined. For example, in a TWS only one cell's field is given and then repeated.
Namelist SOLENOID	
In this namelist the magnetic fields produced by solenoids are specified. For each given field the user can specify the respective parameters, the most important of which are presented below:	
FILE_BFieLD()	The input file describing the solenoid field
MaxB()	Peak field
S_pos()	Solenoid position

Other namelists of Astra are:
QUADRUPOLE, DIPOLE, SCAN, APERTURE and FEM

6.1.3 Plotting programs

ASTRA supports graphics programs for the representation of the lattice and the visualisation of the results. The program 'fieldplot' shows the plots of the longitudinal fields of the various components. The program 'postpro' creates the plots of the beam parameters in a given point in the z-axis, usually the phase spaces. Finally, the program 'lineplot', produces the plots of the longitudinal evolution of various metrics.

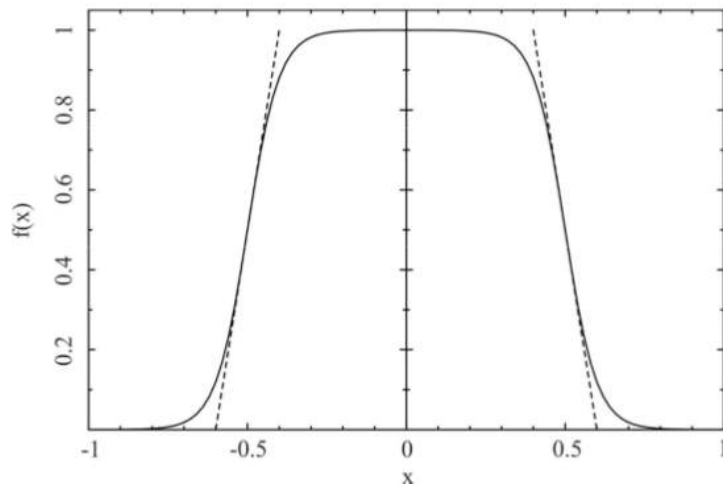
6.2 Parameters and Distributions Used

Initial particle distribution

The program provides a variety of distributions. Here, only the ones used in the simulations are presented. The laser in all simulations has a Flattop temporal profile (see Appendix B) and a radially uniform transverse one.

Temporal profile

The Flattop distribution requires two parameters : the rise-fall time and the length of the constant part.



F.6.1 Plateau distribution with $L = 1$ and fall/rize time $rt = 0.2$. Straight lines according to the definition of rt

TABLE 6.3 : Parameters of Plateau distribution			
Dimension	Keyword	Parameter	Unit
temporal	Dist_z='Plateau'	Lt, rt	ns

Momentum distribution

In the case of a beam generated by a photocathode, the average kinetic energy is required in order to determine the thermal emittance according to (B.9) or

$$\epsilon_{x,y} = \sigma_{x,y} \frac{1}{\sqrt{3}} \sqrt{\frac{2E_{kin}}{m_0 c^2}}$$

Although in the semiconductor case, the relation (B.16) is not supported. So, half the MTE is inserted as the kinetic energy so that the thermal emittance is computed correctly.

The momentum distribution is considered to be isotropic (in 3D) with emission angles into a half sphere.

The respective relations are:

$$p_x^2 + p_y^2 + p_z^2 = P^2 = E_{kin}^2 + 2E_{kin}$$

$$\sigma p_x = \sigma p_y = \frac{P}{\sqrt{3}}$$

$$\sigma p_z = \frac{P}{2\sqrt{3}}$$

$$p_{z,mean} = \frac{P}{2}$$

TABLE 6.4 : Parameters of Isotropic distribution			
Dimension	Key word	Parameter E _{kin}	unit
p _x , p _y , p _z	Dist_pz = 'isotropic'	LE	keV

It is important to underline that ASTRA does not simulate the emission process as described in Appendix B. It get user-defined distributions obtained from the respective theory.

Other generator parameters are described in Ch.6.1.1.

Transverse distribution

The transverse distribution is set to be radially uniform and the parameters that need to be specified are presented in Table

TABLE 6.5 : Parameters of Radially uniform distribution			
Dimension	Key word	Parameter E_{kin}	unit
transverse x, y	Dist_pz = 'radial uniform'	Lx or sig_x	mm

6.3 References

[6.1] ASTRA documentation (http://www.desy.de/~mpyflo/Astra_manual/Astra-Manual_V3.2.pdf)

7. Genetic algorithms in Photoinjector optimisation

7.1 Algorithms Generally Used for optimisation

The number of parameters affecting a linear accelerator's performance, the unpredictable effect of space charge forces on the beam evolution and the careful combination of the tunable parameters required set a limit to the effectiveness of manual testing of parameters. Such parameters are presented in Table 7.1 and their effects are coupled so optimisation of individual parameters may not lead close to the optimum output beam. As a consequence, existing knowledge on optimisation algorithms and techniques are of increasing interest for accelerator design optimisation.

Knob	Physics effect	Comment
Laser spot size on cathode	Invariant envelope matching	Iris set according to simulated optimum
Transverse laser profile	Emittance x - y symmetry	Tuned to maximum homogeneity and symmetry
Longitudinal laser profile	Collective effects in the gun	Tuned to flat top (lower emittance)
Laser alignment	Orbit, dispersion	Standard beam-based alignment
Gun phase	Minimization of energy spread	Minimization of horizontal beam size in spectrometer
Gun gradient	Invariant envelope matching	Set to design energy using spectrometer (7.1 MeV)
Gun solenoid alignment	Orbit, dispersion	Standard beam-based alignment
Gun solenoid field	Invariant envelope matching	Emittance-based optimization
Corrector quads	x / y coupling	Empirical and systematic tuning
S-band solenoid fields	Invariant envelope matching, x - y coupling	Empirical and systematic tuning
Orbit in S-band booster	Wake- and off-axis RF fields	Emittance-driven beam-based alignment
Orbit after S-band booster	Dispersion at screen	Beam-based alignment and local orbit bump

TABLE 7.1

A summary of “knobs” used for emittance minimization.[7.5]

For linear accelerators, some common algorithms are gradient descent algorithms [7.4], stochastic algorithms, the simplex algorithm, neural networks and genetic algorithms. Although in this thesis, a genetic algorithm is used, a report of some other optimisation publications on similar cases will be cited. In [7.3], the use of an optimiser based on the Simplex algorithm is reported used for optimising the Swiss FEL. The Simplex is a linear programming algorithm used for optimising a definite quantity- a Figure of Merit (FOM). In [7.3] the FOM is a linear combination of the mismatch parameter and the emittance at the end of the injector and the reported emittance minimization is 60%.

In [7.5] is recently reported a Bayesian optimiser for the LCLS FEL. Bayesian optimisation is a sequential stochastic design strategy for global optimisation of black-box functions that doesn't require derivatives. [7.6] In [7.7], a neural network inspired by artificial intelligence techniques in video games is proposed for FEL optimisation. High demands from FELs' performance have lead researchers to turn to advanced algorithms and techniques.

The algorithm used for this thesis is a genetic Algorithm.

7.2 Genetic Algorithms

A Genetic Algorithm is an algorithm inspired by biological evolution, thus otherwise named as evolutionary computation. Such algorithms are usually used for optimisation in a wide variety of problems.

In the following terminology the terms have a usage similar to their meaning in biology. A genetic algorithm operates with the following components:

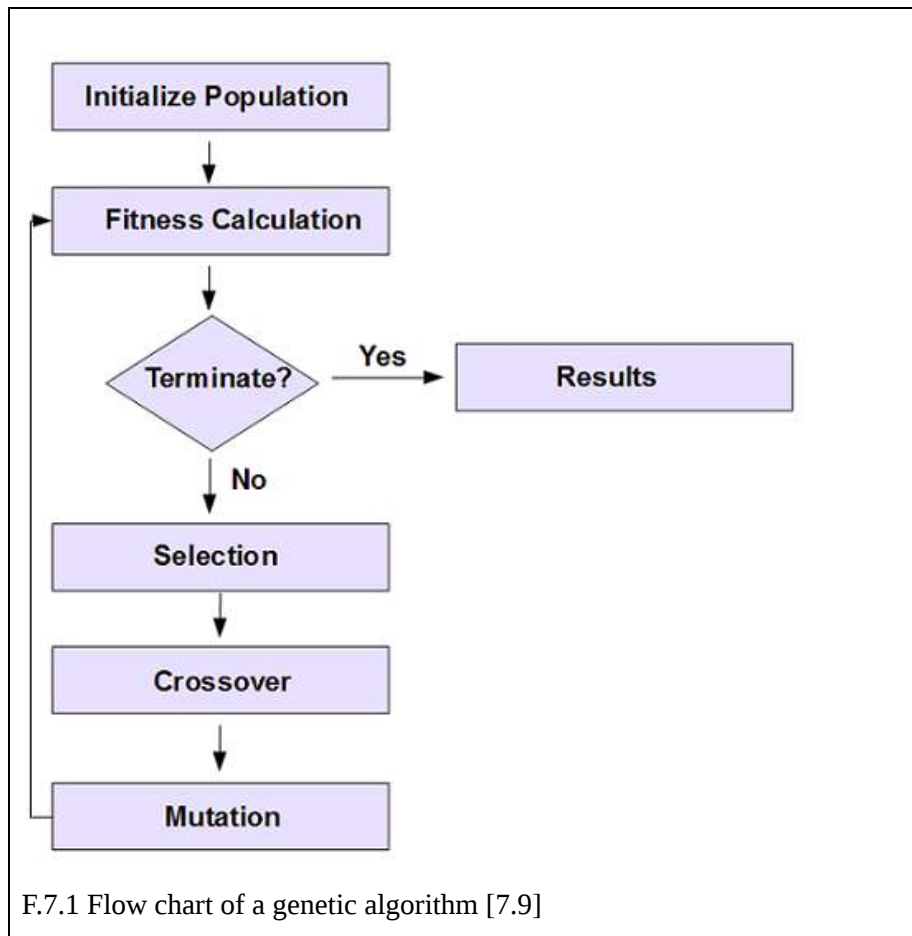
- Genes: Either a bit of information or a block of bits (such as a whole variable) can be called genes. Information from the problem variables are organized into genes. The way they are defined depends on the design
- Chromosomes: A chromosome is a collection of genes organized in a specific order. The chromosome represents a possible set of variables for the problem.
- Individual: Each chromosome corresponds to an individual. An individual is a possible solution to the problem
- Population: All the individuals that exist in a specific point in time are called a population. It is a set of possible solutions
- Fitness Function: It is the function to optimise. The biological analog is the environment on which the individuals need to survive and the population needs to adjust to.

The process of a genetic algorithm consists of the following steps:

Given a clearly defined problem to be solved and a bit string representation for candidate solutions, a simple Genetic Algorithm (GA) works as follows:

1. Start with a randomly generated population of n l -bit chromosomes (candidate solutions to a problem).
2. Calculate the fitness $f(x)$ of each chromosome x in the population.
3. Repeat the following steps until n offspring have been created:
 - a. Select a pair of parent chromosomes from the current population, the probability of selection being an increasing function of fitness. Selection is done "with replacement," meaning that the same chromosome can be selected more than once to become a parent.
 - b. With probability p_c (the "crossover probability" or "crossover rate"), cross over the pair at a randomly chosen point (chosen with uniform probability) to form two offspring. The point can be either in the binary representation of the information (Binary-coded GA) or in the real representation of the numbers (Real-coded GA). If no crossover takes place, form two offspring that are exact copies of their respective parents. (Note that here the crossover rate is defined to be the probability that two parents will crossover in a single point. There are also "multi-point crossover" versions of the GA in which the crossover rate for a pair of parents is the number of points at which a crossover takes place.)
 - c. Mutate the two offspring at each locus with probability p_m (the mutation probability or mutation rate), and place the resulting chromosomes in the new population. If n is odd, one new population member can be discarded at random.
4. Replace the current population with the new population.
5. Go to step 2.

Each iteration of this process is called a Generation. [7.8]



7.3 GIOTTO Algorithm for ASTRA

GIOTTO is a Real-coded genetic code for demanding beam dynamics optimisations designed to run with the ASTRA Space Charge Tracking Algorithm. GIOTTO was designed by A. Bacci, INFN/Milan, Italy. The development was done in modern Fortran. It takes advantage of ASTRA's output files user interface to process data. Also, it can be run in parallel using the MPI library.

The algorithm gets input from a configuration file, where all the necessary parameters are defined. These parameters can be classified as the problem's parameters, the algorithm's parameters and the file inputs, as well as a fitness function. The Astra and Generator program files and respected input files have to be provided. The problem parameters include the parameters that the user aims to optimise. Their permitted range depends on the user. The algorithm parameters include the number of generations, the number of genes of each chromosome, the population size and the parameters that will be presented below and are characterized as user-defined.

The population:

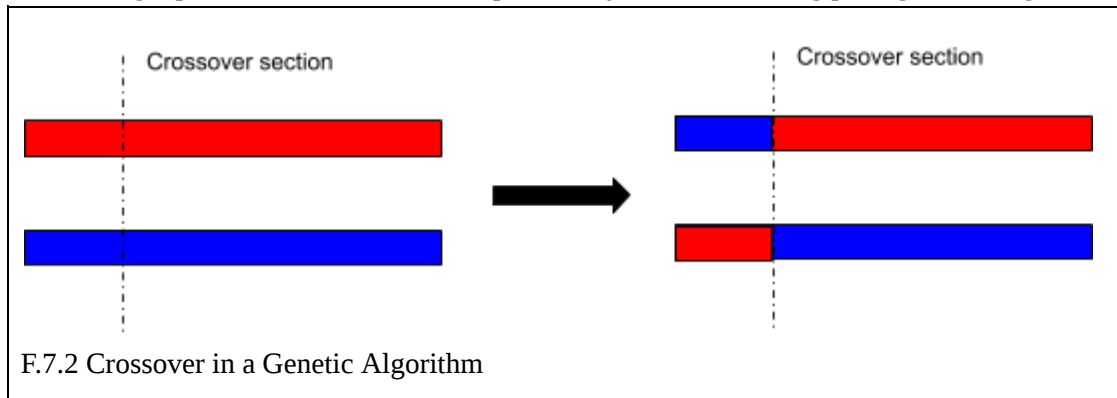
As rule of thumb the number of individuals each generation should have should be near the value $(\text{number of genes})^2$. The intuition behind the rule, is that there must be a good chance in all generations that most of the genes will be selected as a crossover point (see Crossover below)

Selection:

In the selection step, the parents are chosen based on roulette-wheel rule. Each individual, has a probability to be chosen proportional to their fitness function.

Crossover:

The algorithm uses a single point crossover operator, meaning that the chromosomes of the parents are cut in a single point chosen with uniform probability and the occurring parts get rearranged.



Mutation:

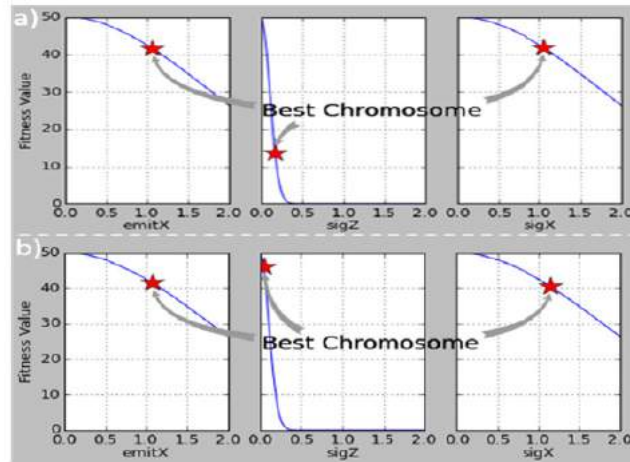
The mutation operator causes mutation on at most one allele (gene) per chromosome with a small mutation probability. The probability depends on the variation of the population, it rises for uniform populations.

Regeneration:

The regeneration is not a mandatory step in a genetic algorithm but with careful handling can lead to faster an optimal results. After a certain number of steps that is user-defined, the population is regenerated around the best yet chromosome with a user-defined variation range. This process is implemented by the regeneration operator. The best chromosome is also maintained (elitism operator). The usefulness of regeneration lies on the acceleration it provides to convergence of the algorithm. After a user-defined number of regenerations the range of variation is reopened in order to avoid entrapment in local minima.

Fitness Function:

The Fitness Function is a function that the algorithm tries to maximize or minimize. GIOTTO is a single criterion optimisation algorithm that can implement multiobjective optimisation, meaning that the fitness function can contain more than one figures of merit (eg. emittance, transverse size etc.). The function is user defined in Reverse Polish Notation and has no restrictions on its form. The recommended strategy from the creator of the code is to define the fitness function as a sum of Gaussian or Lorentzian curves centred in the goal values. GIOTTO tries to maximize the function so it performs optimisation with respect to all parameters. A Gaussian curve is steeper and almost vanishes the probability of survival for a chromosome with performance away from the target. On the other hand a Lorentzian curve is smoother and allows some not optimal chromosomes to survive, giving the population a greater variety. For lattices that already are close to optimum both fitness functions can operate effectively. In unoptimized lattice a Gaussian fitness function is unlikely to perform an effective simulation.



F.7.3 Graphical representation of the fitness function equation pieces. a) Offspring not yet optimised, b) offspring satisfying the optimisation [7.1]

7.3.1 Running GIOTTO

In order to perform an optimisation, GIOTTO requires the Astra and Generator executables, the respective input files that describe a lattice that can operate, a configuration file and the necessary electric and magnetic field files. The configuration file contains 7 sections, out of which three were used. The first concerns the parameters of the algorithm :

- Astra executable
- Astra input file
- Generator exe
- Generator input file
- Number of genes : is equal to the numbers of the parameters to be optimised
- Number of individuals : the number of instances, it has to be a multiple of the CPU cores used.
- Number of generations used
- Number of CPUs : the number of CPUs the program can use for parallel running of the Astra instances can be either the system number of CPUs or less
- Fitness function : the fitness function is a Gaussian or Lorentzian function of the figures of merit (for the simulations was the transverse emittance, size and the longitudinal size)

The second part concerns the definition of the fitness function. The definition must be in Reverse Polish notation and uses values from the output files of Astra. In the simulations, the parameters used were the transverse emittance in x-axis, emitX, the transverse size in x-axis, sigX and the longitudinal size, sigZ.

The third part contains all the lattice and beam generation parameters that need to be examined. The information that needs to be provided is the name of the variable and the range in which the algorithm can change the initial value in every new generation. The suggested thing to do for faster convergence of the algorithm is to manually find a good setup and not let the parameters to diverge a lot. Of course, if the lattice cannot be pre-optimised one can perform a not refined optimisation to get to an optimal point and then perform another one closer to a good solution. On the other hand this is exactly what the regeneration process does.

7.4 References

- [7.1] Bacci, et al. “GIOTTO: A Genetic Code for Demanding Beam-Dynamics optimisations.” *DOI*, JACOW, Geneva, Switzerland, 1 June 2016, doi.org/10.18429/JACoW-IPAC2016-WEPOY039.
- [7.2] Negnevitsky, Michael. *Artificial Intelligence: a Guide to Intelligent Systems*. Addison-Wesley, 2008. (Chapter 7)
- [7.3] Bettoni, S., et al. “Low Emittance Injector Design for Free Electron Lasers.” *Physical Review Special Topics - Accelerators and Beams*, vol. 18, no. 12, 2015, doi:10.1103/physrevstab.18.123403.
- [7.4] Prat, Eduard, et al. “Measurements of Cu and Cesium Telluride Cathodes in a Radio-Frequency Photoinjector.” *Physical Review Accelerators and Beams*, American Physical Society, 9 Apr. 2015, dx.doi.org/10.1103/PhysRevSTAB.18.043401.
- [7.5] Duris, et al. “Bayesian optimisation of a Free-Electron Laser.” *ArXiv.org*, 12 Sept. 2019, arxiv.org/abs/1909.05963.
- [7.6] https://en.wikipedia.org/wiki/Bayesian_optimisation
- [7.7] Meier, E., et al. “Development of a Novel optimisation Tool for Electron Linacs Inspired by Artificial Intelligence Techniques in Video Games.” *Nuclear Instruments and Methods in Physics Research Section A: Accelerators, Spectrometers, Detectors and Associated Equipment*, vol. 632, no. 1, 2011, pp. 1–6., doi:10.1016/j.nima.2010.12.203.
- [7.8] Mitchell, Melanie. *An Introduction to Genetic Algorithms*. MIT, 1998.
- [7.9] <https://apacheignite.readme.io/docs/genetic-algorithms>

8. Laser and Material Parameters Choice

8.1 Material Parameters

For the simulations below, two different photocathode materials are examined, Cu and Cs₂Te, the most common semiconductor used for photoemission. Cu is a very common metal used in photocathodes it has low cost and is also durable, while a great interest is shown on Cs₂Te in the recent years. Cs₂Te has a very high QE, which means that high charges are produced with small laser pulse energy. Also, the emission delay it has is appealing because it smoothes out any spikes and anomalies a laser pulse may have [8.1].

It is important to keep in mind that any theoretical values used in the simulations below might differ in any experiment.

The beam charge is arbitrarily set to 75pC. The electrical field on cathode is in all guns 100 MV/m. For the delay see Appendix B , the distribution is assumed to be isotropic as the most common choice in bibliography. The QE is an approximate reference value and it was used to calculate the necessary laser pulse energy. It is important to underline here that Cs₂Te has 1000 times greater QE than Cu. Also, the laser spot size/radius(rms) was an arbitrary feasible choice (see space charge limit in Table 8.1) and later it will be optimised. The work function was found in [8.1] , it is a reference value in both cases which might differ in experiments.

All the energies and emittances are calculated by the relevant relations presented in Appendix B.

8.1.1 Space Charge Limit and Minimum Radius

For the choice of the radius is restricted by the saturation level. As presented in Appendix A :

$$\sigma_{SCL} = \epsilon_0 E_0 \sin(\phi_0)$$

assuming a radial transverse profile:

$$r_{min} = \sqrt{\frac{q}{\pi \cdot \sigma_{scl}}}$$

where:

$$\epsilon_0 = 8.8541878128(13) \times 10^{-12} \text{ F} \cdot \text{m}^{-1}$$

For a range of 100 MV/m to 50 MV/m and for charges 10pC , 75pC, 100pC and 200pC the minimum laser spot size is computed in Table 8.1.

TABLE 8.1				
10pC		75pC	100pC	200pC
Field on cathode $E_0 \sin(\varphi_0)$ (MV/m)	r_{\min} (mm)	r_{\min} (mm)	r_{\min} (mm)	r_{\min} (mm)
50	0.085	0.23	0.27	0.38
60	0.078	0.21	0.25	0.35
70	0.072	0.19	0.23	0.32
80	0.067	0.18	0.21	0.25
90	0.064	0.17	0.20	0.29
100	0.060	0.16	0.19	0.27

8.1.1 Cu Photocathode

For the Cu photocathode there are two options for the choice of the kinetic energy. The first one is to use the literature reference values of the work function, which is 4.65 eV according to [8.2]. But, the experimental values are very variant and depend on many variables, such as the surface roughness, the material cleanliness, etc. In [8.3] such measurements demonstrate these differences.

The second one is to use the experimental reference values. For the SwissFEL community, the reference value for the average kinetic energy for a beam produced by a laser pulse of 4.9 eV photon energy ($\lambda = 253$ nm) with 115 MV/m electric field on cathode is 0.63 eV. This value was measured in LCLS [8.6], corresponds to 0.91 pi mm mrad/mm intrinsic emittance and is used for simulations in guns with gradient from 100 to 120 MV/m.

For the simulations the theoretical and experimental values are listed in Table 8.2A.

The measured reference value of $E_{\text{phot}} - \Phi_{\text{eff}} = 0.63$ eV, corresponds to the last set of values in the Table 8.2A. and is almost three times higher than the anticipated one.

In the simulations the abbreviations Cu[A/B/C/D] are used for reference to each case.

TABLE 8.2A								
A. Literature reference work function 4.65 eV / laser 4.90 eV								
E_{cathode} (MV/m)	Φ_{Schottky} (eV)	$\lambda / E_{\text{phot}}$ (nm/ eV)	Φ_{eff} (eV)	Φ_{exc} (eV)	E_{kin} (eV)	ϵ_{th} (pi mm mrad/m m) no Schottk y	ϵ_{th} (pi mm mrad/m m) with Schottk y	$\epsilon_{x,y}$ for laser rms radius 0.2mm (pi mm mrad)
100	0.379	253/ 4.90	4.271	0.629	0.314	0.40	0.64	0.12
B. Literature reference work function 4.65 eV / laser 4.73 eV								
E_{cathode} (MV/m)	Φ_{Schottky} (eV)	$\lambda / E_{\text{phot}}$ (nm/ eV)	Φ_{eff} (eV)	Φ_{exc} (eV)	E_{kin} (eV)	ϵ_{th} (pi mm mrad/m m) no Schottk y	ϵ_{th} (pi mm mrad/m m) with Schottk y	$\epsilon_{x,y}$ for laser rms radius 0.2mm (pi mm mrad)
100	0.379	262/ 4.73	4.271	0.459	0.23	0.23	0.55	0.11
C. [8.6] effective work function 4.52eV / laser 4.90 eV								
E_{cathode} (MV/m)	Φ_{Schottky} (eV)	$\lambda / E_{\text{phot}}$ (nm/ eV)	Φ_{eff} (eV)	Φ_{exc} (eV)	E_{kin} (eV)	ϵ_{th} (pi mm mrad/m m) no Schottk y	ϵ_{th} (pi mm mrad/m m) with Schottk y	$\epsilon_{x,y}$ for laser rms radius 0.2mm (pi mm mrad)
115	0.406	253/ 4.90	4.52	0.38	0.19	-	0.50	0.10
D. [8.6] Experimental reference values work function 4.52eV /laser 4.90 eV								
$E_{\text{kin}} = \frac{E_{\text{photon}} - \Phi_{\text{eff}}}{2}$ (eV)						ϵ_{th} (pi mm mrad/mm) no Schottky		
0.63						0.91		

8.1.1 Cs₂Te Photocathode

For Cs₂Te the same holds. Either the theoretical reference values or the experimental ones as presented in [8.1] or Appendix B can be used. The values for the two cases are listed in Table 8.2B.

TABLE 8.2B									
A. Theoretical values work function 3.5 eV/ laser 4.73 eV									
Φ_w (eV)	E_{cathode} (MV/m)	Φ_{Schottky} (eV)	$\lambda / E_{\text{phot}}$ (nm/eV)	Φ_{eff} (eV)	Φ_{exc} (eV)	E_{kin} (eV)	ϵ_{th} (pi mm mrad/mm) no Schottky	ϵ_{th} (pi mm mrad/mm) with Schottky	$\epsilon_{x,y}$ for laser rms radius 0.2mm (pi mm mrad)
3.5	100	0.379	262/ 4.73	3.121	1.61	1.61	0.90	1.02	0.20
B. Experimental values [8.1] work function 3.5 eV/ laser 4.73 eV									
$E_{\text{kin}} = E_{\text{photon}} - \Phi_{\text{eff}}$ (eV)						ϵ_{th} (pi mm mrad/mm) no Schottky			
2.2						1.2			

8.2 Cu vs Cs₂Te

There are several pros and cons on choosing either of the two materials. To begin with, semiconductors have several orders of magnitude higher QE, specifically Cs₂Te has 1000 times higher QE than Cu. This, gives the opportunity to use lower laser energy for higher charge production. Also, semiconductors have non negligible emission delay. This has consequences to the shape of the beam thus space charge forces. But, the delay can smooth out the non uniformities in transverse laser profile (see Appendix B4 and [8.1]). Both materials need laser wavelength in the UV range, although semiconductors may also emit in the visible range. The ones examined, emit in non excluded ranges, so they can be used with same lasers, for instance 4.73 eV photon energy / 262 nm wavelength.

As for the cost, the metallic photocathodes are generally cheaper and have a longer life expectancy. Specifically, Cu photocathodes may last several years of operation, while semiconductors last from several hours to several months. The reason for this is that the semiconductors are vulnerable to contamination and require very high vacuum, in contrast with the more tolerant metals. Cs₂Te is the least sensitive to contaminants and can last up to 4 months which makes it more attractive as a choice. Consequently, semiconducting photocathodes are high maintenance.

What is more, the two materials show similar behaviour and comparable emittances, as reported in [8.3]. In this report, it is also observed that transverse emittance of the same photocathode material can vary under the same conditions in different measurements $\pm 0.4 \text{ mm mrad/mm}$ with statistical error of the difference $\pm 0.4 \text{ mm mrad/mm}$.

8.3 Laser Parameters

For the laser the SwissFEL UV Ti:Sapphire laser system parameters were used.

Laser specifications	
Maximum pulse energy on cathode	60 μ J
Central wavelength	250–300 nm
Bandwidth (FWHM)	1–2 nm
Pulse repetition rate	100 Hz
Double-pulse operation	yes
Delay between double pulses	50 ns
Laser spot size on cathode (rms) (10 pC / 200 pC)	0.1 / 0.27 mm
Minimum pulse rise-time	<0.7 ps
Pulse duration (FWHM)	3–10 ps
Longitudinal intensity profile	various
Transverse intensity profile	Uniform
Laser-to-RF phase jitter on cathode (rms)	<100 fs
UV pulse energy fluctuation	<0.5% rms
Pointing stability on cathode (relative to laser diameter)	<1% ptp

TABLE.8.3 Gun laser characteristics for SwissFEL.

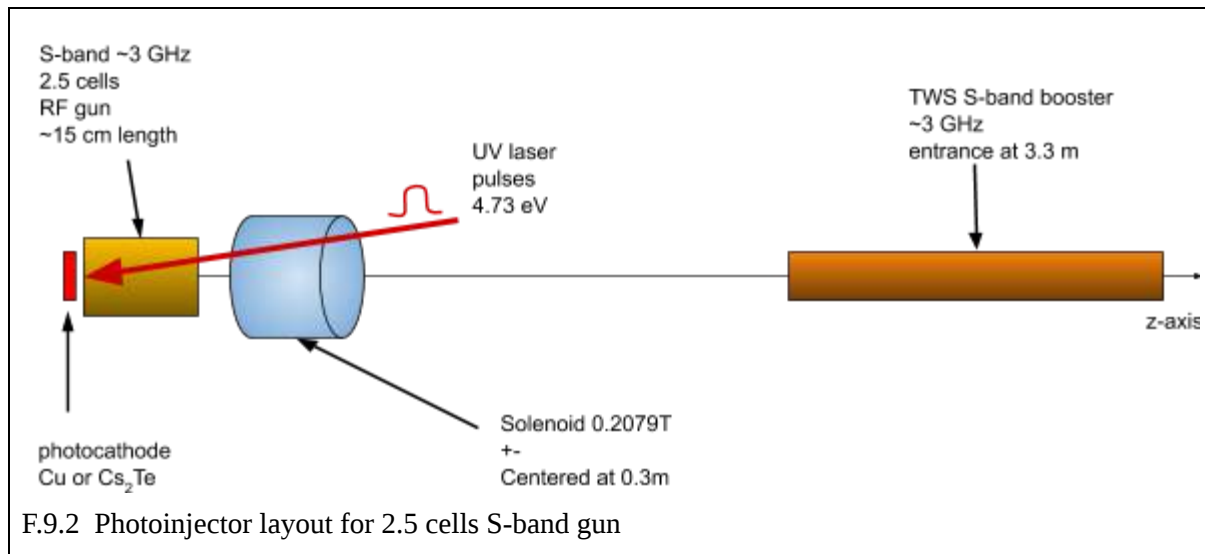
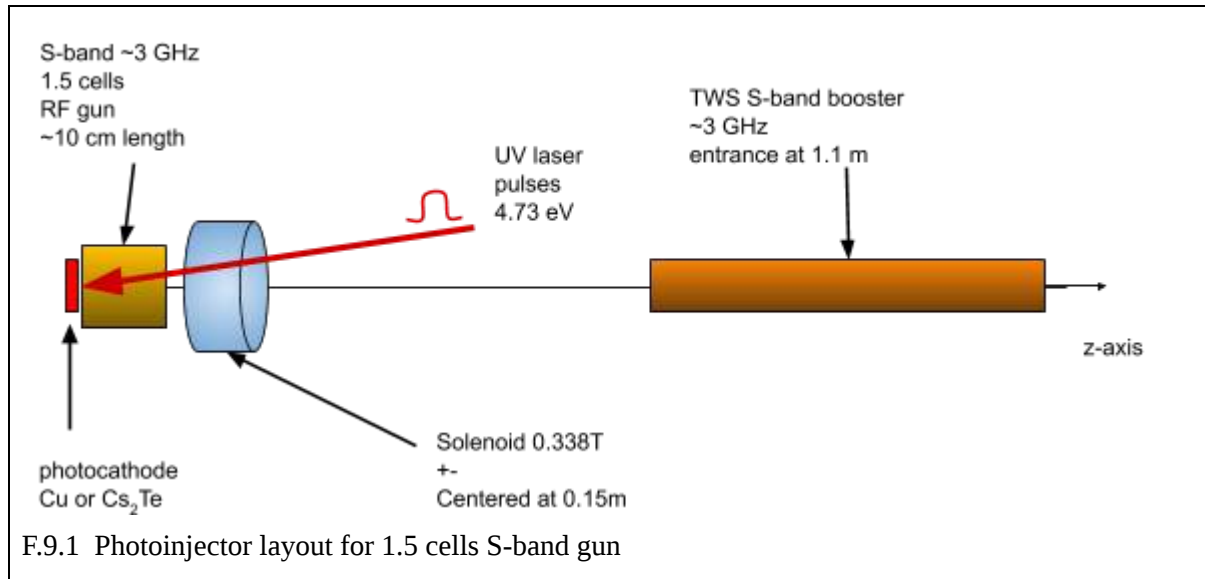
The longitudinal profile is a Flattop as presented in Appendix B. As reported in [8.7], three different sets of crystals in the laser system provide the three pulse durations of 3.6, 6.7 and 10 ps for electron bunch production. So, in the simulations the possible choices are out of these values.

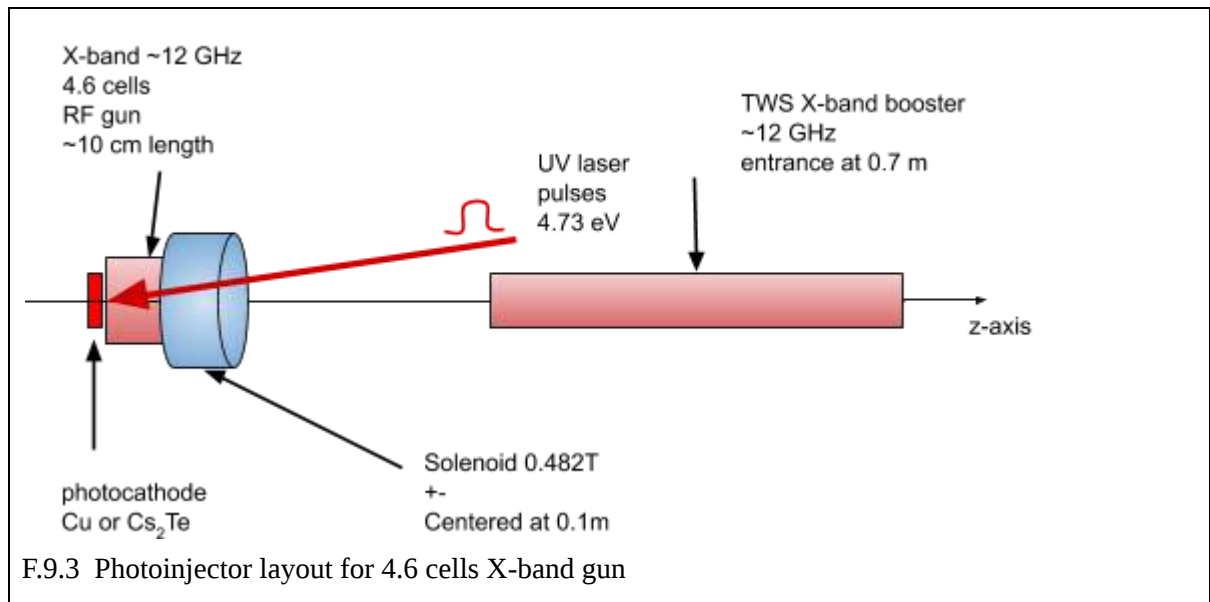
8.3 References

- [8.1] Rao, Triveni, and David H. Dowell. *An Engineering Guide to Photoinjectors*. CreateSpace Independent Publishing, 2013.
- [8.2] Schaer, and Mattia. "RF Traveling-Wave Electron Gun for High Brightness Photoinjectors." *RF Traveling-Wave Electron Gun for High Brightness Photoinjectors - Research Collection*, ETH Zürich, 1 Jan. 1970, doi.org/10.3929/ethz-a-010749949.
- [8.3] Prat, Eduard, et al. "Measurements of Cu and Cesium Telluride Cathodes in a Radio-Frequency Photoinjector." *Physical Review Accelerators and Beams*, American Physical Society, 9 Apr. 2015, dx.doi.org/10.1103/PhysRevSTAB.18.043401.
- [8.4] Jensen, Kevin L., et al. "Delayed Photo-Emission Model for Beam Optics Codes." *Journal of Vacuum Science & Technology B, Nanotechnology and Microelectronics: Materials, Processing, Measurement, and Phenomena*, vol. 35, no. 2, 2017, doi:10.1116/1.4968511.
- [8.5] Spicer, William E., and Alberto Herrera-Gomez. "Modern Theory and Applications of Photocathodes." *Photodetectors and Power Meters*, 1993, doi:10.1117/12.158575.
- [8.6] Ding, Y., et al. "Measurements and Simulations of Ultralow Emittance and Ultrashort Electron Beams in the Linac Coherent Light Source." *Physical Review Letters*, vol. 102, no. 25, 2009, doi:10.1103/physrevlett.102.254801.
- [8.7] Milne, Christopher, et al. "SwissFEL: The Swiss X-Ray Free Electron Laser." *Applied Sciences*, vol. 7, no. 7, 2017, p. 720., doi:10.3390/app7070720.

9. ASTRA Simulations

In F.9.1 - F.9.3 the benchmark layouts of the simulated photoinjectors are presented. The parameters change in the optimisation process and the changes are stated when necessary.

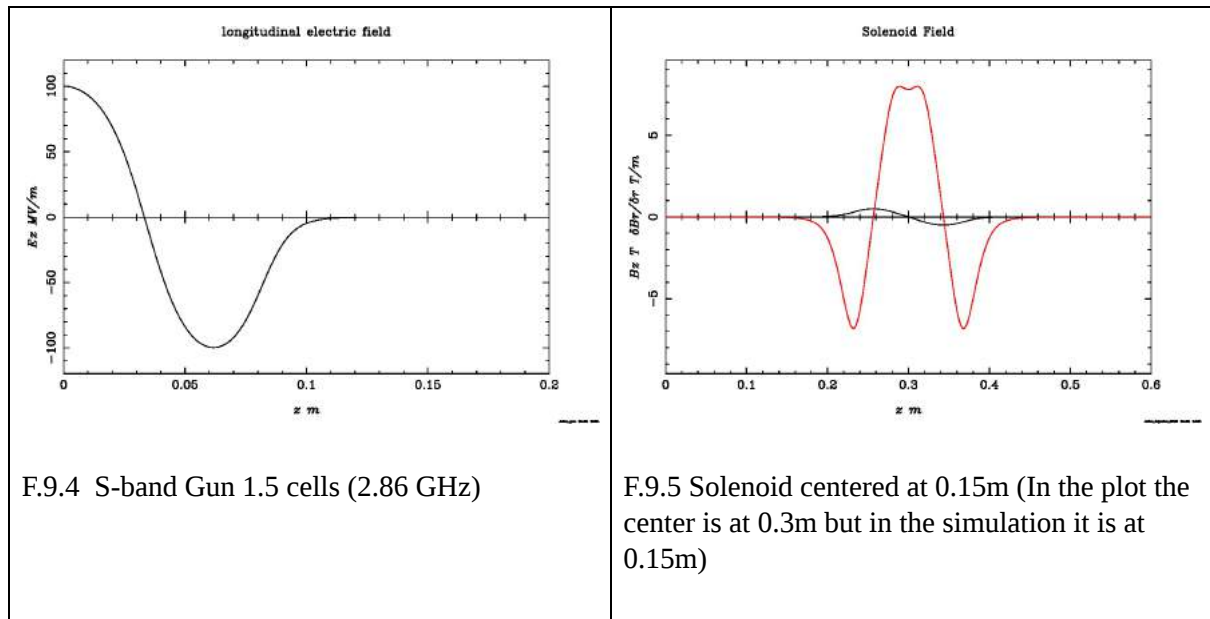


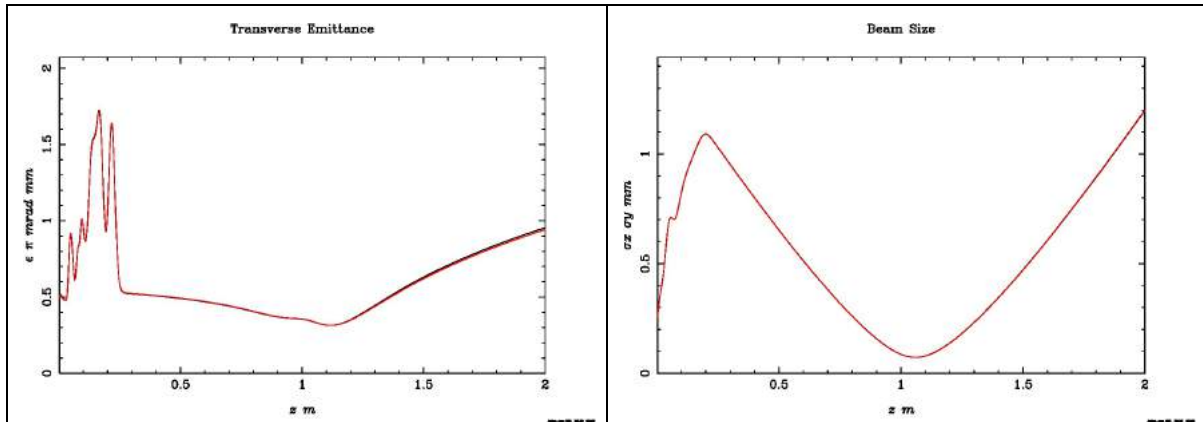


9.1 Space charge field simulation

Below, the beam of Cs₂Te A is simulated through a gun of 1.5 cells and gradient 100 MV/m and a solenoid of peak field 0.338T (F.9.1). The laser pulse duration is 6.7 psec and the charge is 100 pC. This layout is a proposed gun for the XLS Collaboration.

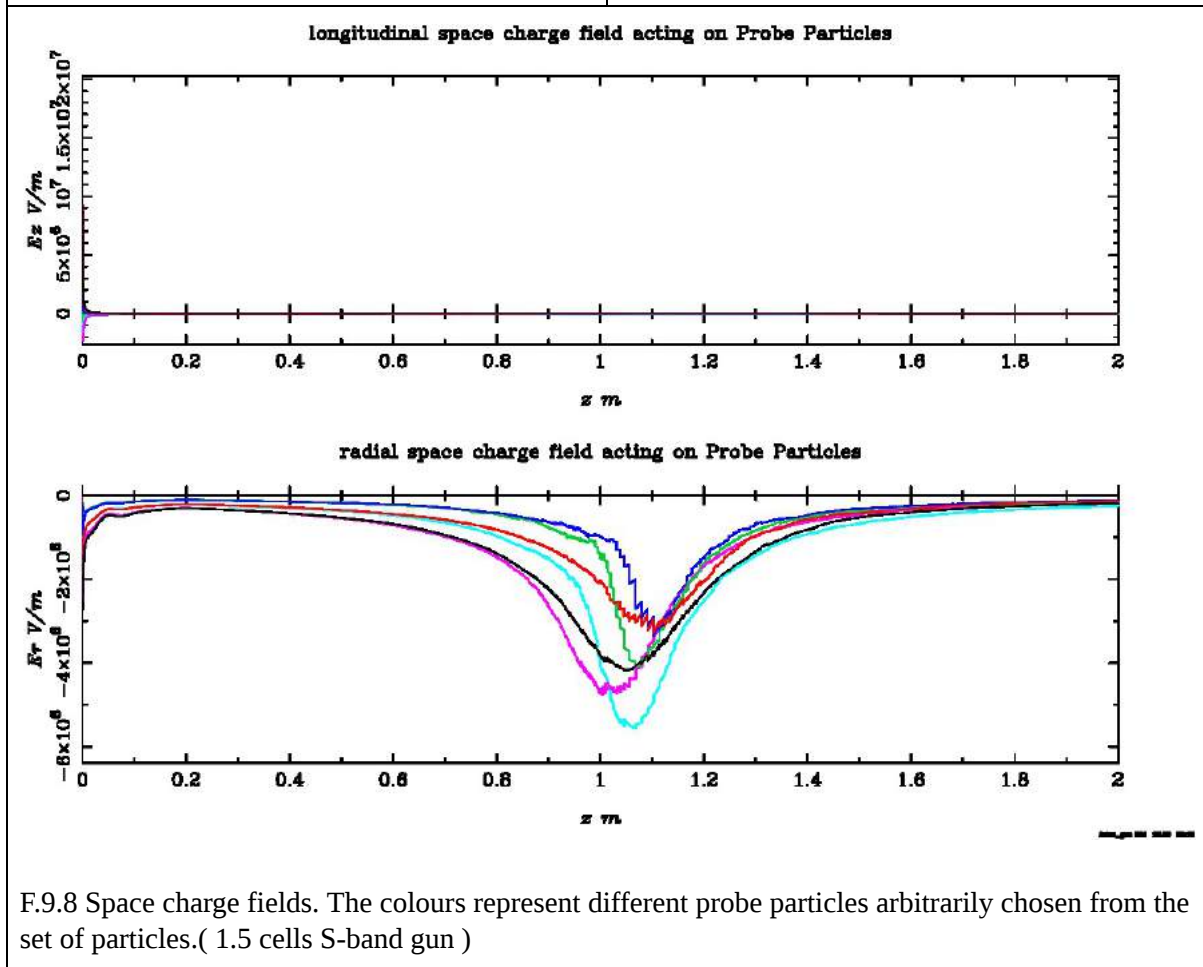
The respective fields on z-axis are show in F.9.4 and F.9.5.





F.9.6 Transverse Emittance evolution

F.9.7 Transverse beam size evolution



F.9.8 Space charge fields. The colours represent different probe particles arbitrarily chosen from the set of particles.(1.5 cells S-band gun)

The beam waist in this lattice is at $z=1.06\text{m}$ where the emittance locally maximizes, making this position the entrance of the booster - TWS (Travelling Wave Structure). At the beam waist the transverse space charge fields maximize as expected by (A.42), where R is minimum. The longitudinal component of the space charge field is only significant close to the cathode, where the beam has almost no length. The final value of the transverse size is close to 0.6mm and is formed at the beginning of the acceleration. As mentioned, the reason is that the beam becomes quickly relativistic so the longitudinal component is insignificant. (see Chapter A.3)

9.2 Emittance evolution inside the gun

Another phenomenon worth pointing out is the ‘spikes’ in emittance inside the gun. This phenomenon is observed in all guns simulated in following Chapters. Examples of all guns used in the thesis are presented in Table 9.1

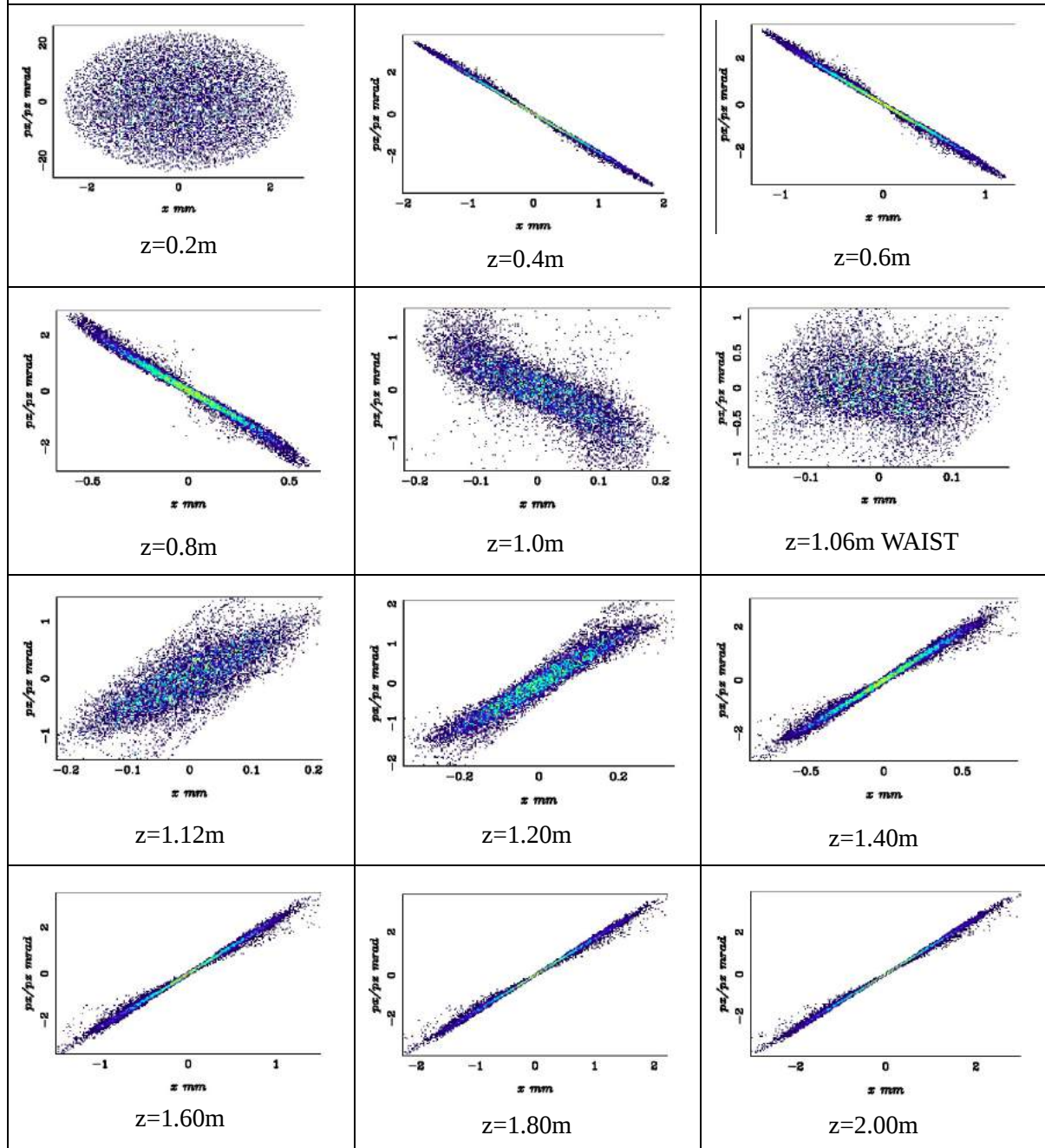
TABLE 9.1 : Emittance near the gun in 3 RF gun cases.		
<p>(I) 1.5 cells S-band gun Cu photocathode Solenoid F.9.5</p>	<p>(II) 2.5 cells S-band gun Cu photocathode Solenoid No3 of Chapter 10 Table 10.2</p>	<p>(III) 4.6 cells X-band gun Cu photocathode Solenoid Table 11.2</p>

In the first decimeters of the z-axis there are steep fluctuations in the emittance evolution. The reason this happens is that the beam is in the high accelerating field of the gun and the solenoid field is either absent (II) inside the gun or weak (I), (III). Later on, the accelerating field is absent and the emittance is more linear. In (II) there are two local maximums after the gun. These are formed because of the fringe fields of the solenoid.

9.2 Beam drift

In the same setup as above (F.9.1), the beam turns from convergent to divergent as presented in Appendix A (see F.A.6). The simulated beam ‘s transverse phase space is presented in various positions in the z-axis to show the evolution from convergent to divergent.

TABLE 9.2: Evolution of phase space through solenoid and drift space.
The beam turns from convergent to divergent in phase space (x, p_x) (see Appendix A)



At 0.20m the beam is inside the solenoid. Right after solenoid focusing at $z=0.40m$ a convergent beam is observed. As the beam gets closer to the waist, the phase space is less stretched and rounder. Away from the waist, the distribution is becoming more elliptical. It is obvious, as well, that the phase space has no ellipse-like shape near or at the waist. The main reason for this is the space charge forces that insert non-linear effects.

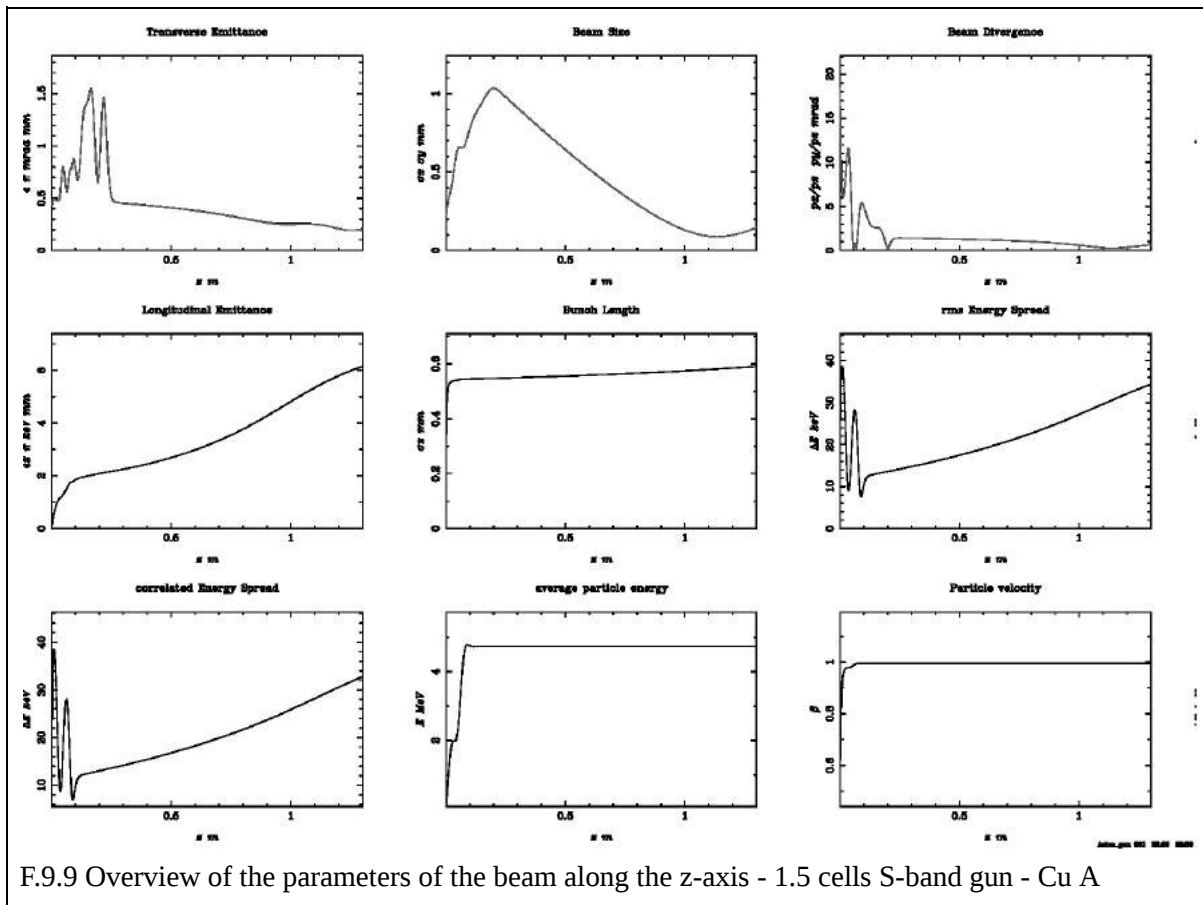
9.3 Beam Distributions and Comparison through Gun - Solenoid

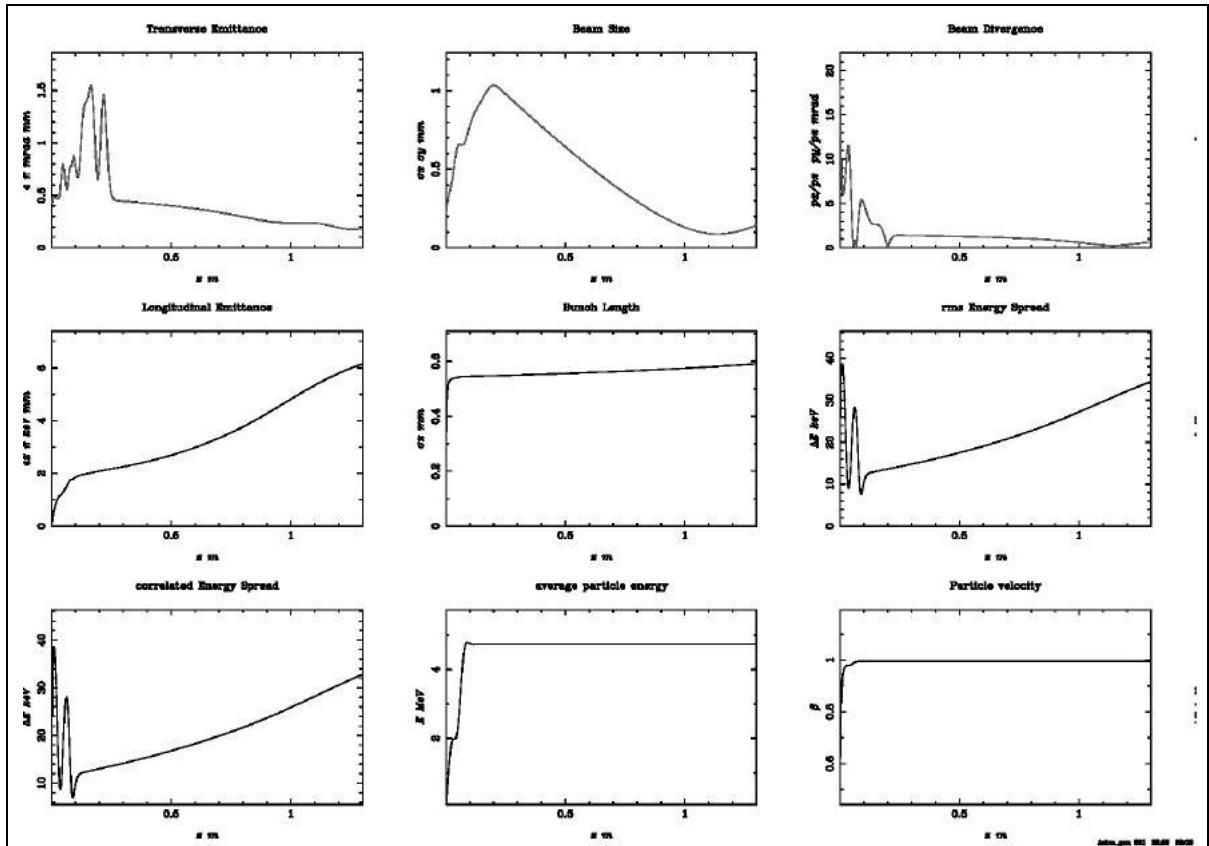
In this part of the simulations, a comparison of the performance of theoretical values of the kinetic energy of each beam presented in Chapter 8 with the experimental ones is presented. Cu A, C and D are compared to each other as well as Cs₂Te A and B. The laser pulse length in the S-band cases can take the values 6.7psec and in the X-band case 2.0psec. Although as already presented in [8.3] great differences are not expected in the RF S-band. In practice, the examination concerns the effect of changing the thermal emittance and the emission delay.

9.3.1 1.5 cells gun S-band

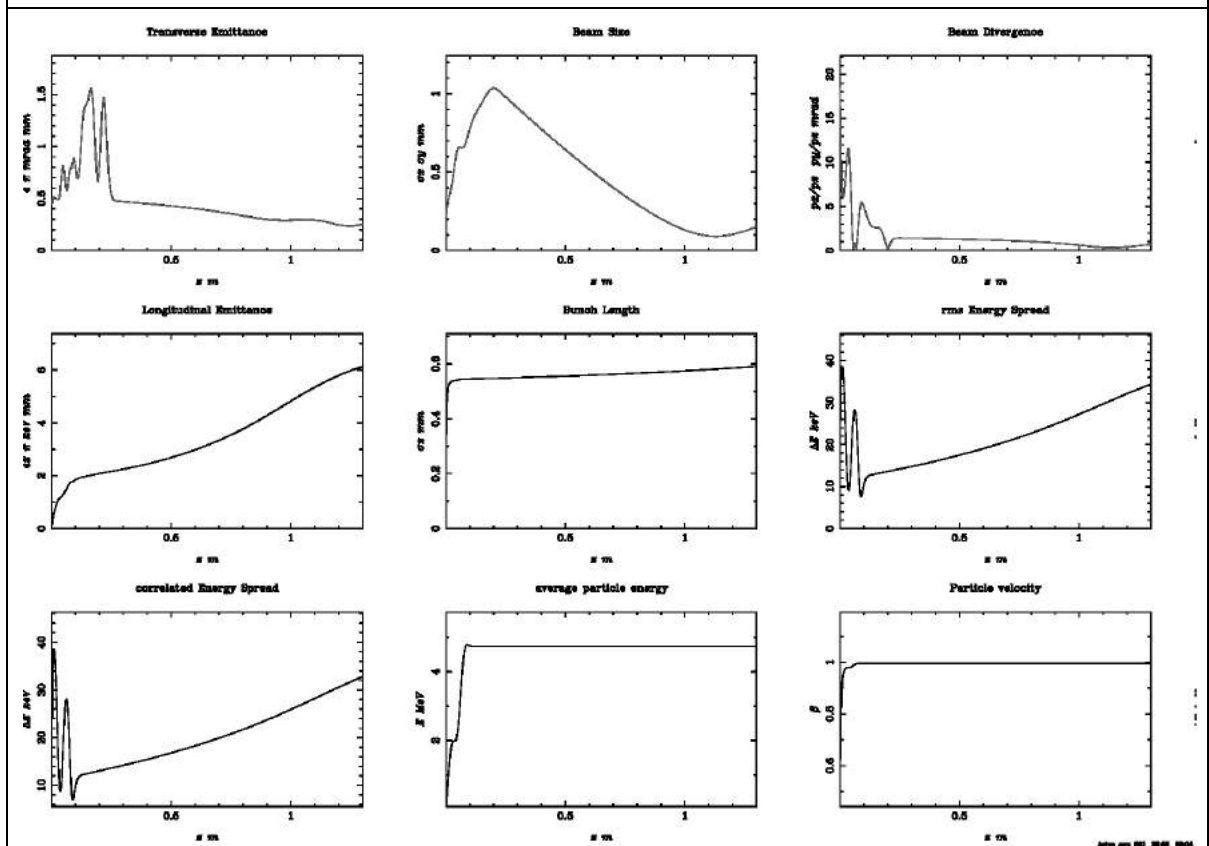
Cu

Below, the results obtained for Cu photocathodes in cases A, C and B are presented:



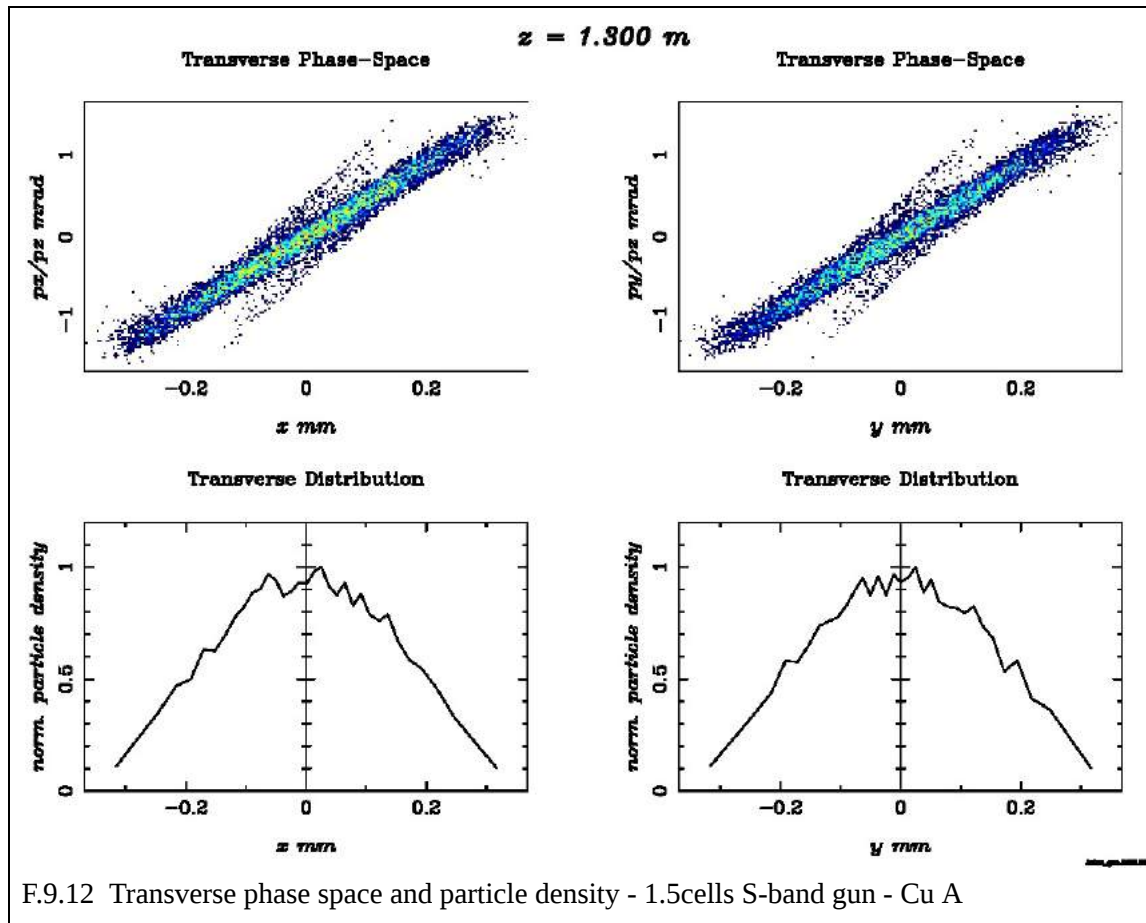


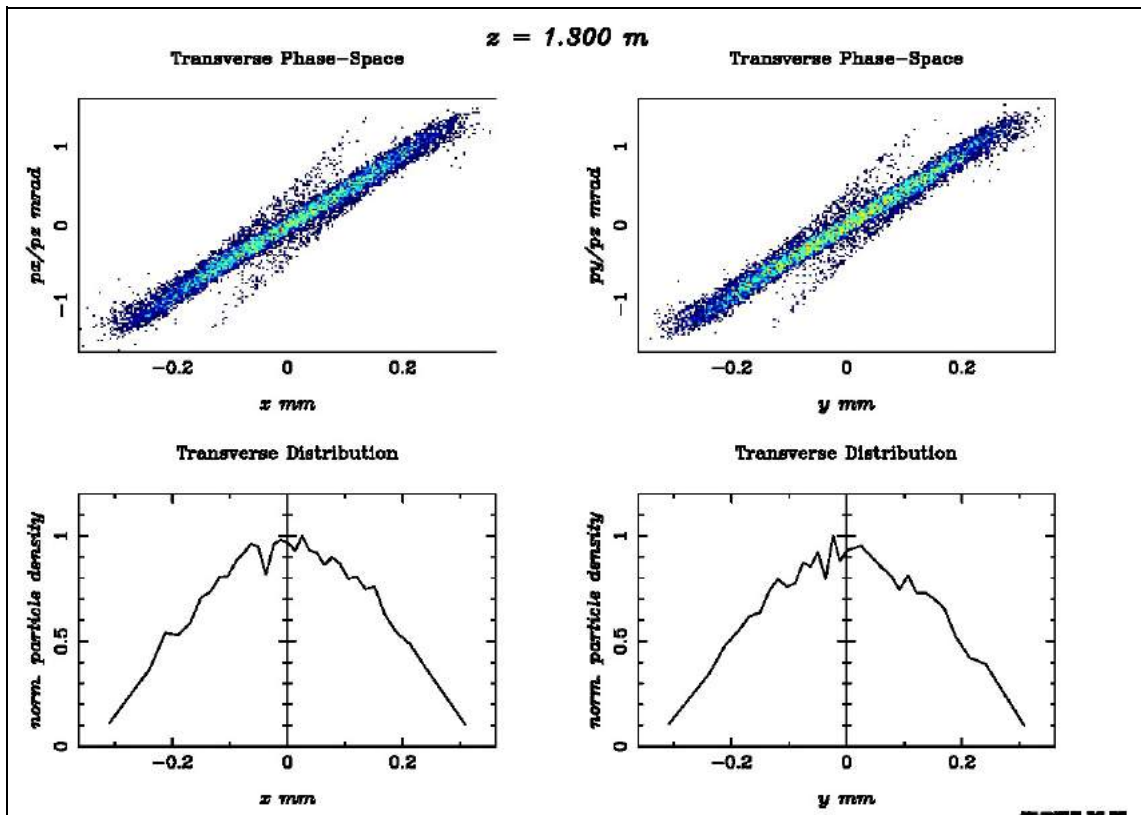
F.9.10 Overview of the parameters of the beam along the z-axis - 1.5 cells S-band gun - Cu C



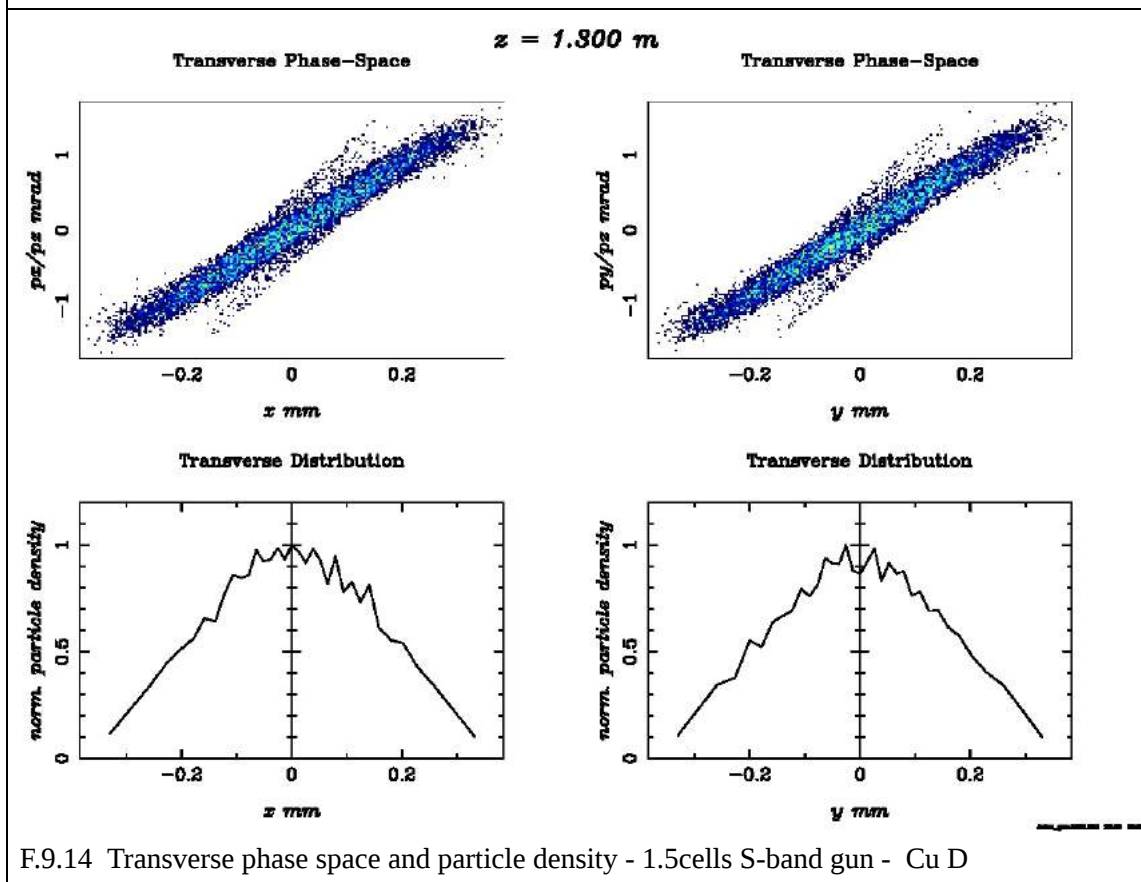
F.9.11 Overview of the parameters of the beam along the z-axis - 1.5 cells S-band gun - Cu D

The lattices are almost identical, proving what (A.38) indicates, that when the space charge forces are not significant the betatron function evolution is dependent on the lattice. Of course, there are space charge forces in all cases but the initial size is the same so the difference is not that significant.





F.9.13 Transverse phase space and particle density - 1.5cells S-band gun - Cu C



F.9.14 Transverse phase space and particle density - 1.5cells S-band gun - Cu D

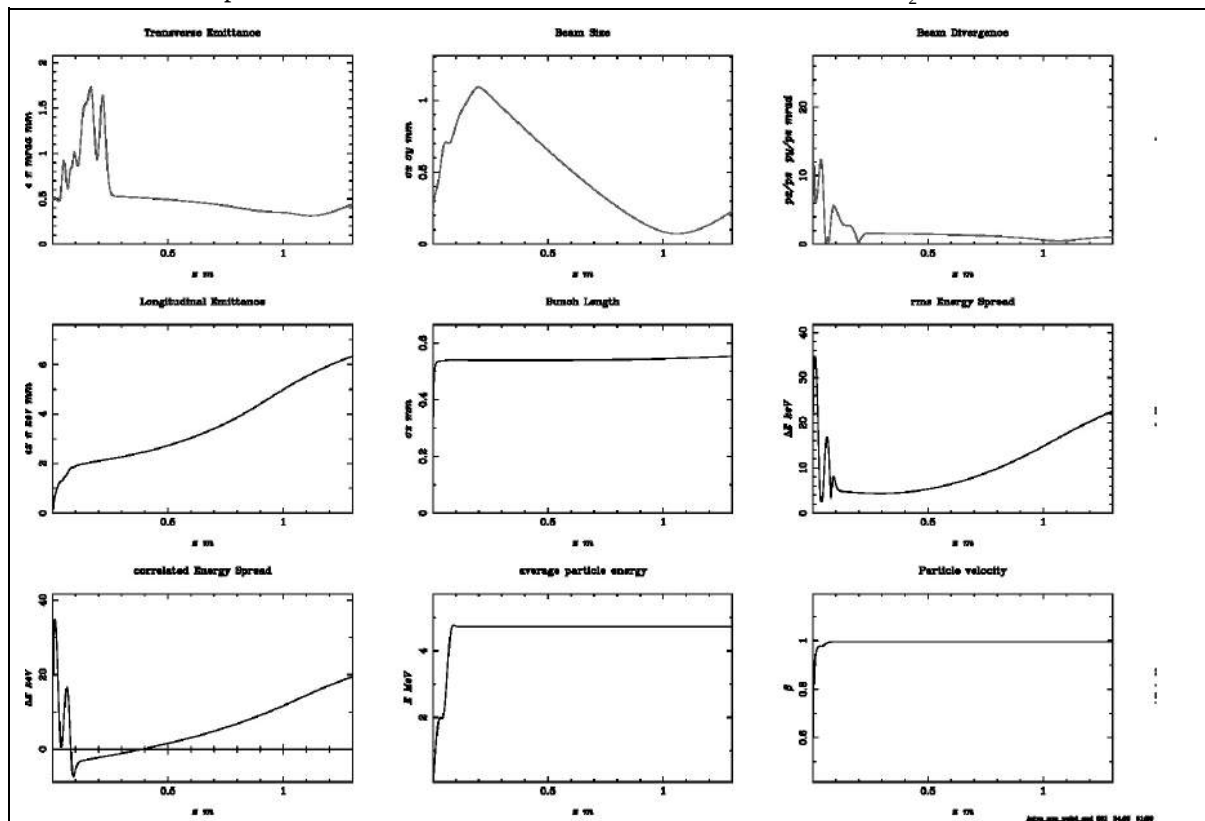
The morphology of the phase space is identical, due to the identical lattice, the only thing changed is the area which is obviously greater in the Cu D case because of the greater thermal emittance.

TABLE 9.3 Cu thermal emittance effects on RF gun performance on 1.5 cells S-band gun							
	Beam waist position (m)	Minimum trans. Size (mm) (waist)	Emittance on waist (pi mm mrad)	Minimum emittance (pi pi mm mrad)	Particle energy (MeV)	Brightness (nC/mrad mm ²)	Bunch Length (mm)
Cu A	1.134	0.089	0.24	0.19	4.726	2.756	0.591
Cu C	1.136	0.088	0.22	0.18	4.276	3.413	0.591
Cu D	1.129	0.091	0.28	0.24	4.276	1.786	0.591

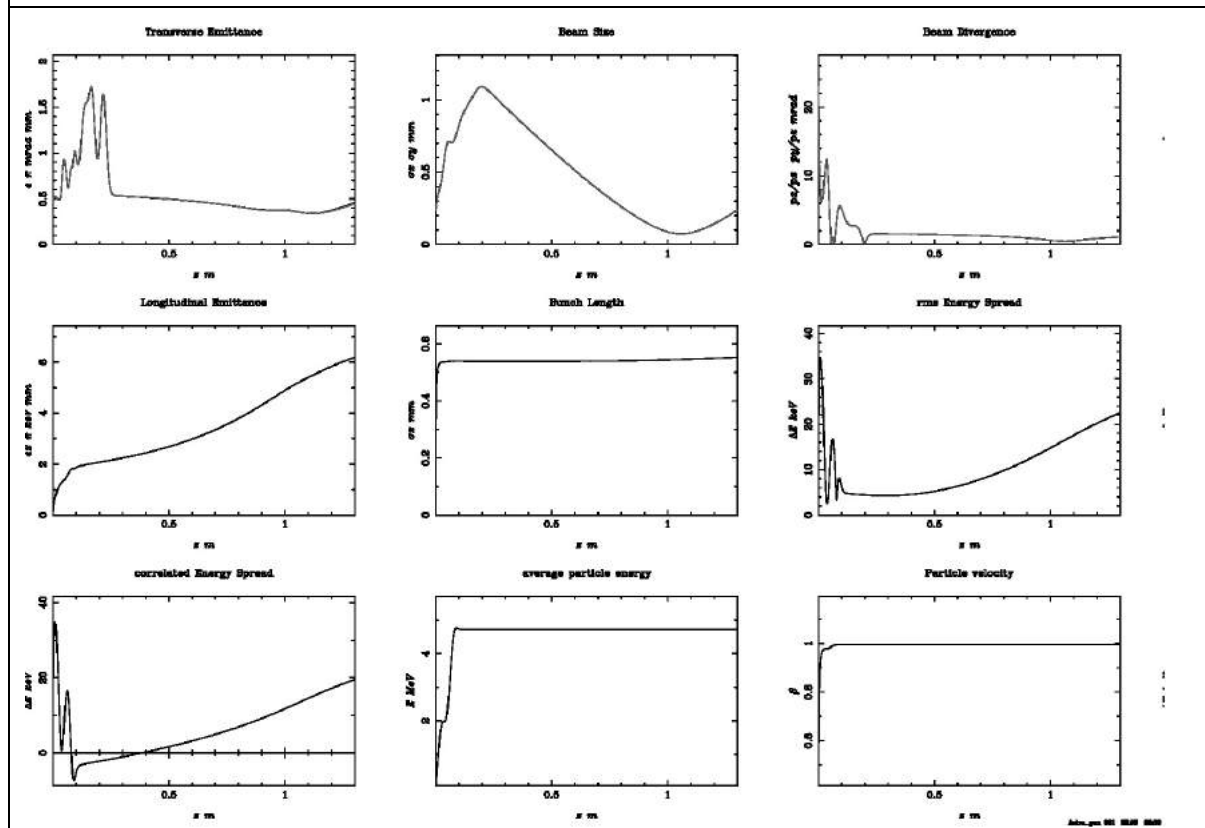
Observing Table 9.3, the energy gain is irrelevant of the thermal emittance, while brightness is considerably higher for the least emittance, as expected by the inversely proportional relation between the two in (A.29). The waist position changes slightly, in centimeter accuracy it is invariant. The same holds for the size on waist. The bunch length is also invariant.

Cs₂Te

The same procedure was followed for the two distributions of the Cs₂Te.



F.9.15 Overview of the parameters of the beam along the z-axis - 1.5 cells S-band gun - Cs₂Te A



F.9.16 Overview of the parameters of the beam along the z-axis- 1.5 cells S-band gun - Cs₂Te B

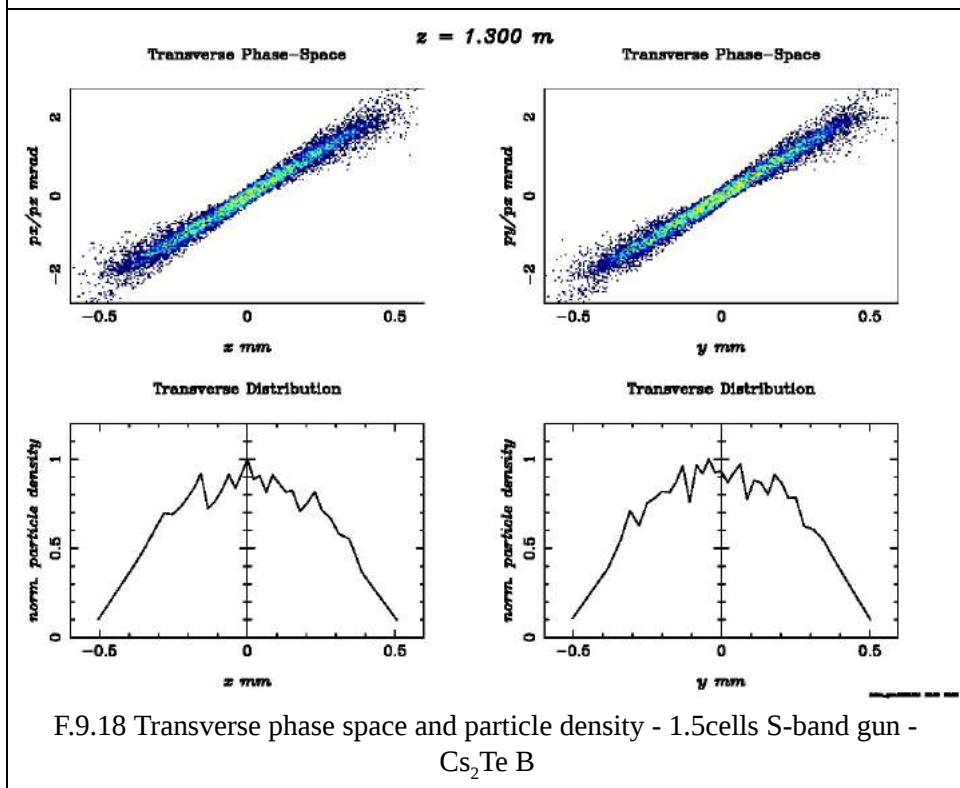
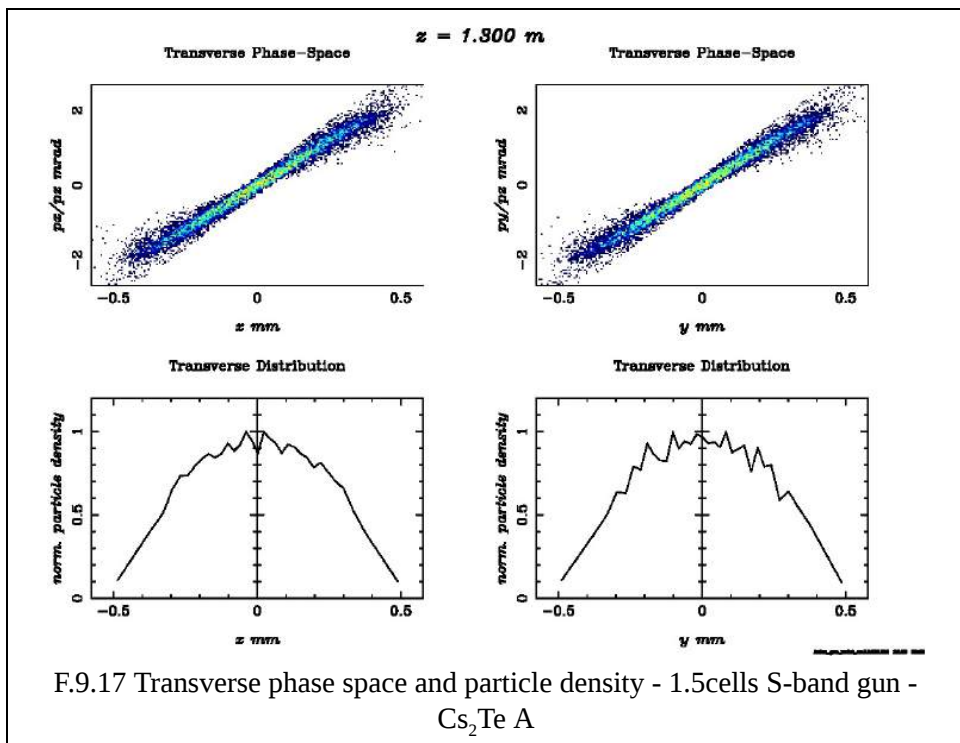
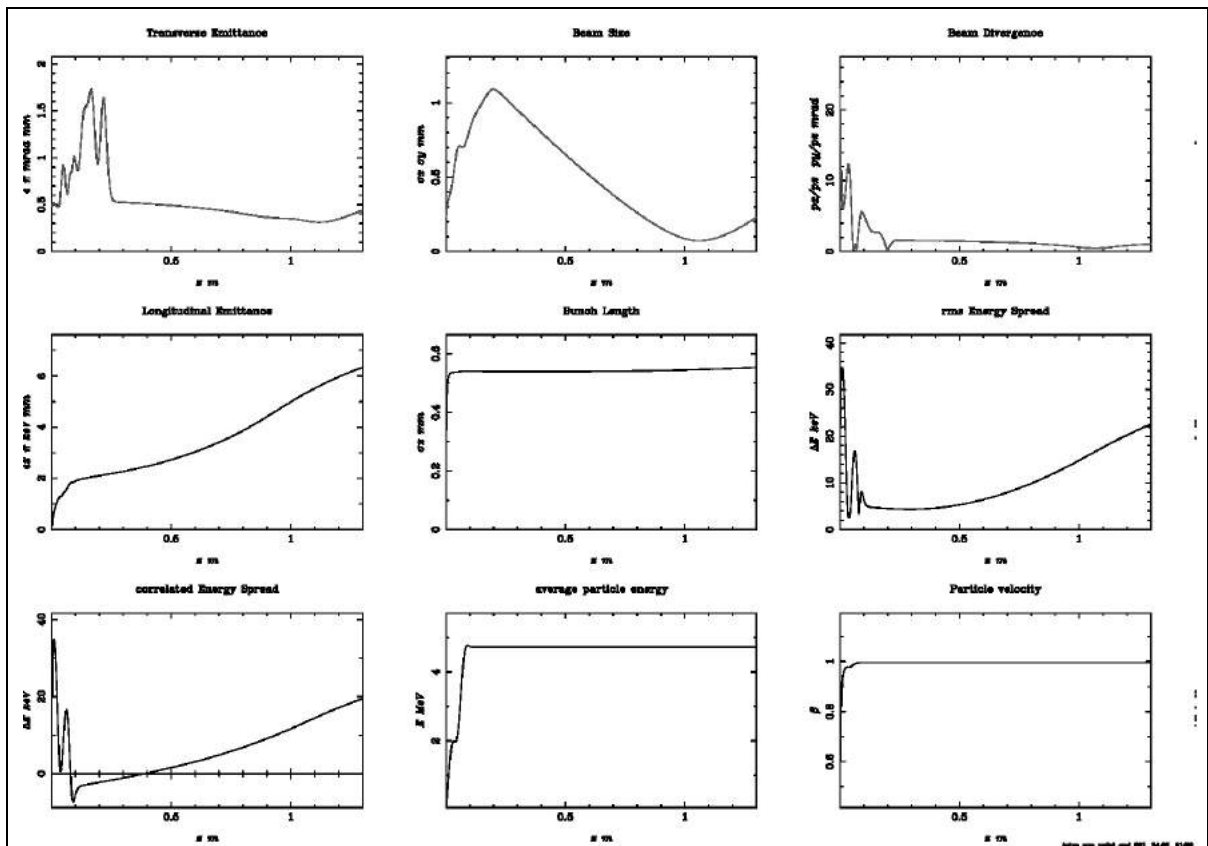


TABLE 9.4 Cs ₂ Te thermal emittance effects on RF gun performance on 1.5 cells S-band gun							
	Beam waist position (m)	Minimum trans. Size (mm) (waist)	Emittance on waist (pi mm mrad)	Minimum emittance (pi pi mm mrad)	Particle energy (MeV)	Brightness (nC/mrad mm ²)	Bunch Length (mm)
Cs ₂ Te A	1.060	0.072	0.33	0.31	4.709	2.002	0.585
Cs ₂ Te B	1.056	0.074	0.36	0.34	4.709	1.937	0.553

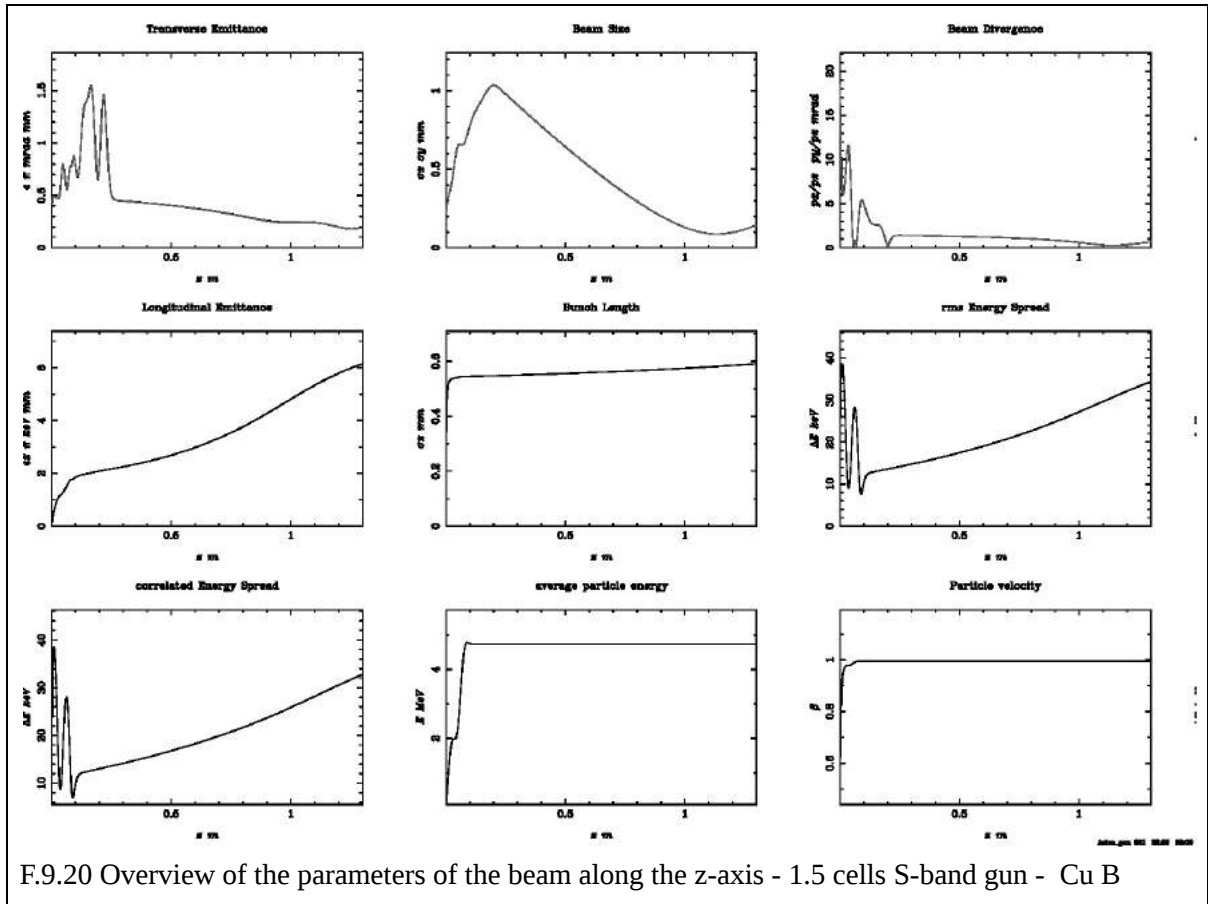
The same conclusions hold here, according to Table 9.4. The only thing worth to point out is that the energy gain / injection energy is lower in this case than in the Cu case presented above. The reason behind this difference is the fact that the initial gun phase is not optimal or adjusted to the delay the semiconductor introduces. Also, that the bunch length differs slightly.

Cu vs Cs₂Te

A comparison of the beams occurring of the same laser 4.73eV/262 nm for Cu and Cesium_Telluride is performed below. The work functions will be from literature references, meaning distributions Cu B and Cs₂Te A.

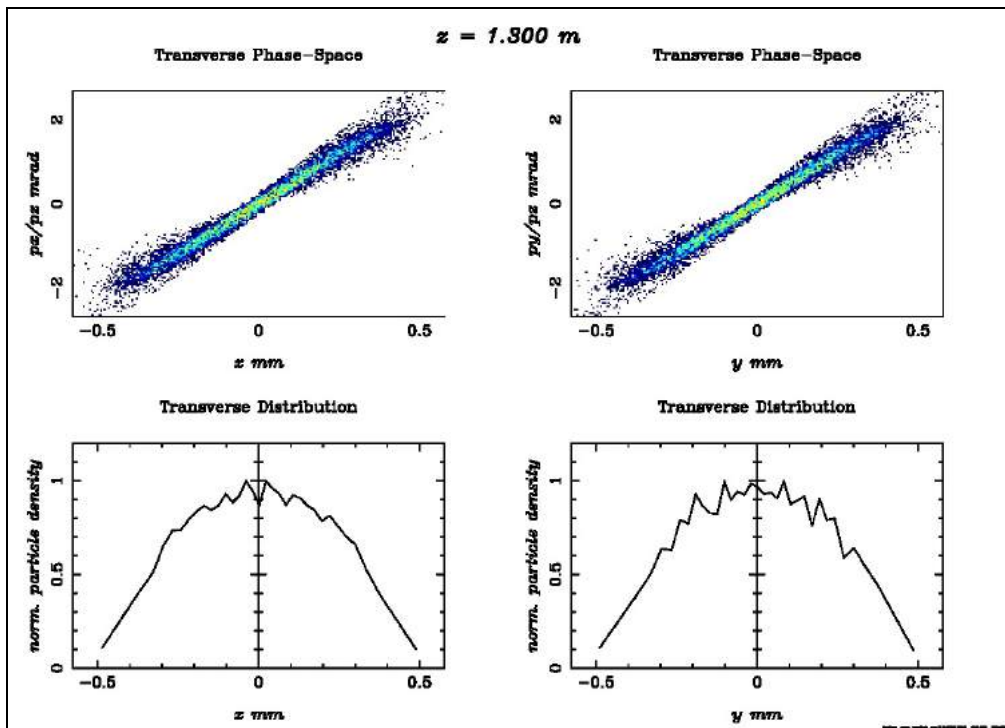


F.9.19 Overview of the parameters of the beam along the z-axis- 1.5 cells S-band gun - Cs₂Te A

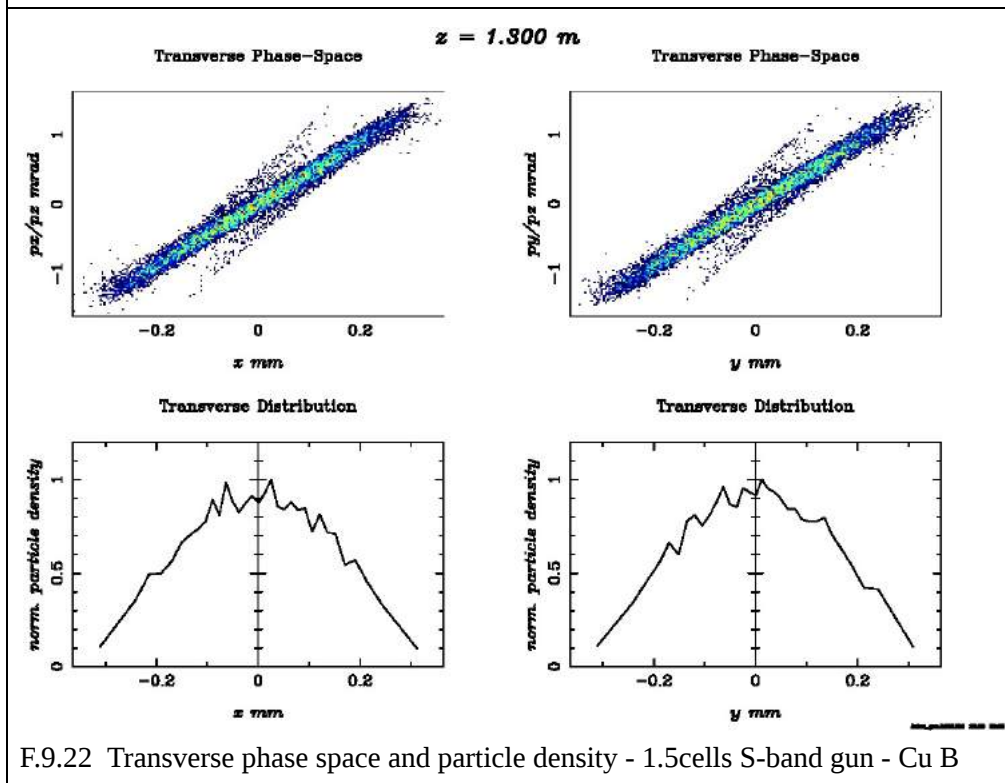


F.9.20 Overview of the parameters of the beam along the z-axis - 1.5 cells S-band gun - Cu B

Again, as shown in F.9.19 and F.9.20, the evolution of the quantities is similar, but here there are significant differences. The emittance of Cu is lower and the beam waist position is different. Also, in the Cs₂Te case the Energy spread is lower (see comment of relation A.35). As shown before, the change in kinetic energy, does not affect that observably the waist position and energy spread. The only variable that differs is the emission delay.



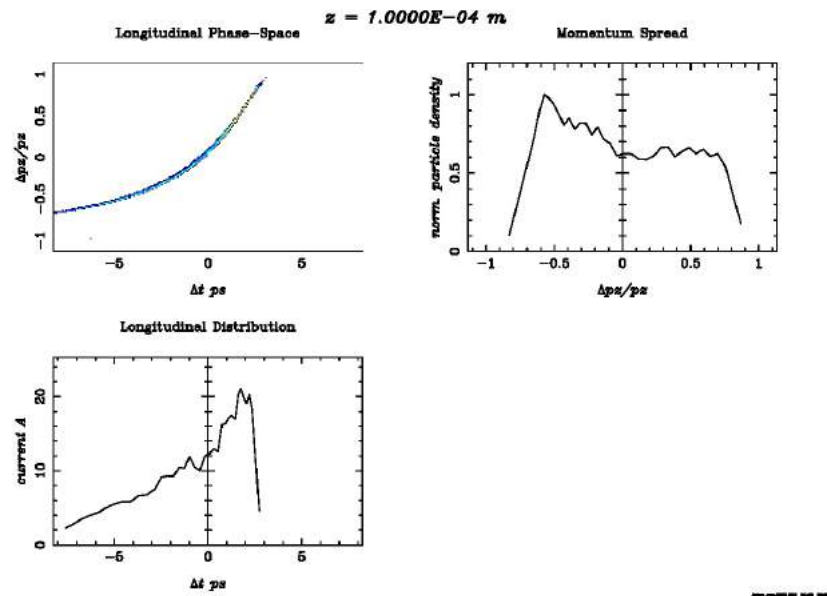
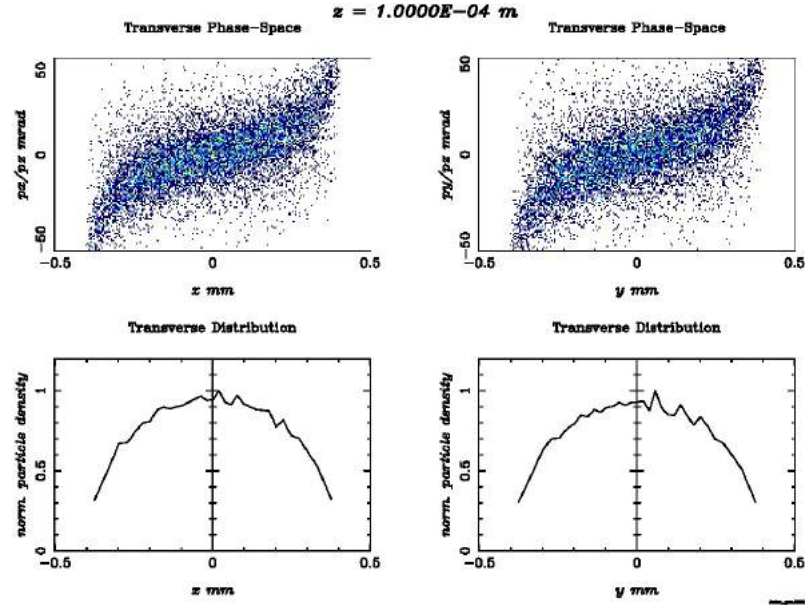
F.9.21 Transverse phase space and particle density - 1.5cells S-band gun - Cs₂Te A

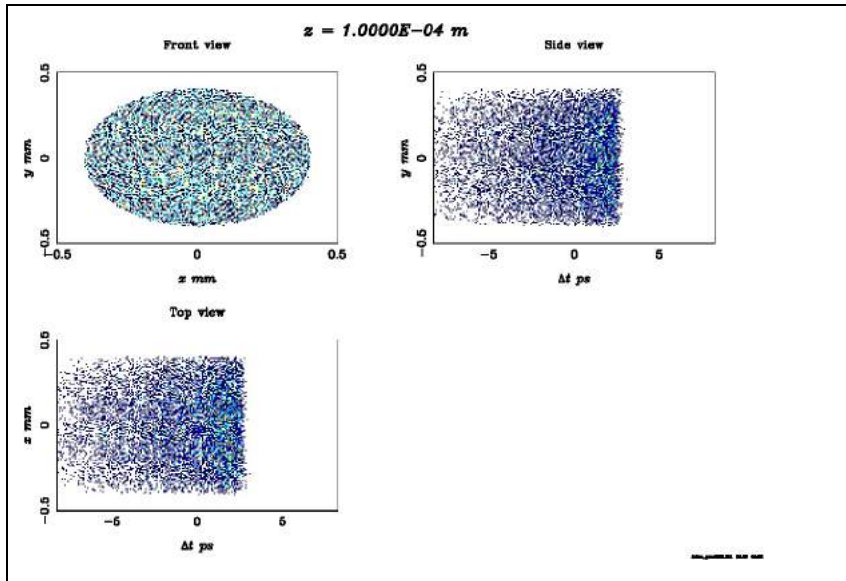


F.9.22 Transverse phase space and particle density - 1.5cells S-band gun - Cu B

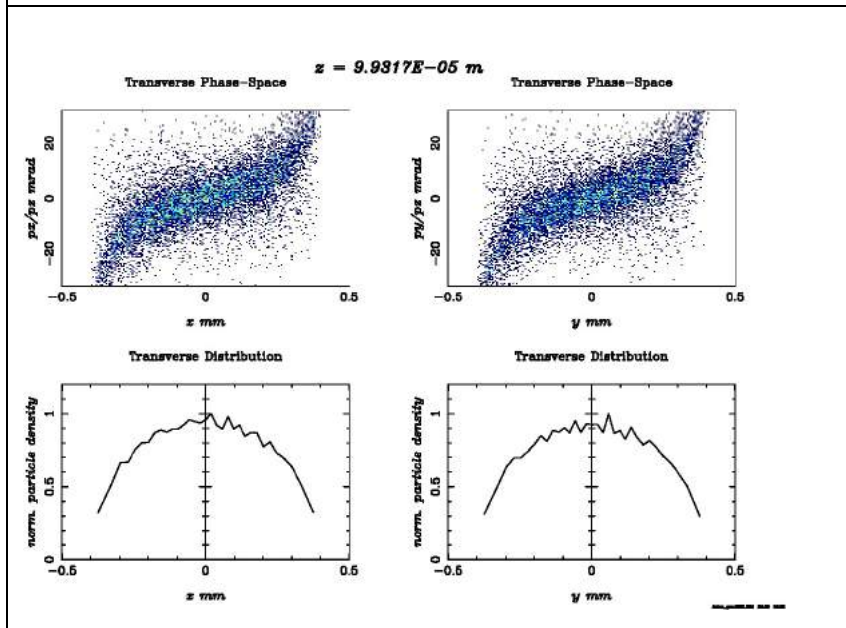
The morphology of the phase space of Cu, F.9.22, is more linear at the edges while in Cs₂Te, F.9.21, it is more linear at the centre. Also, in Cs₂Te case the electron density is more spread than in Cu's.

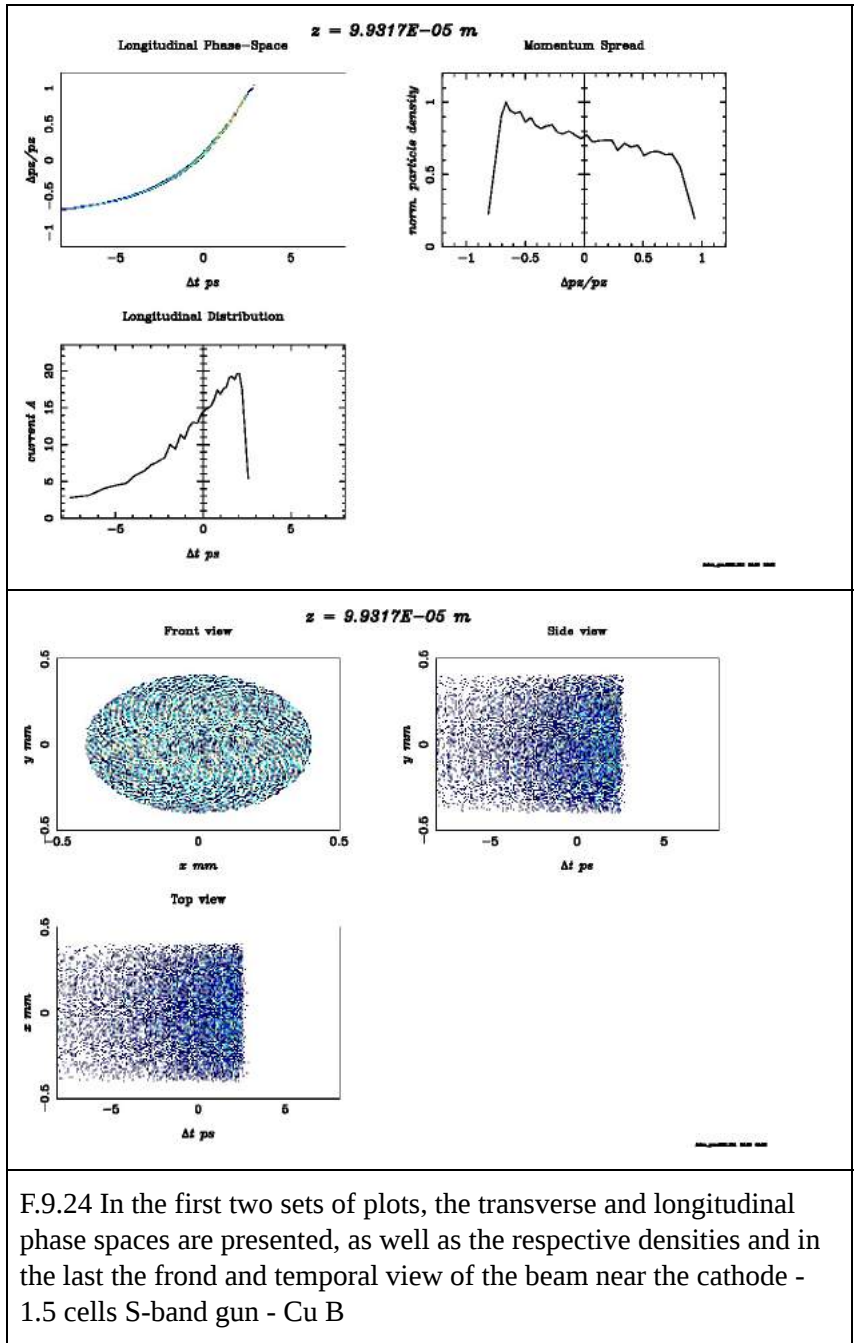
Near the cathode at $z=10^{-4}$ m





F.9.23 In the first two sets of plots, the transverse and longitudinal phase spaces are presented, as well as the respective densities and in the last the front and temporal view of the beam near the cathode - 1.5 cells S-band gun - $\text{Cs}_2\text{Te A}$





F.9.24 In the first two sets of plots, the transverse and longitudinal phase spaces are presented, as well as the respective densities and in the last the front and temporal view of the beam near the cathode - 1.5 cells S-band gun - Cu B

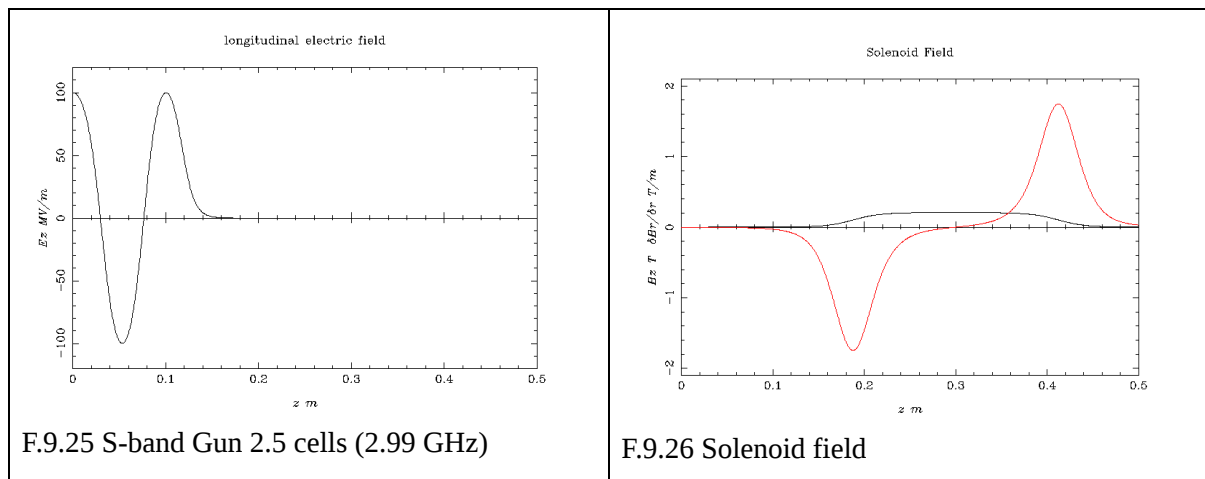
The delay in emission is observable in the temporal distributions, F.9.24 and F.9.23, as well as the alteration it causes to the current.

TABLE 9.5 Comparison of Cu and Cs ₂ Te photocathodes performance on 1.5 cells S-band gun							
	Beam waist position (m)	Minimum trans. Size (mm) (waist)	Emittance on waist (pi mm mrad)	Minimum emittance (pi pi mm mrad)	Particle energy (MeV)	Brightness (nC/mrad mm ²)	Bunch Length (mm)
C ₂ Te A	1.060	0.072	0.33	0.31	4.709	2.002	0.585
Cu B	1.134	0.088	0.23	0.18	4.726	3.171	0.591

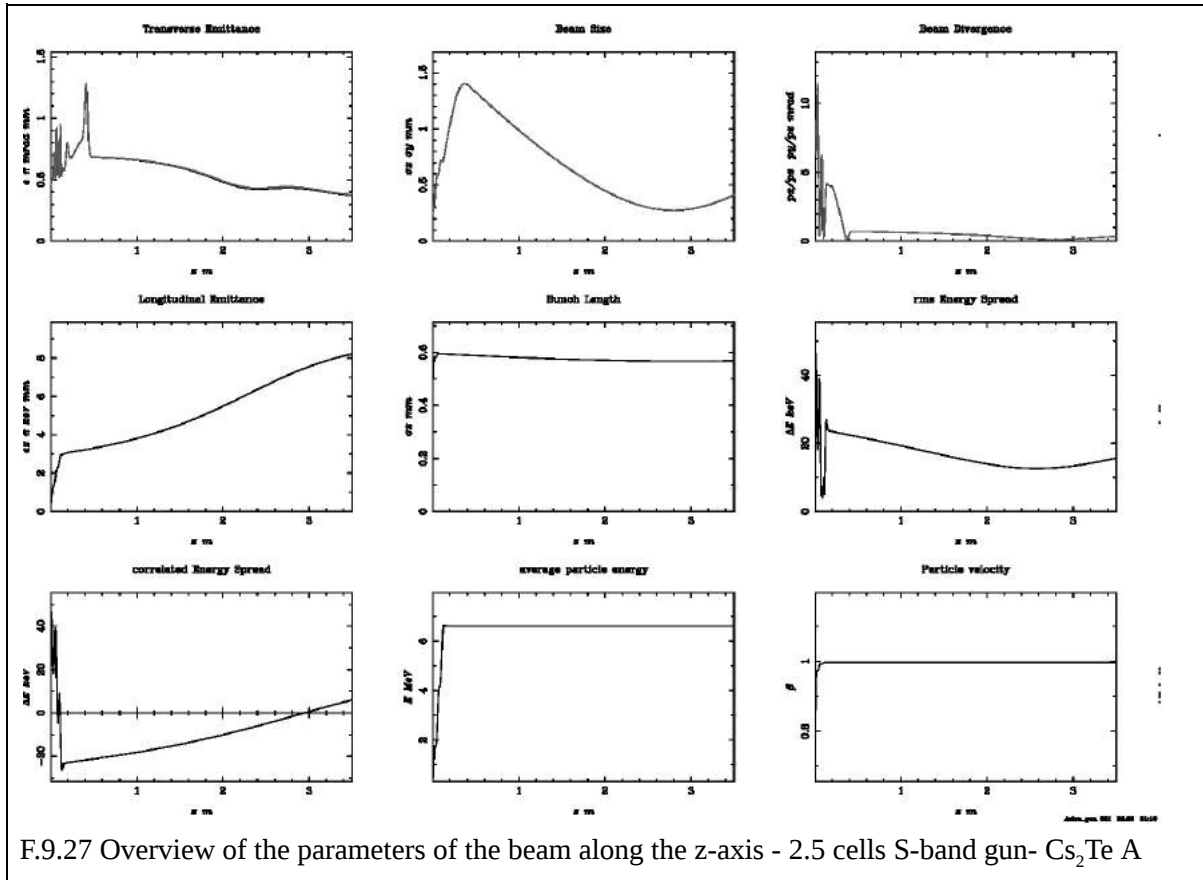
The beam waist position's alteration is not negligible now, as can be seen in Table 9.5, meaning that if the different cathodes are used over identical lattices the *Ferrario Working Point (FWP) condition* may not be met. The waist size also is lower for the semiconductor in contrast with the respective emittance. The semiconductor, as said above, has slightly less injection energy than that of the Cu due to the not optimum initial phase of the gun. In addition, the bunch length of the beam from Cs₂Te is lower than the bunch length of Cu, due to the large difference of the emission delay between the two materials.

9.3.2 2.5 cells gun S-band

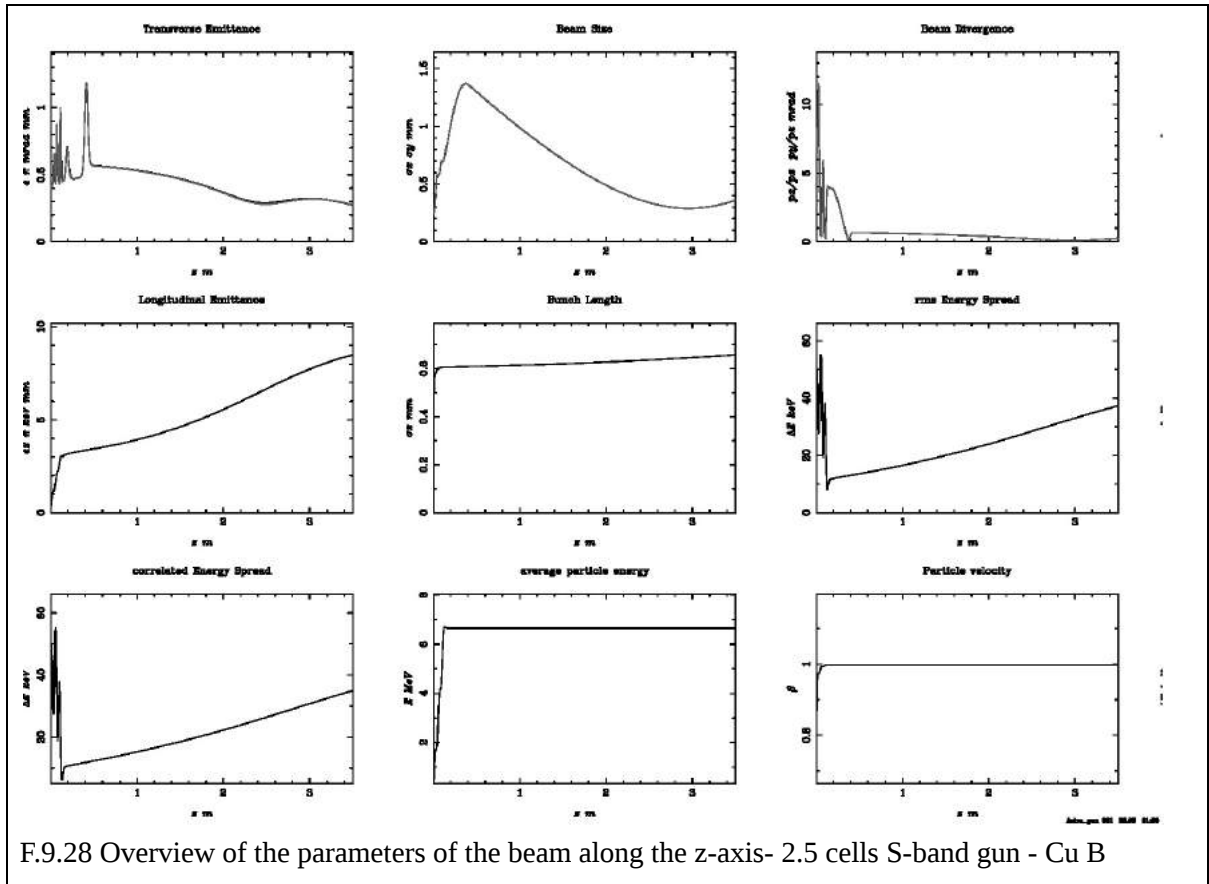
The same simulations were performed for a 2.5 cells gun in S-band. But the quality of the results is the same as above. Meaning that the change of the thermal emittance does not change the evolution of the beam. Comparing the Cu photocathode with the Cs₂Te, according to F.9.27-F9.28, the latter alters the waist position a bit by shifting it closer to the photocathode, the emittance is also higher for Cs₂Te, but the initial thermal emittance was higher as well.



For reference, the results of Cooper B and Cs₂Te A are presented.

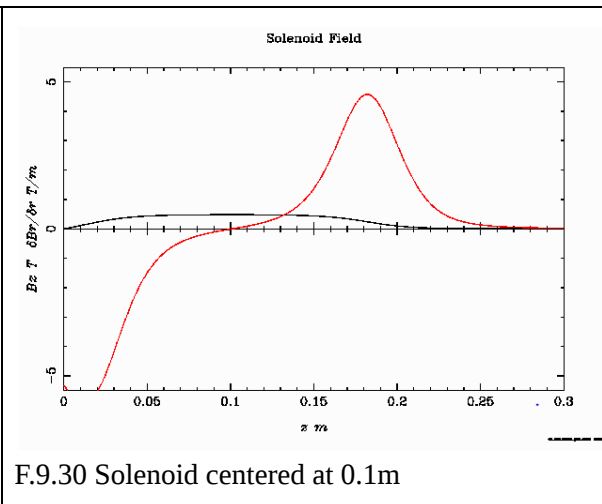
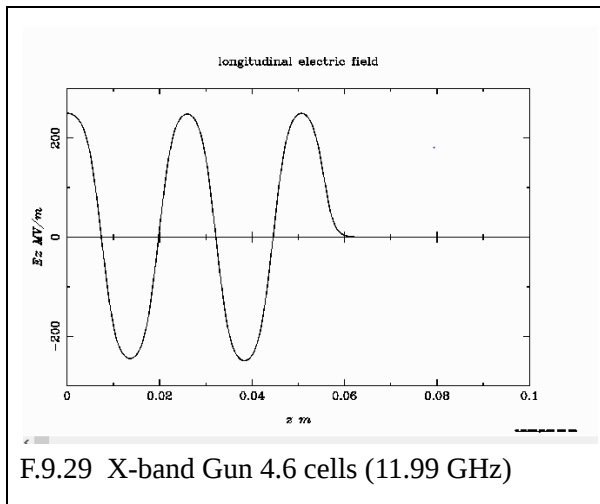


F.9.27 Overview of the parameters of the beam along the z-axis - 2.5 cells S-band gun- Cs₂Te A

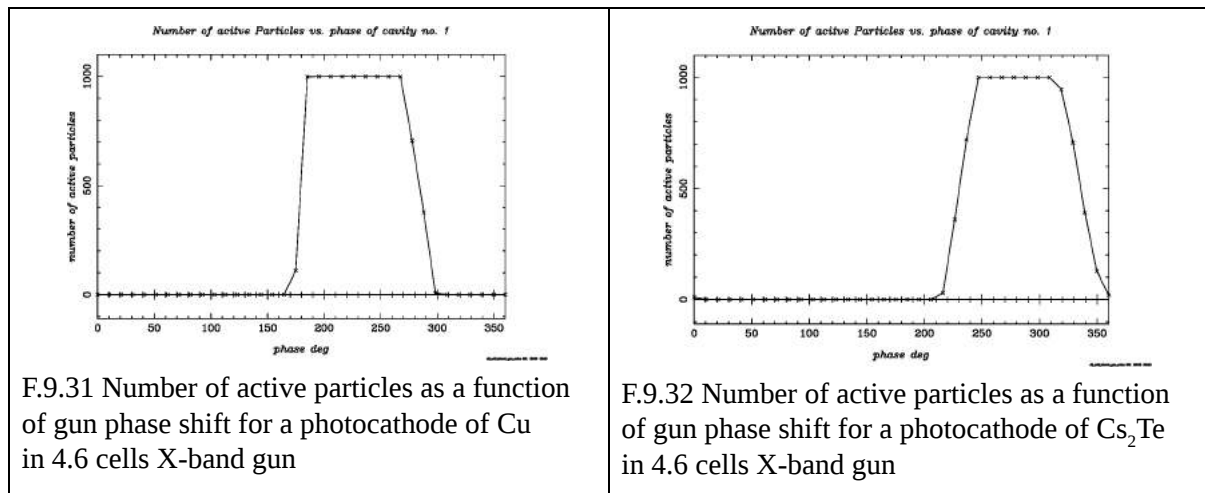


9.3.3 4.6 cells gun X-band

The 4.6 cells X-band gun geometry, F.9.29 and simulations are presented below. The longitudinal components of the Gun, Solenoids and TWS can be found in F.9.29 and 9.30. In the X-band case the laser pulse duration has been set to 2 psec, as it is indicated in Table 4.4 where the maximum pulse duration must be less than 2.3 psec.



In this X-band case, the materials could not operate both for the same initial phase of the gun, because the emission delay of Cs_2Te is comparable to the duration of the pulse; while the emission delay of Cu is negligible.



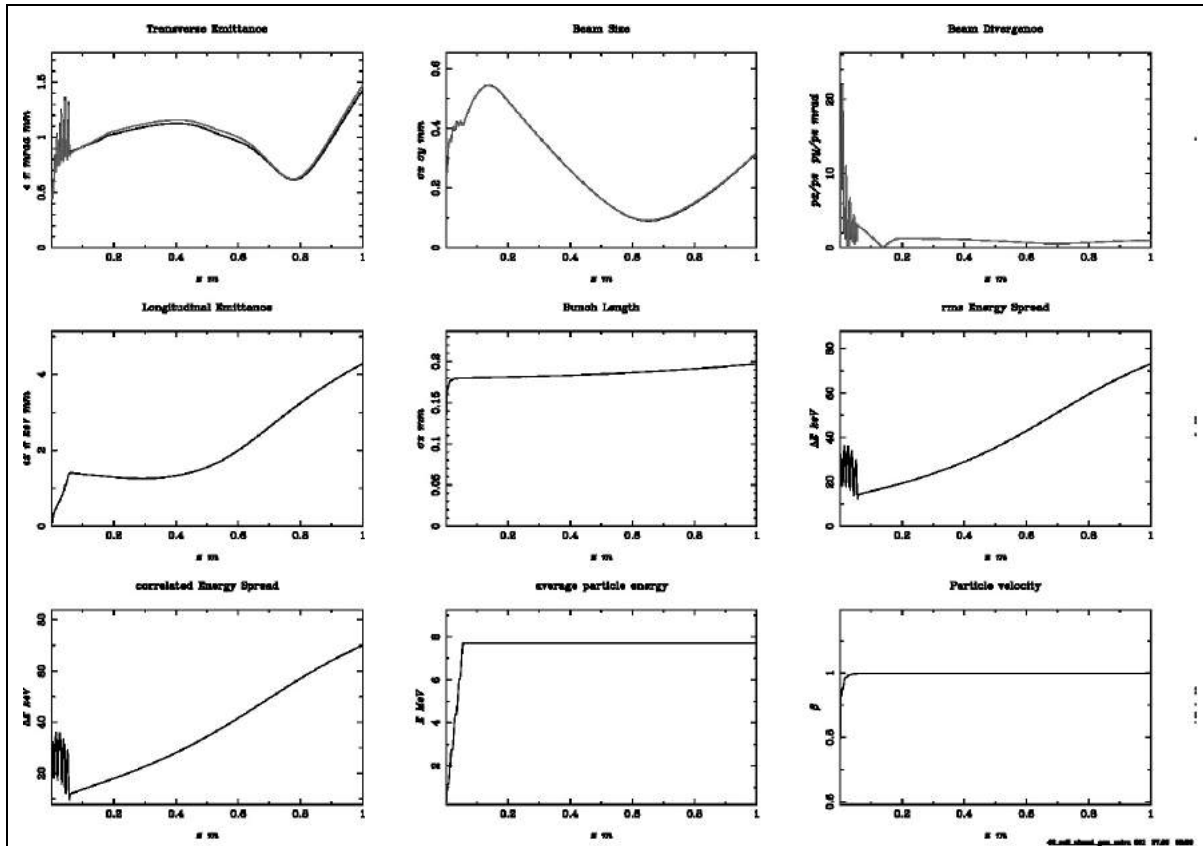
As shown in F.9.31 and F.9.32, the feasible phases for Cu are between 180 and 280 degrees, while for Cs_2Te they are from 235 to 340 degrees approximately. Phases from 235 to 280 are feasible for both photocathodes but they may not give optimal results for both.

After a series of scans of the initial phase for Cs_2Te 240 degrees were chosen as an optimal solution for the gun phase. For Cu the proposed phase of 197 degrees was used.

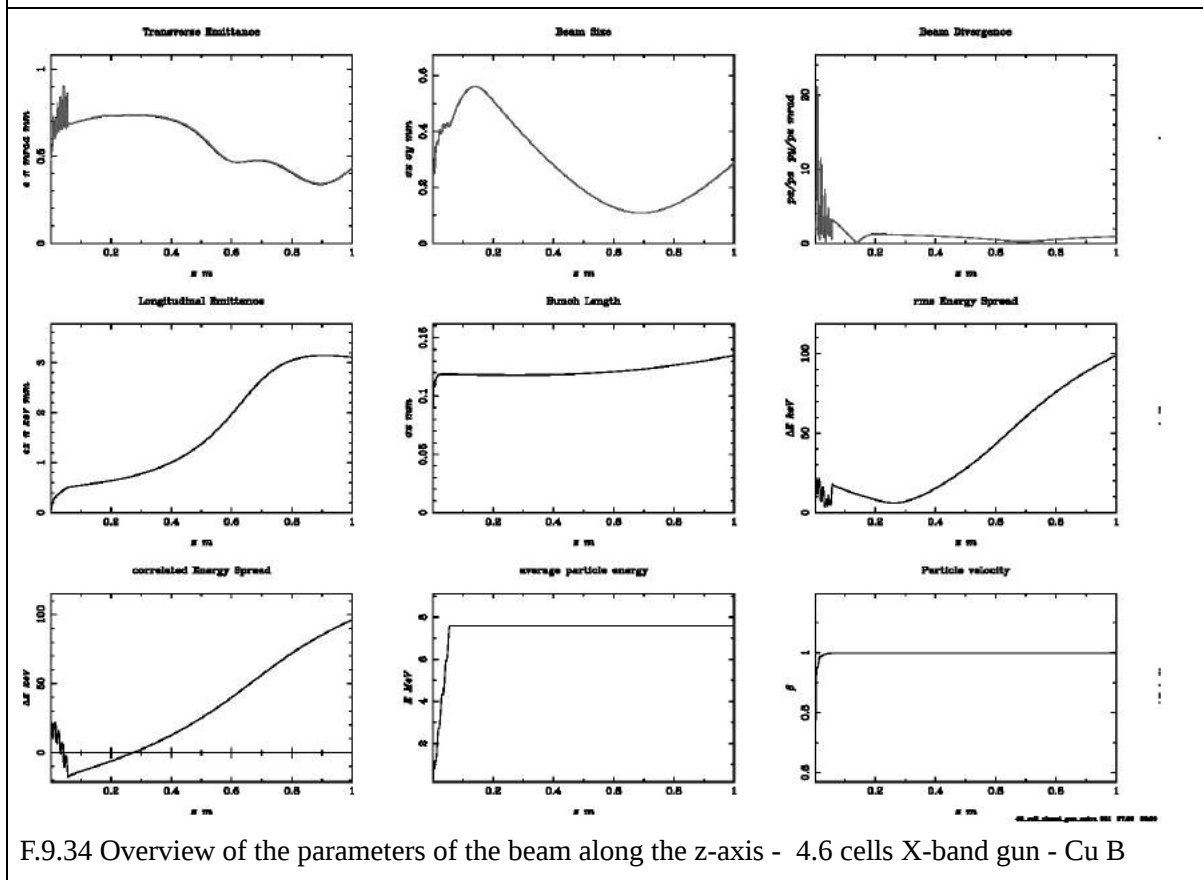
For this gun there will not be a presentation of the comparison of results among the same materials, as the conclusions were the same as in the other two RF guns in the S-band. The most worth mentioning results occur from the comparison of the materials.

Cu vs Cs_2Te

The comparison below concerns the beams occurring of the same laser 4.73 eV / 262 nm for Cu and Cesium_Telluride. The work functions will be from literature reference, meaning distributions Cu B and Cs_2Te A.



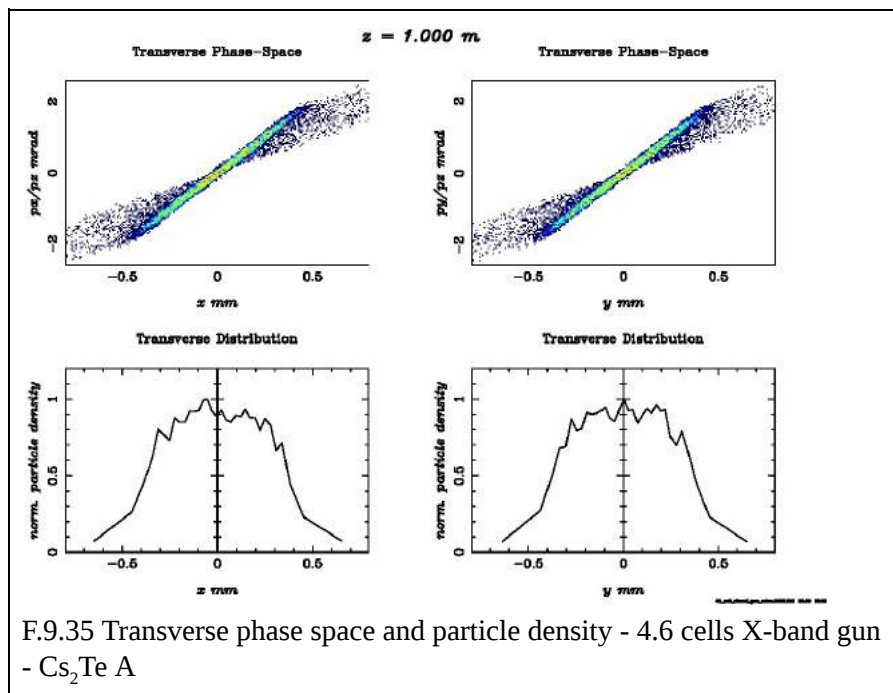
F.9.33 Overview of the parameters of the beam along the z-axis - 4.6 cells X-band gun - Cs₂Te A

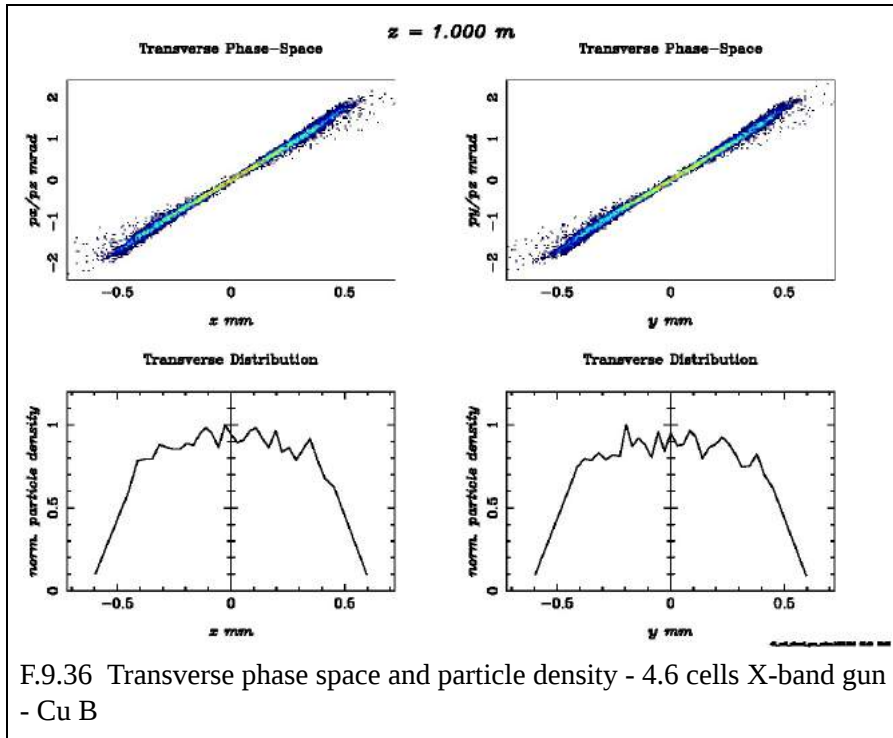


F.9.34 Overview of the parameters of the beam along the z-axis - 4.6 cells X-band gun - Cu B

In contrast with the previous S-band guns, here the differences are more intense. The emission delay is very high in comparison with the pulse length altering the shape and symmetry of the beam, thus the space charge forces. In the Cu case a double emittance minimum is observed, as presented in Chapter 5. Comparing these results to F.5.1, the Cs₂Te delay inserts an extra non-uniformity in the temporal profile of the beam, similar to increasing the τ variable (rise/fall time of the laser). So, in the semiconductor, one cannot take advantage from the second minimum occurring at the end of the booster (see Ch. 5).

What is more, in the first case not even the *FWP* can be met, as in the waist position the emittance is not minimum at any case, it does have a small gradient, which is not zero. In the contrary, in Cu in the waist position conveniently occurs the emittance maximum. Also, the bunch length is remarkably smaller for Cu.



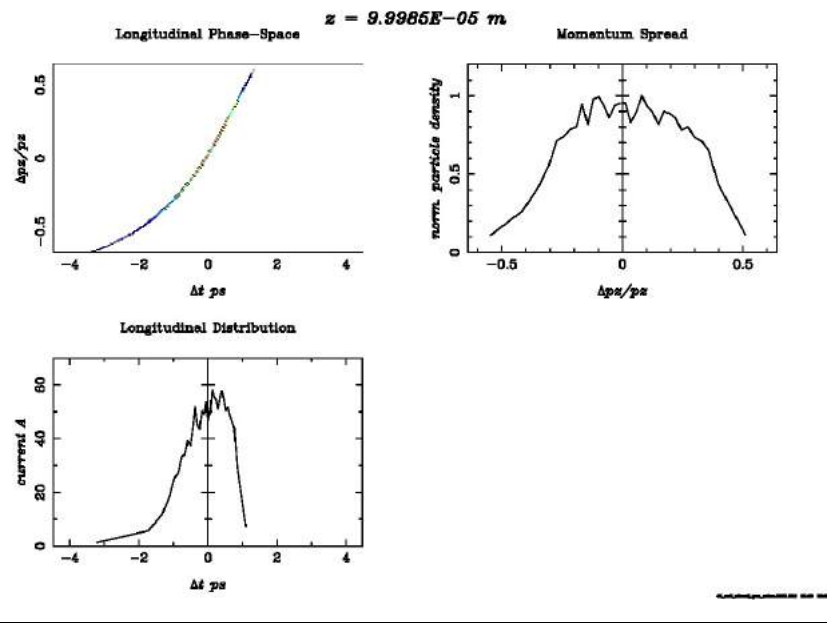
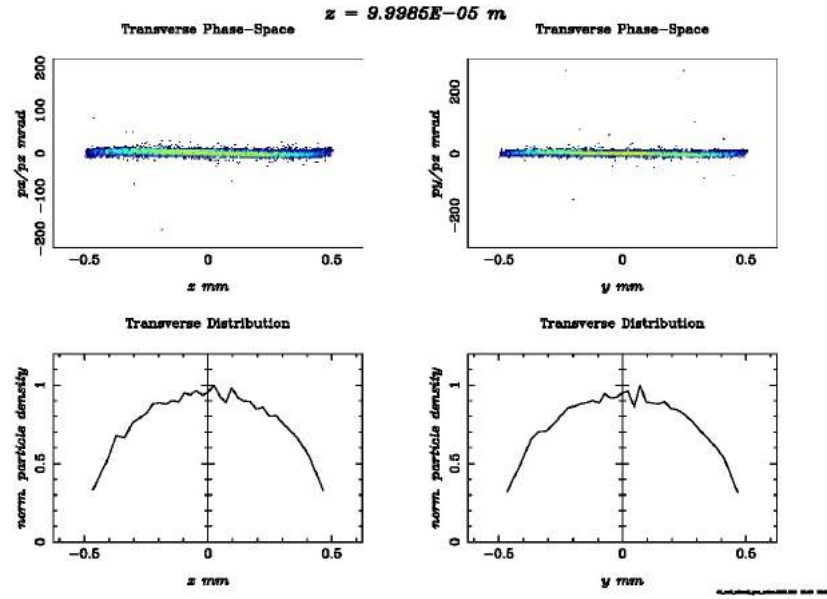


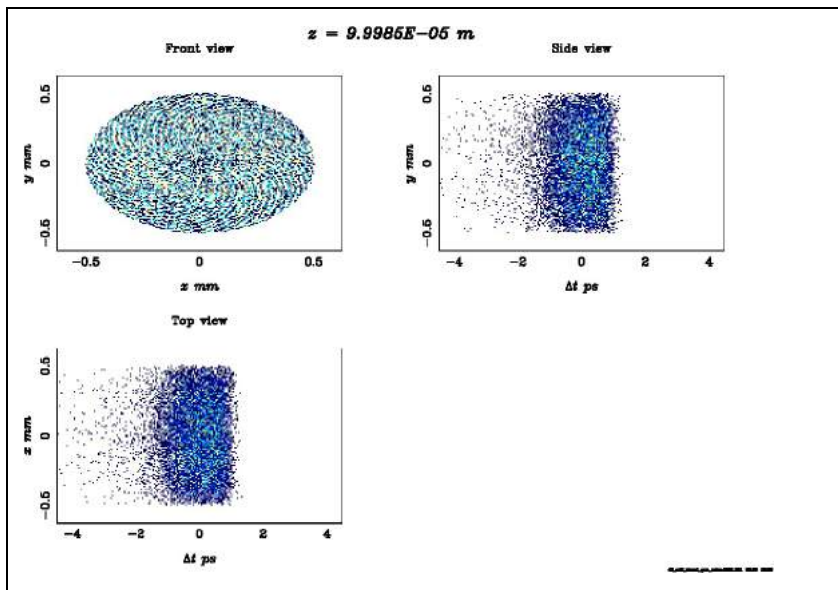
F.9.36 Transverse phase space and particle density - 4.6 cells X-band gun - Cu B

The morphology of the phase space of Cu is more linear (F.9.36), while in Cs_2Te (F.9.35) long tails and dispersion at the edges of the phase-space are observed. Also, in Cs_2Te case the electron density is more intense near the centre but there is considerable dispersion. Cu shows a more uniform/flattop particle density.

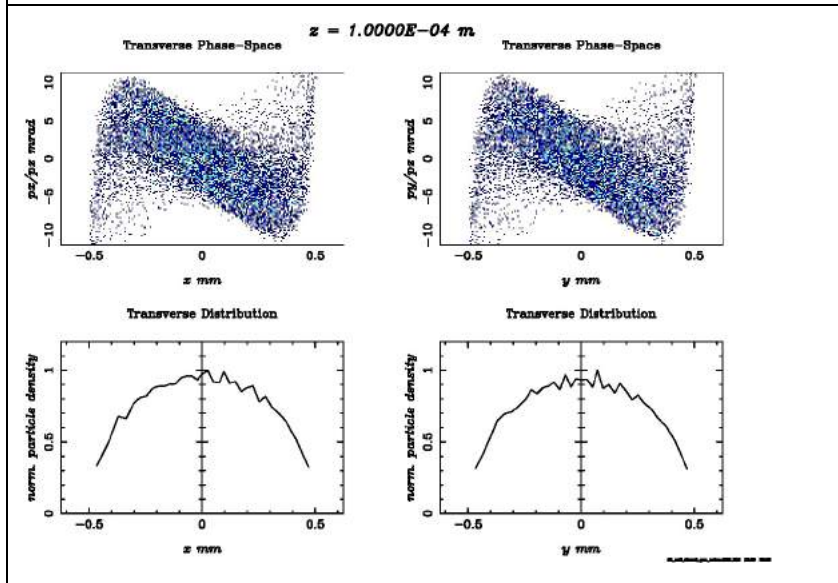
Near the cathode, right after emission the phase spaces and beam transverse and temporal views are presented in F.9.37 and F.9.38.

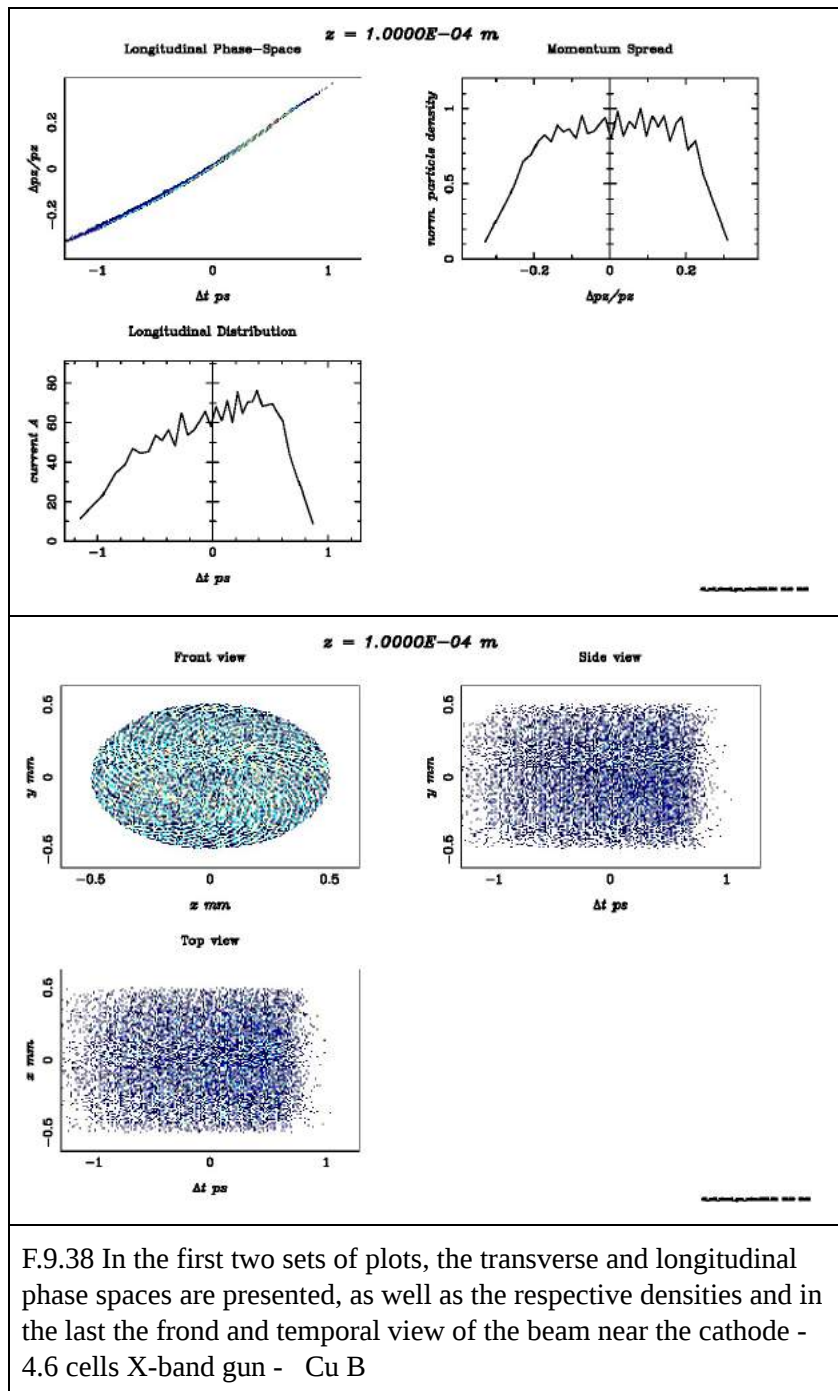
Near the cathode at $z=10^{-4}$ m





F.9.37 In the first two sets of plots, the transverse and longitudinal phase spaces are presented, as well as the respective densities and in the last the front and temporal view of the beam near the cathode - 4.6 cells X-band gun - Cs₂Te A

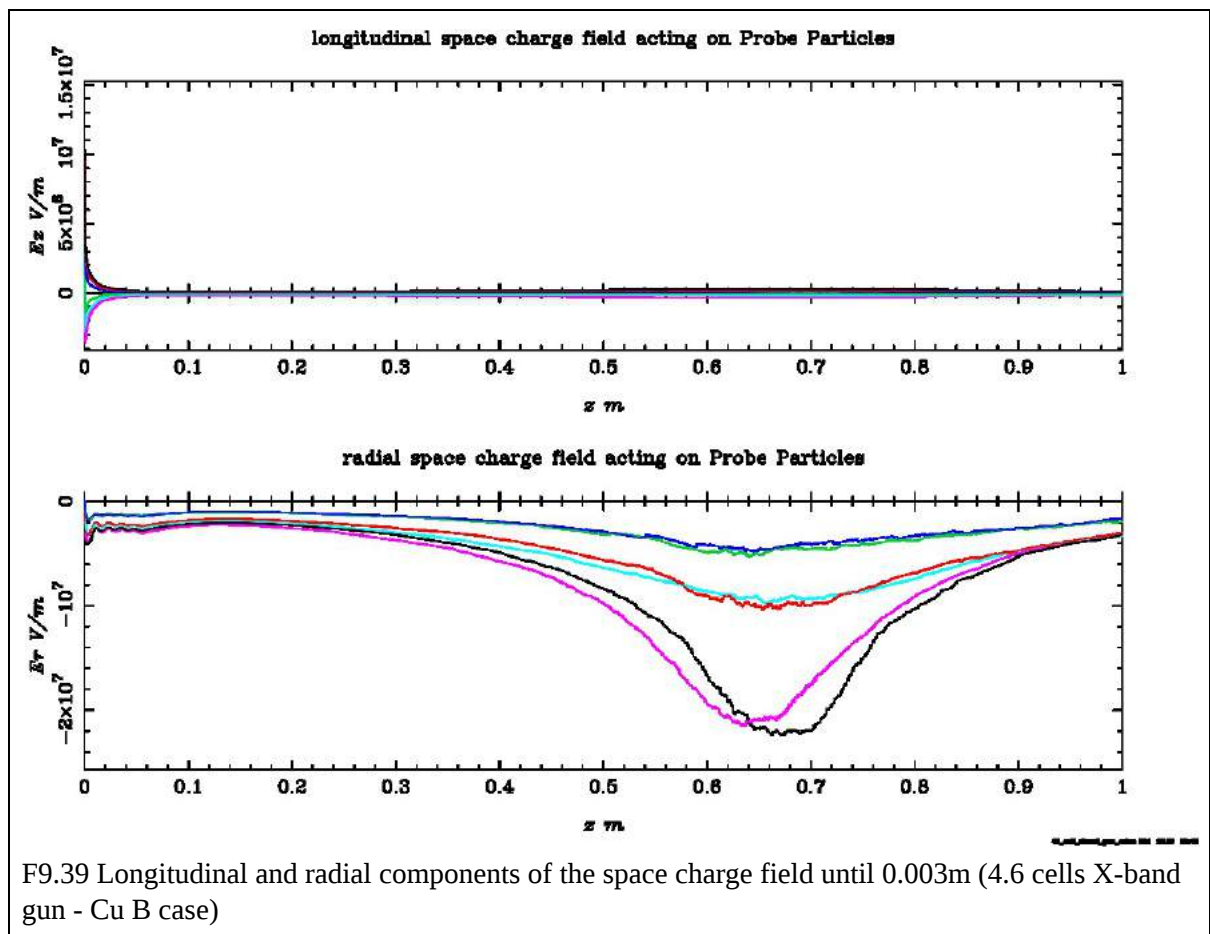


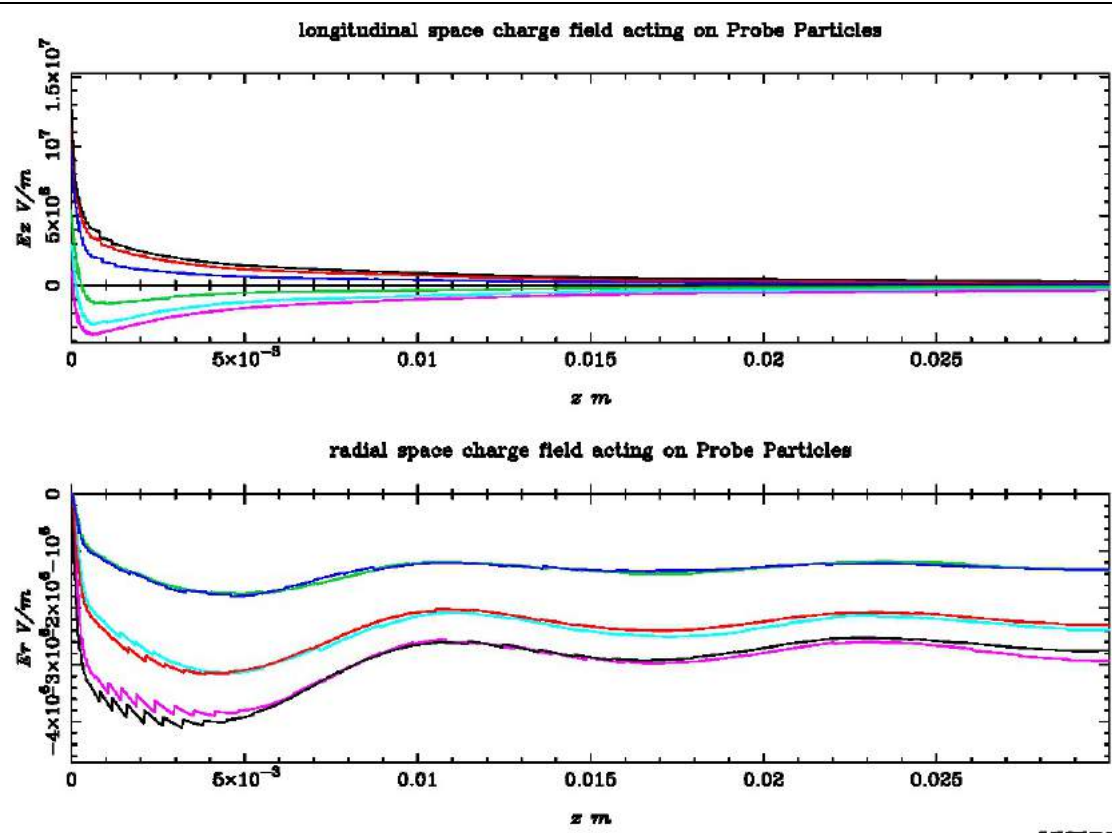


The delay in emission is obvious in the temporal distributions, as well as the alteration it causes to the current. The current in the semiconductor case has a very long tail due to the delay, while in the metallic photocathode case, all distributions are more symmetric. Of course, one has to keep in mind that the distributions are in the beginning of the acceleration so partly the asymmetry is due to the electrical field rise.

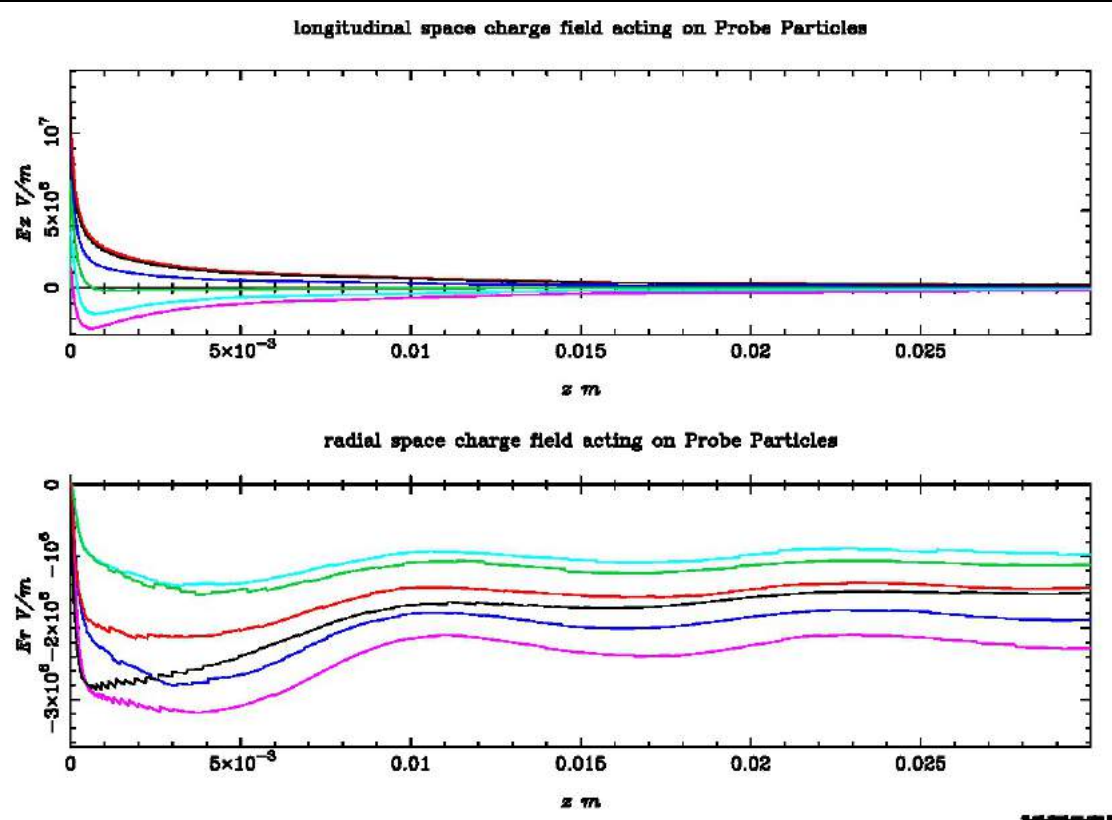
TABLE 9.6 Comparison of Cu and Cs ₂ Te photocathodes performance on 4.6 cells X-band gun							
	Beam waist position (m)	Minimum trans. Size (mm) (waist)	Emittance on waist (pi mm mrad)	Minimum emittance (pi pi mm mrad)	Particle energy (MeV)	Brightness (nC/mrad mm ²)	Bunch Length (mm)
Cs ₂ Te A	0.652	0.091	0.882	0.443	7.709	1.196	0.197
Cu B	0.690	0.109	0.476	0.340	7.600	3.539	0.135

The beam waist position's alteration is not negligible here (Table 9.6). The waist size also is lower for the semiconductor, like in the S-band case, but the values are still close, in contrast with the respective emittance. The beam generated from the metal photocathode results in half the emittance on waist position. The semiconductor has slightly more energy gain / injection energy than Cu. In addition, the bunch length for Cu is also lower, maybe due to the gun phase as the longitudinal space charge forces seem to be greater for the Cu near , as shown below in F.9.39-F.9.42.

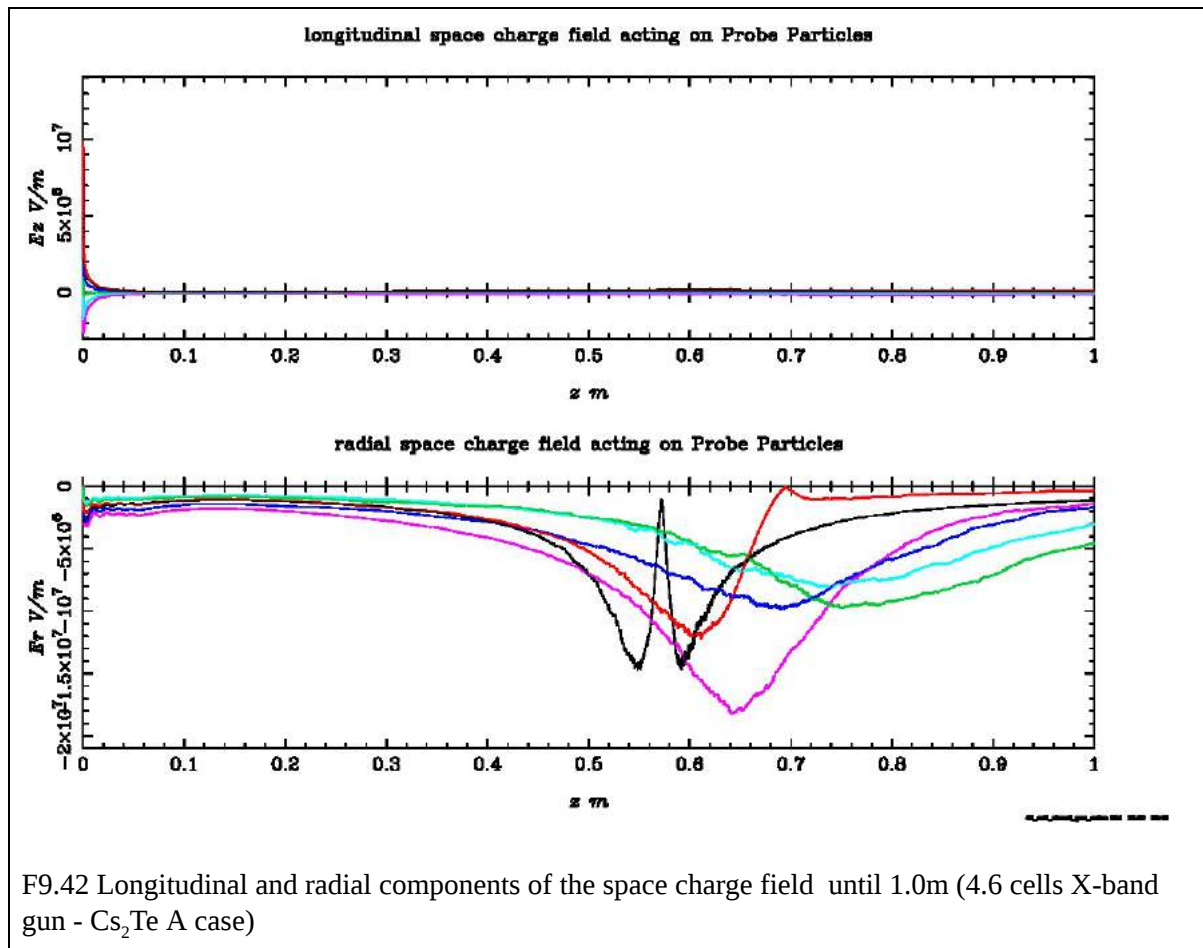




F9.40 Longitudinal and radial components of the space charge field until 1.0m (4.6 cells X-band gun - Cu B case)



F9.41 Longitudinal and radial components of the space charge field until 0.003m (4.6 cells X-band gun - Cs₂Te A case)



Near the waist where the space charge forces are important, the Cu case has a symmetry around the waist position, while in the semiconductor such a symmetry is missing and the evolution of the space charge forces does not follow a strict pattern, as shown in F.9.42.

9.3.4 Conclusions

In the S-band guns tested and simulated, the change of photocathode is not affecting the results in a way that the cathodes cannot be substituted with one another. So, both cathodes can be used for the same of similar setups. In the X-band, though, the introduction of the emittance delay altered the output in a way that the lattice could not be operative with different materials. So, in an X-band, a careful tuning of the parameters needs to be done so that the Cs₂Te can operate, or even both the cathodes can operate on the same lattice.

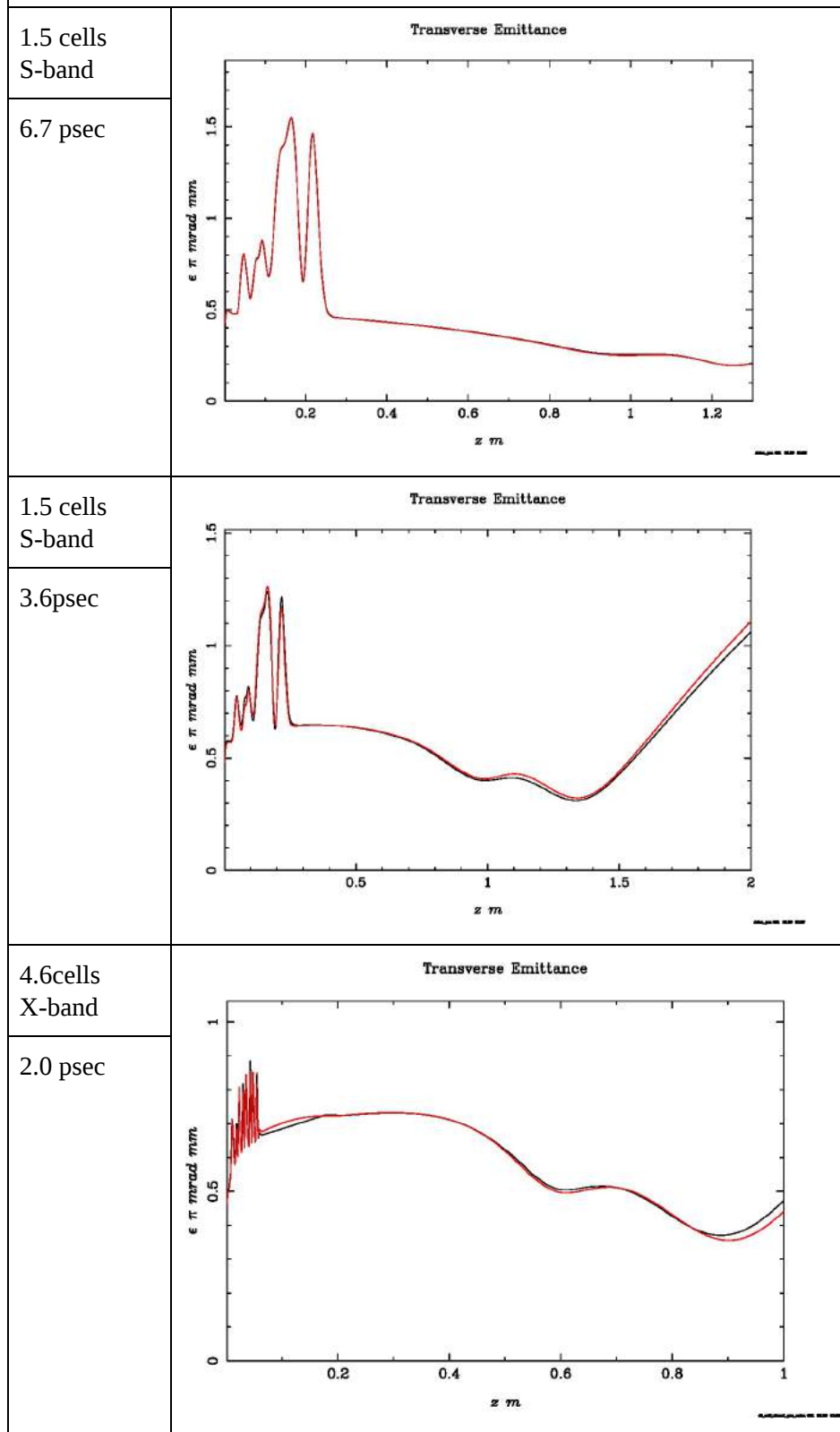
9.4 Double emittance minimum

In this part of the simulations a double emittance minimum in the S-band is presented. Altering the beam profile in the 1.5 cells gun presented before, a double emittance minimum occurred. The change performed was just inserting a smaller pulse of 3.6 psec duration and 0.5 psec rise/fall time.

The results of the S-band are compared with the X-band case shown before in Chapter 9.3.3 with the previous pulse. Also, the material used for these simulations was Cu A.

TABLE 9.7

Transverse emittance along the z-axis in 3 gun cases.
Double emittance minimum observation.



As shown in Table 9.7, the double minimum exist in all cases, even though in the first it is faint. By making the beam shorter and altering the gun phase from 0.0 to 3.0 degrees an intense double

minimum was achieved. The minimum and the local maximum emittance are high compared to the initial case in the S-band and slightly lower compared to the X-band gun. So, there is no reason to switch to a short beam in the 1.5 cells S-band gun, except for the case the TWS is chosen to be in the X-band, where a short pulse is mandatory.

10. Photoinjector optimisation 1.5 cells S-band

In this Chapter , the method and the results of the optimisations of 1.5 cells injector are presented. The optimisation was performed in four steps. The first step was to simulate the gun with four solenoids that were proposed as possible combinations (without the TWS). Out of those, only two feasible solutions were taken into account for further analysis.

As a second step, the unoptimised lattices chosen were simulated until the first TWS for later comparison. After that, the gun alone was simulated, testing different solenoid positions, so that an optimal beam waist could be located. Optimal case means a waist with small transverse size and small emittance local maximum. The booster entrance was then located in the beam waist position chosen (FWP see Chapter 5) .

The third step is optimising the lattices created at the second step using the algorithm GIOTTO, as it was presented in Chapter 7. To be more specific, in this step the the optimisation concerns the variables: the laser spot size, the initial phases, the solenoid position and maximum and the TWS electric peak field, without the TWS solenoids magnetic field.

In the last step, the TWS solenoids' magnetic fields were inserted and the optimisation was performed for the peak fields and positions of the solenoids, along with the laser spot size.

Until step two, both materials were taken into account, Cs₂Te and Cu. The distributions used were Cs₂Te A and Cu D with laser spot radius 0.20mm . The reason for choosing the reference values for Cs₂Te and the experimental ones for Cu, is to remove the thermal emittance as a parameter that affects the results, because these cases have almost the same thermal emittance. Reference [8.3] supports this choice, as it proves there are small differences in performance and emittance for the two materials under the same lattice in S-band. This leaves the emission delay as the exclusive variable that is examined for comparison.

After step two, only the Cu case could be optimised, because GIOTTO does not yet support the parameter of ASTRA Tau which represents the emittance delay (τ). Although, as proved in previous simulations substituting the photocathode after the optimisation probably will give substantial results.

10.1 Cavities

The electric and magnetic fields of the various components of the 1.5 cells S-band gun photoinjector are presented with respect to the z-axis in Tables 10.1 - 10.3 .

RF-Gun

TABLE 10.1 1.5 cells RF gun S-band	
Number of cells	1.5
Frequency (GHz)	2.856
Peak Field (MV/m)	100

Solenoids

TABLE 10.2 Four different solenoid fields	
Solenoid No1	0.5
Peak Field (T)	

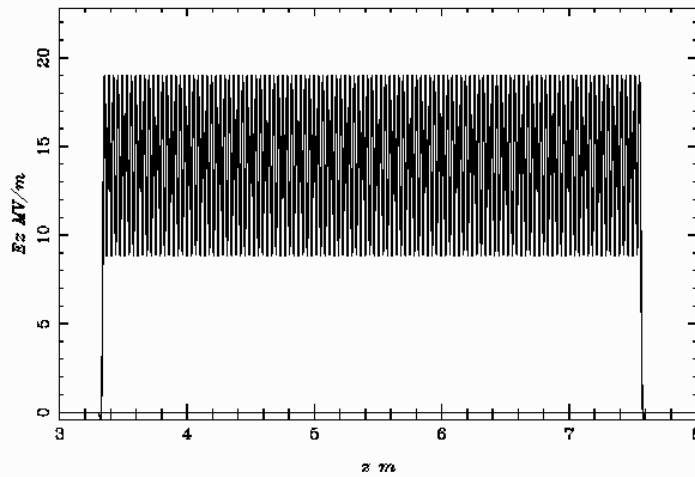
Solenoid No2	0.338	
Peak Field (T)		
Solenoid No3	0.2079	
Peak Field (T)		
Solenoid No4	0.75	
Peak Field (T)		

Travelling Wave Structures (TWS)

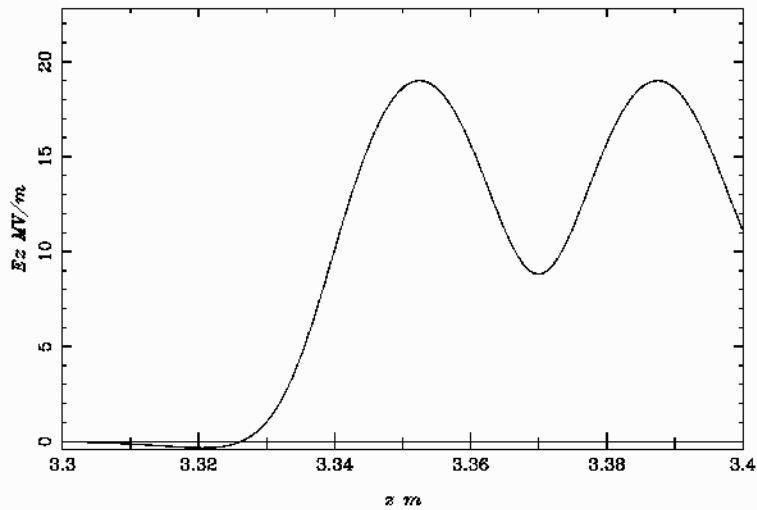
TABLE 10.3
Travelling Wave structure field

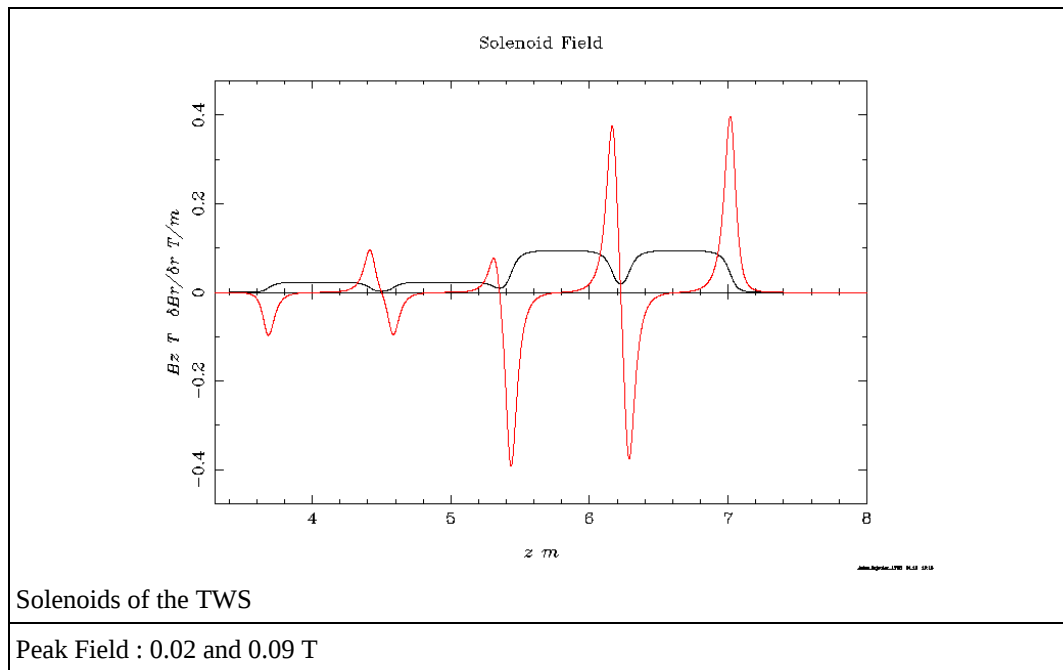
Number of cells	120
Frequency (GHz)	2.856
Peak Field (MV/m)	19

longitudinal electric field



longitudinal electric field





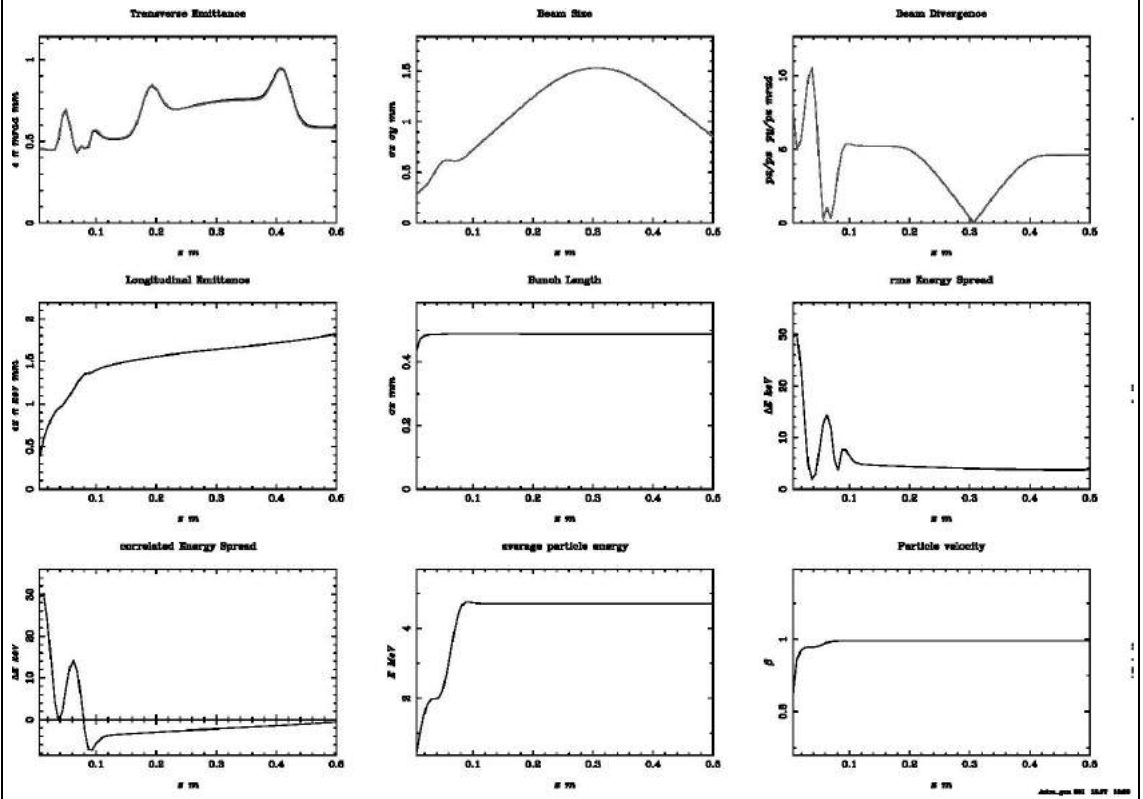
10.2 STEP 1. Solenoid choice

All solenoids were centered at 0.3m for this step. For the solenoid choice, the results of each solenoid for the most important beam parameters are presented. The ones taken in account mostly are presented in Table 10.4. Furthermore, not only the final values were taken into account, but also, the way these value evolve along the z-axis in Tables 10.4 and 10.5.

TABLE.10.4
 Overview of the parameters of the beam along the z-axis in the four solenoid cases.
 All solenoids are centered at 0.3m

Solenoid	Cs ₂ Te		
No1			
No2			

No3



No4

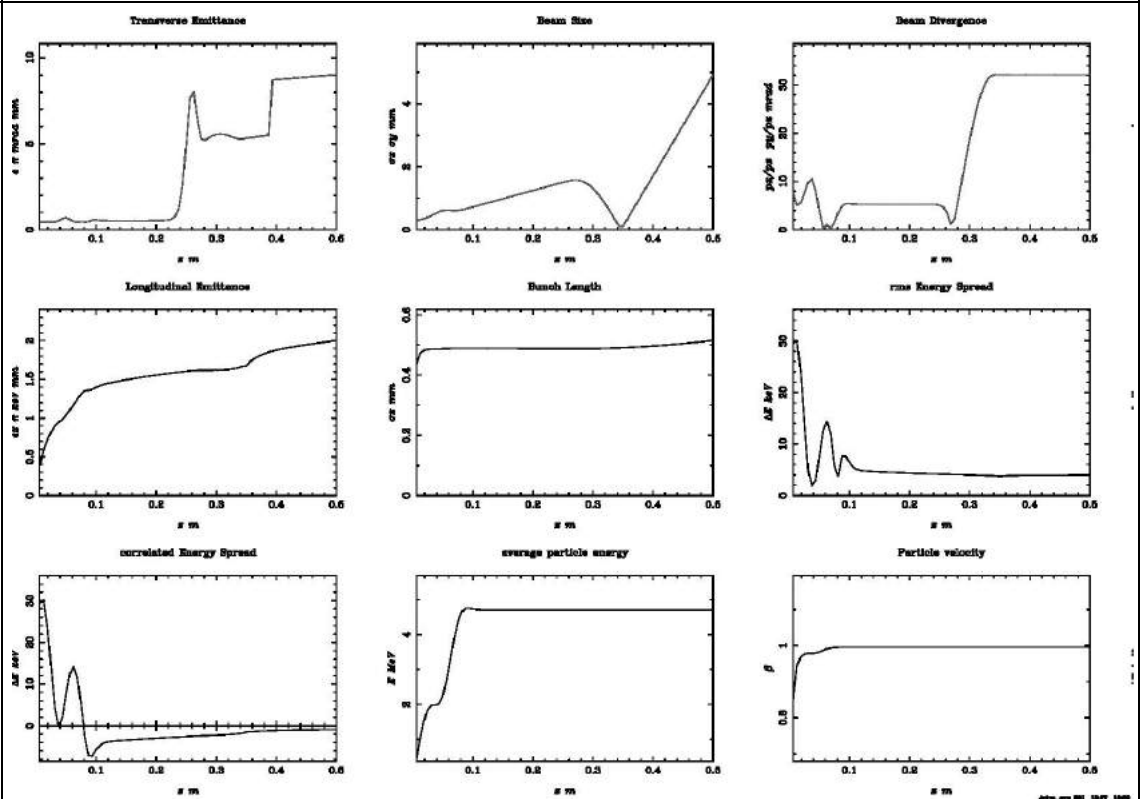
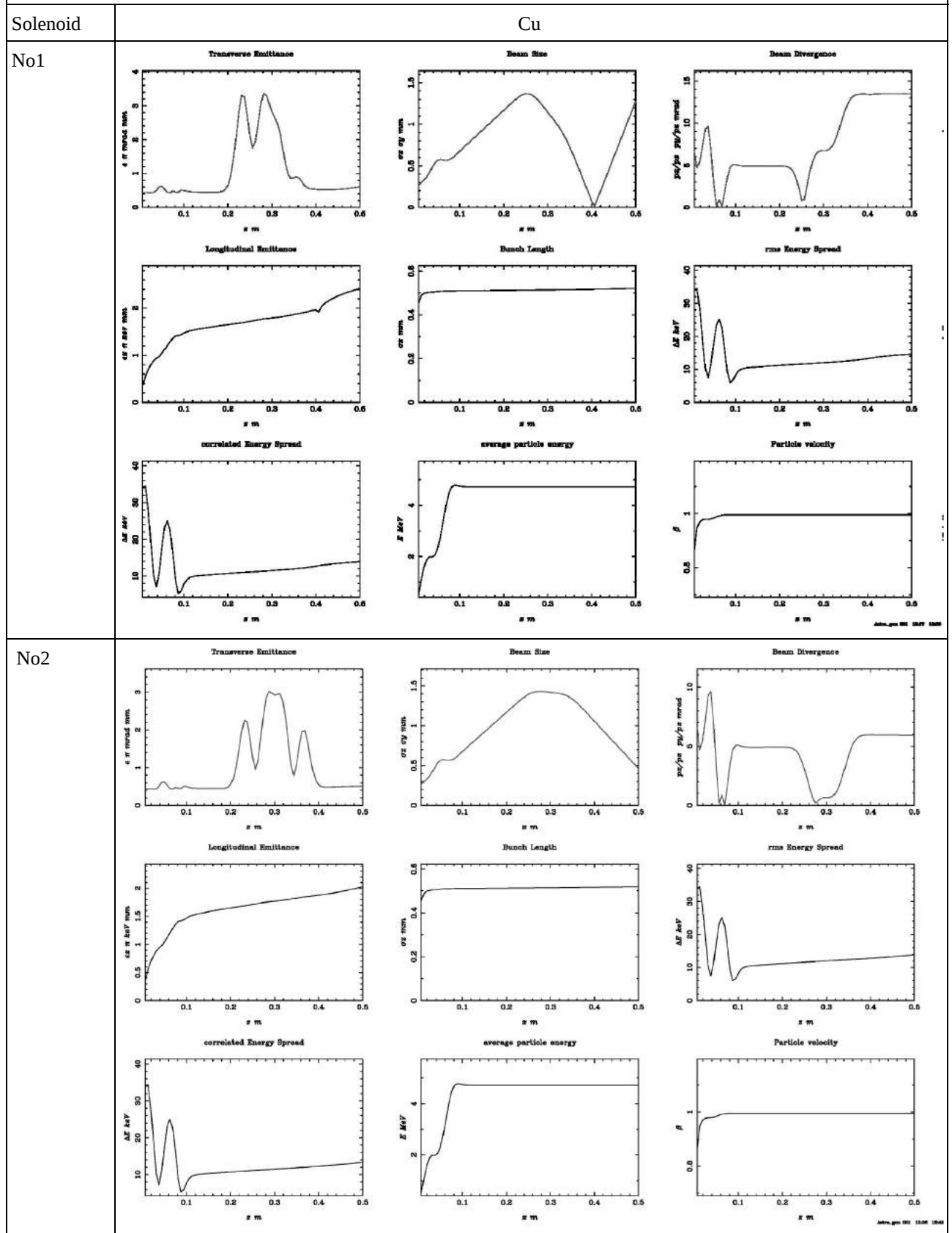
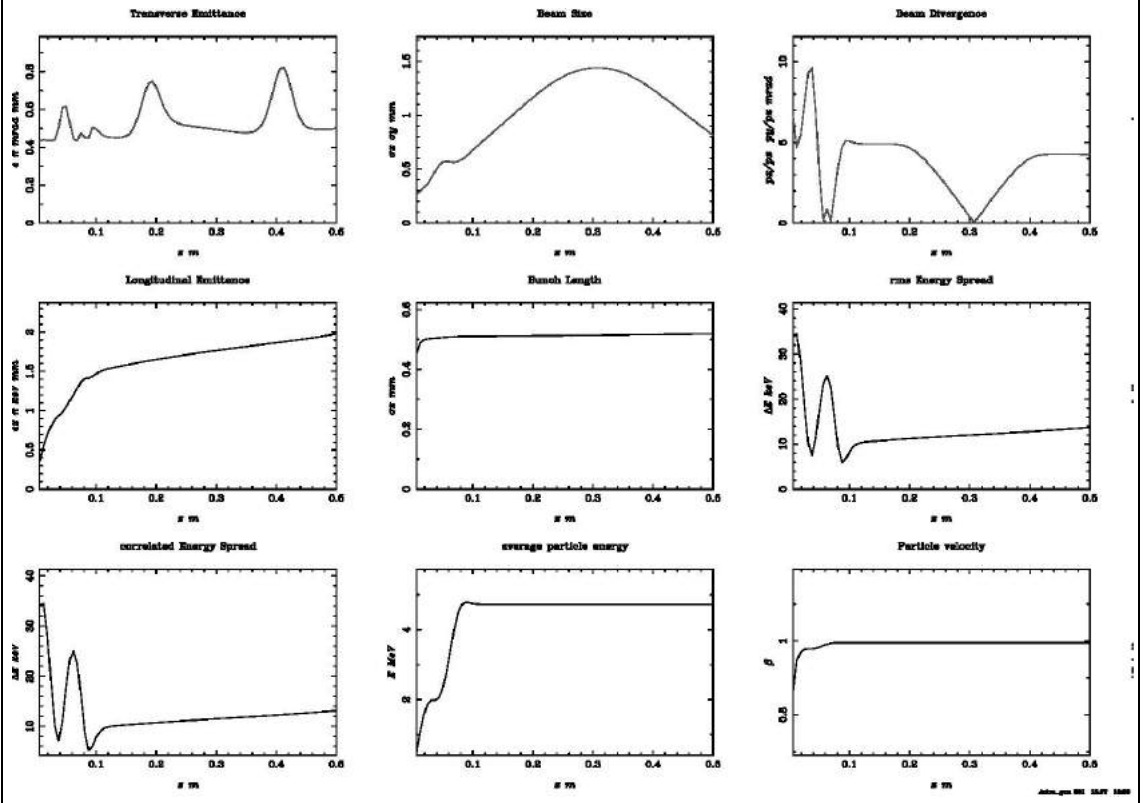


TABLE.10.5
 Overview of the parameters of the beam along the z-axis in the four solenoid cases.
 All solenoids are centered at 0.3m



No3



No4

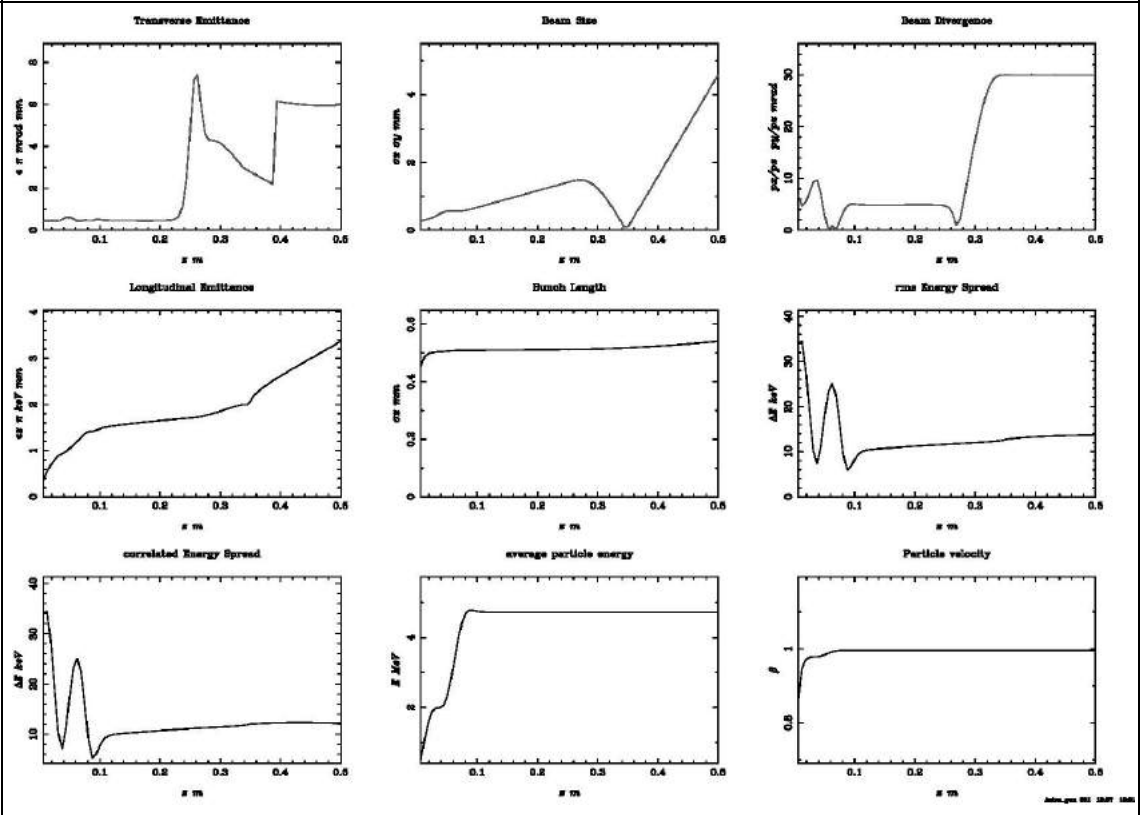


TABLE.10.6		
Overview of the most important parameters of the beam at the end of the simulation- somewhere in drift space - in the four solenoid cases.		
Solenoid No1	Cs₂Te	Cu
Transverse Emittance (pi mm mrad)	1.5	0.6
Beam size rms (mm)	1.4	1.3
Bunch Length rms (mm)	0.49	0.52
Solenoid No2	Cs₂Te	Cu
Transverse Emittance (pi mm mrad)	0.68	0.51
Beam size rms (mm)	0.47	0.51
Bunch Length rms (mm)	0.48	0.52
Solenoid No3	Cs₂Te	Cu
Transverse Emittance (pi mm mrad)	0.59	0.5
Beam size rms (mm)	0.85	0.81
Bunch Length rms (mm)	0.47	0.52
Solenoid No4	Cs₂Te	Cu
Transverse Emittance (pi mm mrad)	9.0	6.0
Beam size rms (mm)	4.9	4.6
Bunch Length rms (mm)	0.51	0.54

Comparison of solenoids

The first and the last solenoids are not suitable for the gun, most probably because of their high magnetic field, and they result in a waist very close to the solenoid- very small focal length- and also to a high variant envelope through the lattice. The second and the third seem to be more suitable and will be examined in the following procedure. As long as the different materials are concerned, the comparison is not reliable, because the lattices are not optimal.

In conclusion, the solenoids to be examined are:

	1.5 cells
Solenoid No1	X
Solenoid No2	OK
Solenoid No3	OK
Solenoid No4	X

10.3 STEP 2. Optimal beam waist

Without any change of the maximum value of the magnetic field, various positions of the solenoids have been tested in order to set an optimal working point.

10.3.1 Solenoid No 2

Cs₂Te

After a series of position scans between 0.1 and 0.6 m, the conclusion was that the solenoid shall be close to the Gun structure, which ends at 0.1m . Thus, the positions between 0.1m and 0.2m were taken into account for a more refined scan. The optimal results are presented in Table 10.7.

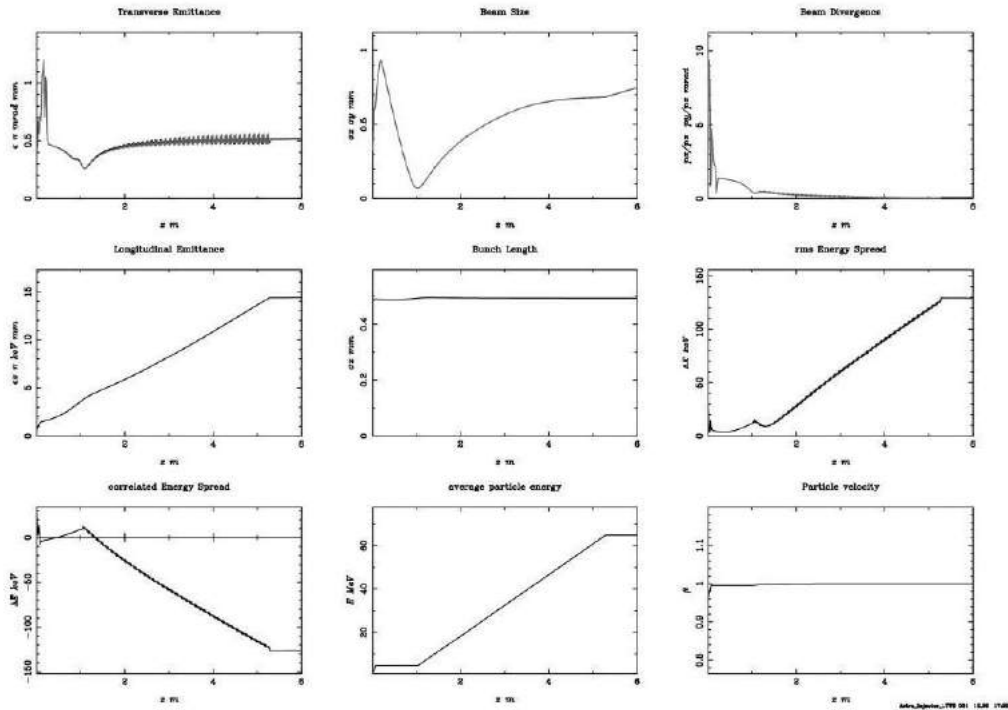
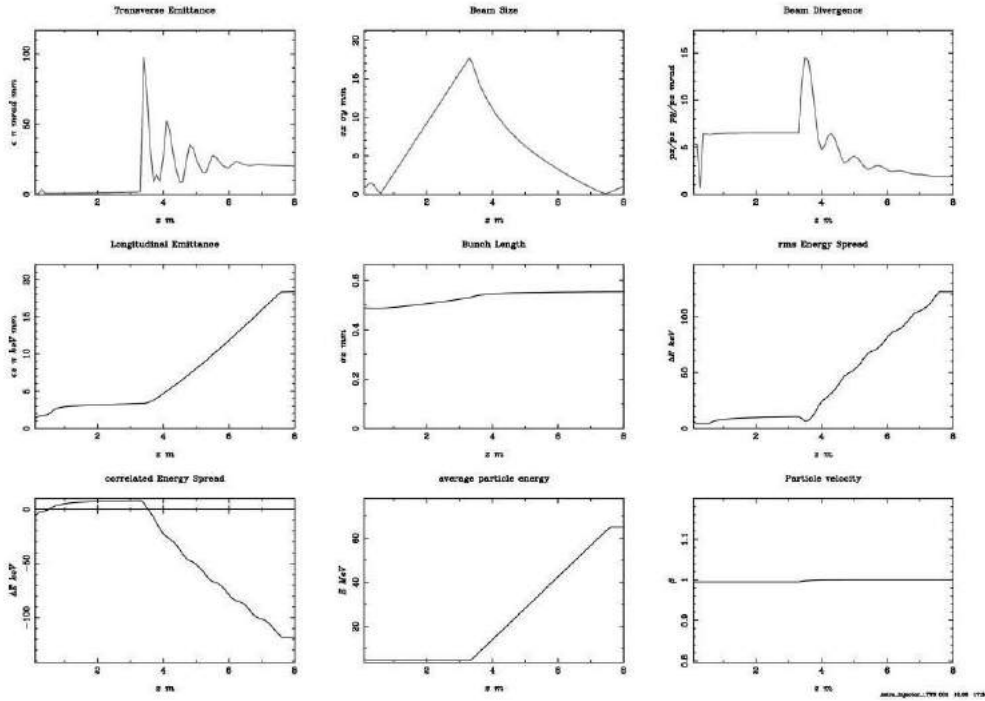
Run number	Solenoid position(m)	Beam waist position (m)	Minimum trans. Size (mm) (waist)	Emittance on waist (pi mm mrad)	Minimum emittance (pi pi mm mrad)	Position of min. Emittance (m)
4	0.14	1.2	0.16	0.36	0.28	1.5
5	0.15	1.01	0.08	0.32	0.28	1.09
6	0.16	0.86	0.04	0.32	0.32	0.9

The position of choice was 0.15m , as it provides the same emittance on waist as the third choice, as shown in Table 10.7, greater transverse size but more space for diagnostics in the beginning of the beam line. The first TWS (Travelling Wave Structure) entrance and the solenoids were shifted to the beam waist position 1.01m. The respective results are presented in Table 10.8, below:

optimisation	Transverse Size (mm)	Emittance (pi pi mm mrad)	Longitudinal Size (mm)	Brightness	Divergence
Before	1.0	20	0.55	$\ll \ll 10^{-3}$	1.9
After	0.75	0.51	0.49	0.3	0.087

TABLE.10.9

Overview of the parameters of the beam along the z-axis for the injector until the first TWS exit before and after the solenoid and TWS shift



Cu (Cu)

An identical procedure was followed for the Cu cathode case, as well, and the optimal results are presented below in Table 10.10:

TABLE.10.10 Three candidate solenoid positions and their results						
Run number	Solenoid position(m)	Beam waist position (m)	Minimum trans. Size (mm) (waist)	Emittance on waist (pi mm mrad)	Minimum emittance (pi pi mm mrad)	Position of min. Emittance (m)
4	0.14	1.2	0.18	0.31	0.22	1.6
5	0.15	1.09	0.08	0.26	0.22	1.2
6	0.16	0.9	0.04	0.27	0.26	0.9

The position of choice is 0.15m , as it provides the least emittance on waist. It is true that this choice does not provide the least transverse size, but the last choice shows the emittance minimum being on the waist position which is not desirable.

Comparison:

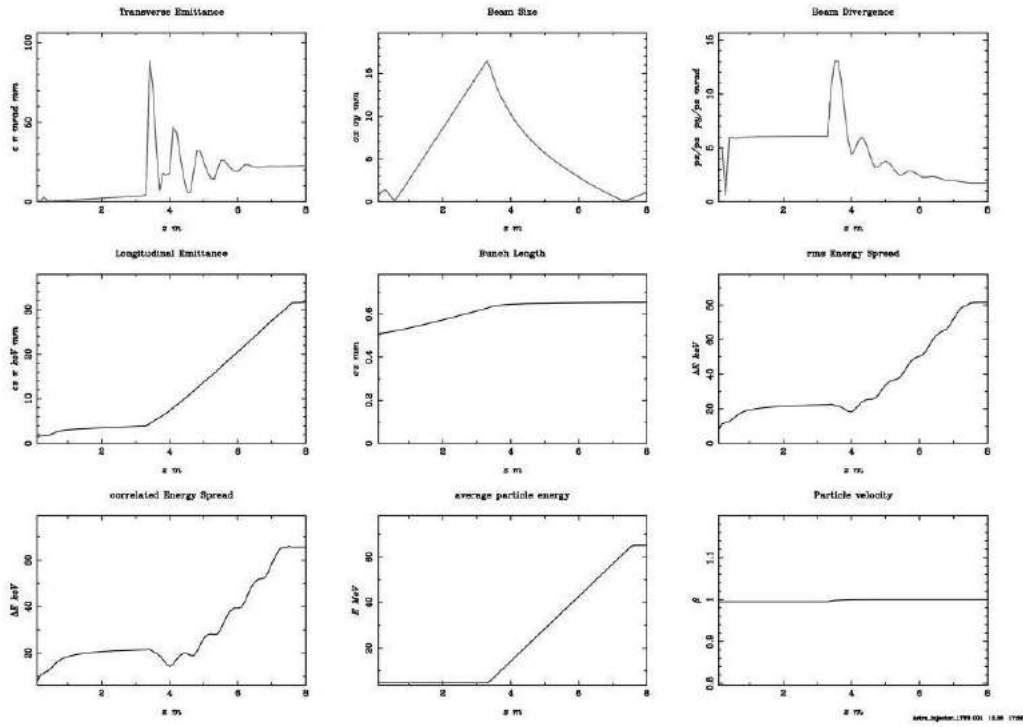
The beam waist position , as in previous simulations, differs several centimeters. The Cs₂Te photocathode case results in greater transverse emittance on waist although the rms radius is almost the same. The beam waist is also closer to the cathode for Cs₂Te. The optimal solenoid position in accuracy of centimeters is the same for both materials.

After having concluded in the position of 0.15m for the solenoid, the first TWS (Travelling Wave Structure) along with its solenoids is shifted to the beam waist position. The respective results are presented below in Table 10.11:

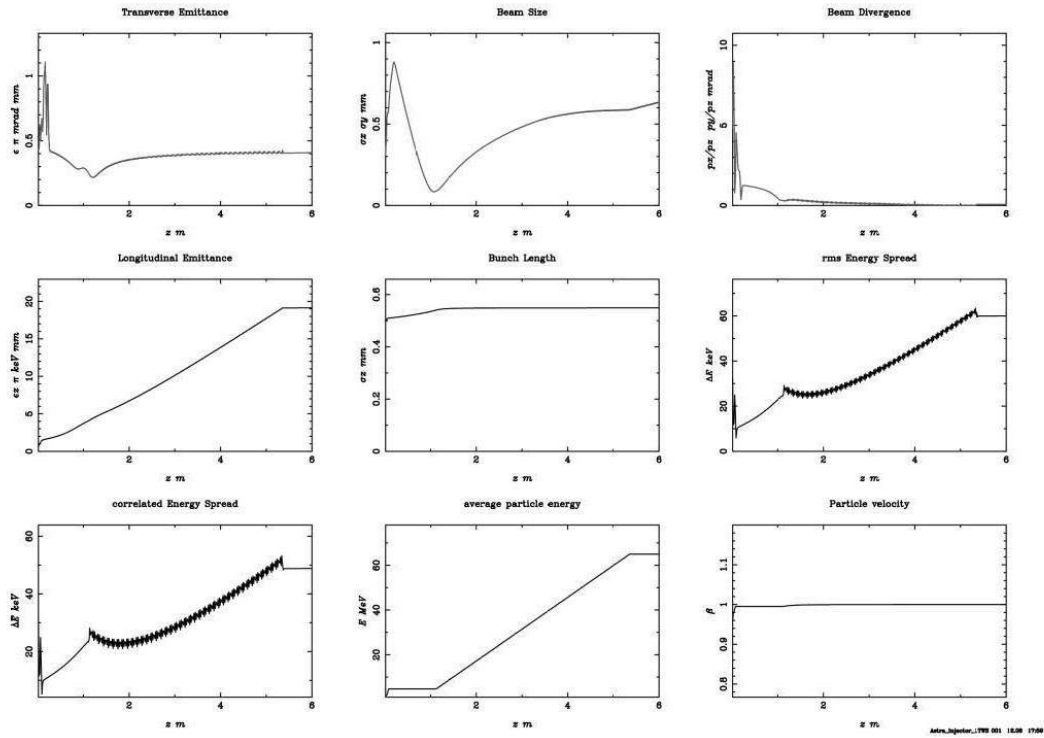
TABLE.10.11 Comparison of the results of the injector until the first TWS exit before and after the solenoid and TWS shift					
optimisation	Transverse Size (mm)	Emittance (pi pi mm mrad)	Longitudinal Size (mm)	Brightness	Divergence
Before	1.12	22.6	0.65	$\ll 10^{-3}$	1.8
After	0.63	0.41	0.55	0.5	0.07

TABLE.10.12

Overview of the parameters of the beam along the z-axis for the injector until the first TWS exit before and after the solenoid and TWS shift



Before – 0.3m solenoid – 3.3m First TWS



After – 0.15m – 1.01m First TWS

Comments on both materials:

It is obvious that the transverse emittance has decreased dramatically as well as its oscillation, proving the value of the *Ferrario Working Point*. All the important parameters have been improved. The oscillations seem to be denser in Cs₂Te optimised lattice but this is only because of the different resolution used during the simulation. The lattices presented above are not optimal, but they had been improved only by correctly shifting the solenoid position. Further optimisation was required, of course, and it was performed in the analysis presented later on, using the code GIOTTO (Chapter 7)

Comparison of the materials:

One should anticipate the Cu to result in less emittance than the Cs₂Te case, which is not valid here. That is because the lattice is not identical so the two results cannot be directly subject to comparison, as the positions of the TWS structures are different. The longitudinal size is greater for Cu as in simulations of Chapter 9.

10.3.2 Solenoid No 3

Cs₂Te

After a series of position scans between 0.1 and 0.6 m, the conclusion was that the solenoid shall be close to the Gun structure, which ends at 0.1m . Thus, the positions between 0.15 m and 0.25 m were taken into account for a more refined scan. The optimal results are presented in Table 10.13.

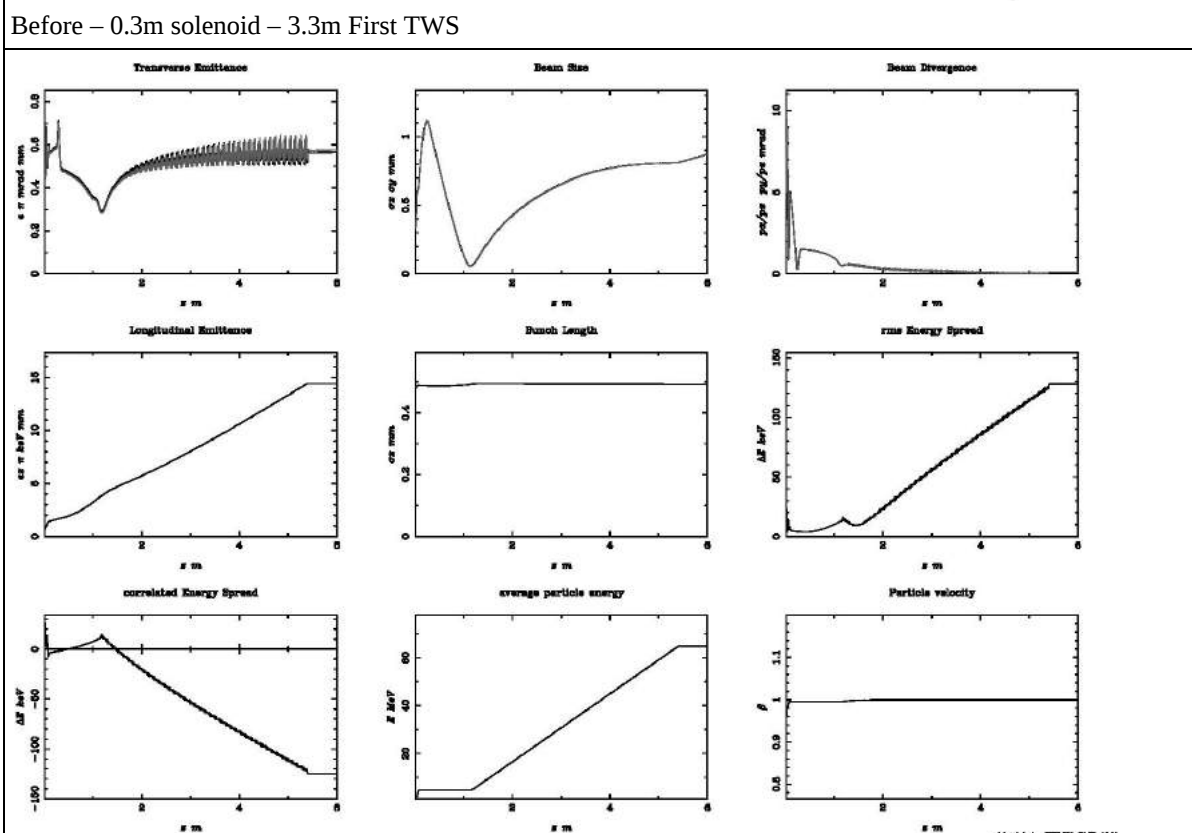
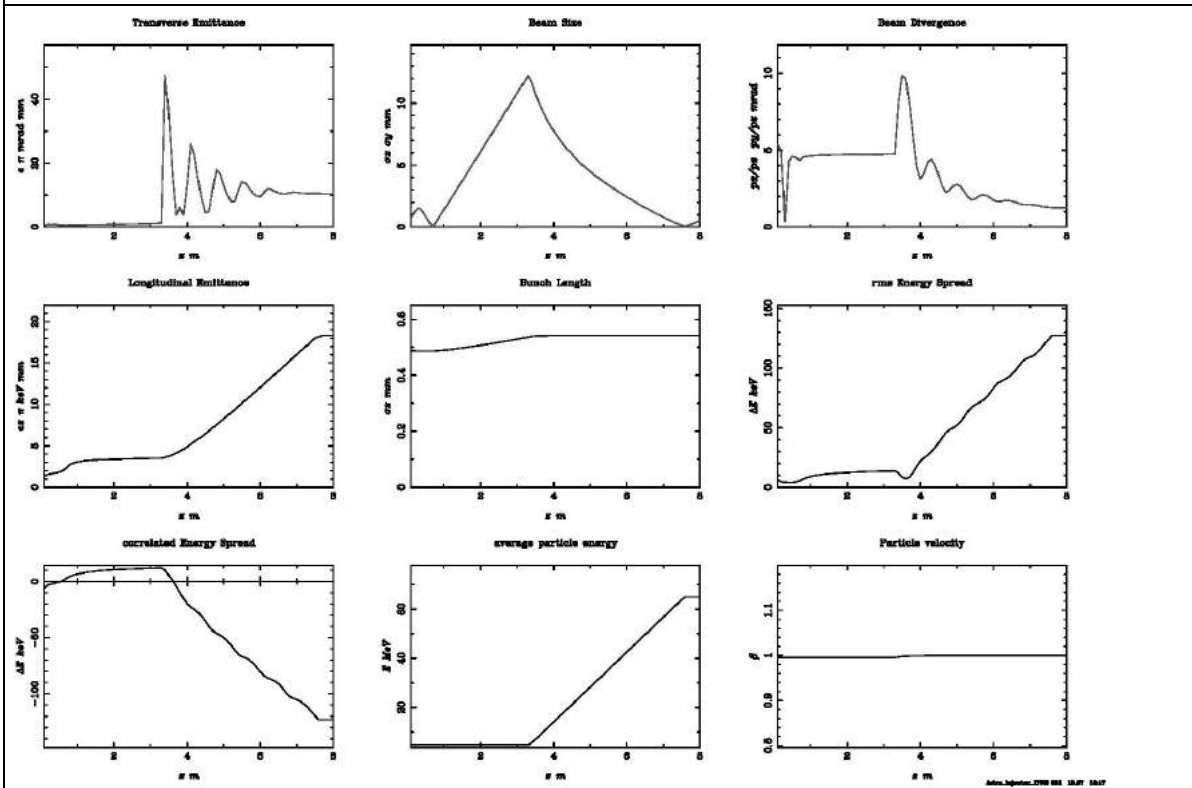
Run number	Solenoid position(m)	Beam waist position (m)	Minimum trans. Size (mm) (waist)	Emittance on waist (pi mm mrad)	Minimum emittance (pi pi mm mrad)	Position of min. Emittance (m)
4	0.18	1.31	0.11	0.32	0.27	1.46
5	0.19	1.13	0.058	0.32	0.30	1.16
6	0.20	0.98	0.039	0.32	0.32	1.01

The position of choice was 0.19m , as it provides the same emittance on waist as all the other choices, greater transverse size than the latter but more space for diagnostics in the beginning of the beam line and also less momentum divergence (A.23). The first TWS (Travelling Wave Structure) entrance was then set to the beam waist position and the solenoids were shifted accordingly. The respective results are presented below in Table 10.14:

optimisation	Transverse Size (mm)	Emittance (pi pi mm mrad)	Longitudinal Size (mm)	Brightness (nC/mrad mm ²)	Divergence (mrad)
Before	0.5	10	0.55	$\ll 10^{-2}$	1.2
After	0.88	0.58	0.5	0.25	0.1

TABLE.10.15

Overview of the parameters of the beam along the z-axis for the injector until the first TWS exit before and after the solenoid and TWS shift



Comparison with Solenoid No2 :

TABLE.10.16					
Comparison of the results of the injector until the first TWS exit of the two solenoids after their and the TWS shift					
	Transverse Size (mm)	Emittance (pi pi mm mrad)	Longitudinal Size (mm)	Brightness (nC/mrad mm ²)	Divergence (mrad)
Solenoid No2	0.75	0.51	0.49	0.3	0.087
Solenoid No3	0.88	0.58	0.5	0.25	0.1

As Table 10.16 indicates, Solenoid No 2 seems to provide slightly better results than No 3. But the difference is not enough to make a safe comparison.

Cu(Cu)

After the same procedure that was followed above for Cs₂Te, the three candidates solenoid positions were chosen and their results are presented in Table 10.17.

TABLE.10.17						
Three candidate solenoid positions and their results						
Run number	Solenoid position(m)	Beam waist position (m)	Minimum trans. Size (mm) (waist)	Emittance on waist (pi mm mrad)	Minimum emittance (pi pi mm mrad)	Position of min. Emittance (m)
4	0.18	1.35	0.13	0.30	0.23	1.58
5	0.19	1.16	0.062	0.28	0.24	1.24
6	0.20	1.01	0.037	0.29	0.28	1.05

The position of choice was 0.19m , as it provides a similar emittance on waist with all the other choices, greater transverse size than the latter but more space for diagnostics in the beginning of the beam line and also less momentum divergence (A.23). The first TWS (Travelling Wave Structure) entrance was then set to the beam waist position and the solenoids were shifted accordingly.

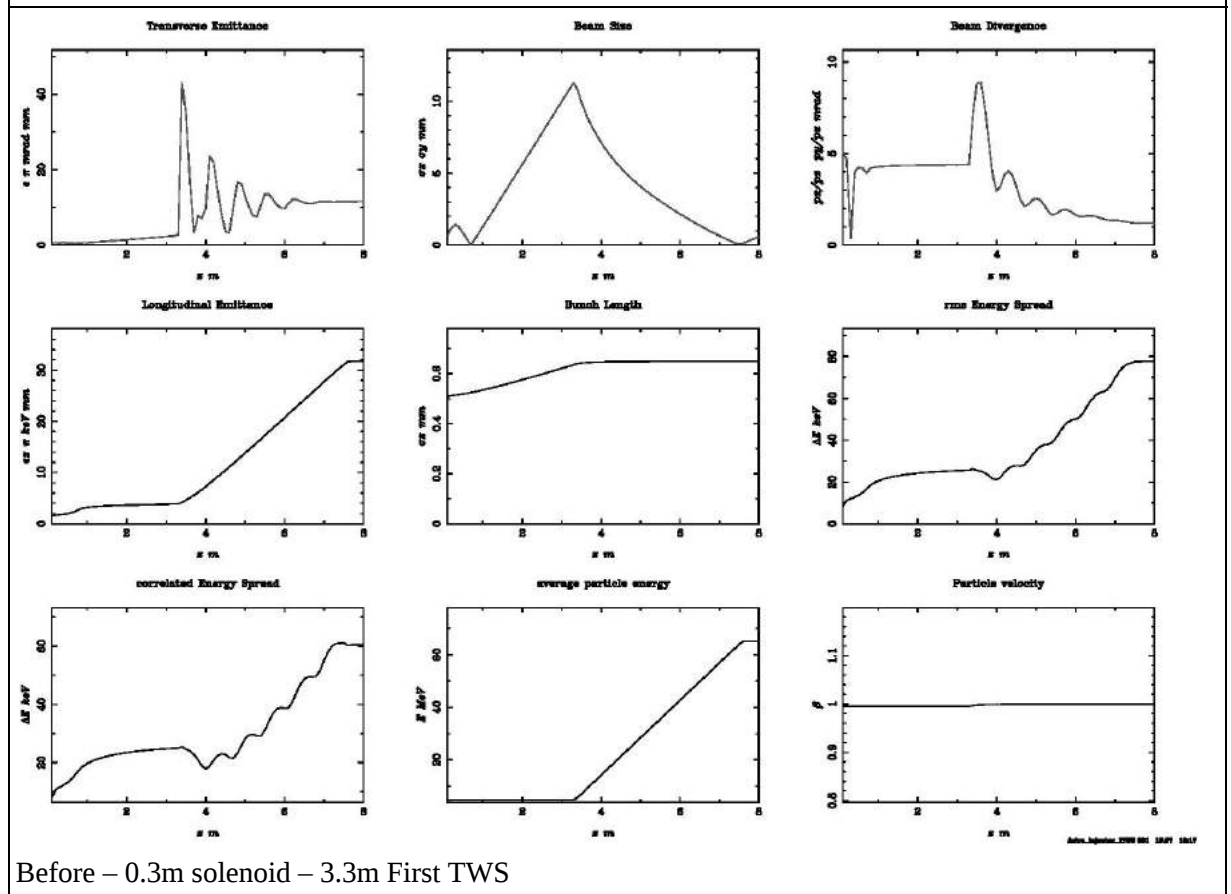
Comparison between the materials:

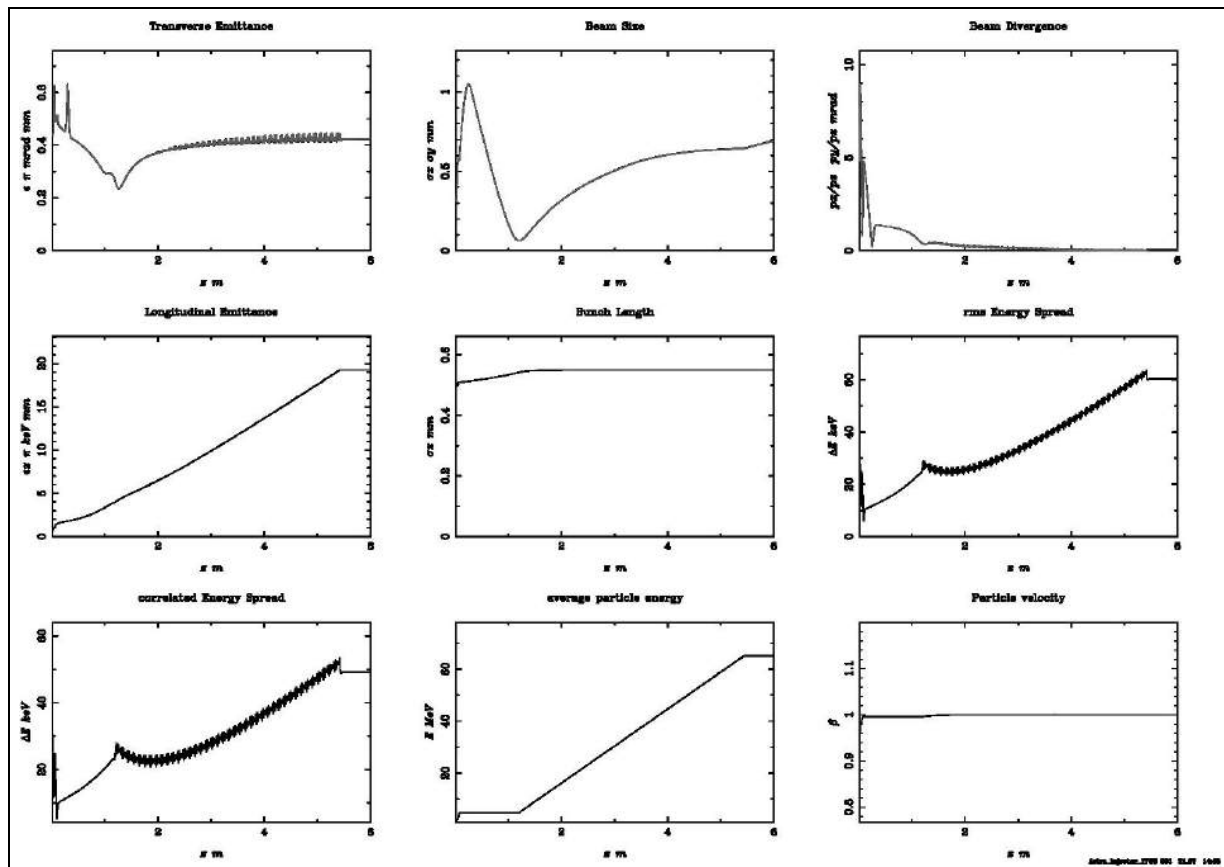
The differences that concern the lattice are slightly increased in comparison with the previous setup, even though this increase is not intense. The waist position is closer to the cathode in the Cs₂Te cathode case, as it was for the previous solenoid. As for the emittance, it is greater for Cs₂Te.

After having concluded in the position of 0.19m for the solenoid, the first TWS (Travelling Wave Structure) was shifted to the beam waist position. The results are presented in Table 10.18.

TABLE.10.18					
Comparison of the results of the injector until the first TWS exit before and after the solenoid and TWS shift					
optimisation	Transverse Size (mm)	Emittance (π π mm mrad)	Longitudinal Size (mm)	Brightness (nC/mrad mm ²)	Divergence (mrad)
Before	0.6	12	0.65	$\ll 10^{-2}$	1.2
After	0.7	0.42	0.55	0.5	0.083

TABLE.10.19
Overview of the parameters of the beam along the z-axis for the injector until the first TWS exit before and after the solenoid and TWS shift





After – 0.19m – 1.16m First TWS

Comments for both materials:

The transverse emittance has decreased from 10 to 0.5 pi mm mrad and 12 to 0.42 pi mm mrad and also its oscillation margins have been significantly limited, proving the FWP (Chapter 5). All the important parameters have been improved, as well. The oscillations again seem to be denser in the optimised lattice but this is only because of the different resolution used during the simulation. The lattice is not optimal, yet, but it was improved only by correctly shifting the solenoid position. Further optimisation was required and it is presented in the analysis later on, using Genetic optimisation algorithm (GIOTTO).

Comparison with Cs2Te case:

The Cu case resulted in less emittance than the Cs2Te case, as well as in greater longitudinal size. The oscillations in the Cu case seem to be more effectively dumped than in Cs₂Te case, indicated that the TWS was more effectively matched to the waist position meeting the FWP.

Comparison with Solenoid No2:

TABLE.10.20					
Comparison of the performance of the two cases of injectors with different solenoids after the solenoid and TWS position shift.					
	Transverse Size (mm)	Emittance (pi pi mm mrad)	Longitudinal Size (mm)	Brightness (nC/mrad mm ²)	Divergence (mrad)
Solenoid No2	0.63	0.41	0.55	0.5	0.07
Solenoid No3	0.7	0.42	0.55	0.5	0.083

Just like in the Cs₂Te case, Solenoid No 2 seems to provide better results but the difference is not enough to make a safe comparison and in further optimisation (e.g. more careful position scanning, or more fine Runge-Kutta steps) the results may differ.

10.4 STEP 3. GIOTTO optimisation of the Gun and TWS

At this point, it should be mentioned that due to lack of resources the optimisations were stopped before finishing the 400 generations that were predefined. The algorithm was interrupted only if the best individual was the same for several generations. So the choice can be considered safe. For the rest of the chapter, for each GIOTTO optimisation, all the user defined parameters used are presented in the first section of the sub-chapter.

10.4.1 Solenoid No 2

The parameters that were used for the first GIOTTO optimisation are in Table 10.21. The population size should be close to $7^2 = 49$ and a multiple of the cores used by GIOTTO. Although the best number to choose would be 48 or 52, 36 was chosen instead due to long computation time.

TABLE.10.21 Algorithm parameters overview	
Number of genes	7
Number of individuals	36
Number of generations used	134
Number of CPUs	4
Fitness function	Lorentzian
Parameters of fitness function	SigX,emitX,SigZ

TABLE.10.22 Parameters before and after optimisation			
Parameters	Initial value	Range	Final value
Laser spot size (rms) / sig_x (mm)	0.20	0.02	0.166
Phase shift of the gun / Phi(1) (degrees)	0.0	5.0	3.26
Phase shift of the TWS / Phi(2) (degrees)	0.0	20.0	-14.8
Peak field of TWS / MaxE(2) (MV/m)	19	5.0	24.16
Entrance position of TWS / C_pos(2) (m)	1.09	0.1	1.186

Peak field of the gun's solenoid / MaxB(1) (T)	0.338	0.03	0.346
Position of the gun's solenoid / S_pos(1) (m)	0.15	0.03	0.125

The Fitness function:

The fitness function, as mentioned in Chapter 7, is a function that the algorithm tries to maximize. The quantities that need to be minimized are the transverse emittance, the transverse size and the longitudinal size. So, a function that maximizes around the wanted values is what one should define.

The functions of choice were a Lorentzian and a Gaussian function. A Lorentzian is less sharp around its maximum value than a Gaussian; this means that a Lorentzian fitness function allows a wider variety of individuals to survive the next generation. So, if the lattice is not near the optimum the individuals may be “trapped” in a local optimum and become very similar, which will ruin the process that needs a variety of genes-individuals to be functional.

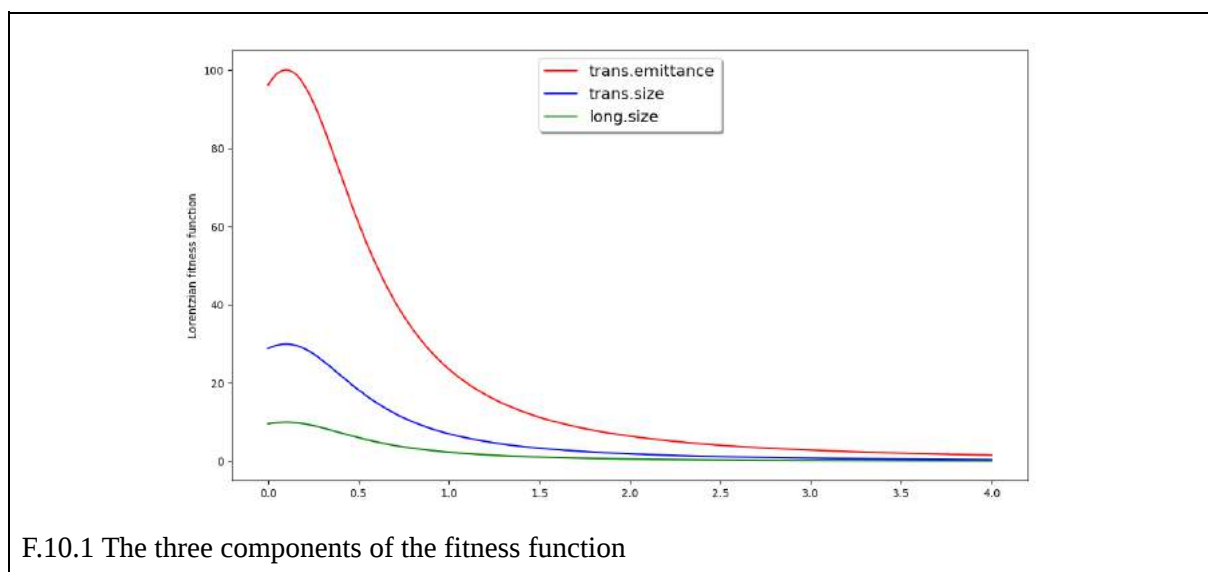
A Gaussian function was firstly tested, but ,due to lack of computing resources, the individuals that could be created were not enough to keep the required variety in a “Gaussian environment” that is steeper. Three figures of merit were used, the transverse emittance centered at 0.1 pi mm mrad, the transverse size centered at 0.2mm and the longitudinal size centered at 0.3mm. The Lorentzian function used is the one below.

In Reverse Polish Notation :

```
0.5 sqr emitX 0.10 - sqr 0.5 sqr + / 100 *
0.5 sqr sigX 0.20 - sqr 0.5 sqr + / 30 * +
0.5 sqr sigZ 0.30 - sqr 0.5 sqr + / 10 * +
```

or

$$F = 100 * \left(\frac{0.5^2}{0.5^2 + (\text{emitX} - 0.10)^2} \right) + 30 * \left(\frac{0.5^2}{0.5^2 + (\text{sigX} - 0.20)^2} \right) + 10 * \left(\frac{0.5^2}{0.5^2 + (\text{sigZ} - 0.30)^2} \right) \quad (10.1)$$



F.10.1 The three components of the fitness function

TABLE.10.23 Target values of the figures of merit	
Parameter	Target value
Emittance (π mm mrad) x-axis	0.1
Transverse Size (mm) x-axis	0.2
Longitudinal Size (mm)	0.3

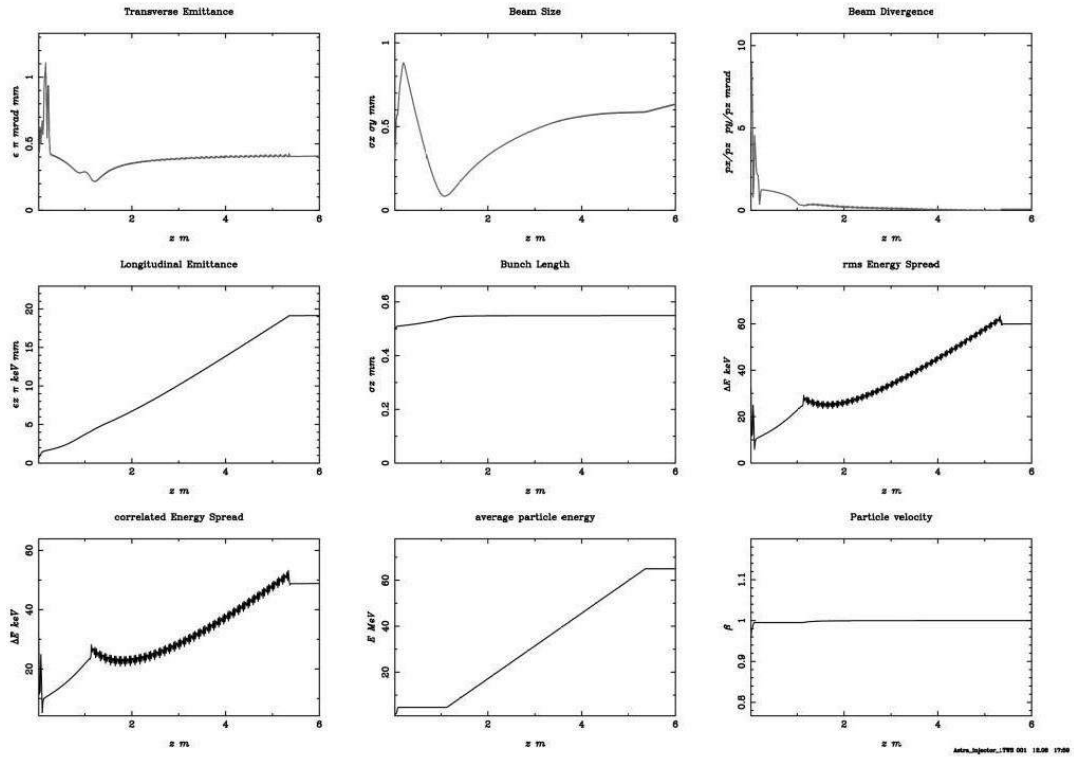
The desirable transverse size is smaller than 0.2 mm, but without the solenoids it could not be achieved in previous attempts of optimisation. So a higher value was targeted for this step. The fitness function was adjusted respectively in the next step of optimisation.

Final Results

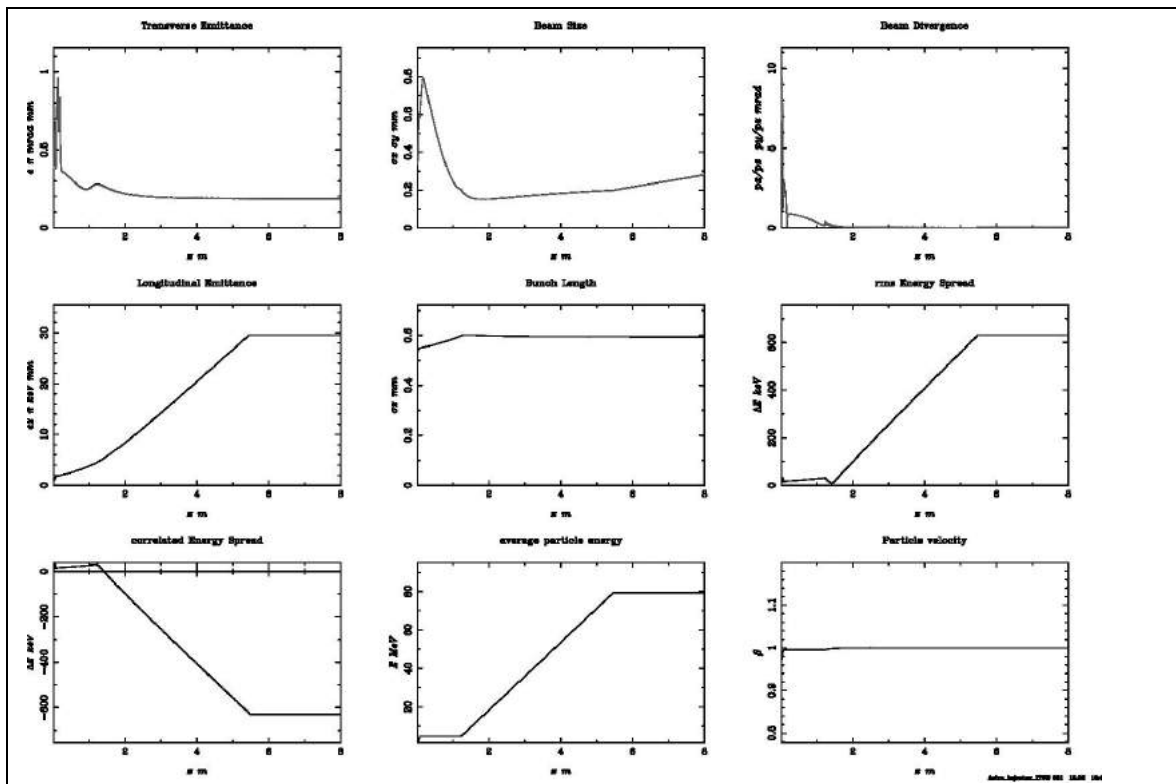
TABLE.10.24 Values of the figures of merit before and after optimisation (without TWS solenoids)		
	Before	After
Emittance (π mm mrad) x-axis	0.41	0.188
Transverse Size (mm) x-axis	0.63	0.218
Longitudinal Size (mm)	0.55	0.595
Divergence (mrad)	0.07	0.033
Emittance (π mm mrad) y-axis	-	0.191
Transverse Size (mm) y-axis	-	0.220

TABLE.10.25

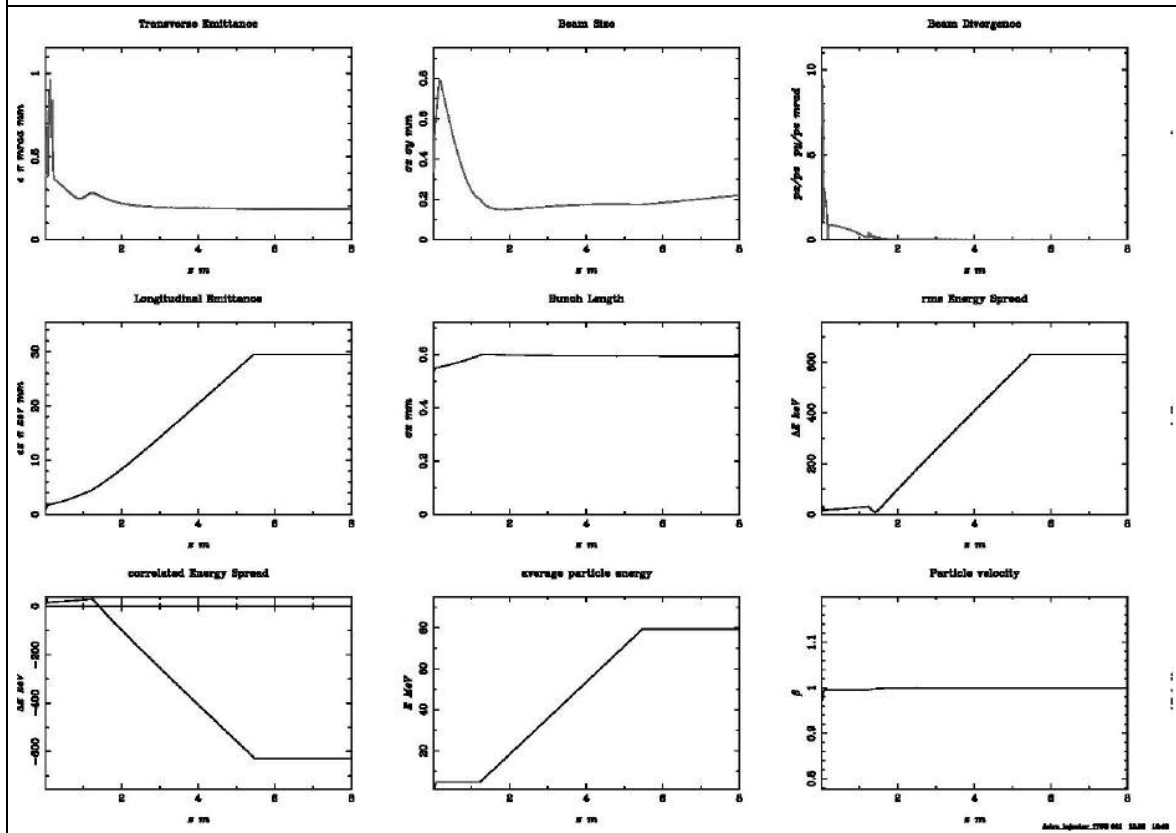
Overview of the parameters of the beam along the z-axis for the injector until the first TWS exit before and after optimisation. Two cases are presented after optimisation, one with the TWS solenoids absent (as it was during optimisation) and one with the solenoids shifted according to the TWS shift.



Before GIOTTO optimisation



After Giotto optimisation – with no solenoids of the TWS



After Giotto optimisation – with the solenoids shifted according to the TWS shift

Comments:

As shown in Tables 10.24 and 10.25, after the first optimisation, all the beams parameters have been obviously improved the the oscillations have been successively dumped , meaning that the *Ferrario Working Point* was automatically and successfully met. The lattice is not ready yet because there are no solenoids around the TWS. The application of the solenoid fields seem to improve the results, as it is shown in Table 10.25, although further optimisation will be applied.

10.4.2 Solenoid No 3

In Table 10.26 the algorithm parameters used for the genetic algorithm are presented. The population size should be close to $7^2 = 49$ and a multiple of the cores used by GIOTTO, thus 3. Although the best number to choose would be 48 or 51, 42 was chosen instead due to long computation time.

TABLE.10.26 Algorithm parameters overview	
Number of genes	7
Number of individuals	42
Number of generations used	150
Number of CPUs	3
Fitness function	Lorentzian
Parameters of fitness function	SigX,emitX,SigZ

TABLE.10.27 Parameters before and after optimisation			
Parameters	Initial value	Range	Final value
Laser spot size (rms) / sig_x (mm)	0.20	0.02	0.183
Phase shift of the gun / Phi(1) (degrees)	0.0	5.0	-1.14
Phase shift of the TWS / Phi(2) (degrees)	0.0	20.0	-42.4
Peak field of TWS / MaxE(2) (MV/m)	19	5.0	14.4
Entrance position of TWS / C_pos(2) (m)	1.15	0.1	1.309
Peak field of the gun's solenoid / MaxB(1) (T)	0.2079	0.03	0.202
Position of the gun's solenoid / S_pos(1) (m)	0.19	0.03	0.178

The Fitness function:

The Lorentzian function used was the same as in the previous optimisation.

In Reverse Polish Notation :

$$0.5 \text{ sqr emitX } 0.10 - \text{ sqr } 0.5 \text{ sqr } + / 100 *$$

$$0.5 \text{ sqr sigX } 0.20 - \text{ sqr } 0.5 \text{ sqr } + / 30 * +$$

$$0.5 \text{ sqr sigZ } 0.30 - \text{ sqr } 0.5 \text{ sqr } + / 10 * +$$

or

$$F = 100 * \left(\frac{0.5^2}{0.5^2 + (\text{emitX} - 0.10)^2} \right) + 30 * \left(\frac{0.5^2}{0.5^2 + (\text{sigX} - 0.20)^2} \right) + 10 * \left(\frac{0.5^2}{0.5^2 + (\text{sigZ} - 0.30)^2} \right) \quad (10.2)$$

Parameter	Target value
Emittance (π mm mrad) x-axis	0.1
Transverse Size (mm) x-axis	0.2
Longitudinal Size (mm)	0.3

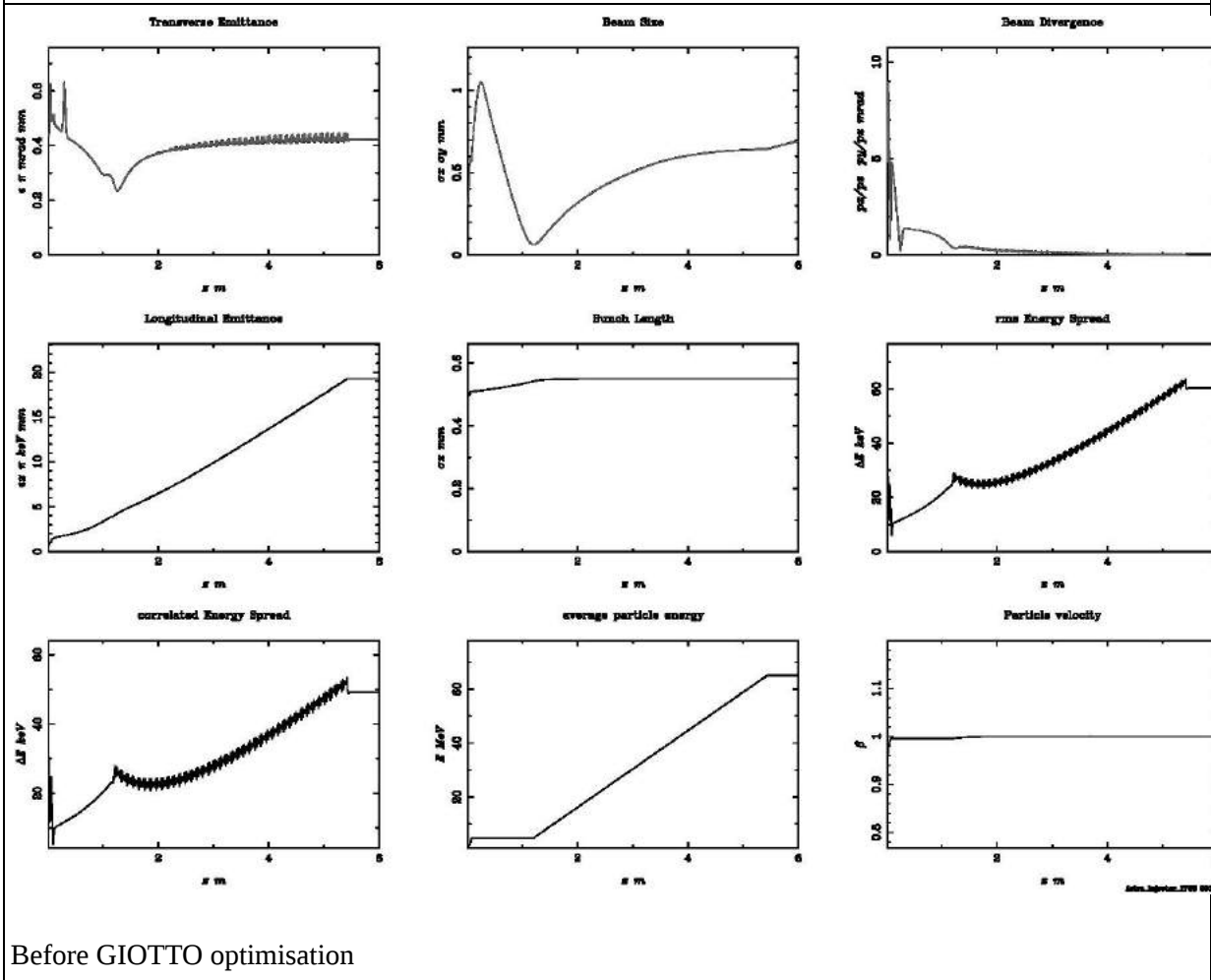
The desirable transverse size is smaller than 0.2 mm, but without the solenoids it could not be achieved in previous attempts of optimisation. So a higher value was targeted for this step. The fitness function was adjusted respectively in the next step of optimisation.

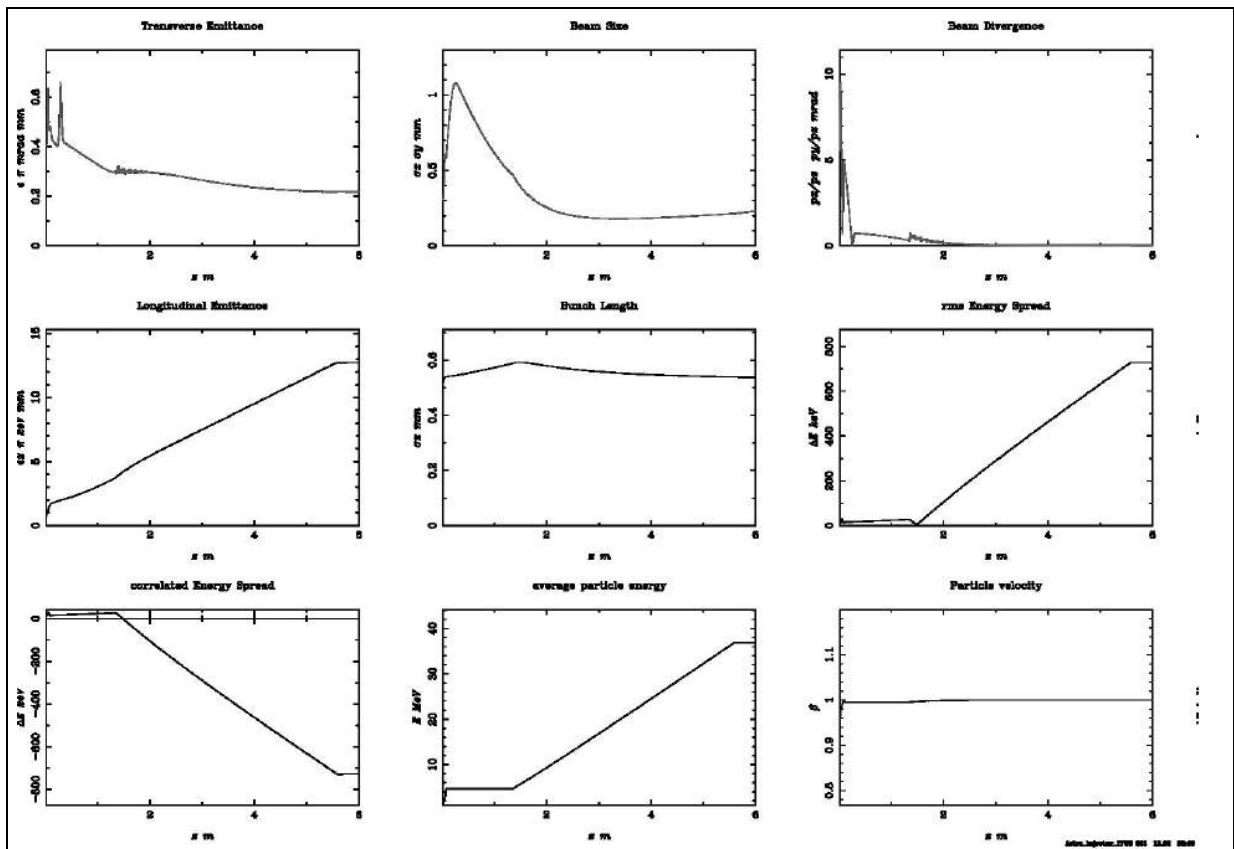
Final Results

	Before	After
Emittance (π mm mrad) x-axis	0.42	0.232
Transverse Size (mm) x-axis	0.7	0.258
Longitudinal Size (mm)	0.55	0.495
Divergence (mrad)	0.083	0.052
Emittance (π mm mrad) y-axis	-	0.225
Transverse Size (mm) y-axis	-	0.254

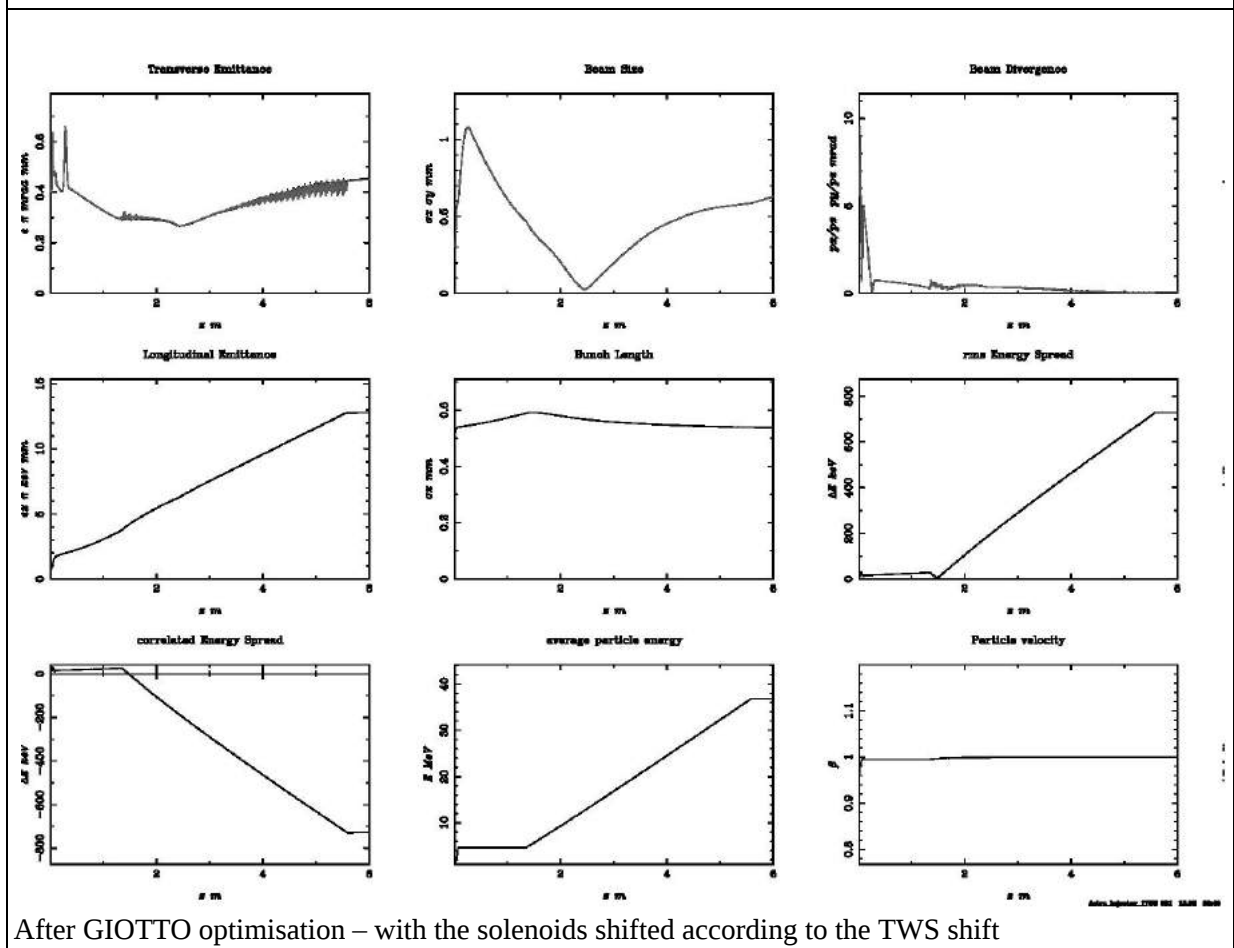
TABLE.10.30

Overview of the parameters of the beam along the z-axis for the injector until the first TWS exit before and after optimisation. Two cases are presented after optimisation, one with the TWS solenoids absent (as it was during optimisation) and one with the solenoids shifted according to the TWS shift.





After Giotto optimisation – with no solenoids of the TWS



After Giotto optimisation – with the solenoids shifted according to the TWS shift

Comments:

After optimisation, the transverse emittance decreased in half its original value, Table 10.29, the beam radius decreased ~60% and the bunch length was slightly decreased, as well. According to Table 10.30, the oscillations without the TWS solenoids seem to have been dumped effectively. Although, the application of the solenoids seem to enhance the remaining oscillations, destroy the emittance. and unacceptably increase the transverse size Thus, further optimisation seems necessary.

10.4.3 Comments and conclusions

It is remarkable that the input parameters did not change dramatically, although completely changed the beam's profile and performance, proving how sensitive the beam is to proper combination and tuning of parameters. Another point worth mentioning, is that although the solenoids have been set to zero, in this step, the performance is satisfactory enough. As shown in later analysis, the solenoids will not alter significantly the emittance evolution but only the transverse size focusing.

Another fact to underline is that in relation (A.35) it is indicated that if the energy spread is significant, so will be the emittance growth even at drift space. It is obvious that GIOTTO minimized the quantity without a user definition; it came 'naturally' with the minimization of the emittance.

10.5 STEP 4. GIOTTO optimisation

At this point, it should be mentioned that due to lack of resources the optimisations were stopped before finishing the 400 generations that were predefined. The algorithm was interrupted only if the best individual was the same for several generations. So the choice can be considered safe.

10.5.1 Solenoid No 2

In Table 10.31 the algorithm parameters used for the genetic algorithm are presented. The population size should be close to $9^2 = 81$ and a multiple of the cores used by GIOTTO, thus 4. Although the best number to choose would be 80 or 84, 48 was chosen instead, due to long computation time and lack of computational resources.

TABLE.10.31 Algorithm parameters overview	
Number of genes	9
Number of individuals	48
Number of generations used	57
Number of CPUs	4
Fitness function	Gaussian
Parameters of fitness function	SigX,emitX,SigZ

Comments:

The number of generations used is relatively low because there was no improvement after a small number of generations and the results were satisfactory enough. As for a fitness function a Lorentzian one was firstly tested but it was not useful, because the fitness value of all the individuals became very high too soon, so there was no diversity in the population to correctly perform the algorithm. As a

result, a Gaussian was preferable.

TABLE.10.32 Parameters before and after optimisation			
Parameters	Initial value	Range	Final value
Laser spot size (rms) / sig_x (mm)	0.166	0.02	0.162
Peak field TWS Solenoid No 1 MaxB(2) (T)	0.023026	0.08	0.086768
Peak field TWS Solenoid No 2 MaxB(3) (T)	0.023026	0.08	-0.0580967
Peak field TWS Solenoid No 3 MaxB(4) (T)	0.094228	0.08	0.151768
Peak field TWS Solenoid No 4 MaxB(5) (T)	0.094228	0.08	0.151741
Position TWS Solenoid No 1 S_pos(2) (m)	1.19	0.2	1.527
Position TWS Solenoid No 2 S_pos(3) (m)	2.09	0.2	2.016
Position TWS Solenoid No 3 S_pos(4) (m)	2.94	0.2	3.062
Position TWS Solenoid No 4 S_pos(5) (m)	3.79	0.2	3.723
Phase shift of the gun / Phi(1) (degrees)	3.26	-	3.26
Phase shift of the TWS / Phi(2) (degrees)	-14.8	-	-14.8
Peak field of TWS / MaxE(2) (MV/m)	24.16	-	24.16

Entrance position of TWS / C_pos(2) (m)	1.186	-	1.186
Peak field of the gun's solenoid / MaxB(1) (T)	0.346	-	0.346
Position of the gun's solenoid / S_pos(1) (m)	0.125	-	0.125

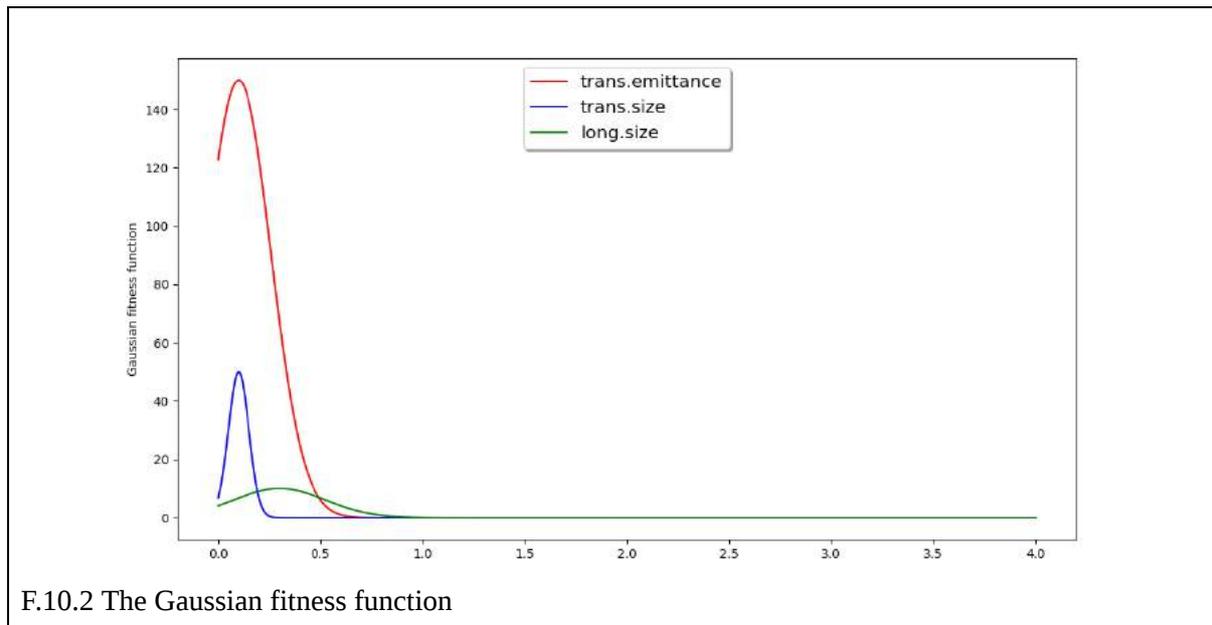
The Fitness function:

The Gaussian function used is in Reverse Polish Notation :

```
emitX 0.1 - 0.05 / sqr -1. * exp 150 *
sigX 0.1 - 0.005 / sqr -1. * exp 50 * +
sigZ 0.30 - 0.1 / sqr -1. * exp 10 * +
```

or

$$F = 150 * e^{\frac{-(emitX-0.1)^2}{0.05}} + 50 * e^{\frac{-(sigX-0.1)^2}{0.005}} + 10 * e^{\frac{-(sigZ-0.3)^2}{0.1}} \quad (10.3)$$



Once again, the weight factors were chosen so that the transverse emittance is the most preferable variable for optimisation. Also, the denominators represent a precision preference, so the blue line - transverse size- is steeper for greater accuracy. In the emittance, the required accuracy is lower in order to provide diversity to the individuals with a greater algorithm performance as a purpose. It is obvious, though, that the function is more steep and practically zero away from the center of the Gaussians.

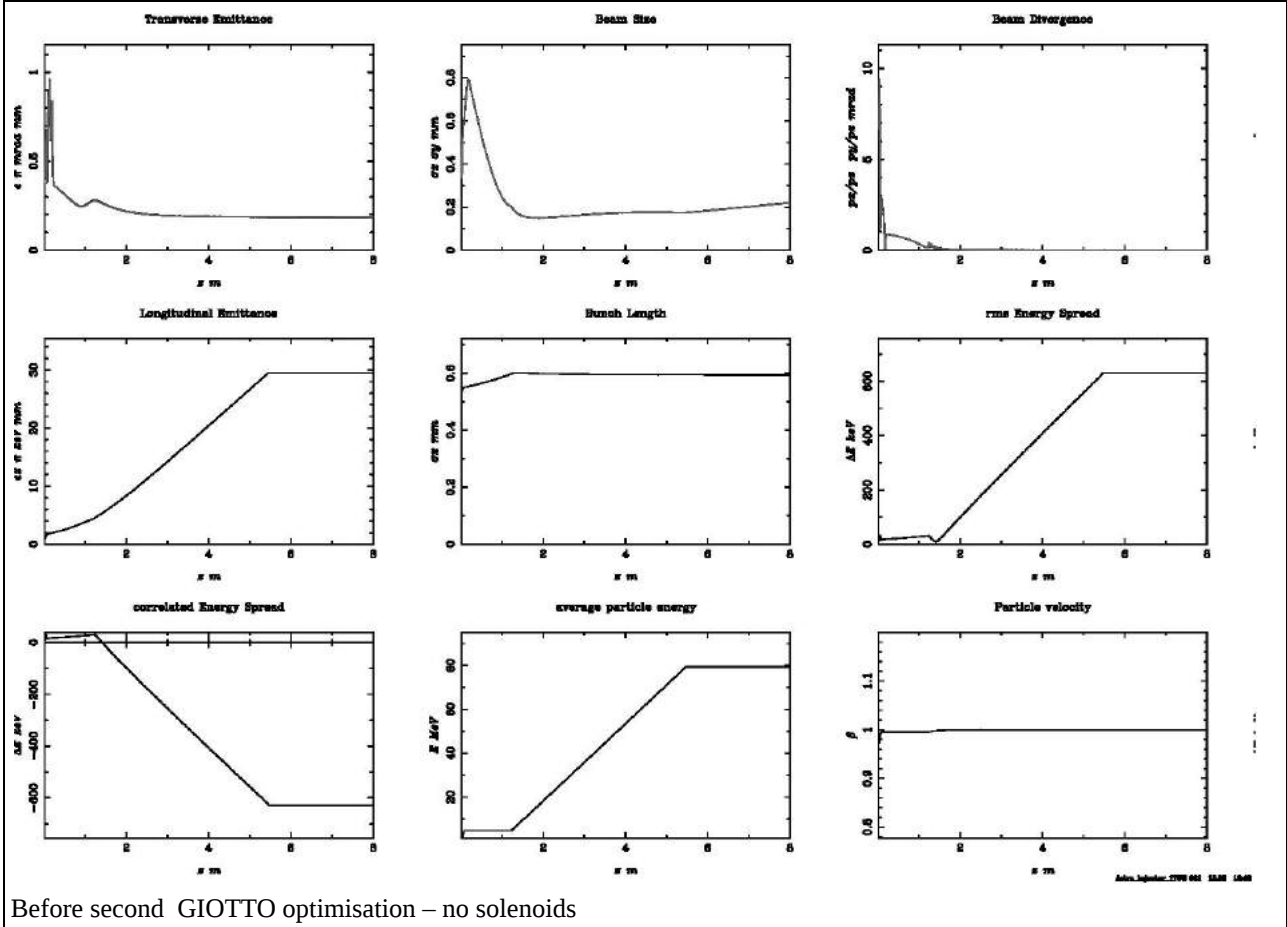
TABLE.10.33 Target values of the figures of merit	
Parameter	Target value
Emittance (π mm mrad) x-axis	0.1
Transverse Size (mm) x-axis	0.1
Longitudinal Size (mm)	0.3

Final Results

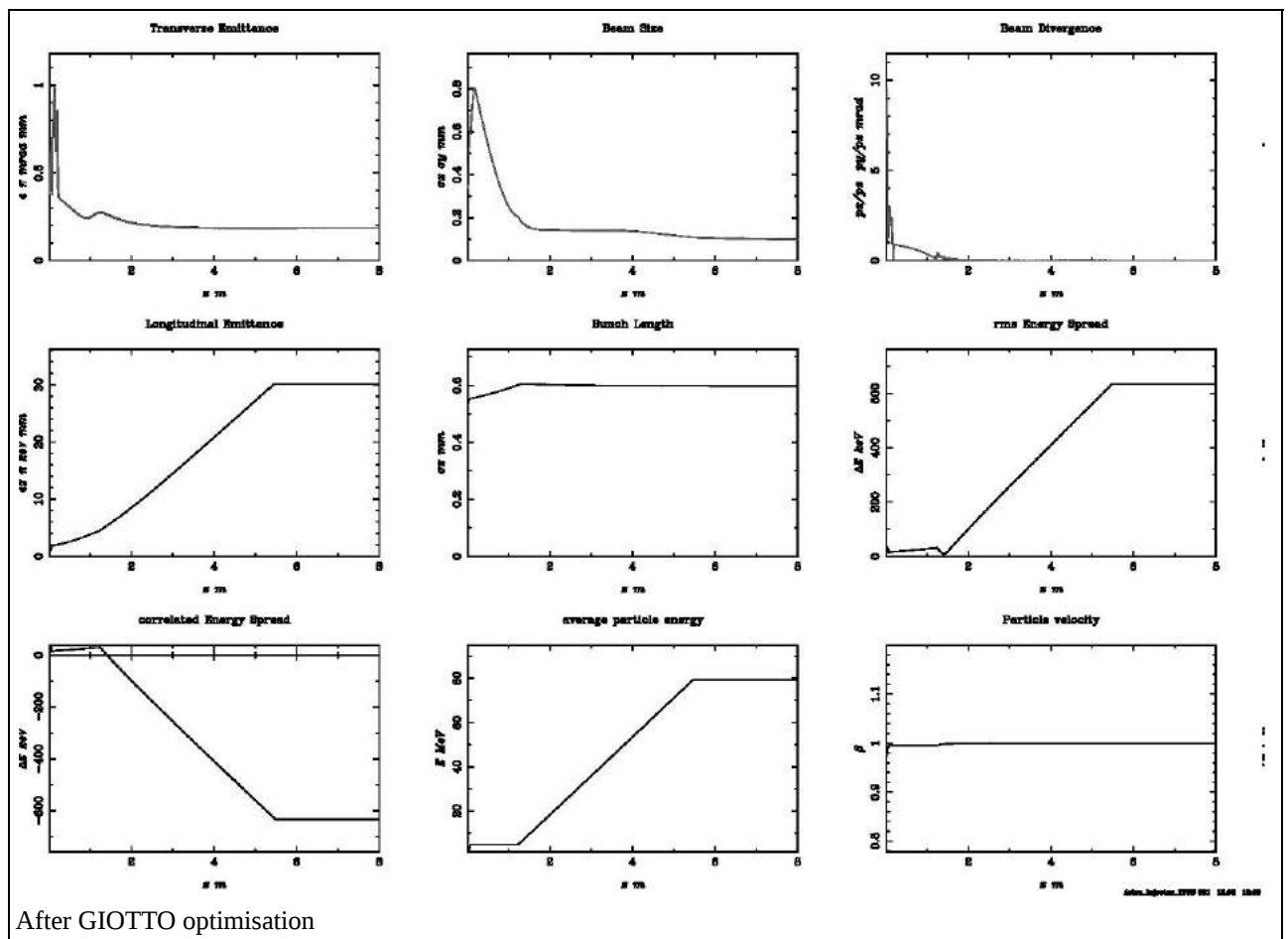
TABLE.10.34 Values of figures of merit before and after optimisation		
	Before	After
Emittance (π mm mrad) x-axis	0.188	0.195
Transverse Size (mm) x-axis	0.218	0.10
Longitudinal Size (mm)	0.595	0.598
Divergence (mrad)	0.033	0.013
Emittance (π mm mrad) y-axis	0.191	0.196
Transverse Size (mm) y-axis	0.220	0.10

TABLE.10.35

Overview of the parameters of the beam along the z-axis for the injector until the first TWS exit before and after optimisation.



Before second GIOTTO optimisation – no solenoids



Comments:

The transverse emittance, as shown in Table 10.34, has insignificantly increased while the transverse size has been halved due to the TWS solenoids application. The change in longitudinal size is also insignificant and the beam has become less. The emittance oscillation remain absent, Table 10.35, while the rest of the output parameters remain unaffected.

What has been done is that although, the laser spot size has shrunk very close to the saturation threshold to provide smaller transverse size, increasing the space charge forces, these are compensated by proper focus from the TWS solenoids.

10.5.2 Solenoid No 3

In Table 10.36 the algorithm parameters used for the genetic algorithm are presented. The population size should be close to $9^2 = 81$ and a multiple of the cores used by GIOTTO, thus 4. Although the best number to choose would be 80 or 84, 60 was chosen instead, due to long computation time and lack of computational resources.

TABLE.10.36 Algorithm parameters overview	
Number of genes	9
Number of individuals	60
Number of generations used	91
Number of CPUs	4
Fitness function	Lorentzian
Parameters of fitness function	SigX,emitX,SigZ

TABLE.10.37 Parameters before and after optimisation			
Parameters	Initial value	Range	Final value
Laser spot size (rms) / sig_x (mm)	0.183	0.02	0.180
Peak field TWS Solenoid No 1 MaxB(2) (T)	0.13026	0.08	0.023703
Peak field TWS Solenoid No 2 MaxB(3) (T)	0.023026	0.08	0.042084
Peak field TWS Solenoid No 3 MaxB(4) (T)	0.094228	0.08	0.095061
Peak field TWS Solenoid No 4 MaxB(5) (T)	0.094228	0.08	0.123116
Position TWS Solenoid No 1 S_pos(2) (m)	1.309	0.2	1.452
Position TWS Solenoid No 2 S_pos(3) (m)	2.209	0.2	2.263
Position TWS Solenoid No 3 S_pos(4) (m)	3.009	0.2	3.051

Position TWS Solenoid No 4 / S_pos(5) (m)	3.909	0.2	3.987
Phase shift of the gun / Phi(1) (degrees)	-1.14	-	-1.14
Phase shift of the TWS / Phi(2) (degrees)	-42.4	-	-42.4
Peak field of TWS / MaxE(2) (MV/m)	14.4	-	14.4
Entrance position of TWS / C_pos(2) (m)	1.309	-	1.309
Peak field of the gun's solenoid / MaxB(1) (T)	0.202	-	0.202
Position of the gun's solenoid / S_pos(1) (m)	0.178	-	0.178

The Fitness function:

The Lorentzian function used was the one below, which is the same as in the previous optimisation.

In Reverse Polish Notation :

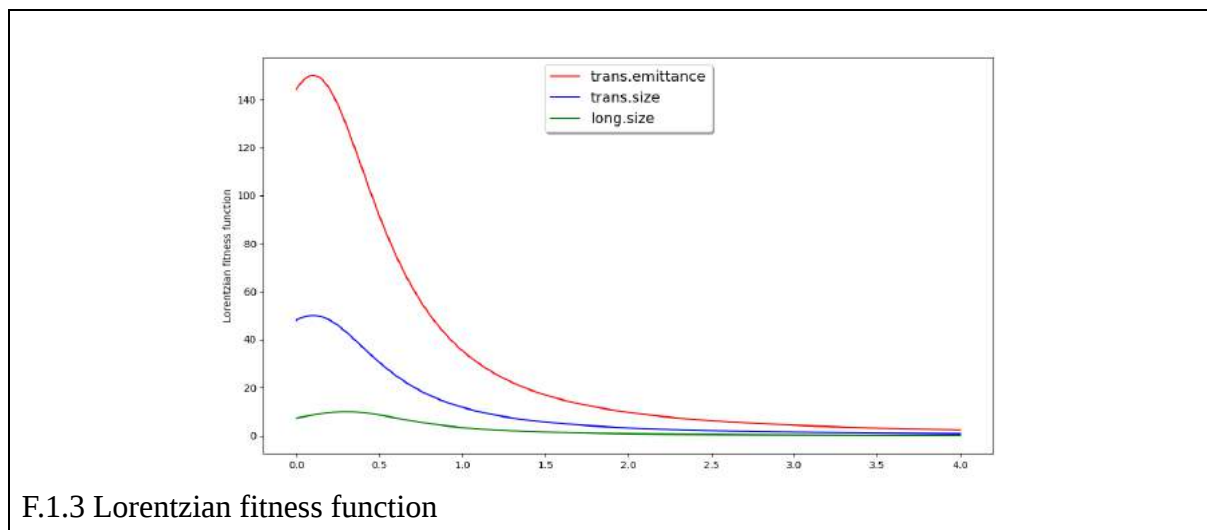
0.5 sqr emitX 0.10 - sqr 0.5 sqr + / 150 *

0.5 sqr sigX 0.10 - sqr 0.5 sqr + / 50 * +

0.5 sqr sigZ 0.30 - sqr 0.5 sqr + / 10 * +

or

$$F = 150 * \left(\frac{0.5^2}{0.5^2 + (\text{emitX} - 0.10)^2} \right) + 50 * \left(\frac{0.5^2}{0.5^2 + (\text{sigX} - 0.10)^2} \right) + 10 * \left(\frac{0.5^2}{0.5^2 + (\text{sigZ} - 0.30)^2} \right) \quad (10.4)$$



F.1.3 Lorentzian fitness function

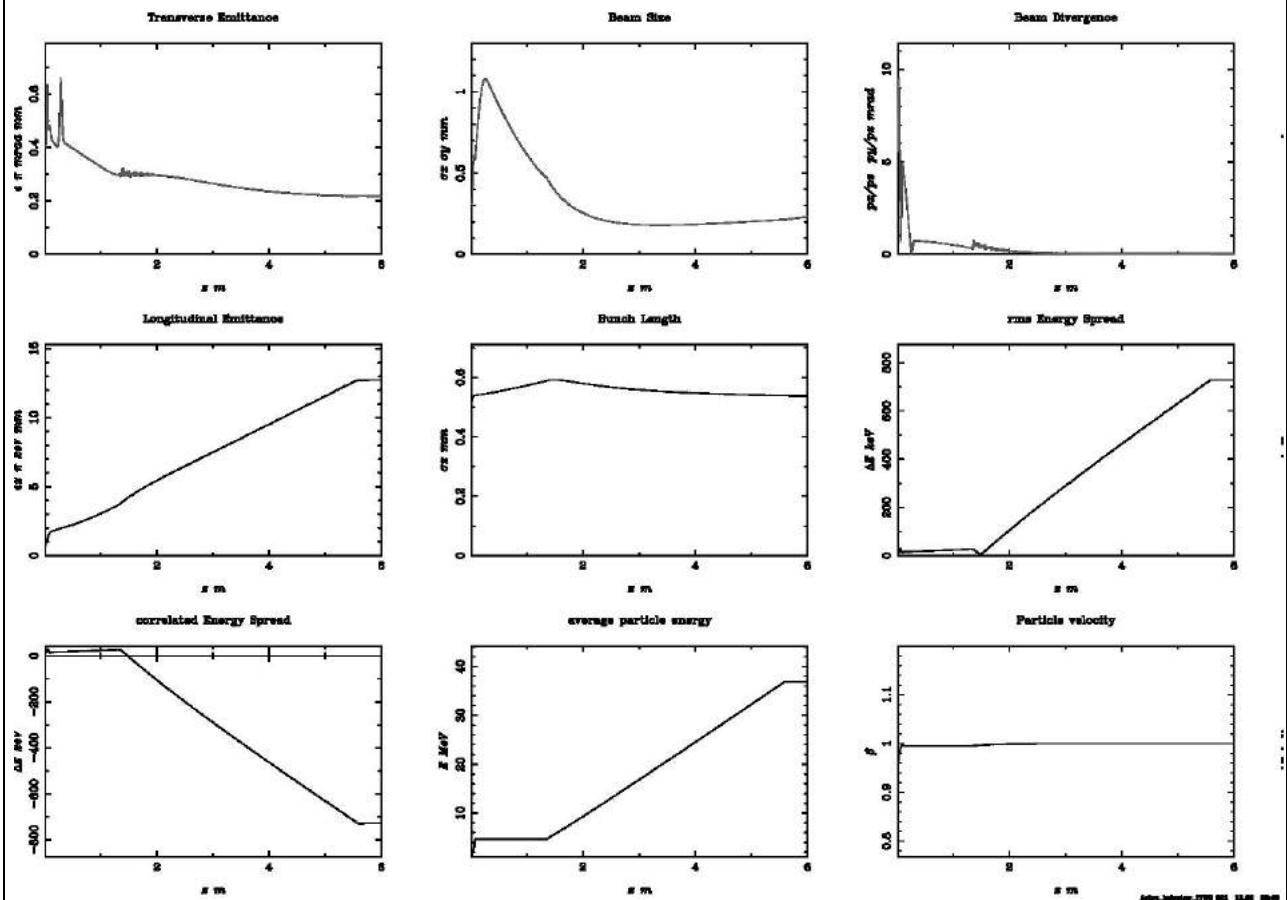
TABLE.10.38 Target values of the figures of merit	
Parameter	Target value
Emittance (π mm mrad) x-axis	0.1
Transverse Size (mm) x-axis	0.1
Longitudinal Size (mm)	0.3

Final Results

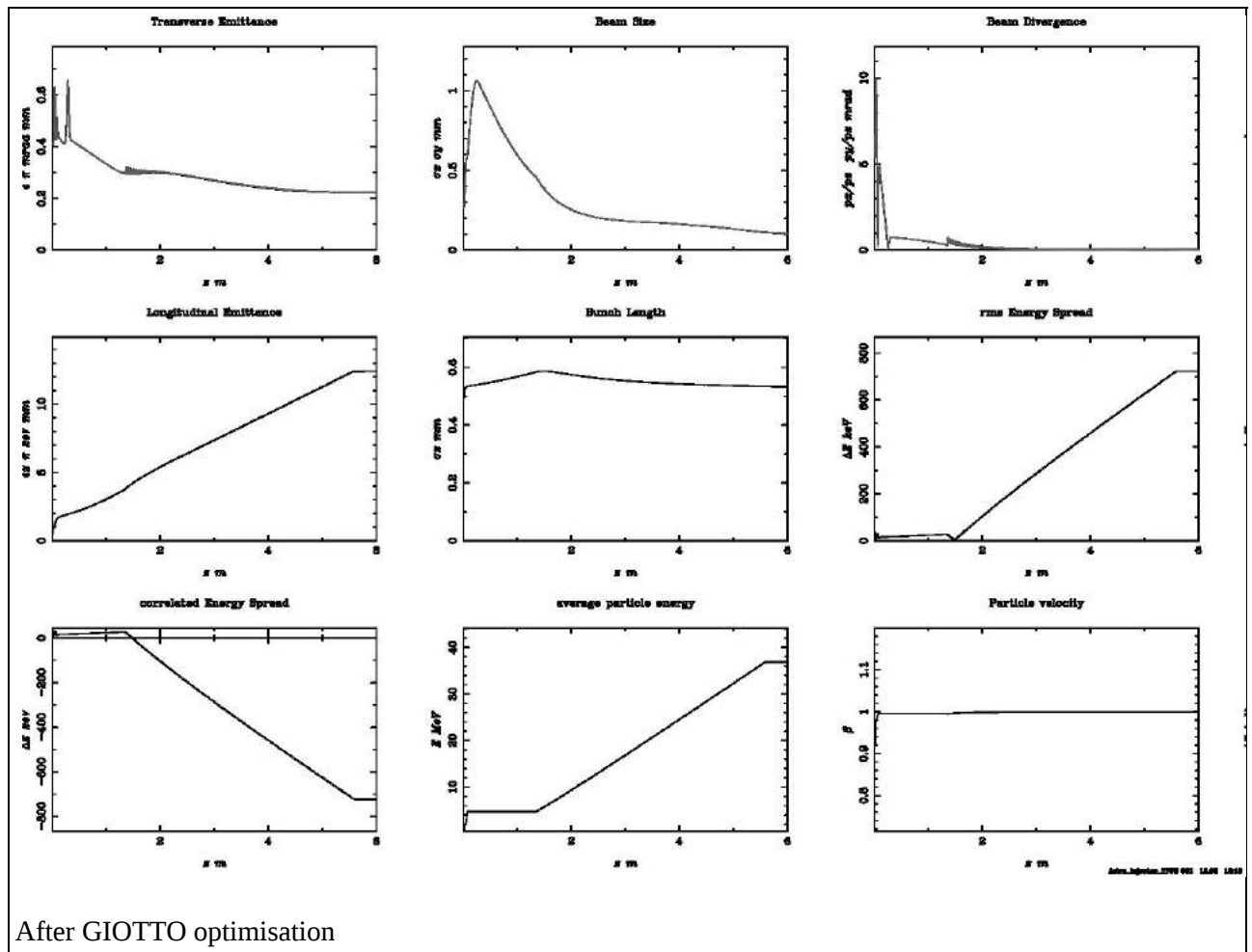
TABLE.10.39 Values of figures of merit before and after optimisation		
	Before	After
Emittance (π mm mrad) x-axis	0.232	0.224
Transverse Size (mm) x-axis	0.258	0.106
Longitudinal Size (mm)	0.495	0.533
Divergence (mrad)	0.052	0.032
Emittance (π mm mrad) y-axis	0.225	0.234
Transverse Size (mm) y-axis	0.254	0.109

TABLE.10.40

Overview of the parameters of the beam along the z-axis for the injector until the first TWS exit before and after optimisation.



Before second GIOTTO optimisation – no solenoids



Comments:

The right application of solenoid fields seem to improve all the parameters. To begin with, the emittance has been decreased, Table 10.39, unlike the previous lattice case. The transverse size has reached the goal and there are no oscillations of the emittance inside the booster. But, the transverse emittance in this case is greater than the one in the second case in a percentage of 15% approximately. The longitudinal size in the solenoid No 3 case has decreased, even though the laser pulse duration is the same in both cases. The rest of the parameters remain intact, as shown in Table 10.40.

10.6 Final Lattice with the second Booster

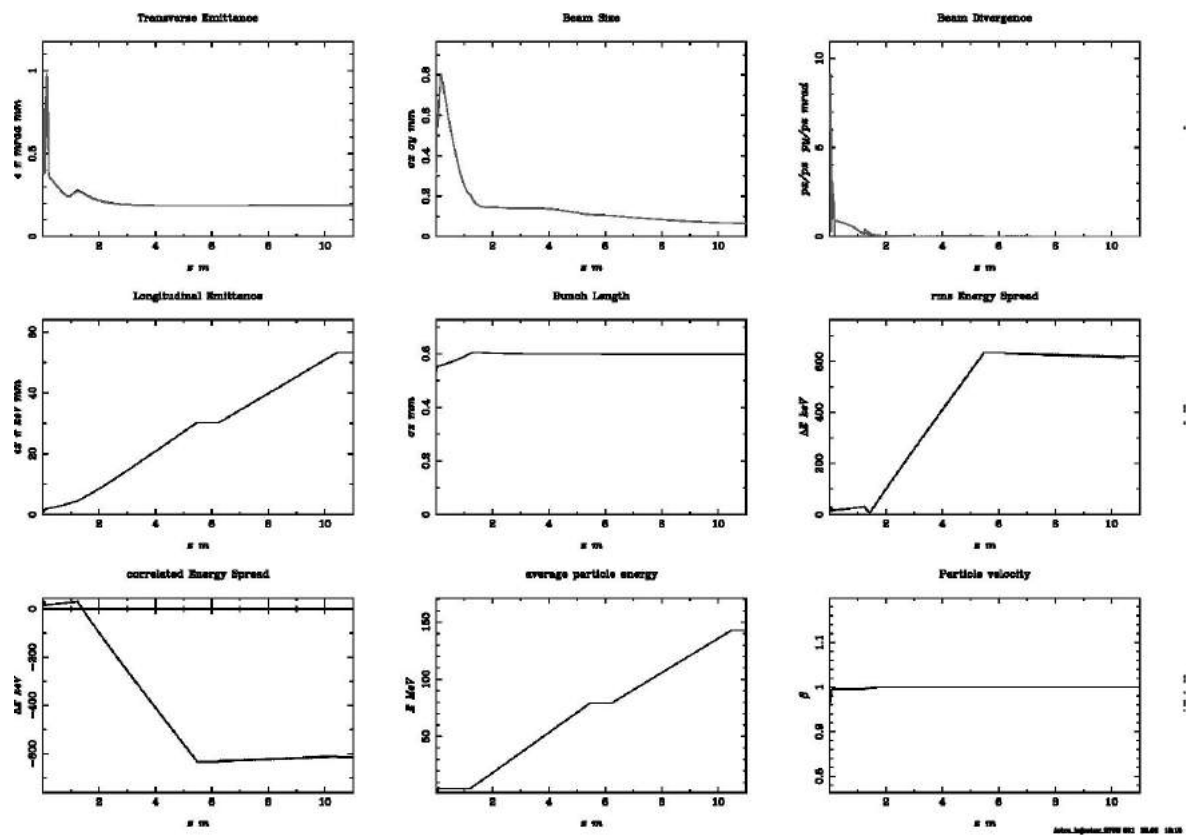
In this section, the results of a final lattice of the whole injector – until the end of the second booster - are presented for both the materials examined. For a more precise analysis, the same procedure should have been followed for the Cs₂Te photocathode, but the GIOTTO code has not yet been extended to work for an emission latency case (τ). The second booster was left intact and just shifted according to the shift of the first booster.

10.6.1 Solenoid No 2

Cu

TABLE.10.41

Overview of the beams parameters along the z-axis until the end of the second TWS. All solenoids are present. The transverse emittance, the final brightness of the beam, the final phase space and the final views (front and sides) of the beam are presented separately.



Overview

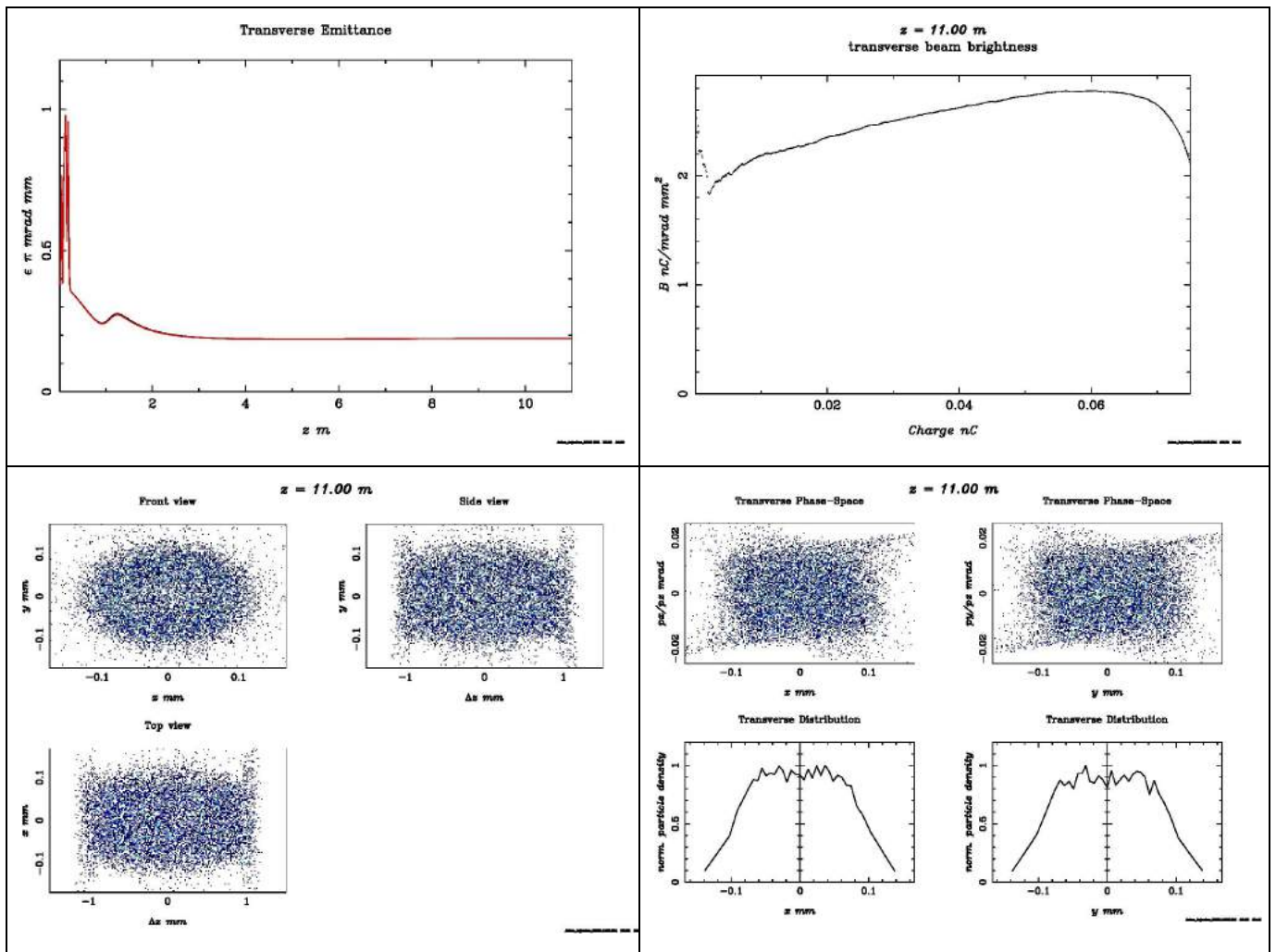
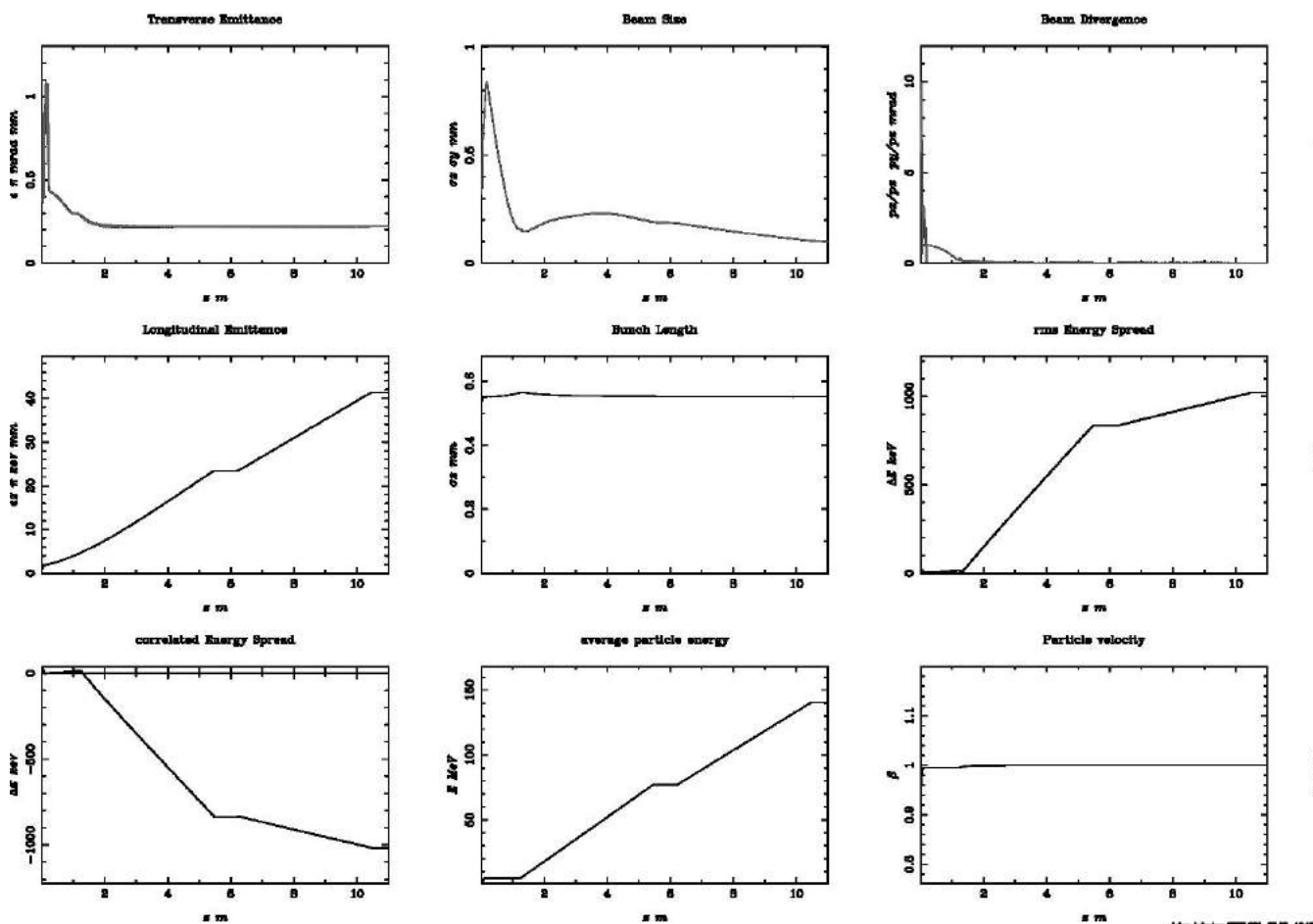


TABLE.10.42 Final values of the figures of merit		
Emittance (π mm mrad) x-axis	0.190	<u>Comments:</u> The transverse emittance freezes and the oscillations are completely damped. Also, the transverse size decreases at the end of the second booster and the peak brightness is high. The RF focusing of the linac is matched to the invariant envelope to damp the emittance to its final value at a relativistic energy. (5.1) The phase space of the beam, Table 10.41, is similar to the shape shown for the waist position $z=1.06$ in Table 9.2. This indicates that the beam's emittance 'freezes' inside the linac, as expected (Chapter 5) from meeting the FWP. Also, the front view of the beam, Table 10.41, is very symmetric, as expected and the side views have a satisfactory symmetry, as well.
Transverse Size (mm) x-axis	0.067	
Longitudinal Size (mm)	0.597	
Divergence (mrad)	0.010	
Emittance (π mm mrad) y-axis	0.190	
Transverse Size (mm) y-axis	0.067	
Maximum Brightness (nC/mrad mm ²)	2.780	

Cesium – Telluride

TABLE.10.43

Overview of the beams parameters along the z-axis until the end of the second TWS. All solenoids are present. The transverse emittance, the final brightness of the beam, the final phase space and the final views (front and sides) of the beam are presented separately.



Overview

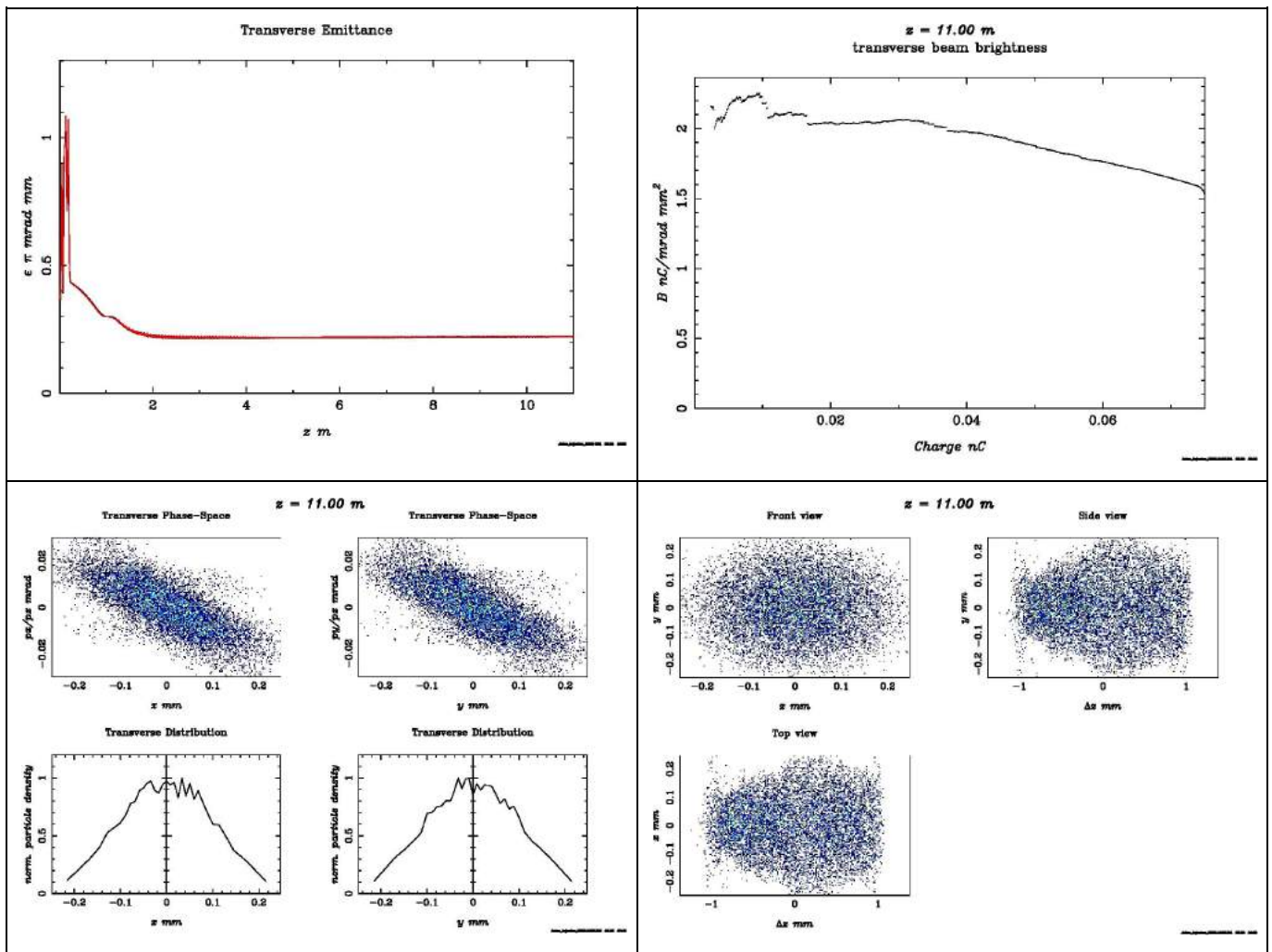


TABLE.10.44 Final values of the figures of merit		
Emittance (π mm mrad) x-axis	0.221	<p style="text-align: center;"><u>Comments:</u></p> <p>From table 10.43, a similar behaviour as the previous photocathode case is observed. In comparison with the Cu case, for Cs₂Te the result is that the transverse emittance and size are both greater, but the longitudinal size is decreased.</p> <p>It is also important to observe that the peak brightness seems to be higher, although the peak is observed at low charge while at the Cu case the brightness is almost constantly high for all charges.</p> <p>What is more, the oscillations are present at the beginning of the first booster even though they are not intense and later not observable.</p> <p>The phase space of the beam, Table 10.43, is similar to the shape shown right before the waist position $z=1.0$ in Table 9.2. This indicates that the beam's emittance 'freezes' inside the linac, as expected (Chapter 5) but the</p>
Transverse Size (mm) x-axis	0.099	
Longitudinal Size (mm)	0.551	
Divergence (mrad)	0.012	
Emittance (π mm mrad) y-axis	0.222	

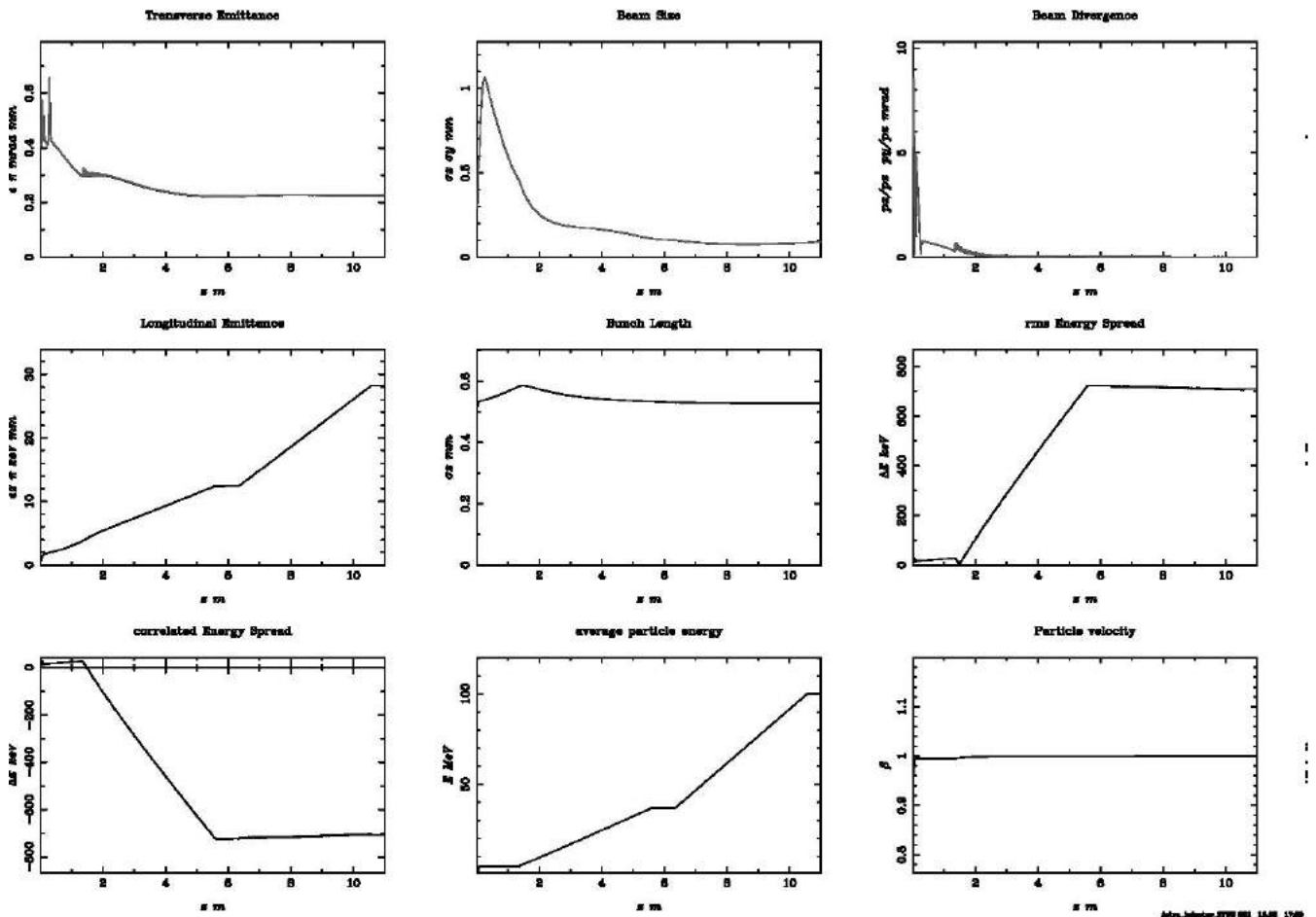
Transverse Size (mm) y-axis	0.099	emittance that froze was not the one at the waist. That happened because it is not the same waist for Cs ₂ Te as it was for Cu. What is shown here is a stability around the FWP, with a close to the point setup being able to operate in a satisfactory way. Another thing indicated here, is that the waist for Cs ₂ Te case was closer to the TWS than for Cu, due to the emission delay, leaving the emittance to the converging part from drift space.
Maximum Brightness (nC/mrad mm ²)	2.849	The front view of the beam is symmetric, in contrast with the side views, because if the alteration of the temporal profile the emission delay introduces.

10.6.2 Solenoid No 3

Cu

TABLE.10.45

Overview of the beams parameters along the z-axis until the end of the second TWS. All solenoids are present. The transverse emittance, the final brightness of the beam, the final phase space and the final views (front and sides) of the beam are presented separately.



Overview

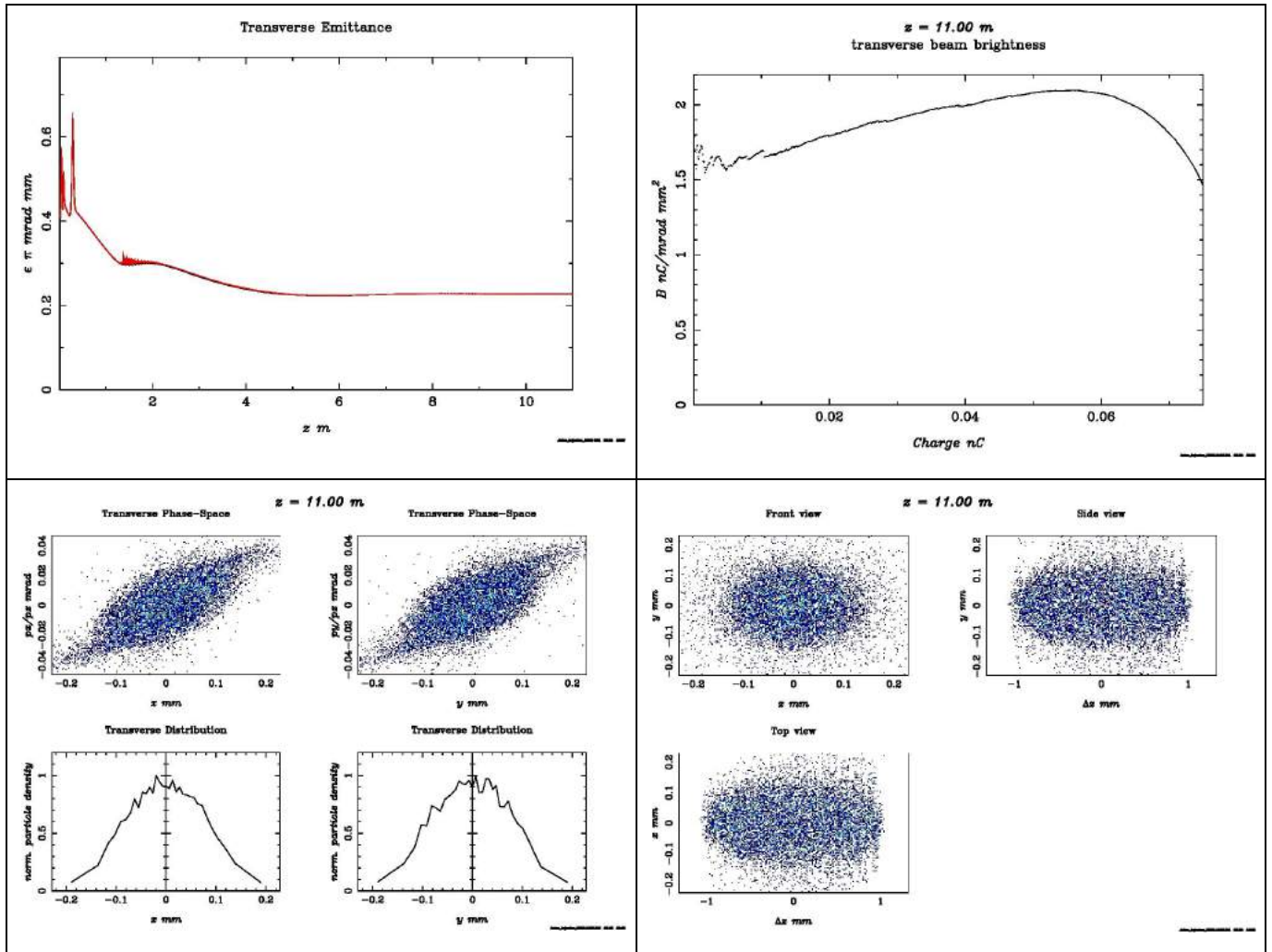


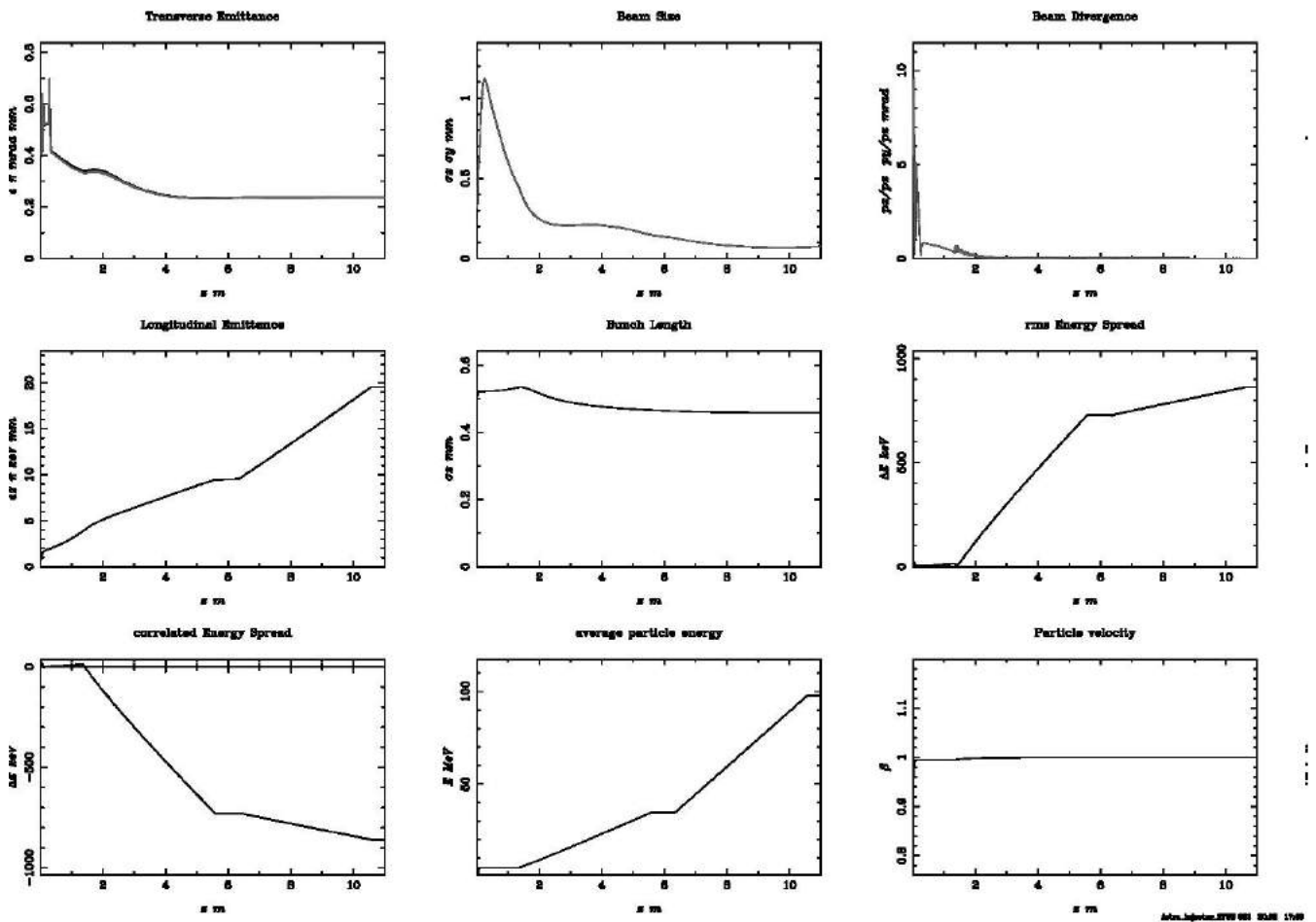
TABLE.10.46 Final values of the figures of merit		
Emittance (π mm mrad) x-axis	0.227	<u>Comments:</u> In this lattice, the final emittance and size are greater than the previous one and the brightness is lower. The transverse phase space is more linear, though, and the longitudinal size slightly smaller. Also, the energy gain is 10 MV/m increased with respect to the previous lattice. The RF focusing of the linac is matched to the invariant envelope to damp the emittance to its final value at a relativistic energy. (5.1) The phase space of the beam, Table 10.45, is similar to the shapes shown for the waist position $z=1.06$ and right after that, $z=1.12$ m, in Table 9.2. This indicates that the beam's emittance 'freezes' inside the linac, as expected (Chapter 5) from meeting the FWP. The phase space is not exactly like the one presented for the waist, but a the one occurring in a small distance after the waist, indicating that the emittance 'freezing' happened a little
Transverse Size (mm) x-axis	0.091	
Longitudinal Size (mm)	0.528	
Divergence (mrad)	0.019	
Emittance (π mm mrad) y-axis	0.227	

Transverse Size (mm) y-axis	0.091	after the waist, at the diverging part from drift space, proving the stability of the FWP. Also, the front view of the beam, Table 10.41, is very symmetric, as expected and the side views have a satisfactory symmetry, as well.
Maximum Brightness (nC/mrad mm ²)	2.096	

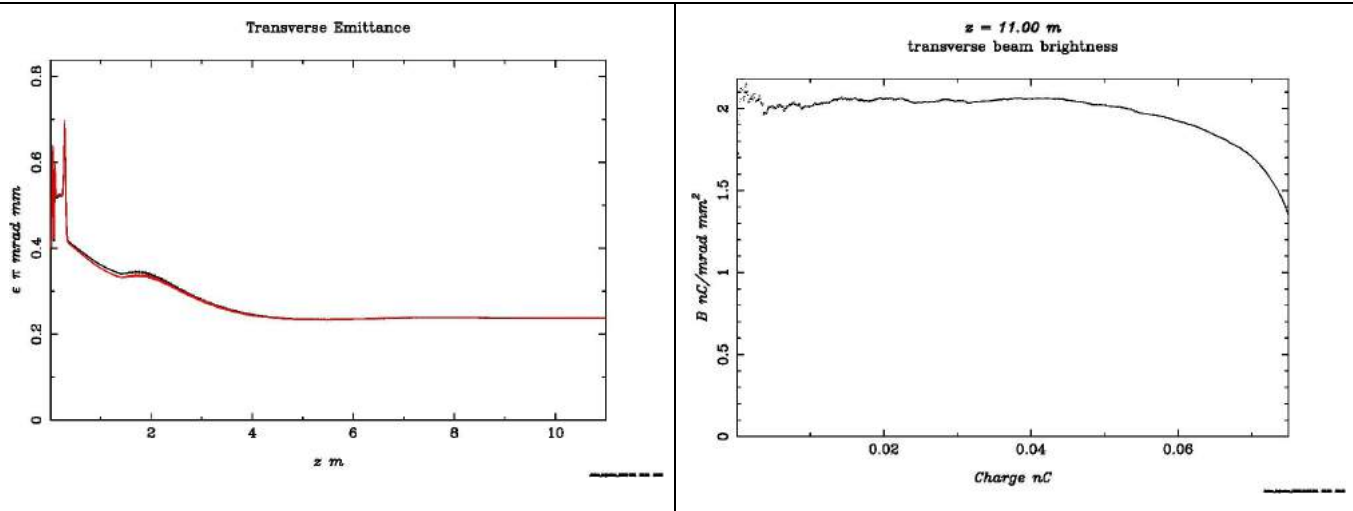
Cesium – Telluride

TABLE.10.47

Overview of the beams parameters along the z-axis until the end of the second TWS. All solenoids are present. The transverse emittance, the final brightness of the beam, the final phase space and the final views (front and sides) of the beam are presented separately.



Overview



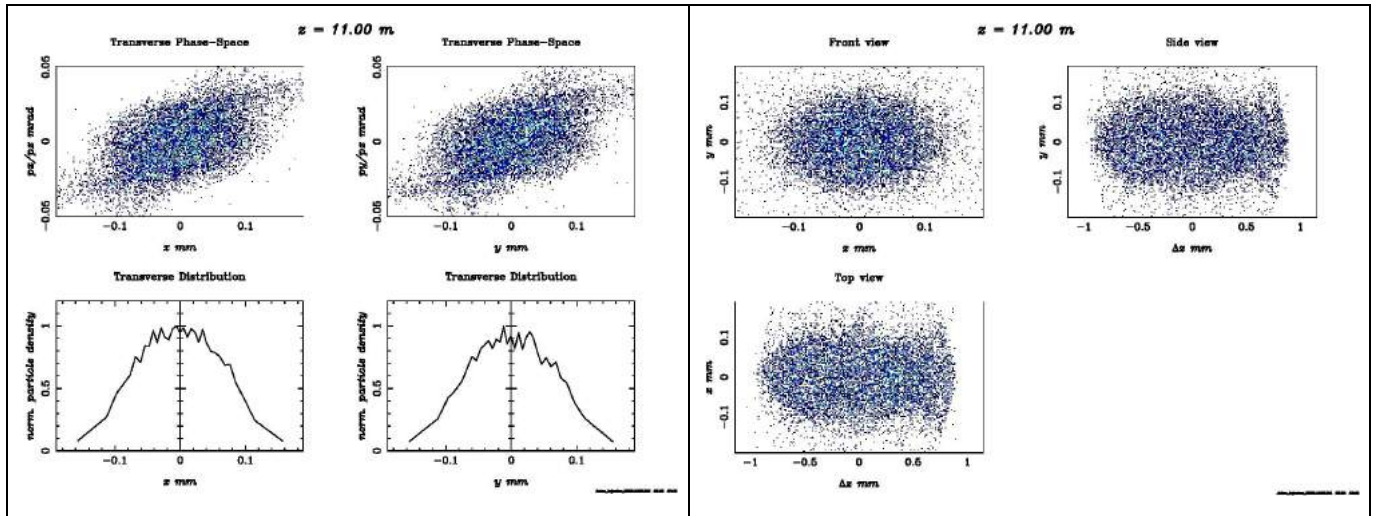


TABLE.10.48
Final values of the figures of merit

		<u>Comments:</u>
Emittance (π mm mrad) x-axis	0.237	<p>Concerning this photocathode case results, the emittance is similar to the Cu case with this solenoid, Table 10.46, and the transverse size decreased. So is the longitudinal size, which is the least of all for cases. The divergence is also smaller, the brightness similar and the oscillations of the emittance are not obvious unlike in the previous simulation.</p> <p>All these differences occurred due to the emission delay of the semiconductor. The explanation occurs if the transverse phase space is observed. The phase space of the beam, Table 10.47, is similar to the shape shown for the waist position $z=1.06$, in Table 9.2. This indicates that the beam's emittance 'freezes' inside the linac, as expected (Chapter 5) from meeting the FWP. The emission delay of the Cs_2Te shifted the waist closer to the photocathode right where it was needed and not met in the Cu photocathode case.</p> <p>The front view of the beam remains symmetric as expected but the side views are not, apparently because of the emission delay (τ).</p>
Transverse Size (mm) x-axis	0.076	
Longitudinal Size (mm)	0.459	
Divergence (mrad)	0.020	
Emittance (π mm mrad) y-axis	0.237	
Transverse Size (mm) y-axis	0.076	
Maximum Brightness ($\text{nC}/\text{mrad mm}^2$)	2.087	

There might not have been an optimisation exclusively for the Cesium- Telluride photocathode, but the optimised lattice for Cu works for both in the S-band.

10.6.3 Conclusions

Although, the optimisation process is a time-consuming process, the time it requires cannot be compared to time a manual optimisation would take to reach a satisfactory solution. Thus, the algorithmic optimisation, and especially the genetic algorithm optimisation, is recommended, as it provides optimal results in a relatively small amount of time.

In the S-band Gun the different photocathode materials do not result in great differences in the injected beam. Which means that the same lattice can operate with both photocathodes without great consequences. Although, if optimised separately, the optimum lattice may differ because of the emission delay, consequently of the different initial phase required and the alteration of the space charge forces and bunch shape which leads to differences in the plasma oscillations (differences in the slices). In the S-band the emittance delay of 0.4 psec is approximately 0.43 degrees in the RF period (10.1) which is a tolerable 'error'.

$$\frac{2\pi t}{T} = \frac{x^\circ \cdot 2\pi}{360^\circ} \quad (10.5)$$

What was observed after the optimisation, was that exchanging the photocathode material could either slightly improve or deteriorate the final performance. It is the stability of the FWP that allows small diversions from the waist without great consequences. In the solenoid No1 case, the algorithm centered the entrance of the TWS almost exactly on the waist position. So, changing the cathode to Cs₂Te shifted the waist closer to the TWS and the emittance 'froze' at the converging part from drift space. The result was slightly greater emittance and deteriorated performance. On the contrary, in solenoid No3 case, the algorithm did not manage to accurately centre the TWS entrance on waist, letting the emittance to 'freeze' at a diverging point from the drift space close to the waist. The difference in distances is only several mm. When the photocathode material changed the waist position was shifted away from the photocathode and closer to the TWS entrance. This made the waist to be centered more effectively to the booster entrance meeting the FWP. The shift of the waist by Cs₂Te that was shown in sub-chapter 10.3, was about a shift closer to the cathode and not away from it. But, the RF and solenoid focusing and the phase shift have changed, so has the waist shift.

The Cs₂Te photocathode may result in greater emittance and rms beam size, but due to the high Quantum Efficiency of the material, using the same energy of a laser pulse one can create much greater charges, or the same charge with less pulse energy. Also, it can be possible to create the same charge with shorter pulses (also less pulse energy), thus shorter bunch length.

11. Photoinjector optimisation 4.6 cells X-band

In this chapter the results of the optimisation of a 4.6 cells X-band gun proposed for the CompactLight Collaboration (XLS) are presented [35].

The beam used was Cu D with an initial radius 0.2 mm, Flattop temporal distribution with 0.2 psec duration and 0.05 psec rise/fall time.

11.1 Cavities

The electric and magnetic fields of the various components of the 1.5 cells S-band gun photoinjector are presented with respect to the z-axis in Tables 11.1 - 11.3 .

RF-Gun

		TABLE 11.1 4.6 cells X-band RF gun
Number of cells	4.6	
Frequency (GHz)	11.99	
Peak Field (MV/m)	250	

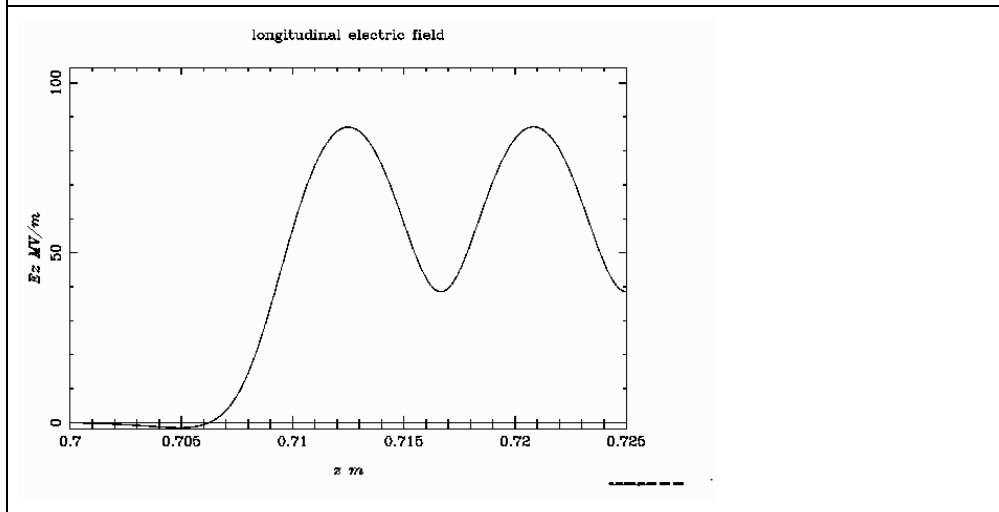
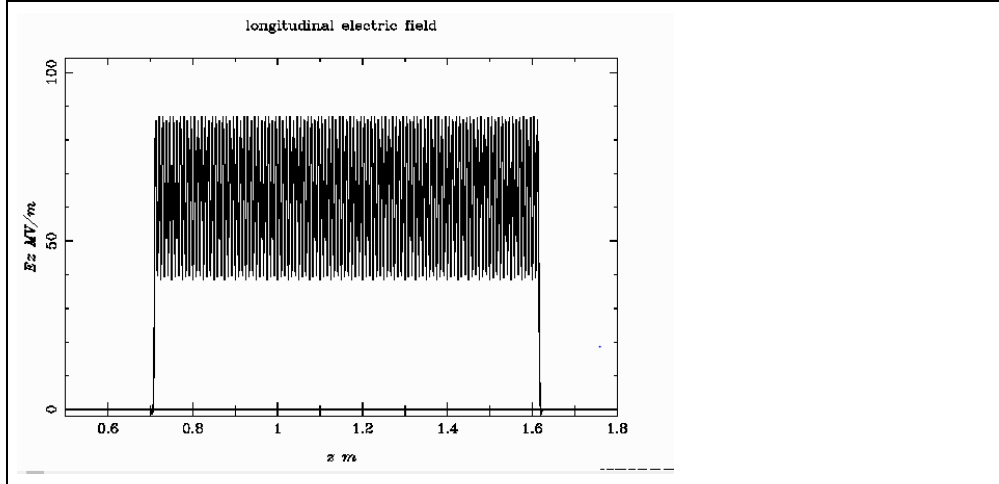
Solenoid

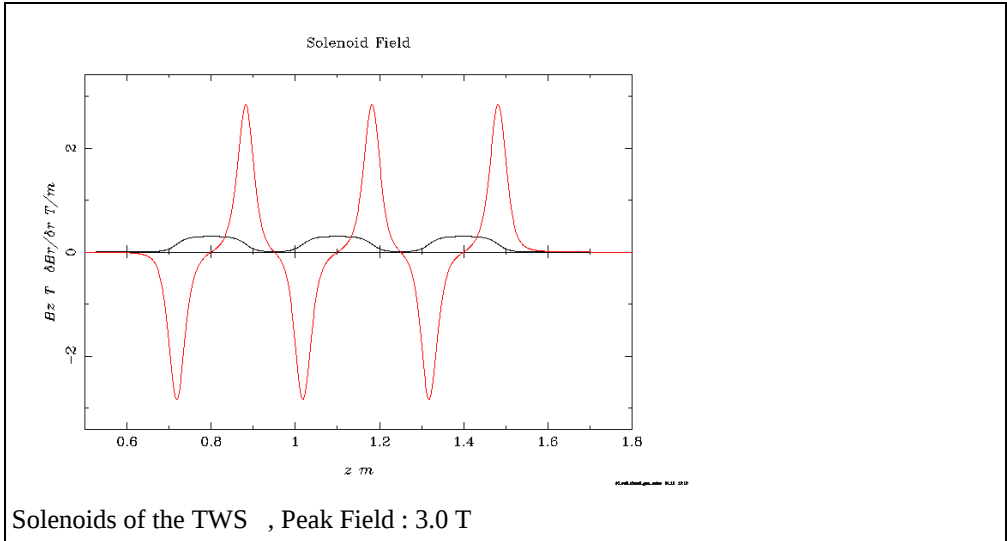
		TABLE 11.2 Solenoid field
Solenoid	0.482	
Peak Field (T)		

Travelling Wave Structures (TWS)

TABLE 11.3
Travelling Wave Structure field

Number of cells	108
Frequency (GHz)	11.99
Peak Field (MV/m)	87





11.2 Optimisation

The original lattice was already close the optimal for the beam injected. The procedure followed for optimisation was similar to the previous at Chapter 10. The pre-optimising procedure was not followed, only the third step of GIOTTO optimisation. The material comparison on the given lattice is presented in Chapter 9. The optimisation, as before, is only run for Cu case.

The parameters that were used for the first GIOTTO optimisation are in Table 10.21. The population size should be close to $6^2 = 36$ and a multiple of the cores used by GIOTTO, thus 4. The population size was defined exactly 36 individuals and the generations were left to reach 231/400, where 400 was the predefined number of generations.

TABLE.11.4	
Algorithm parameters overview	
Number of genes	6
Number of individuals	36
Number of generations used	231
Number of CPUs	4
Fitness function	Lorentzian
Parameters of fitness function	SigX,emitX,SigZ

TABLE.11.5 Parameters before and after optimisation			
Parameters	Initial value	Range	Final value
Laser spot size (rms) / sig_x (mm)	0.2	0.05	0.11
Phase shift of the gun / Phi(1) (degrees)	197	10.0	207
Phase shift of the TWS / Phi(2) (degrees)	21	20.0	61
Peak field of TWS / MaxE(2) (MV/m)	87	5.0	84
Entrance position of TWS / C_pos(2) (m)	0.7	0.2	0.77
Peak field of the gun's solenoid / MaxB(1) (T)	0.482	0.05	0.483

The Fitness function:

The fitness function was chosen to be Lorentzian:

In Reverse Polish Notation :

0.5 sqr emitX 0.05 - sqr 0.5 sqr + / 100 *

0.5 sqr sigX 0.05 - sqr 0.5 sqr + / 30 * +

0.5 sqr sigZ 0.10 - sqr 0.5 sqr + / 10 * +

or

$$F = 100 * \left(\frac{0.5^2}{0.5^2 + (\text{emitX} - 0.05)^2} \right) + 30 * \left(\frac{0.5^2}{0.5^2 + (\text{sigX} - 0.05)^2} \right) + 10 * \left(\frac{0.5^2}{0.5^2 + (\text{sigZ} - 0.10)^2} \right) \quad (11.1)$$

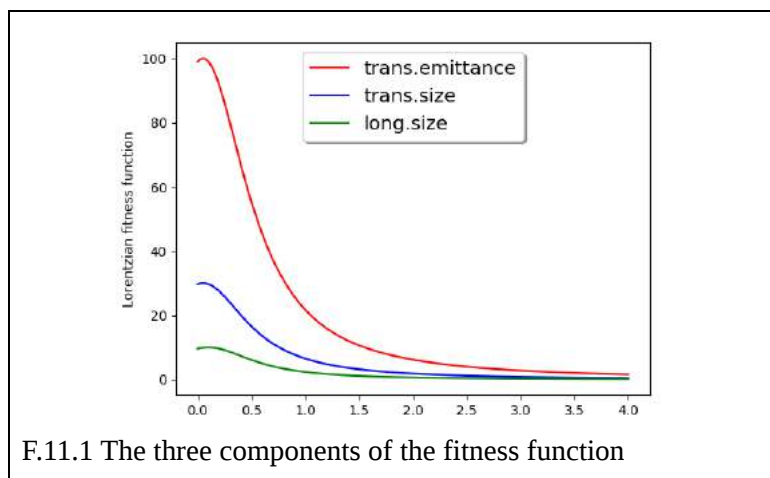


TABLE.11.6 Target values of figures of merit	
Parameter	Target value
Emittance (π mm mrad) x-axis	0.05
Transverse Size (mm) x-axis	0.05
Longitudinal Size (mm)	0.1

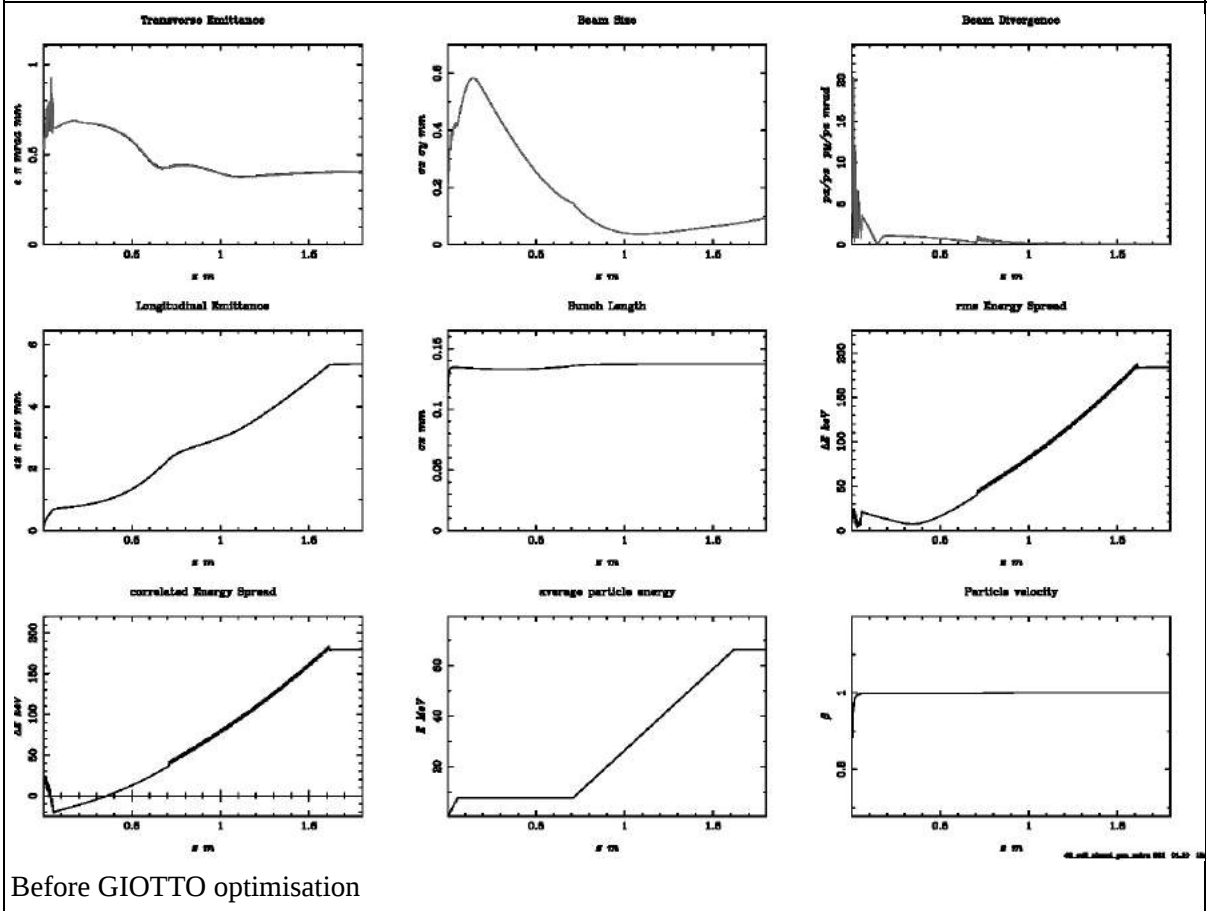
The target values, Table 11.6, seem to be very small but the function is a Lorentzian so the population could evolve with variety. The final results are for the lattice without the solenoids in the TWS structure are presented in Table 11.7.

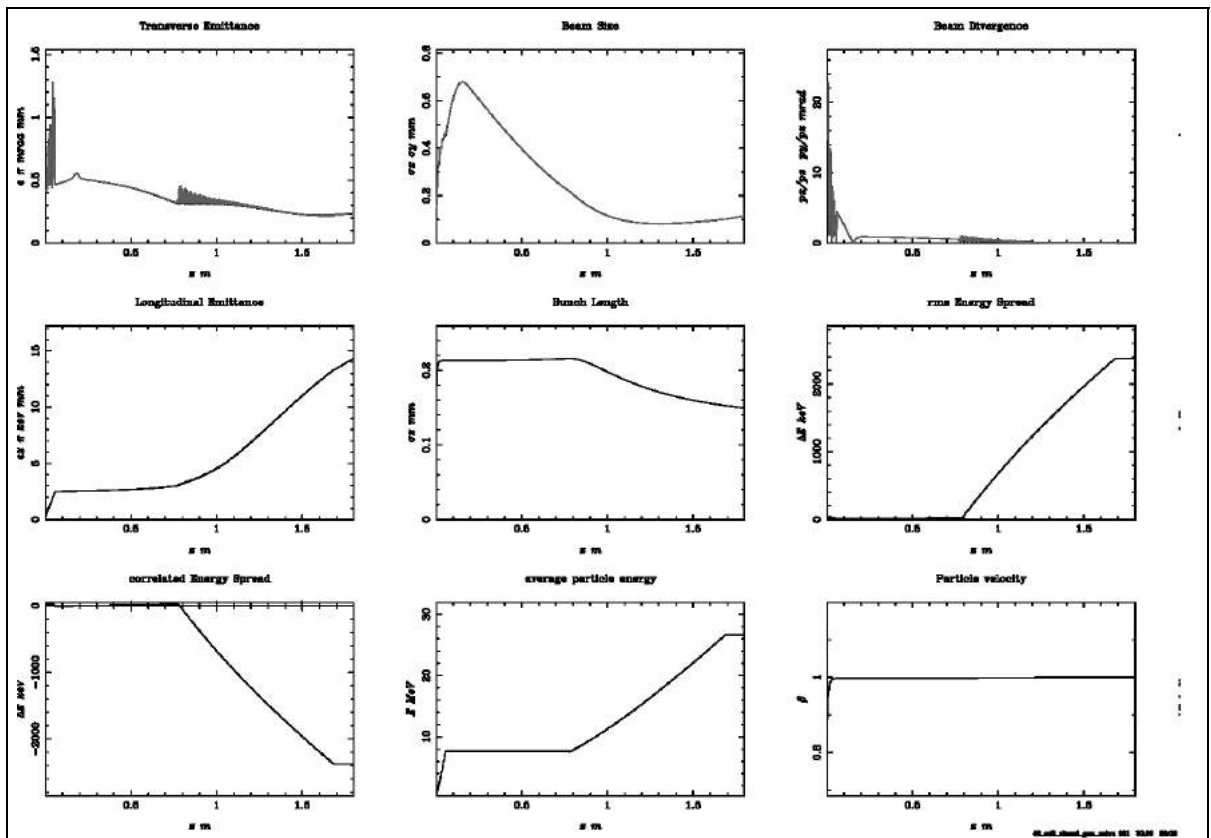
Final Results

TABLE.11.7 Figures of merit before and after optimisation		
	Before	After
Emittance (π mm mrad) x-axis	0.406	0.238
Transverse Size (mm) x-axis	0.093	0.115
Longitudinal Size (mm)	0.138	0.149
Divergence (mrad)	0.119	0.13
Emittance (π mm mrad) y-axis	0.406	0.240
Transverse Size (mm) y-axis	0.093	0.115

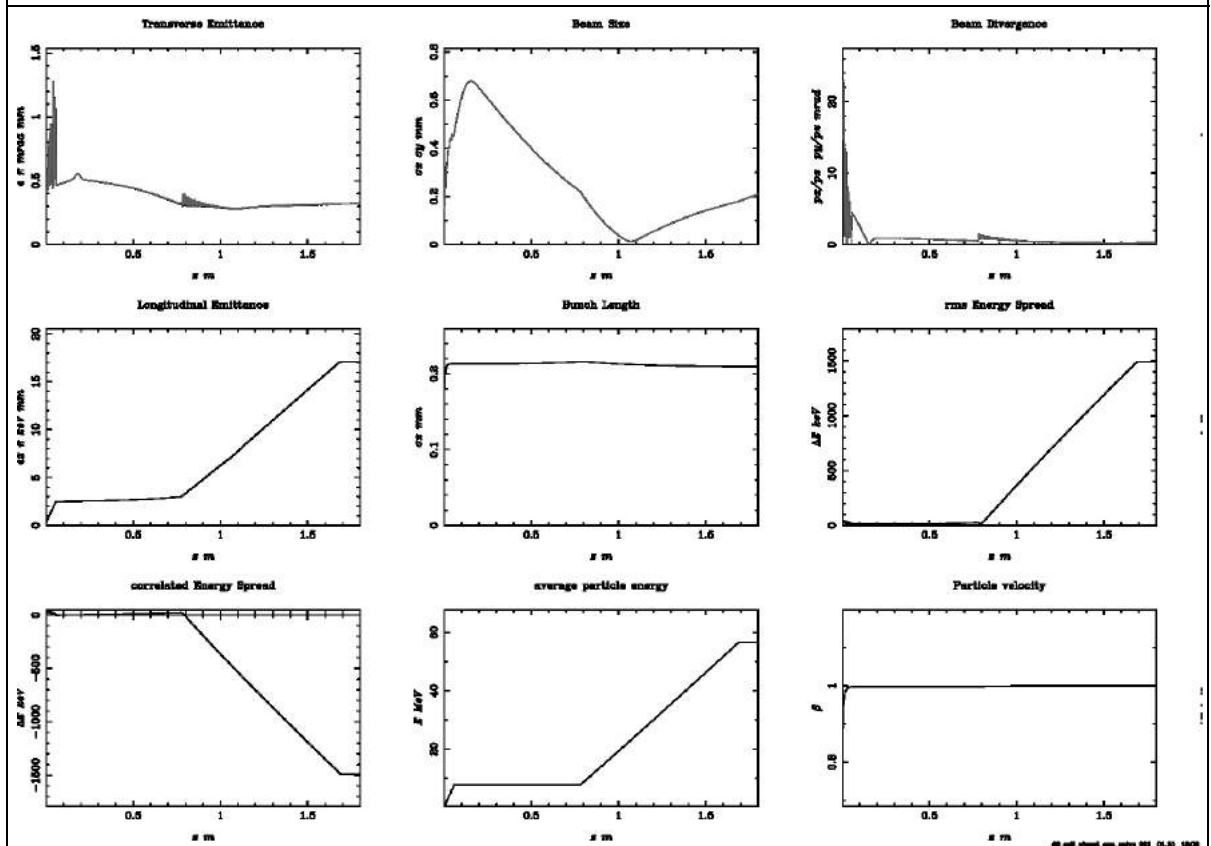
TABLE.11.8

Overview of the parameters of the beam along the z-axis for the injector until the first TWS exit before and after optimisation. Two cases are presented after optimisation, one with the TWS solenoids absent (as it was during optimisation) and one with the solenoids shifted according to the TWS shift.





After Giotto optimisation – with no solenoids of the TWS

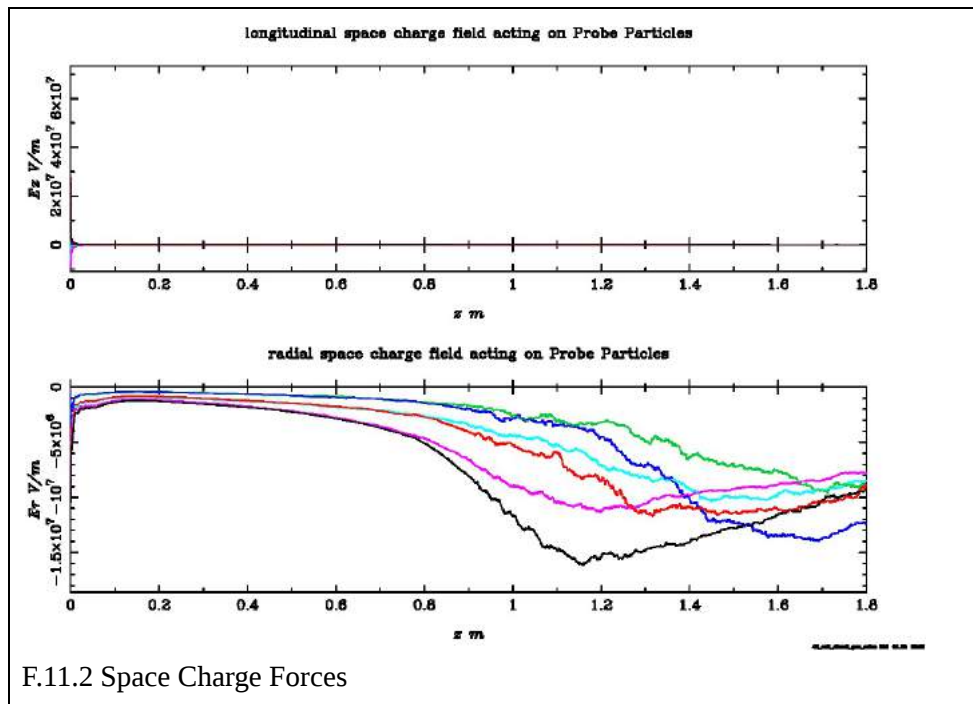


After Giotto optimisation – with the solenoids shifted according to the TWS shift

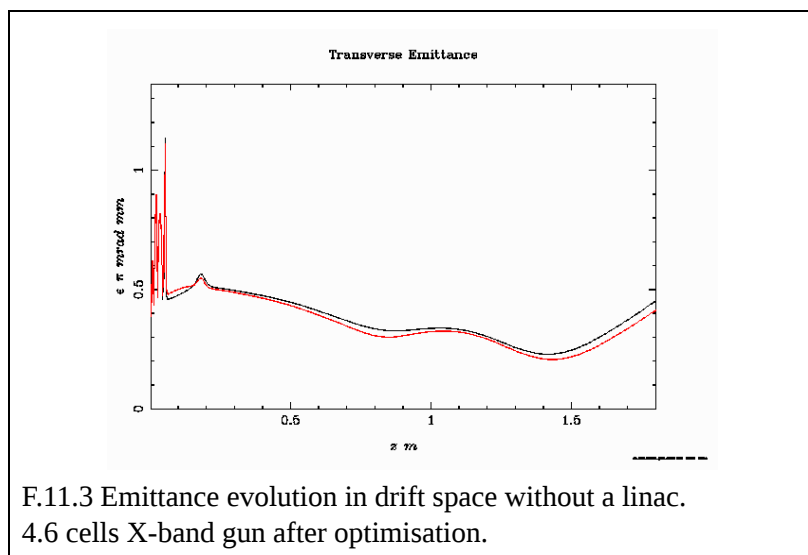
According to Table 11.7, the transverse emittance is almost halved and the other quantities are slightly changed. An interesting effect that was not observed is the S-band in such intensity is the bunch shortening. At the initial lattice the longitudinal size is constantly small, while in the other cases the initial size is greater but it reduces at waist position. This happens because of the acceleration (A.57)

Also, in the ‘optimised’ the energy spread is one order of magnitude higher than the initial. But, according to (A.35) the relation should be the opposite. This raised questions, along with the space charges below and the intense oscillations, and the lattice was revised in terms of accordance with the FWP.

The space charge forces of the results seem to constantly be significantly increased after the linac entrance, F.11.2.



Because of the high space charge, the beam waist position after the optimisation was sought. After a test without the linac, the following was obtained, F.11.2.



In $z = 0.77\text{m}$ the emittance is a local minimum and not a maximum, as required from the FWP. So the criterion of the working point is not met. Shifting the linac with the solenoids to 1.1 m where the waist really is, the results of the new lattice were obtained and shown in Table 11.9.

TABLE 11.9

Overview of the parameters of the beam along the z-axis for the optimised injector until the first TWS exit after TWS, without the respective solenoids, shift to 1.1m entrance. The transverse emittance and size are presented separately.

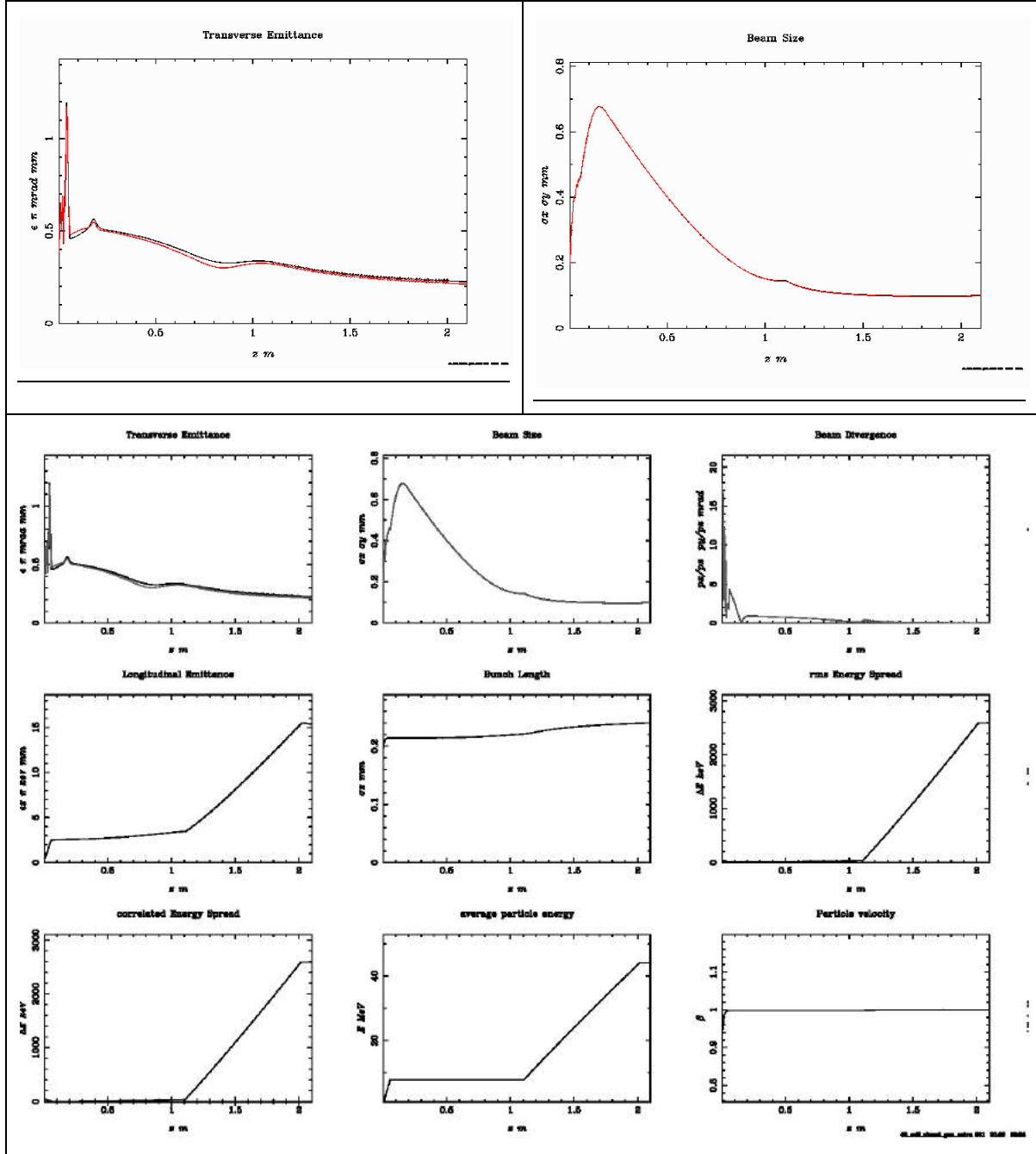


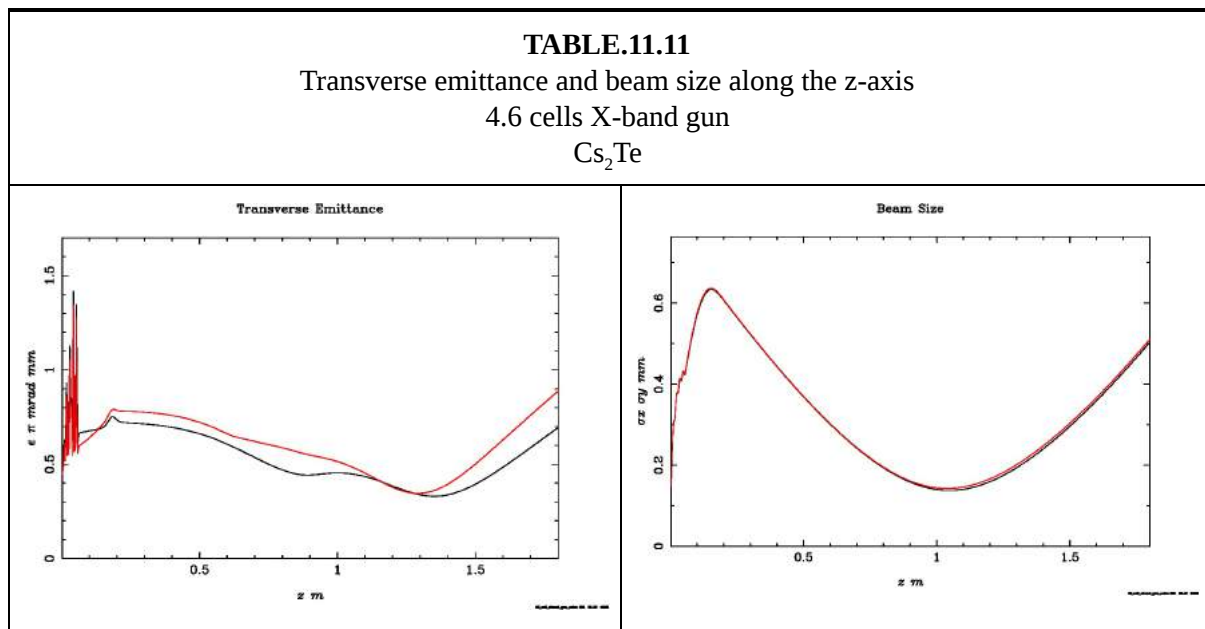
TABLE.11.10		
Figures of merit at the exit of the first TWS on the optimised injector, after TWS, without the respective solenoids, shift to 1.1m entrance.		
	Before	After
Emittance (π mm mrad) x-axis	0.238	0.225
Transverse Size (mm) x-axis	0.153	0.102
Longitudinal Size (mm)	0.149	0.24
Divergence (mrad)	0.13	0.005
Emittance (π mm mrad) y-axis	0.240	0.212
Transverse Size (mm) y-axis	0.153	0.997

The transverse profile, according to Table 11.10, has been improved by all means in exchange for a greater bunch length. The bunch length increased in contrast with the the previous simulation, almost doubled. Also the beam is far less divergent than before and the oscillations of the emittance have vanished.

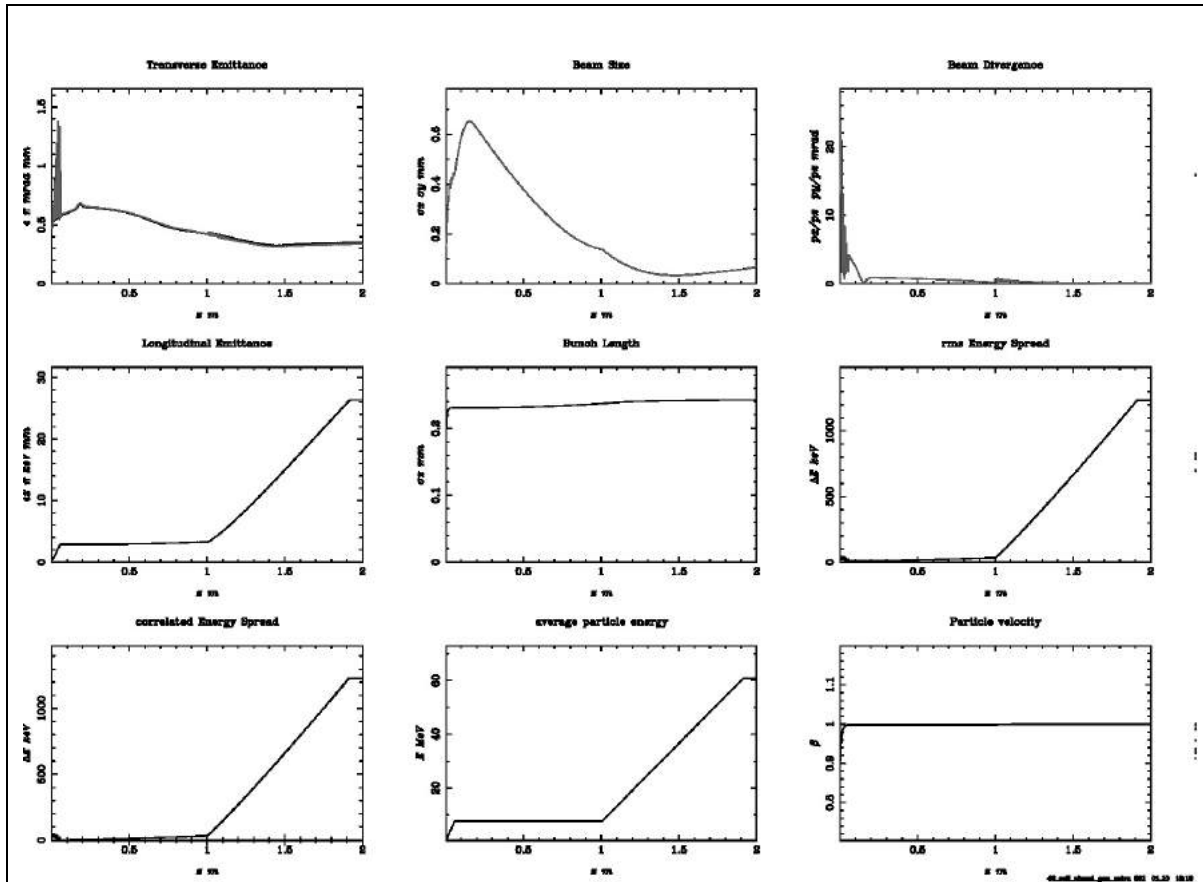
Cs₂Te

This photocathode, as shown in Chapter 9 and as tested in with simulations, cannot work on the same lattice because of the initial phase and the shift of the beam waist position. A series of scans on the permitted initial phases on the optimised lattice showed that an optimal phase of the gun to get a minimal local maximum at waist would be 236 degrees. The rest of the parameters remain intact.

There is a double emittance minimum which was not observed in Chapter 9. The FWP is observed at $z = 1.0$ m, Table 11.11.



The whole lattice with the solenoids was shifted according to the linac shift and simulated. An overview of the output is presented in F.11.3. The results for Cu in Table 11.12 are the ones occurred with shift of the solenoids with respect to the entrance of the linac, $z=1.1\text{m}$.



F.11.4 Overview of the parameters of the beam along the z-axis for the optimised injector until the first TWS exit after TWS and respective solenoids shift to 1.0m booster entrance.

TABLE 11.12

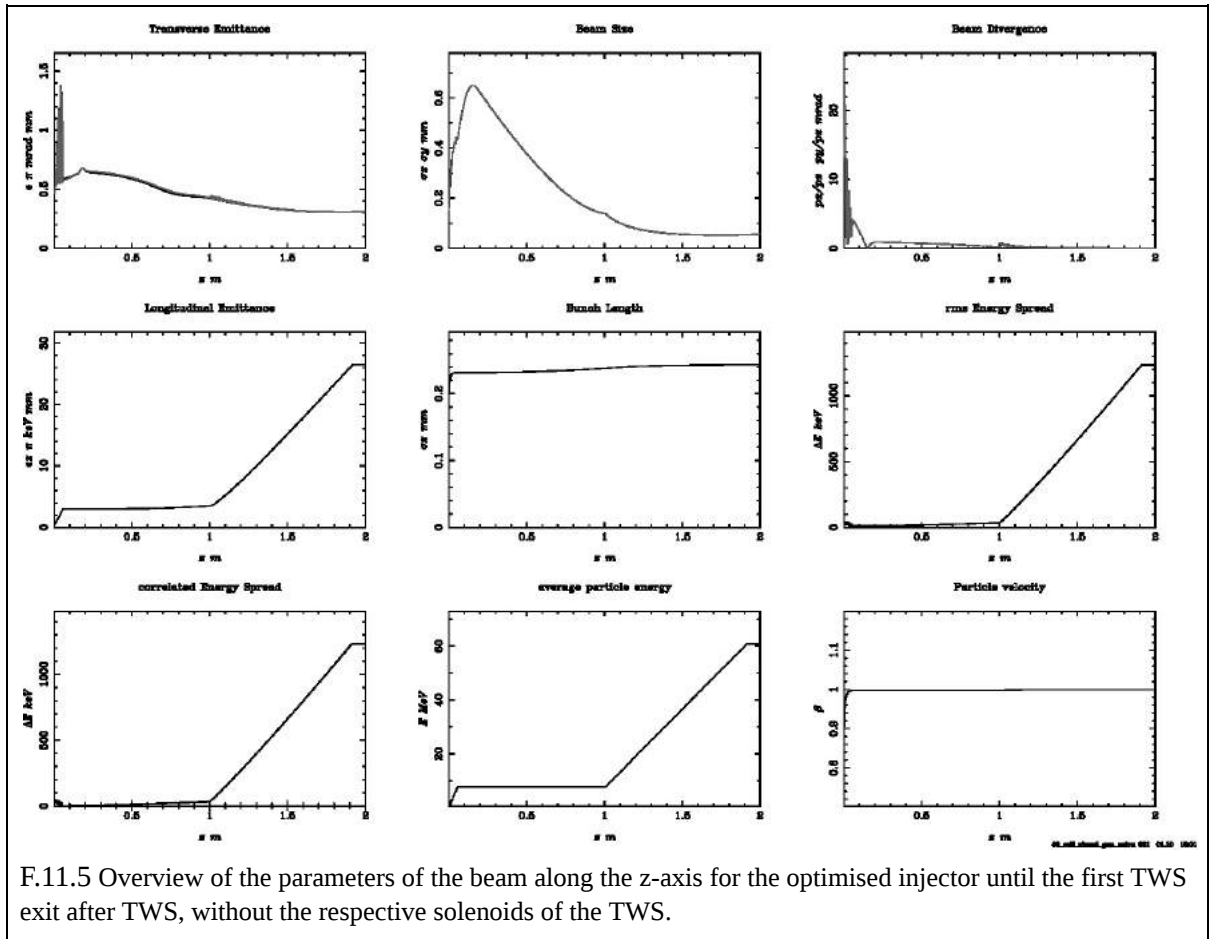
Comparison of the figures of merit in the cases of Cu and Cs₂Te photocathode for the respective optimised lattices. The following results concern the optimal lattices with the TWS solenoids, Table 11.3, shifted accordingly.

	Cu	Cs ₂ Te
Emittance (π mm mrad) x-axis	0.324	0.349
Transverse Size (mm) x-axis	0.210	0.067
Longitudinal Size (mm)	0.21	0.24
Divergence (mrad)	0.27	0.11
Emittance (π mm mrad) y-axis	0.210	0.338
Transverse Size (mm) y-axis	0.997	0.067

The Cu with the solenoids seems to have greater transverse emittance and divergence , compared to the simulations without the solenoids. Which means that the solenoid's distribution needs to be optimised.

Comparing the two materials, Cs₂Te seems to result in half the transverse size and divergence but in slightly greater emittance.

The respective results for Cs₂Te without the solenoids of the TWS are :



F.11.5 Overview of the parameters of the beam along the z-axis for the optimised injector until the first TWS exit after TWS, without the respective solenoids of the TWS.

TABLE 11.13		
Comparison of the figures of merit in the cases of Cu and Cs ₂ Te photocathode for the respective optimised lattices. The following results concern the optimal lattices without the TWS solenoids.		
	Cu	Cs ₂ Te
Emittance (pi mm mrad) x-axis	0.225	0.309
Transverse Size (mm) x-axis	0.102	0.058
Longitudinal Size (mm)	0.24	0.24
Divergence (mrad)	0.005	0.06
Emittance (pi mm mrad) y-axis	0.212	0.310
Transverse Size (mm) y-axis	0.997	0.058

The relevant results seem to have the same behaviour as with the solenoids. The Cu case results in much less emittance and divergence. On the other hand, the transverse size is increased and the longitudinal size has been left intact.

11.6.3 Conclusions

The optimisation of the X-band in Cu apparently was successful as the transverse emittance halved leaving the transverse size intact. Intensifying the beam profile by narrowing the laser transverse size, the beam waist shifted away from the cathode while the emittance decreased. Even though the initial transverse size of the laser is double the final, the transverse size at the end of the first TWS is almost the same. This happens because the transverse size has been matched to the linac (5.1)

As a result of the simulations, the two materials were not able to operate under the exact same parameter setup. The reason for this is the emission delay of the semiconductor. The 0.4 psec emission delay represents, according to (10.5), 1.7 degrees in the RF period at 12 GHz. The emission has to occur during 10 degrees of the RF period and 1.7 degrees represent 17% of that time. So, the emission delay in short pulses alters the beam profile, thus the slices' profile, and the plasma oscillations. Also, it corresponds to a different initial phase of the gun, on which the Cu photocathode does not operate optimally.

12. Conclusions and Suggestions for further analysis

The goal of this diploma thesis was to study the beam dynamics in the photoinjector part of an X-Ray Free Electron Laser, compare the beams generated by two different photocathode materials and, finally, present the pros and cons of each material choice for the operation of XFEL of CompactLight (XLS) Collaboration project.

The materials that were subject to study were Copper/Cu (metal) and Cesium-Telluride/Cs₂Te (semiconductor), that are the most commonly used photocathodes for electron beam generation in Linear Accelerators. The two materials have a very close emittance which makes their comparison easier, as it only relies on the parameter of the emission delay (τ) or emission latency. As it observed, the emission delay changes the dynamics of the beam in a way that is not destructive of the results in the S-band frequencies (3 GHz). In the first optimised layout, the substitution of the cathode with a semiconductor did not disturb the performance. The waist of the beam shifted several millimeters closer to the TWS and, as a result, the beam emittance ‘froze’ at a convergent phase space near the waist (Table 9.2). So, the performance was slightly worse.

On the other hand, in the X-band frequencies (12 GHz) the laser pulse duration is limited to up to 2 psec. This makes the emission delay of Cs₂Te, 0.4 psec, comparable to the RF period and the 2 psec emission duration threshold. As a consequence, the two materials require different initial phases in the gun and have different waist positions, meaning that in the X-band the cathodes are not exchangeable. Although, both can operate in both bands with comparable results. The Cs₂Te did not produce satisfactory emittance in the X-band but optimising its lattice individually was not possible, so this observation is not conclusive but subject to further analysis. GIOTTO did not lead the lattice to work on the *Ferrario Working Point* so this was achieved manually by performing an appropriate shift to the TWS, showing that the parameter choice in optimisation must be very careful to avoid such phenomena. After the shift the performance was optimised for Cu and even more for Cs₂Te, that appeared to have a waist even closer to the TWS entrance, even though for different gun phase. In conclusion, both materials can operate theoretically in the X-band in different gun setups showing similar performance. Additionally, the durability of the materials in the high gradients of the X-band frequencies (250 MV/m) needs to be studied and investigated.

What is more, for the operation of the X-band gun the laser system that was taken for granted in the S-band (Swiss FEL laser) cannot be used. The reason is that the minimum laser pulse length that it can be produced with a flattop profile is 3.6 psec and the maximum the X-band requires is approximately 2 psec.

The main advantage of the semiconductor in both cases is its high Quantum Efficiency, which allows the same charge to be produced with 1000 times less laser pulse energy (see Appendix B.5). This means less power consumption and the possibility to drive the laser to other targets and use it otherwise. Even though the laser power required is less, the Cs₂Te photocathodes are costly to manufacture, buy and maintain as they require very high vacuum and last from some hours up to several months. On the other hand the Cu photocathodes are both cheap and long lasting, and also are more tolerant to imperfect vacuum conditions [25].

What is more, the Cs₂Te is reported to smooth the spikes of a Flattop laser temporal profile due to the emission delay[25]. Such phenomena should be simulated with other tools of emission simulation for detailed results from the emission process and the final beam.

As shown before, an algorithmic optimisation of the lattice can result in distributions a manual optimisations would take a very long time to get to. A genetic algorithm is one of these cases. It does not require knowledge of the nature of the problem, but makes a smart choice of parameters

based on principles of biology and it can apply to many fields of study such as accelerators. These principles concern the survival of the stronger, that in this case is translated to the high probability of selection of the more appropriate parameter set.

In general, the optimisation process is very complex because of the number of variables and the non-linearity of the problem. So, the process of optimisation should be very careful and repeatedly tested. The genetic algorithm GIOTTO is subject to many user defined algorithm variables. This means that the constraints set by the user may exclude a possible solution or delay the results. Even though the outcome of the optimisations is satisfactory, the results can only be described as optimal solutions rather than optimum ones.

What is more, the optimisations performed were split in two, as independent as possible, parts, due to lack of computational resources. Also the algorithm execution never exceeded 240 generations out of the 400 and often were far less. This means that if the resources were available a more effective optimisation could be performed. Also, the GIOTTO algorithm did not support the delay variable, which means that only the Cu case could be optimised. Thus, a further research on the optimal solution for the semiconductor could lead to more reliable results for the comparison of the two.

In conclusion, Cu and Cs₂Te are exchangeable materials for the photocathode. With proper tuning and optimisation the performance can be drastically improved for both. The thermal emittance of Cs₂Te is slightly higher, giving the Cs₂Te a small disadvantage that can be compensated by its high Quantum Efficiency. Also, the emission delay of the semiconductor is not only important but can, also, require a different setup for proper operation of the injector. Other parameters, such as the cost and the lifetime of the cathodes must be taken into account and, of course, more refined optimisation can lead to results even even closer to the CompactLight Collaboration final goals.

13. Bibliography

- [1] Bacci, et al. "GIOTTO: A Genetic Code for Demanding Beam-Dynamics optimisations." *DOI*, JACOW, Geneva, Switzerland, 1 June 2016, doi.org/10.18429/JACoW-IPAC2016-WEPOY039.
- [2] Bakr, Mahmoud & Vashchenko, Grygorii & Khojoyan, Martin & Krasilnikov, M. & Stephan, F.. (2015). BEAM DYNAMICS SIMULATION FOR THE UPGRADED PITZ PHOTO INJECTOR APPLYING VARIOUS PHOTOCATHODE LASER PULSES.
- [4] Bettoni, S., et al. "Low Emittance Injector Design for Free Electron Lasers." *Physical Review Special Topics - Accelerators and Beams*, vol. 18, no. 12, 2015, doi:10.1103/physrevstab.18.123403.
- [5] Cianchi, A., et al. "High Brightness Electron Beam Emittance Evolution Measurements in an Rf Photoinjector." *Physical Review Special Topics - Accelerators and Beams*, vol. 11, no. 3, 2008, doi:10.1103/physrevstab.11.032801.
- [6] D'auria, G & Di Mitri, S. & Rochow, Regina & Trieste, Sincrotrone & Latina, Italy & Liu, Xiongyi & Rossi, Carlo & Schulte, D & Cortes, H & Clarke, Jim & Dunning, David & Thompson, N & Goryashko, V & Jacewicz, M & Ruber, R & Dowd, R & Zhu, D & Aksoy, Australia & Negris, Z & Zhang, L. (2019). CompactLight DESIGN STUDY. 10.18429/JACoW-IPAC2019-TUPRB032.
- [7] Ding, Y., et al. "Measurements and Simulations of Ultralow Emittance and Ultrashort Electron Beams in the Linac Coherent Light Source." *Physical Review Letters*, vol. 102, no. 25, 2009, doi:10.1103/physrevlett.102.254801.
- [8] Duris, et al. "Bayesian optimisation of a Free-Electron Laser." *ArXiv.org*, 12 Sept. 2019, arxiv.org/abs/1909.05963.
- [9] Falone, Antonio & Adelman, A. & Raguin, Jean-Yves & Stingelin, Lukas. (2011). RF Gun Studies for the SwissFEL Injector.

- [10] Ferrario, M., et al. "Homodyn Study For The Lcls Rf Photo-Injector." *The Physics of High Brightness Beams*, 2000, doi:10.1142/9789812792181_0037.
- [11] Ferrario, Massimo. "Space Charge Mitigation." *CERN Yellow Reports: School Proceedings*, dx.doi.org/10.23730/CYRSP-2018-001.177.
- [12] Hernandez-Garcia, C., et al. "Charge Production Studies from Cs₂Te Photocathodes in a Normal Conducting RF Gun." *Nuclear Instruments and Methods in Physics Research Section A: Accelerators, Spectrometers, Detectors and Associated Equipment*, vol. 871, 2017, pp. 97–104., doi:10.1016/j.nima.2017.06.051.
- [13] Hernandez-Garcia, C., et al. "Charge Production Studies from Cs₂Te Photocathodes in a Normal Conducting RF Gun." *Nuclear Instruments and Methods in Physics Research Section A: Accelerators, Spectrometers, Detectors and Associated Equipment*, vol. 871, 2017, pp. 97–104., doi:10.1016/j.nima.2017.06.051.
- [14] J.-Y. Raguin, PSI, CH-5232 Villigen, Switzerland (2012). *The Swiss FEL S-Band Accelerating Structure : RF Design*. ISBN 978-3-95450-122-9
- [15] Jensen, Kevin L., et al. "Delayed Photo-Emission Model for Beam Optics Codes." *Journal of Vacuum Science & Technology B, Nanotechnology and Microelectronics: Materials, Processing, Measurement, and Phenomena*, vol. 35, no. 2, 2017, doi:10.1116/1.4968511.
- [16] Livingston, Milton Stanley., and John Paul. Blewett. *Particle Accelerators*. McGraw-Hill, 1962.
- [17] Maurizio. "Linear Accelerators." *CERN Document Server*, CERN, 29 Mar. 2013, arxiv.org/ct?url=https://dx.doi.org/10.5170/CERN-2013-001.225&v=e1312714.
- [18] Meier, E., et al. "Development of a Novel optimisation Tool for Electron Linacs Inspired by Artificial Intelligence Techniques in Video Games." *Nuclear Instruments and Methods in Physics Research Section A: Accelerators, Spectrometers, Detectors and Associated Equipment*, vol. 632, no. 1, 2011, pp. 1–6., doi:10.1016/j.nima.2010.12.203.

- [19] Milne, Christopher, et al. "SwissFEL: The Swiss X-Ray Free Electron Laser." *Applied Sciences*, vol. 7, no. 7, 2017, p. 720., doi:10.3390/app7070720.
- [20] Mitchell, Melanie. *An Introduction to Genetic Algorithms*. MIT, 1998.
- [21] Negnevitsky, Michael. *Artificial Intelligence: a Guide to Intelligent Systems*. Addison-Wesley, 2008.
- [22] Prat, Eduard, et al. "Emittance Measurements and Minimization at the SwissFEL Injector Test Facility." *Physical Review Special Topics - Accelerators and Beams*, vol. 17, no. 10, 2014, doi:10.1103/physrevstab.17.104401.
- [23] Prat, Eduard, et al. "Measurements of Cu and Cesium Telluride Cathodes in a Radio-Frequency Photoinjector." *Physical Review Accelerators and Beams*, American Physical Society, 9 Apr. 2015, dx.doi.org/10.1103/PhysRevSTAB.18.043401.
- [24] Raguin, Jean-Yves & Bopp, M & Citterio, A & Scherer, A. (2012). The Swiss FEL RF Gun: RF Design and Thermal Analysis.
- [25] Rao, Triveni, and David H. Dowell. *An Engineering Guide to Photoinjectors*. CreateSpace Independent Publishing, 2013.
- [26] Schaer, and Mattia. "RF Traveling-Wave Electron Gun for High Brightness Photoinjectors." *RF Traveling-Wave Electron Gun for High Brightness Photoinjectors - Research Collection*, ETH Zürich, 1 Jan. 1970, doi.org/10.3929/ethz-a-010749949.
- [27] Spicer, William E., and Alberto Herrera-Gomez. "Modern Theory and Applications of Photocathodes." *Photodetectors and Power Meters*, 1993, doi:10.1117/12.158575.
- [28] Wangler, Thomas P. *RF Linear Accelerators*. Wiley-VCH Verlag, 2017.
- [29] Wiedemann, Helmut. *Particle Accelerator Physics: with 264 Figures*. Springer, 2007.
- [30] <https://www-ssrl.slac.stanford.edu/stohr/xfels.pdf>
- [31] <https://apacheynite.readme.io/docs/genetic-algorithms>
- [32] https://en.wikipedia.org/wiki/Particle_accelerator#Low-energy_machines_and_particle_therapy
- [33] <https://en.wikipedia.org/wiki/Undulator>
- [34] https://en.wikipedia.org/wiki/Bayesian_optimisation
- [35] Personal Communication, A. Avni

Appendix A. Particle Beam Dynamics

A.1 Single Particle Dynamics

In this part of the chapter the theory of linear particle beams is discussed, thus a single particle, in the most important electromagnetic fields. Also, the matrix formalism in linear beam dynamics will be presented and will be useful later on the analysis.

The following analysis focuses on the linear approximation of motion in the magnetic fields of a dipole, a quadrupole, a multipole and the drift space, where there is absence of any field. A dipole is used for bending a beam's trajectory, while quadrupoles and multipoles are used for focusing of the beam. Especially, if the quadrupole results in focusing on a plane eg. x-plane, it will result in defocusing on the other plane eg. y-plane.

Let us assume a quadrupole and a dipole that bends only in the x-plane. The respective magnetic fields in the x and y- plane are:

$$B_x = -gy \quad (\text{defocusing})$$

$$B_y = B_{y0} + gx, \quad (\text{focusing and bending})$$

B_{y0} : dipole field, g : quadrupole gradient

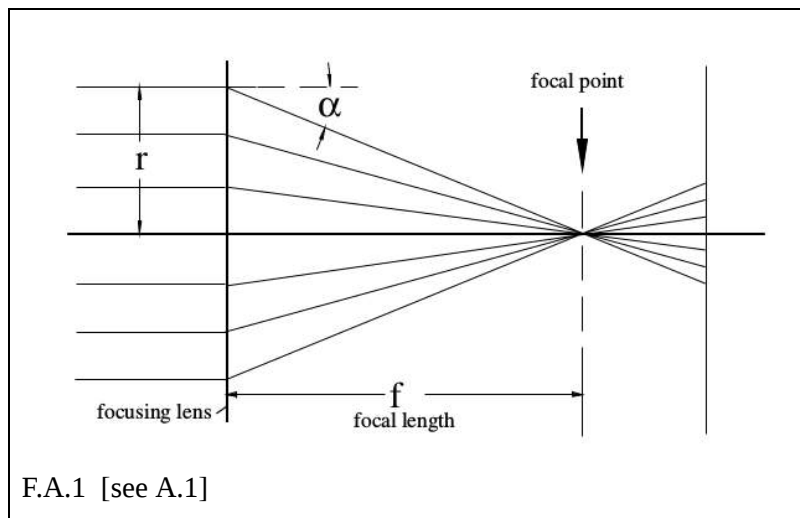
Using the equations of motion presented in Chapter 3 of [A.1] and their linear approximation, one can obtain the approximate solutions of motion :

$$x'' + (k_0 + \kappa_{0x}^2)x = 0 \quad (\text{A.1})$$

$$y'' - k_0 y = 0 \quad (\text{A.2})$$

The $k_0 + \kappa_{0x}^2$ term describes the focusing effects from quadrupoles and a pure geometrical focusing from bending in a sector magnet.

From k_0 and κ_{0x} the focal length of the quadrupole can be found. The focal length is the distance from the quadrupole where the beam is focused to a point, like the figure below.



and is defined as $f = -\frac{L}{a}$ where r : distance from the axis of the centre of the quadrupole
 a : the deflection angle.

In this case, a is defined, if (A.1) or (A.2) are integrated over a short distance Δz .

$$\int y'' dz = - \int k_0 y dz \Rightarrow y' - y_0' = - k_0 y \Delta z \Rightarrow a = - k_0 y \Delta z \Rightarrow - \frac{y}{a} \Rightarrow$$

$$\frac{1}{f} = k_0 \Delta z \quad (A.3)$$

The parameters k_0 and κ_{0x} derive directly from the magnetic field as factors of the magnetic field 's Taylor expansion (see [A.1] ch. 2). But, they are a function of the variable z , which makes it impossible for the equations (A.1) and (A.2) to be solved in general.

From these equations the magnet strength parameter is obtained: $K(z) = k_0(z) + \kappa_{0x}^2(z)$, which is also a function of z and varies as the beam travels through the various parts of the beam line and also varies inside the components when the fields are significantly non-uniform. The most common example should be the fringe magnetic fields that can be important for the evolution of the beam.

To overcome this fact, the matrix formalism makes one assumption and one mathematical trick. The assumption is that all the magnetic fields are considered to be uniform, thus called "hard-edged" and the model respectively called the "hard-edge model". Now, the parameter K is constant inside each component and (A.1) and (A.2) can be written as:

$$u'' + K u = 0 \quad (A.3), \quad u = x, y \text{ and } K = \text{constant}$$

which is the equation of an harmonic oscillator.

Let $C(z)$ be the cosine part of the solution and $S(z)$ be the sine part, then the transformation matrix is formed as :

$$\begin{pmatrix} u(z) \\ u'(z) \end{pmatrix} = \begin{pmatrix} C_u(z) & S_u(z) \\ C'_u(z) & S'_u(z) \end{pmatrix} \begin{pmatrix} u_0 \\ u'_0 \end{pmatrix}$$

The transformation matrix is:

$$M = \begin{pmatrix} C(z) & S_u(z) \\ C'_u(z) & S'_u(z) \end{pmatrix} \quad (A.4)$$

Important Transformation Matrices :

Drift space :

$K = 0$, so:

$$\mathcal{M}_d(\ell|0) = \begin{pmatrix} 1 & \ell \\ 0 & 1 \end{pmatrix} \quad (A.5)$$

where l is the length of the drift space

Quadrupole :

Focusing :

$$\mathcal{M}_{QF}(\ell|0) = \begin{pmatrix} \cos \varphi & \frac{1}{\sqrt{k}} \sin \varphi \\ -\sqrt{k} \sin \varphi & \cos \varphi \end{pmatrix} \quad (\text{A.6})$$

Defocusing :

$$\mathcal{M}_{QD}(\ell|0) = \begin{pmatrix} \cosh \varphi & \frac{1}{\sqrt{|k|}} \sinh \varphi \\ \sqrt{|k|} \sinh \varphi & \cosh \varphi \end{pmatrix} \quad (\text{A.7})$$

where $\varphi = \sqrt{k}l$, k = the magnet constant and l = the quadrupole length.

Thin lens approximation of a quadrupole

Let $l \rightarrow 0$ and the focal length stays constant.

$$(\text{A.3}) \Rightarrow kl = \text{constant} \Rightarrow \sqrt{k}l \rightarrow 0$$

So the matrices now are:

focusing:

$$M_{QF} = \begin{pmatrix} 1 & l \\ 1/f & 1 \end{pmatrix} \quad (\text{A.8})$$

defocusing :

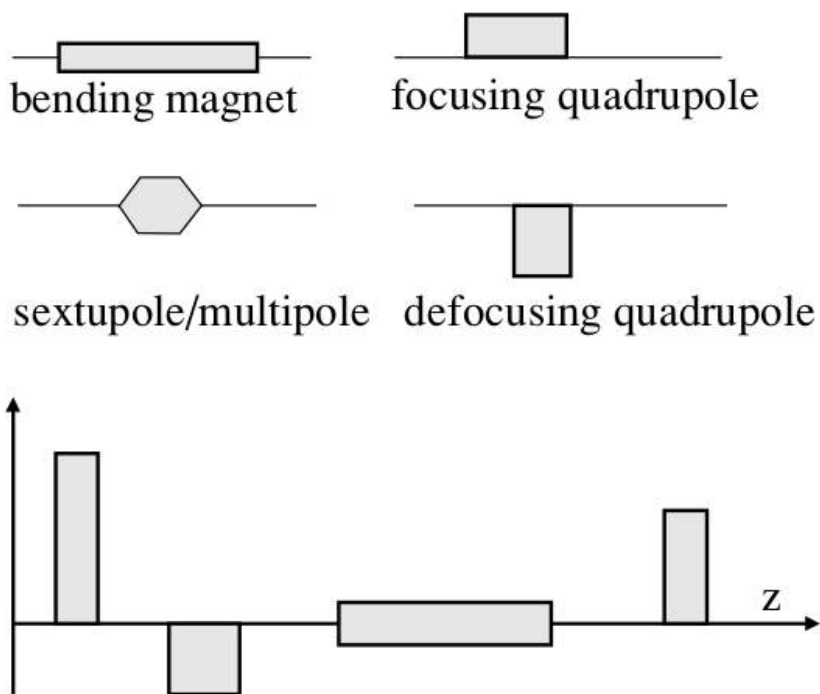
$$M_{QD} = \begin{pmatrix} 1 & l \\ -1/f & 1 \end{pmatrix} \quad (\text{A.9})$$

The reason why this approximation can be considered safe and useful is because usually the length of the quadrupole is insignificant compared to the focal length.

The trick previously mentioned is that it is possible to split the beam line in separate uniform parts . So, in a beam line that can be described using the matrix formalism , the whole beam line or parts of it can be described as a matrix equal to the product of all the matrices describing each part.

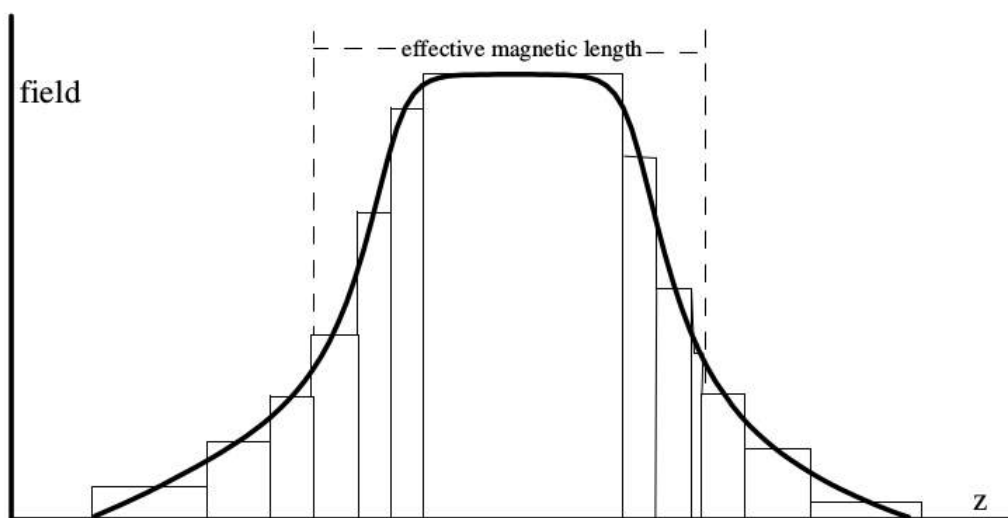
$$M = M_1 \cdot M_2 \cdots M_n$$

The most classic example of that kind is the FODO lattice - channel, which is a lattice of periodical focusing and defocusing quadrupoles that are usually considered as thin lenses. Further discussion is out of the discussion of this thesis.



F.A.2 Symbols for magnets in lattice design and typical distributions of magnets along a beam transport line [see A.1]

The same idea applies in fringe fields where the technique is to split the fringe part into consecutive uniform parts, each one of which has its own transformation matrix.



F.A.3 Decomposition of an actual quadrupole field profile into segments of hard edge quadrupoles [see A.1]

A.2 RF fields and gun geometries

A.3 Particle Beams and Phase Space

Phase Space

Each particle along the beam transport line can be represented by a point in a six dimensional phase space $(x, p_x, y, p_y, \sigma, E)$, where p_x, p_y are the transverse momenta σ is the coordinate along the trajectory and E is the particle energy. Instead of the energy E often the momentum cp or the momentum deviation from the ideal momentum $\Delta p = p - p_0$ or the relative momentum deviation $\Delta p/p_0$ is used.

For small angles :

$$p_x = p_0 x' \quad (\text{A.10a})$$

$$p_y = p_0 y' \quad (\text{A.10b})$$

When the energy of the beam stays constant, instead of the momenta, the slope of the trajectories x' and y' is used. Also, if the transverse momentum is very small compared to the longitudinal ($p_z \gg p_x, p_y$) then $\sin x' \approx x'$ and $\sin y' \approx y'$ (transverse angles) .

If the coupling between the x and y-plane can be ignored the beam can be described by the two transverse distributions (x, x') and (y, y') . This is the case in this thesis.

Then, for example, p_x can be written as:

$$p_x = mu_x + qA_x = m_0 c \beta \gamma x' + qA_x \quad (\text{A.11})$$

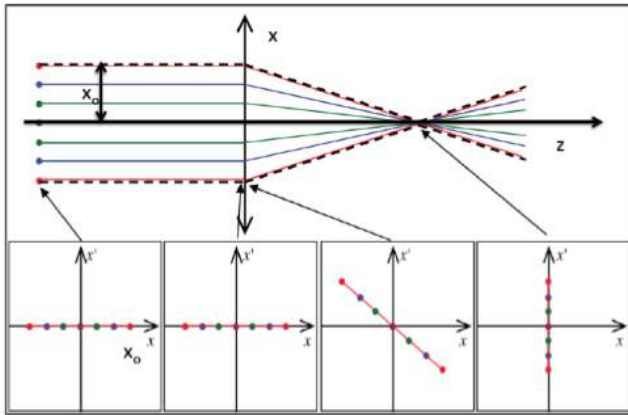
, where m_0 is the rest mass of the particle, $x' = dx/dz$, q is the charge of the particle, and A_x is the x-component of the magnetic vector potential . A similar relation holds for q_y .

Laminarity

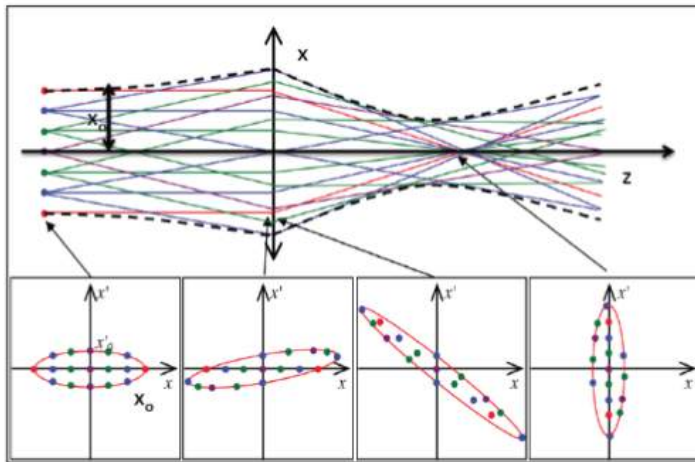
An ideal high-charge particle beam has orbits that flow in layers that never intersect, as occurs in a laminar fluid. Such a beam is often called a laminar beam. Two conditions must be met to have a laminar beam:

1. all particles at a given position must have identical velocities
2. the magnitudes of the slopes of the trajectories in the transverse directions x and y, given by $x'(z) = dx/dz$ and $y'(z) = dy/dz$, where z the direction of propagation, are linearly proportional to the displacement from the z axis of beam propagation.

As an example, below are presented the trajectories and phase space in a laminar and in a non-laminar beam when they propagate through a focal lens.



F.A.4 Particle trajectories and phase space evolution of a laminar beam [see A.2]

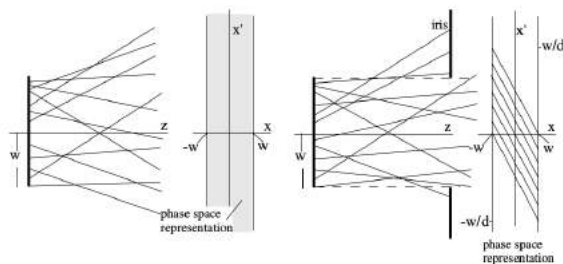


F.A.5 Particle trajectories and phase space evolution of a non-laminar beam [see A.2]

Beam Emittance and Twiss parameters

The beam emittance in the two dimensional phase space is defined as the region occupied by the particles of the beam in this plane. Their numerical values multiplied by π are equal to the area occupied by the beam in the respective phase plane. In higher dimensioned phase spaced the emittance is equal to the respective volume.

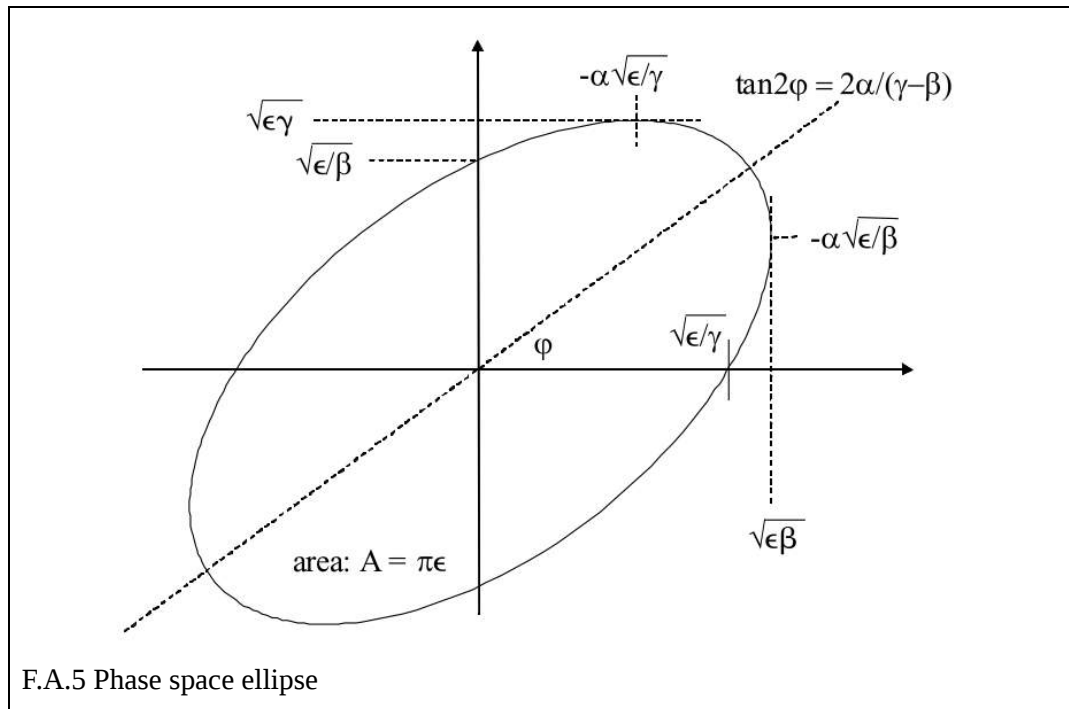
In order to understand better the emittance concept there is a simple example in F.A.4:



FA.4 Beam from a diffuse source in real space and in phase space (left). Reduction of phase space (shaded area) due to beam restriction by an iris aperture (right) [see A.1]

The reason why the phase space is an important tool in beam dynamics is because it can be proved that the density of particles in phase space does not change along a beam transport line, if the forces acting on particles can be derived from macroscopic electric and magnetic fields. This is the known Liouville's theorem and it can be proved either using the analytical Maxwell's equations or the matrix formalism discussed above [see A.1 ch.5.1.1].

Customarily, the phase space of a beam is represented by an ellipse called the phase ellipse. Of course, the shape of the ellipse is not completely arbitrary but derives from the way the differential equation of motion is solved and will be presented later. The general form of the ellipse is presented below:



The ellipse is described by:

$$\gamma x^2 + 2\alpha x x' + \beta x'^2 = \epsilon \quad (\text{A.12a})$$

The area enclosed by the ellipse is the emittance ϵ , defined as :

$$\int_{\text{ellipse}} dx dx' = \pi \epsilon \quad (\text{A.13})$$

From this definition, the emittance is measured in meters-radians (usually pi mm mrad).

In bibliography, the following definition can be found, as well:

$$\gamma x^2 + 2\alpha x x' + \beta (x')^2 = A^2 \quad (\text{A.12b})$$

And the area then is equal to πA^2 so $\epsilon = \pi A^2$ and it is measured in pi-meters-radians.

In the simulations to follow, emittance will be measured in [pi mm mrad]

The parameters α, β, γ , are called the Twiss parameters and are representative of the ellipse's shape and orientation.

From, the geometrical properties of the ellipse one can get :
 $\beta\gamma - \alpha^2 = 1$ (A.14), which is the definition of the parameter γ as well.

From the ellipse it also derives that:

$$\begin{cases} X_{\max} = \sqrt{\beta_x \epsilon_x} \\ (X_{\max})' = -\alpha \sqrt{\frac{\epsilon}{\beta}} \\ X'_{\max} = \sqrt{\gamma_x \epsilon_x} \end{cases} \quad (\text{A.15})$$

Transformation of the Twiss parameters

It is obvious that the Twiss parameters, thus the ellipse shape, change through the beam line. In order to determine the way this happens one can use the matrix formalism transformation matrix :

$$\begin{pmatrix} x(z) \\ x'(z) \end{pmatrix} = \begin{pmatrix} C(z) & S(z) \\ C'(z) & S'(z) \end{pmatrix} \begin{pmatrix} x_0 \\ x'_0 \end{pmatrix}$$

and the equation of the initial ellipse:

$$\gamma_0 x_0^2 + 2\alpha_0 x_0 x'_0 + \beta_0 x_0'^2 = \epsilon$$

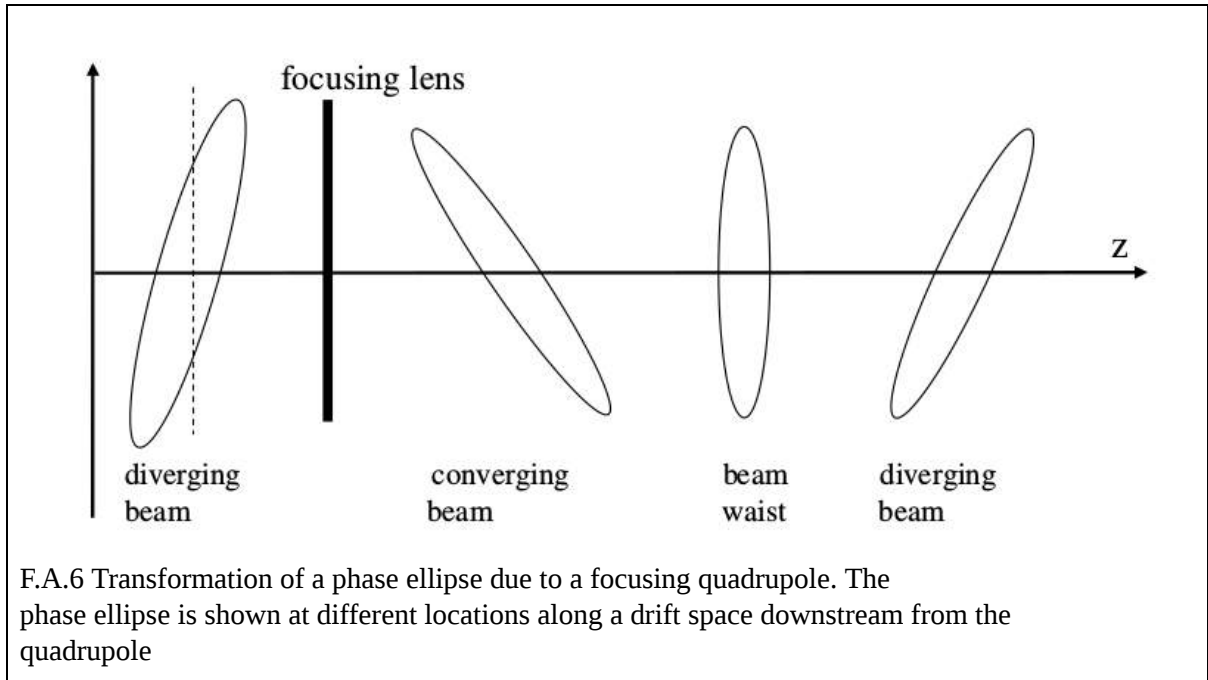
and finally be led to the transformation matrix [A.1] :

$$\begin{pmatrix} \beta(z) \\ \alpha(z) \\ \gamma(z) \end{pmatrix} = \begin{pmatrix} C^2 & -2CS & S^2 \\ -CC' & CS' + C'S & -SS' \\ C'^2 & -2C'S' & S'^2 \end{pmatrix} \begin{pmatrix} \beta_0 \\ \alpha_0 \\ \gamma_0 \end{pmatrix} \quad (\text{A.16})$$

For example in drift space the respective matrix is :

$$\begin{pmatrix} \beta(\ell) \\ \alpha(\ell) \\ \gamma(\ell) \end{pmatrix} = \begin{pmatrix} 1 & -2\ell & \ell^2 \\ 0 & 1 & -\ell \\ 0 & 0 & 1 \end{pmatrix} \begin{pmatrix} \beta_0 \\ \alpha_0 \\ \gamma_0 \end{pmatrix}, \quad (\text{A.16a})$$

The latter matrix, describes the transition from a converging beam to a diverging beam in drift space, as γ stays constant, α decreases and β increases. Convergent beams are characterized by a rotated phase ellipse extending from the left upper quadrant to the lower right quadrant while a divergent beam spreads from the left lower to the right upper quadrant. A symmetric phase ellipse signals the location of a waist or symmetry point. [A.1]



The location of the beam waist will prove to be very useful later on.

Betatron function and Hill's equation of motion

The equation of motion of a particle in the lattice , eg. for the x-axis, is:
 $x'' + k(z)x = 0$, where z is the axis of propagation and $k(z)$ is arbitrary and depends on the lattice. A solution of the equation could be the following:

$$x(z) = A\sqrt{\beta(z)}\cos(\psi(z)) \quad (\text{A.17})$$

This equation is called the 1D Hills equation of motion and describes an harmonic variation of the beam envelope along the beam line. $\beta(z)$ is the Twiss parameter that were presented earlier , it is called the betatron function and the other two parameters are defined according to it. It can be proven [A.1] that the phase function is defined from the betatron function and equals to :

$$\psi(z) = \int_0^z \frac{d\bar{z}}{\beta(\bar{z})} + \psi_0 \quad (\text{A.18})$$

The betatron function defines the beam envelope as follows :

$$E(z) = \pm \sqrt{\epsilon\beta(z)} \quad (\text{A.19})$$

It can easily be proved that the ellipse equation derives directly from the Hill's equation (see [A.1] Ch.5.2)

Normalised emittance

Very often instead of the emittance the normalised emittance is used in beam dynamics. The reason behind this choice is that while a beam accelerates it transversely shrinks. So, the normalized emittance is defined as:

$$\varepsilon_N = \varepsilon \cdot (\beta\gamma) \quad (\text{A.20})$$

β, γ are the relativistic parameters.

To explain this choice, one needs to use (A.11)

(A.11) $\Rightarrow x' \approx \frac{p_x}{mc\beta\gamma} \Rightarrow x'$ scales according to $\beta\gamma$. To recover the decrease one can multiply and the result no longer depends on the acceleration.

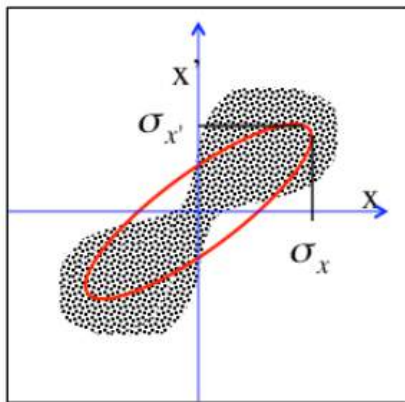
Statistical definition of the emittance

Of course, the definition of the emittance is not very helpful when one wants to measure it, because real-life beams do not have a ideal laminar flow. Non-linear forces distort the shape of the particle distribution and the final distribution may differ a lot from the ellipse. The solution is to form a statistical definition of the emittance so it is possible to use the particle distribution. The ellipse is still used as an equivalent ellipse whose projections on the x and x' -axis (or $y - y'$) are equal to the rms values of the distribution, let it be $f(x, x', z)$. The so called *root mean square (rms) emittance* is defined as [2]:

$$\gamma_x x^2 + 2\alpha_x x x' + \beta_x x'^2 = \varepsilon_{x,rms} \quad (\text{A.21})$$

and the following conditions must be valid, according to F.A.7 and (A.15):

$$\begin{cases} \sigma_x = \sqrt{\beta_x \varepsilon_{x,rms}} \\ \sigma_{x'} = \sqrt{\gamma_x \varepsilon_{x,rms}} \end{cases} \quad (\text{A.22})$$



F.A.7 Typical evolution of phase space distribution (black dots) under the effects of non-linear forces with the equivalent ellipse superimposed (red line).[A.1]

Using (A.22) and (A.21) and the definition of σ_x , $\sigma_{x'}$ and $\sigma_{xx'}$ it is not difficult to show [A.2] that the rms emittance can be computed by:

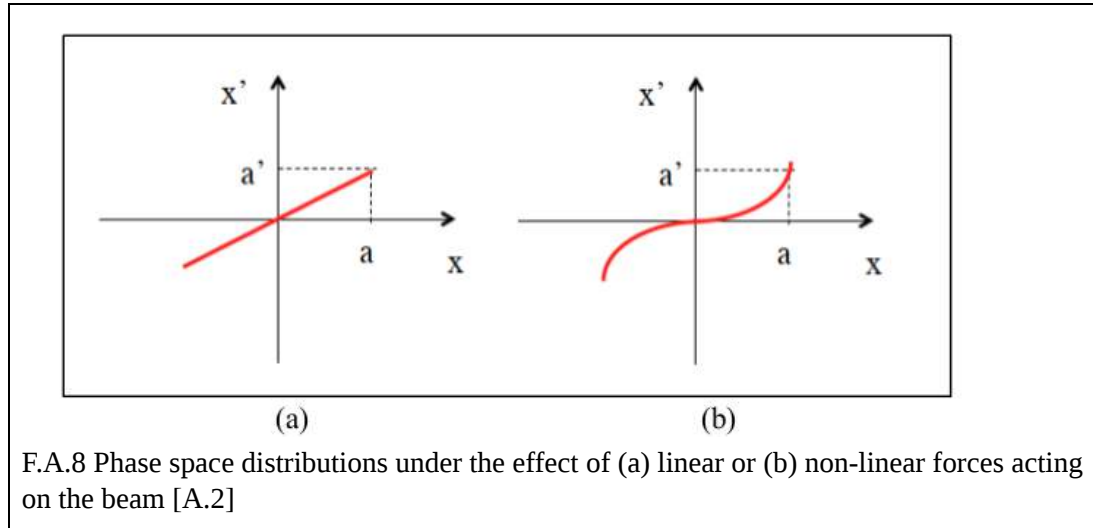
$$\varepsilon_{\text{rms}} = \sqrt{\sigma_x^2 \sigma_{x'}^2 - \sigma_{xx'}^2} = \sqrt{(\langle x^2 \rangle \langle x'^2 \rangle - \langle xx' \rangle^2)} \quad (\text{A.23})$$

This is the emittance that will be used in the simulation part of the thesis.

The statistical definition of the emittance has one very important advantage, it reveals non-linear behaviour of the distribution. For example, for two, zero-area, curves, a straight and a curved line that pass from the axis origin and are of the type $x' = Cx^n$, the following is valid:

$$\varepsilon_{\text{rms}}^2 = C \sqrt{\langle x^2 \rangle \langle x^{2n} \rangle - \langle x^{n+1} \rangle^2} \quad \begin{cases} n=1 \Rightarrow \varepsilon_{\text{rms}} = 0 \\ n>1 \Rightarrow \varepsilon_{\text{rms}} \neq 0 \end{cases} \quad (\text{A.24})$$

In the case of a straight line the emittance is equal to zero, as the area it occupies, but in the curved line it is not. So, the rms emittance, also, reveals distortions from non-linear forces.



In cases of acceleration it is more convenient to use the normalized emittance, which is now defined using the momenta $p_x = m_0 c \beta \gamma x'$ instead of the divergence x' . The reason is because, as shown in (A.20) the value $x'(\beta \gamma)$ is independent of the acceleration.

$$\varepsilon_{n,\text{rms}} = \frac{1}{m_0 c} \sqrt{\sigma_x^2 \sigma_{p_x}^2 - \sigma_{xp_x}^2} = \frac{1}{m_0 c} \sqrt{(\langle x^2 \rangle \langle p_x^2 \rangle - \langle xp_x \rangle^2)} = \sqrt{(\langle x^2 \rangle \langle (\beta \gamma x')^2 \rangle - \langle x \beta \gamma x' \rangle^2)} \quad (\text{A.25})$$

It is interesting to notice that in the relativistic limit the normalized emittance cannot be equal to zero due to the Heisenberg uncertainty relation $\sigma_x \sigma_{p_x} \geq \hbar/2$

So,

$$\varepsilon_{n,\text{rms}}^{QM} \geq \hbar/2m_0c = 1.9 \cdot 10^{-13} m \text{ for the electron.}$$

When the energy and the transverse positions are poorly correlated (A.25) can be written:

$$\varepsilon_{n,\text{rms}}^2 = \langle \beta^2 \gamma^2 \rangle \langle x^2 \rangle \langle x'^2 \rangle - \langle \beta \gamma \rangle^2 \langle xx' \rangle^2 \quad (\text{A.26})$$

The relative energy spread is defined as :

$$\sigma_y^2 = \frac{\langle \beta^2 \gamma^2 \rangle - \langle \beta \gamma \rangle^2}{\langle \beta \gamma \rangle^2} \quad (\text{A.27})$$

From (A.25) and (A.26) :

$$\varepsilon_{n,rms}^2 = \langle \beta^2 \gamma^2 \rangle \sigma_y^2 \langle x^2 \rangle \langle x'^2 \rangle + \langle \beta \gamma \rangle^2 \left(\langle x^2 \rangle \langle x'^2 \rangle - \langle x x' \rangle^2 \right) \quad (\text{A.28a})$$

For $\beta \rightarrow 1$:

$$\varepsilon_{n,rms}^2 = \langle \gamma^2 \rangle \left(\sigma_y^2 \sigma_x^2 \sigma_{x'}^2 + \varepsilon_{rms}^2 \right) \quad (\text{A.28b})$$

If the term is negligible, then the formula $\varepsilon_{n,rms}^2 = \langle \gamma^2 \rangle \varepsilon_{rms}^2$ is also valid [A.2]

According to [A.2], the latter formula is appropriate for conventional accelerators (such the one this thesis is examining) but not in plasma accelerators.

Brightness

The beam brightness combines the emittance and the peak current into a single parameter measuring the electron volume density. The most common practice is to define the transverse, normalized beam brightness, B_n :

$$B_n = \frac{2I}{\pi^2 \varepsilon_{n,x} \varepsilon_{n,y}} \quad (\text{A.29})$$

The beam envelope equation

Using the rms emittance definition and the derivatives of the beam size σ_x the beam envelope equation occurs [A.2]:

$$\sigma_x'' - \frac{1}{\sigma_x} \langle x x'' \rangle = \frac{\varepsilon_{rms}^2}{\sigma_x^3} \quad (\text{A.30})$$

In (A.30), the emittance term can be interpreted physically as an outward pressure on the beam envelope produced by the rms spread in trajectory angle, which is parameterized by the rms emittance

Beam envelope and betatron function in drift space

In matrix formalism the evolution of the beam envelope in drift space is described by (A.16a). The beam waist occurs for $a = 0$, thus in the position $z_w = a_0/\gamma_0$, assuming a_0, β_0, γ_0 to be the initial Twiss parameters. The betatron function then is :

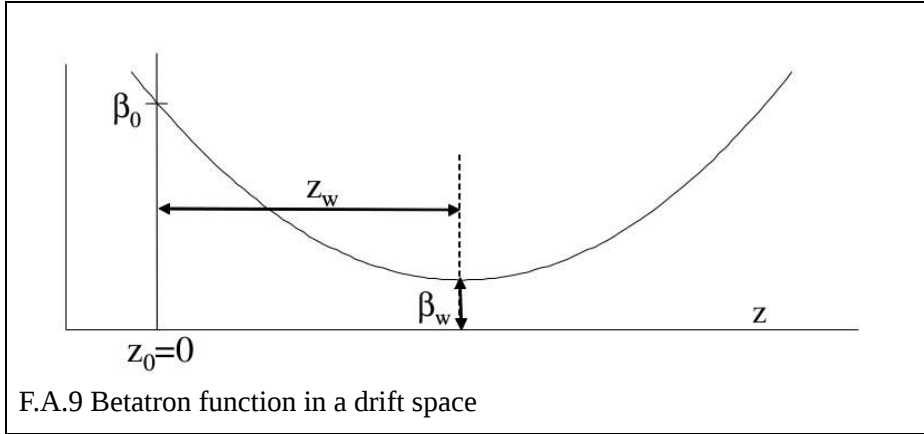
$$\beta(z - z_w) = \beta_w + \frac{(z - z_w)^2}{\beta_w} \quad (\text{A.31})$$

if $L = z - z_w$ is half the length of the drift space, then the optimum β anywhere along the drift space can be obtained if it is optimised with respect to β_w .

$$\frac{d\beta}{d\beta_w} = 0 \Rightarrow \beta_{w,opt} = L \quad (\text{A.32})$$

From (A.18) the phase advance in the waist is equal to $\psi(L) = \arctan(L/\beta_w) \rightarrow \pi/2$ for $L/\beta_w \rightarrow \pi/2$. So, $\psi(L) \leq \pi/2$ and generally in drift space the phase advance cannot exceed π radians (see F.A.6).

$$\Delta\psi_{drift} \leq \pi \quad (\text{A.33})$$



From a statistical point of view, when the phase space distribution is concerned, the rms beam size can be found :

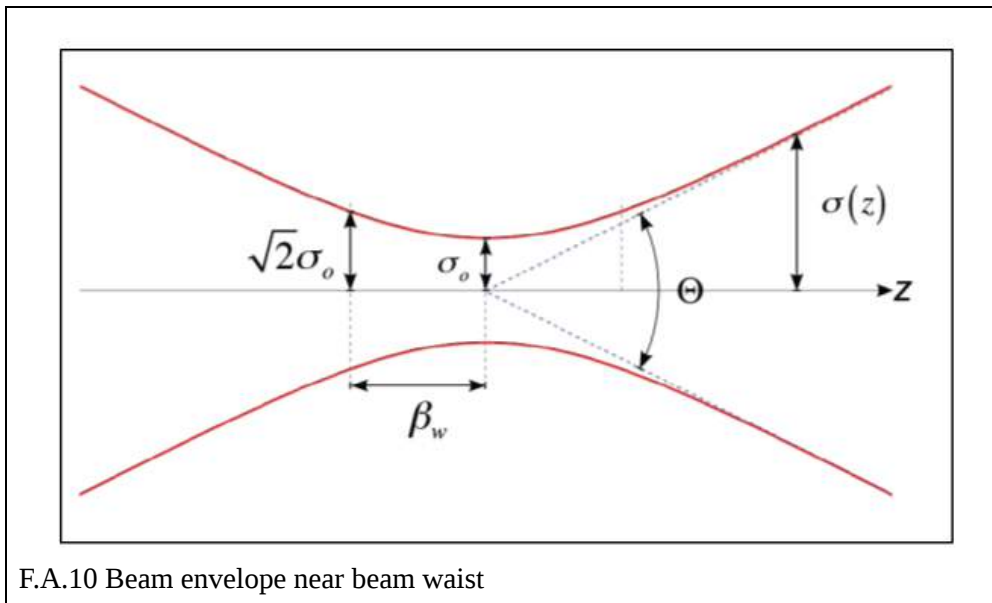
$$(\text{A.22}) \Rightarrow \sigma_x(z) = \sqrt{\beta_x(z)\epsilon_{x,rms}} = \sqrt{\beta_w\epsilon_{x,rms} + \beta_w\epsilon_{x,rms} \cdot \frac{(z-z_w)^2}{\beta_w^2}} \Rightarrow$$

$$\sigma_x(z) = \sigma_0 \sqrt{1 + \frac{(z-z_w)^2}{\beta_w^2}} \quad (\text{A.34})$$

Also,

$$\Theta = \tan^{-1}(\sigma_0/\beta_w) \quad (\text{A.35}) \quad (\tan\Theta = \lim_{z \rightarrow \infty} \sigma(z)/z = \sigma_0/\beta_w)$$

The equation (A.34) can also be obtained from (A.30) with use of the statistical definition of the emittance (A.23) [see A.2]



An important comment here should be made. At the waist the relation $\varepsilon^2 = \sigma_x^2 \sigma_x'^2$ is valid because $\sigma_{xx'} = 0$ in drift space (A.23). With use of (A.34) :

$$\sigma_x(z) = \sigma_{0x'}^2 (z - z_0)^2$$

Inserting the latter to (A.28b) , in the relativistic limit the normalized emittance:

$$\varepsilon_{n,rms}^2(z) = \langle \gamma^2 \rangle \left(\sigma_\gamma^2 \sigma_x'^4 (z - z_0)^2 + \varepsilon_{rms}^2 \right), \quad (A.35)$$

The relation above shows that if the energy spread and the divergence of the beam are significant in an accelerating beam, then in the drift space the normalized emittance will grow significantly even in a drift of length $(z - z_0)$. This conclusion will prove to be very useful in the simulations.

Beam envelope in acceleration

Let us assume an accelerating beam with momentum p , transverse momentum p_x , on which acts a transverse force F_x while accelerating. It can be proven [A.2] that the equation of motion (A.30) is expressed as:

$$\sigma_x'' + \frac{p'}{p} \sigma_x' - \frac{1}{\sigma_x} \frac{\langle x F_x \rangle}{\beta c p} = \frac{\varepsilon_{n,rms}^2}{\gamma^2 \sigma_x^3} \quad (A.36)$$

The important part of this equation is the acceleration term $(+ \frac{p'}{p} \sigma_x')$ that is an oscillation damping term, called “adiabatic damping”, proportional to $\frac{p'}{p}$. The term $\langle x, F_x \rangle$ represents the moment of any external transverse force acting on the beam, such as that produced by a focusing magnetic channel.

Beam envelope in RF focusing

Let us assume a uniform focusing channel (eg solenoid) without acceleration. Then the envelope equation (A.30) will take the form :

$$\sigma_x'' + k_{ext}^2 \sigma_x = \frac{\varepsilon_{rms}^2}{\sigma_x^3} \quad (A.37)$$

which is similar to (A.36) without the damping term. Substituting with (A.22):

$$\beta_x'' + 2k_{ext}^2 \beta_x = \frac{2}{\beta_x} + \frac{\beta_x'^2}{2\beta_x} \quad (A.38)$$

The betatron function is not dependent to the emittance but only depends on the external field.

The equilibrium solution of (A.38) is $\beta_{eq} = 1/k_{ext} = \lambda_\beta/2\pi$ (A.39) [see A.2], where λ_β is called “betatron wavelength” and the corresponding envelope size is $\sigma_x = \sqrt{\varepsilon_{rms}/k_{ext}}$.

Space charge forces and the complete envelope equation

The Coulomb forces created inside the beam can be classified in two regimes:

- a) Collisional regime , dominated by binary collisions caused by close particle encounters
- b) collective regime or space charge regime, dominated by the self-field produced by the particles' distribution.

As long as the Debye length remains small compared with the particle bunch transverse size, the beam is in the space charge dominated regime and is not sensitive to binary collisions.[A.2]

The Debye length is defined as:

$$\lambda_D = \sqrt{\frac{\epsilon_0 \gamma^2 k_B T_b}{e^2 n}} \quad (\text{A.40})$$

When the beam is space charge dominated then the space charge field can be treated as an external field. This field can be described in linear and non-linear terms; the first result in emittance growth because of defocusing and size growth , while the latter result in distortion in the phase space distribution, thus emittance growth.

Let us assume a beam with uniform charge distribution, cylindrical shape of radius R and length L, carrying a current \hat{I} and having a velocity $v_z = \beta c$. Then, the linear component of the longitudinal and transverse space charge field are given approximately by [A.2] [also see A.1 ch.18]:

$$E_z(\zeta) = \frac{\hat{I}L}{2\pi\epsilon_0 R^2 \beta c} h(\zeta) \quad (\text{A.41})$$

$$E_r(r, \zeta) = \frac{\hat{I}r}{2\pi\epsilon_0 R^2 \beta c} g(\zeta) \quad (\text{A.42}),$$

where

$$h(\zeta) = \sqrt{A^2 + (1-\zeta)^2} - \sqrt{A^2 + \zeta^2} - |1-\zeta| + |\zeta|$$

and

$$g(\zeta) = \frac{(1-\zeta)}{2\sqrt{A^2 + (1-\zeta)^2}} + \frac{\zeta}{2\sqrt{A^2 + \zeta^2}}$$

and

$\zeta = z/L$, the normalized longitudinal coordinate.

$A = R/\gamma L$, the beam aspect ratio.

In a relativistic beam $\gamma \rightarrow \infty$, $h(\zeta) \rightarrow 0$ and $g(\zeta) \rightarrow 1$. So, only the radial component is significant. Now, the azimuthal magnetic field component is :

$$B_\theta = \frac{\beta}{c} E_r$$

and the Lorentz force:

$$F_r = e(E_r - \beta c B_\theta) = e(1 - \beta^2) E_r = \frac{e E_r}{\gamma^2} \quad (\text{A.43})$$

Using this force and an arbitrary external transverse force on an accelerating field , eq.(A.30) takes the form:

$$\sigma_x'' + \frac{\gamma'}{\gamma} \sigma_x' + k_{\text{ext}}^2 \sigma_x = \frac{\varepsilon_{n,\text{rms}}^2}{\gamma^2 \sigma_x^3} + \frac{k_{\text{sc}}}{\gamma^3 \sigma_x} \quad (\text{A.44})$$

This equation reveals two regimes of the beam propagation: space charge dominated and emittance dominated (thermal regime). When the beam propagation is space charge dominated by the respective linear components then the beam has a quasi-laminar behaviour [A.2]. A useful measure of the space charge versus emittance effects is the *laminarity parameter* ρ .

$$\rho = \frac{\hat{I} \sigma^2}{2I_A \gamma \varepsilon_n^2} \quad (\text{A.45})$$

where I_A is the Alfvén current defined as: $I_A = 4\pi\varepsilon_0 m_0 c^3 / e = 17\text{kA}$ for electrons.

$\rho < 1 \rightarrow$ thermal regime

$\rho > 1 \rightarrow$ space charge dominated

$\rho = 1 \rightarrow$ transition

The transition energy above which the regime turns from thermal to space charge dominated is:

$$\gamma_{\text{tr}} = \frac{\hat{I} \sigma^2}{2I_A \varepsilon_n^2} \quad (\text{A.46})$$

Space charge dominated regime is typical of low-energy beams. For such applications as linac-driven free electron lasers, peak currents exceeding kA are required.

In the simulations of this thesis, in the photoinjector part, the current had not exceeded 100A while σ is 0.1~0.6 mm and ε is 1~0.15 μm . So, the beams examined in this thesis can be assumed not to be laminar.

Emittance oscillations

In many cases the longitudinal correlation along the beam is non-negligible. A frequent cause is the space charge forces. In such cases the envelope development depends highly on the normalized coordinate ζ along the bunch. The way to treat such cases is to divide the bunch into slices that interact with one another. In the following analysis each slice is treated as a different bunch with its own envelope and the respective quantities will be indexed with s .

The correlations induce along the bunch can result in oscillations of the emittance. These oscillations can be evaluated by the correlated emittance:

$$\varepsilon_{\text{rms,cor}} = \sqrt{\langle \sigma_s^2 \rangle \langle \sigma_s'^2 \rangle - \langle \sigma_s \sigma_s' \rangle^2} \quad (\text{A.47})$$

The total normalized rms emittance is given by the superposition of the correlated and uncorrelated terms as:

$$\varepsilon_{\text{rms,cor}} = \langle \gamma \rangle \sqrt{\varepsilon_{\text{rms}}^2 + \varepsilon_{\text{rms,cor}}^2} \quad (\text{A.48})$$

Now, if one examines the behaviour of a not perfectly matched beam in a focusing channel the envelope equation to solve, assuming space charge domination, is for each slice:

$$\sigma_s'' + k_{\text{ext}}^2 \sigma_s = \frac{k_{\text{sc},s}}{\gamma^3 \sigma_s} \quad (\text{A.49})$$

The stationary solution of this equation is the *Brillouin flow*:

$$\sigma_{r,B} = \frac{1}{k_{ext}} \sqrt{\frac{\hat{I}g(\zeta)}{2\gamma^3 I_A}} \quad (\text{A.50})$$

Let us assume that one slice matches this envelope, then the matching condition for the other slices is:

$$\sigma_{sB} = \sigma_{rB} + \frac{\sigma_{rB}}{2} \left(\frac{\delta I_s}{\hat{I}} \right) \quad (\text{A.51})$$

Now, assuming a slice with a small perturbation δ_s with respect to its equilibrium:

$$\sigma_{sB} = \sigma_{rB} + \frac{\sigma_{rB}}{2} \left(\frac{\delta I_s}{\hat{I}} \right) \quad (\text{A.52})$$

the eq. (A.49) will give a solution :

$$\sigma_s = \sigma_{s,B} + \delta_0 \cos(\sqrt{2}k_{ext}z) \quad (\text{A.53})$$

that reveals a plasma oscillation of frequency $\sqrt{2}k_{ext}$. This solution represents a collective behaviour of the bunch, similar to that of the electrons subject to the restoring force of ions in a plasma.[A.2] The emittance evolution is described by:

$$\varepsilon_{\text{rms,cor}} = \frac{1}{4} k_{ext} \sigma_{rB} \left| \frac{\Delta I}{\hat{I}} \delta_0 \sin(k_{ext}z) \right| \quad (\text{A.54})$$

Envelope oscillations of the mismatched slices induce correlated emittance oscillations that periodically return to zero. The reason behind these oscillations is the coupling between the transverse and longitudinal motion caused by space charge fields.

What has just been described is a beam with a single charge species that exhibits plasma oscillations, which are characteristic of plasmas composed of two-charge species. The reason this occurs in a single charge plasma (beam) is that the external field plays the role of the other species.

Mismatch Parameter

The definition of the mismatch parameter is based on the concept of an elliptical beam in the trace space. More specifically, the mismatch parameter ζ gives an indication of how a particular trace space ellipse described by the Twiss parameters (α, β, γ) is mismatched with respect to a reference ellipse defined by $(\alpha_0, \beta_0, \gamma_0)$:

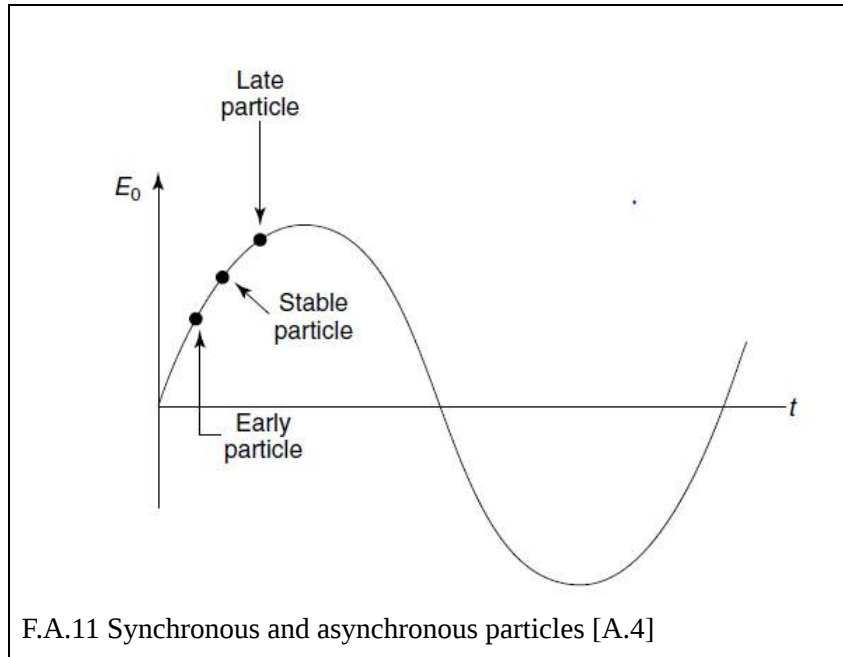
$$\zeta \equiv \frac{1}{2}(\beta_0\gamma - 2\alpha_0\alpha + \gamma_0\beta) \geq 1. \quad (\text{A.55})$$

The reference ellipse is usually the one representing the design optics of the beam line. The term mismatched is used to indicate that the shape of the two ellipses differs, regardless of their area. Similarly to the slice emittance (A.47), also a slice mismatch ζ_s can be defined by inserting $(\alpha_s, \beta_s, \gamma_s)$ the slice Twiss parameters instead of those for the whole bunch in Equation (A.55).

A.3 Longitudinal Beam Dynamics and Phase Space

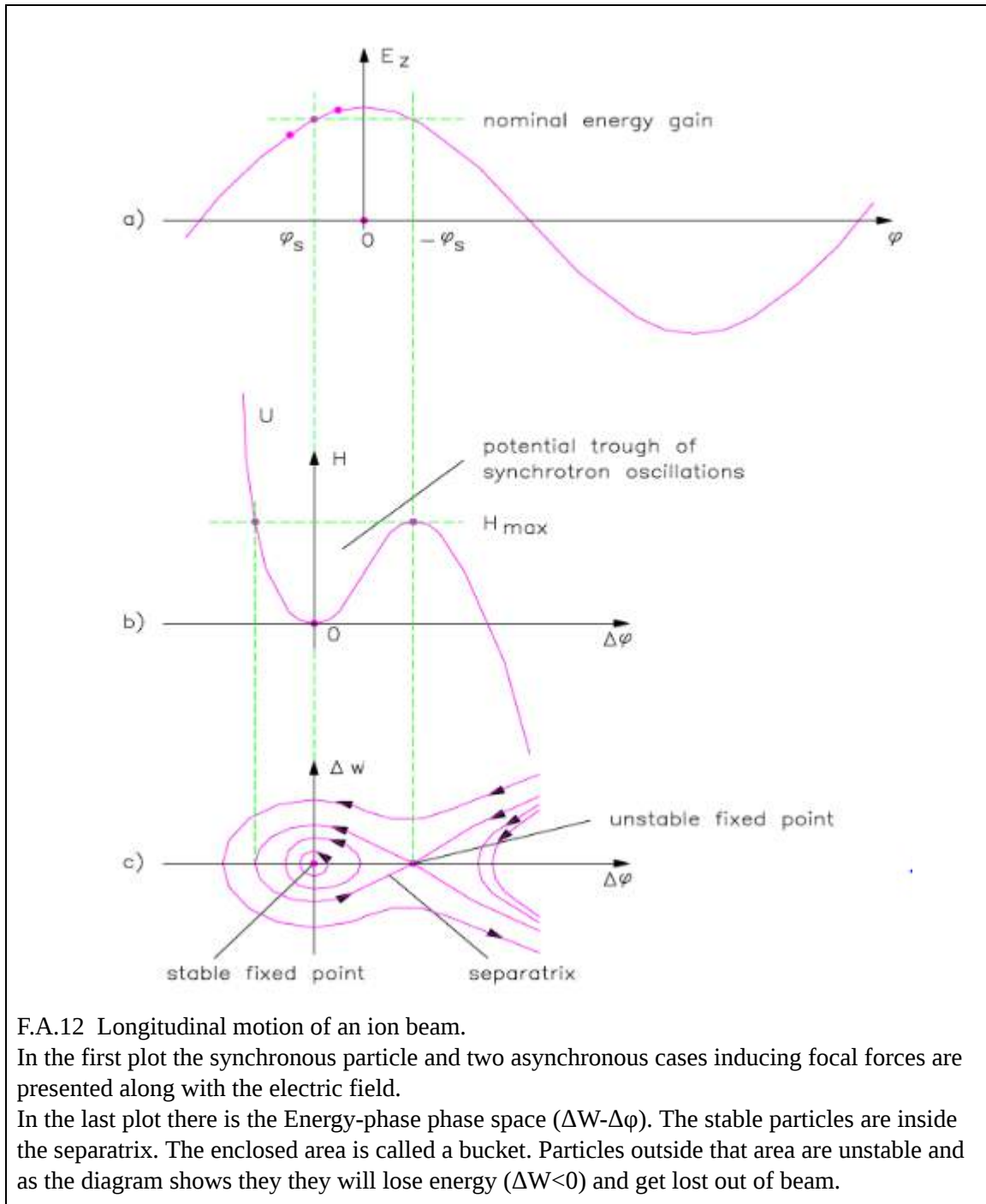
A single particle, which remains in synchronism with the accelerating fields and is called the synchronous particle. Longitudinal focusing is provided by an appropriate choice of the phase

of the synchronous particle relative to the crest of the accelerating wave.[A.4] Particles must be synchronous with the accelerating wave to achieve the maximum acceleration[A.6] A longitudinal restoring force exists when the synchronous phase is chosen corresponding to a field that is rising in time, as shown in F.A.11. The early particles experience, then, a smaller field and the late particles a larger field than the synchronous particle.



The particles have to be injected into the linac on a well-defined phase with respect to the accelerating sinusoidal field, and then they need to maintain this phase during the acceleration process. Linac beams are usually made of a large number of particles with a given spread in phase and in energy. If the injection phase corresponds to the crest of the wave ($\phi = 0^\circ$) for maximum acceleration, particles having slightly higher or lower phases will gain less energy. They will slowly lose synchronicity until they are lost.[A.6] The accelerated particles are formed in stable bunches that are near the synchronous particle, as in F.A.12. Those particles outside the stable region correspond to the completely asynchronous particles and they slip behind in phase and do not experience any net acceleration. [A.4]

In linacs, the same principle of phase stability holds as in synchrotrons: if the injected beam is not centred on the crest of the wave but around a slightly lower phase, a 'synchronous phase' ϕ_s whose typical values are between -20° and -30° , particles that are not on the central phase will oscillate around the synchronous phase during the acceleration process. The resulting longitudinal motion is confined, and the oscillation is represented by an elliptical motion of each particle in the longitudinal phase plane, i.e. the plane $(\Delta\phi, \Delta W)$ of phase and energy difference with respect to the synchronous particle. The relation between the synchronous phase in an accelerating sinusoidal field, and the longitudinal phase plane is presented in F.A.12.



F.A.12 Longitudinal motion of an ion beam.

In the first plot the synchronous particle and two asynchronous cases inducing focal forces are presented along with the electric field.

In the last plot there is the Energy-phase phase space (ΔW - $\Delta\phi$). The stable particles are inside the separatrix. The enclosed area is called a bucket. Particles outside that area are unstable and as the diagram shows they will lose energy ($\Delta W < 0$) and get lost out of beam.

It is interesting to observe that the frequency of longitudinal oscillations, i.e. the number of oscillations in the longitudinal phase plane per unit time, depends on the velocity of the beam. A simple approximate formula for the frequency of small oscillations ω_l can be found, for example, in [A.4]:

$$\omega_l^2 = \omega_0^2 \frac{qE_0 T \sin(-\phi) \lambda}{2\pi mc^2 \beta \gamma^3} . \quad (\text{A.56})$$

where ω_0 and λ are the RF frequency and wavelength, respectively, E_0T is the effective accelerating gradient and ϕ is the synchronous phase. The oscillation frequency is proportional to $\frac{1}{\beta\gamma^3}$: when the beam becomes relativistic, the oscillation frequency decreases rapidly. At the limit of $\beta\gamma^3 \gg 1$ the oscillations will stop and the beam is practically “frozen” in phase and in energy with respect to the synchronous particle.[A.6] .

So, for relativistic electron linacs, after beam injection into electron linacs, the velocities approach the speed of light so rapidly that hardly any phase oscillations take place. The electrons initially slip relative to the wave and rapidly approach a final phase that is maintained all the way to high energy. The final energy of each electron with a fixed phase depends on the accelerating field and on the value of the phase [A.4]

Another important relativistic effect for ion beams is the ‘phase damping’, the shortening of bunch length in the longitudinal plane. This can be understood considering that, as the beam becomes more relativistic, its length in z seen by an external observer will contract due to relativity. A precise relativistic calculation shows that the phase damping is proportional to

$$\Delta\phi = \frac{\text{const}}{(\beta\gamma)^{3/4}} . \quad (\text{A.57})$$

When a beam becomes relativistic, not only will its longitudinal oscillations slow down, but the bunch will also compact around the centre particle.

A.4 Beam Dynamics without space charge

Longitudinal RF field

In order to accelerate electrons, the relevant modes are those with large longitudinal electric fields as shown in Figure 1.2a. Such a cavity is the pillbox cavity F.1.3b. The field components in a Pillbox cavity in a T_{mnp} are:

$$\begin{aligned} E_z &= E_0 J_m(k_{mn}r) \cos(m\theta) \cos(pk_z z) \exp[i(\omega t + \phi_0)] \\ E_r &= -p \frac{k_z}{k_{mn}} E_0 J'_m(k_{mn}r) \cos(m\theta) \sin(pk_z z) \exp[i(\omega t + \phi_0)] \\ E_\theta &= -mp \frac{k_z}{k_{mn}^2} E_0 J_m(k_{mn}r) \cos(m\theta) \sin(pk_z z) \exp[i(\omega t + \phi_0)] \\ B_z &= 0 \\ B_r &= \frac{-i\omega m}{k_{mn}^2 c^2} E_0 J_m(k_{mn}r) \sin(m\theta) \cos(pk_z z) \exp[i(\omega t + \phi_0)] \\ B_\theta &= \frac{-i\omega}{k_{mn} c^2} E_0 J'_m(k_{mn}r) \cos(m\theta) \cos(pk_z z) \exp[i(\omega t + \phi_0)] \end{aligned} \quad (\text{A.58})$$

For reasons of timing and efficient acceleration, the full cell length for most RF guns is $\lambda/2$ and $p = 1$. The above mode equations then give a π phase shift between cells. Since the cathode is at a high field position, its cavity length is half that of a full cell, or $\lambda/4$. Thus most RF guns use the TM_{011} mode whose non-zero field components are:

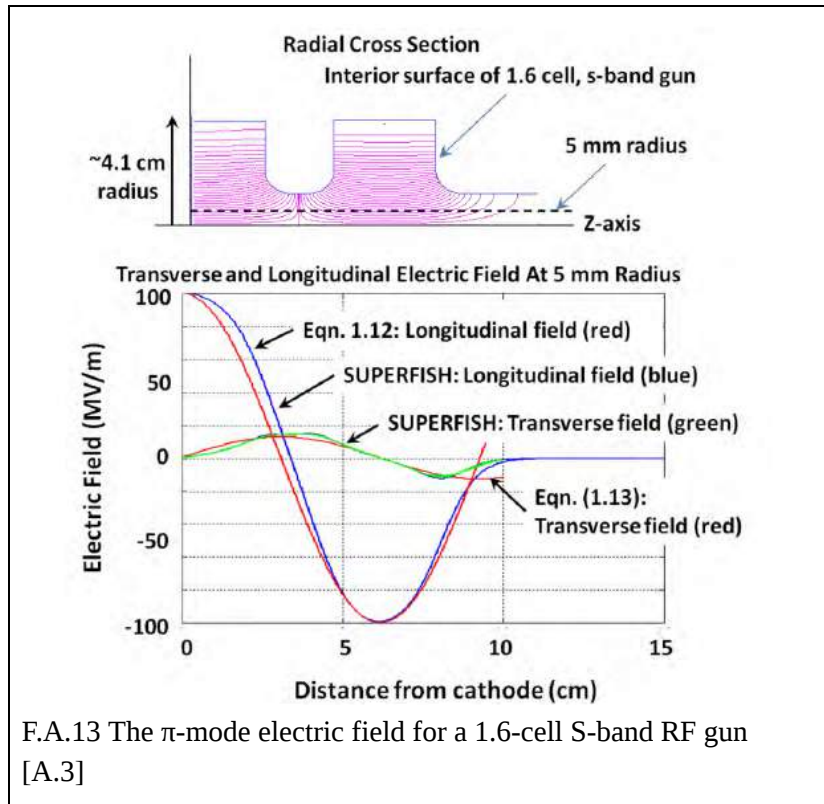
$$E_z = E_0 J_0(k_{01}r) \cos(k_z z) \exp[i(\omega t + \phi_0)]$$

$$E_r = \frac{-k_z}{k_{01}} E_0 J_0'(k_{01}r) \sin(k_z z) \exp[i(\omega t + \phi_0)]$$

$$B_\theta = \frac{-ik_z}{k_{01}c} E_0 J_0'(k_{01}r) \cos(k_z z) \exp[i(\omega t + \phi_0)]$$

(A.59)

This mode is also called the π -mode, because the argument of the cosine function changes by π over a cell length.[A.3]



Transverse RF field

The transverse RF field can be expressed by [A.3] :

$$F_r = e(E_r - \beta c B_\theta) \quad (A.60)$$

using the previous equations:

$$F_r = e \frac{k_z}{k_{01}} E_0 [\beta \cos(k_z z) \sin(\omega t + \phi_0) - \sin(k_z z) \cos(\omega t + \phi_0)] J_0'(k_{01}r) \quad (A.61)$$

At the exit of the gun the same force is expressed as [A.3]:

$$F_r = -e E_0 \frac{k_z r}{2} \sin(\omega t + \phi_0 - k_z z) \quad (A.62)$$

From that expression of the force and the definition of the focal length of the gun:

$$x' = \frac{x}{f_{RF}} \quad (\text{A.63})$$

we can express the gun's focal length as:

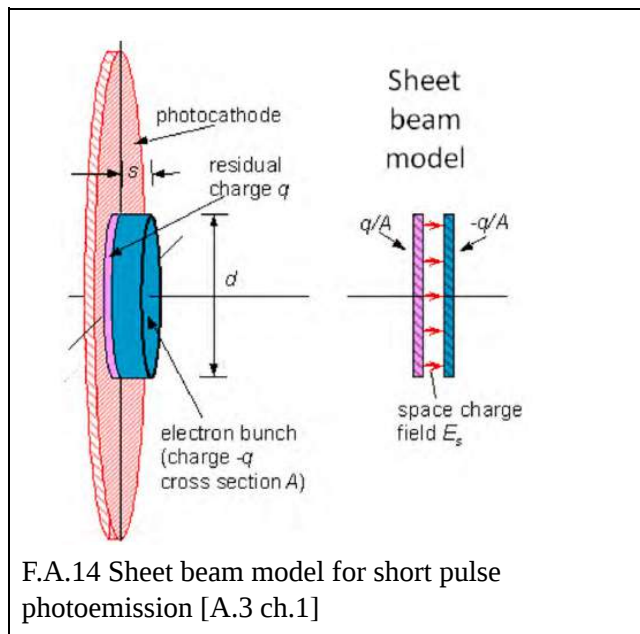
$$f_{RF} = \frac{-2\beta\gamma mc^2}{eE_0 \sin(\phi_e)} \quad (\text{A.64})$$

A.5 Beam Dynamics with space charge

Space Charge Limited Emission

The electrons of a beam in LINAC can be either produced by thermionic emission, by the increase of the cathode temperature, or by photoemission. In photoemission the electrons are produced by a cathode, metallic or semiconducting, excited by a laser. A pulse of specific wavelength will excite the electrons and the energy of the pulse will determine the charge produced.

In the case of photoemission, the bunch charge can be photon limited or space charge limited. The photon limited emission is given by the quantum efficiency (QE) [see Appendix B] times the number of incident photons, and space charge limited emission is given by a sheet beam model.



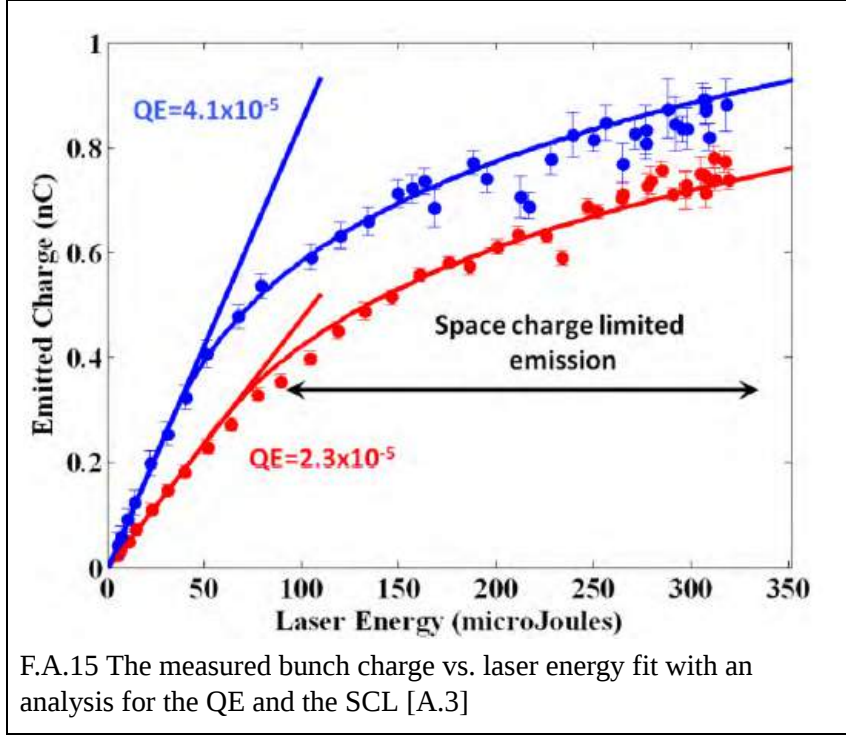
The charge that can be emitted is limited by its own image charge. The threshold is when the electric field produced by the electron bunch itself is equal to the electric field on the cathode. The field induced by the bunch is similar to a capacitor's electrical field. With this said:

$$E_{SCL} = \frac{q}{A\epsilon_0} = \frac{\sigma}{\epsilon_0} = E_{applied}$$

So, the space charge density limit is :

$$\sigma_{SCL} = \varepsilon_0 E_0 \sin(\phi_0) \quad (A.65)$$

In the plot below, the bunch charge is presented with respect to the laser energy. For small charges the relation is linear with the slope depending on the Quantum Efficiency QE and for greater charges, saturation is observed.



F.A.15 The measured bunch charge vs. laser energy fit with an analysis for the QE and the SCL [A.3]

For low laser energies below the SCL, the curve is linear with a slope related to the quantum efficiency, QE :

$$q_{bunch} = \frac{eE_{laser}}{\hbar\omega} QE \quad (A.66)$$

QE is often obtained from the linear portion of the curve (see Fig.A.15)

In a case of a Gaussian laser energy profile, whose energy exceeds the space charge limits, the emitted charge either comes from the region that saturates or from the tails of the laser profile.

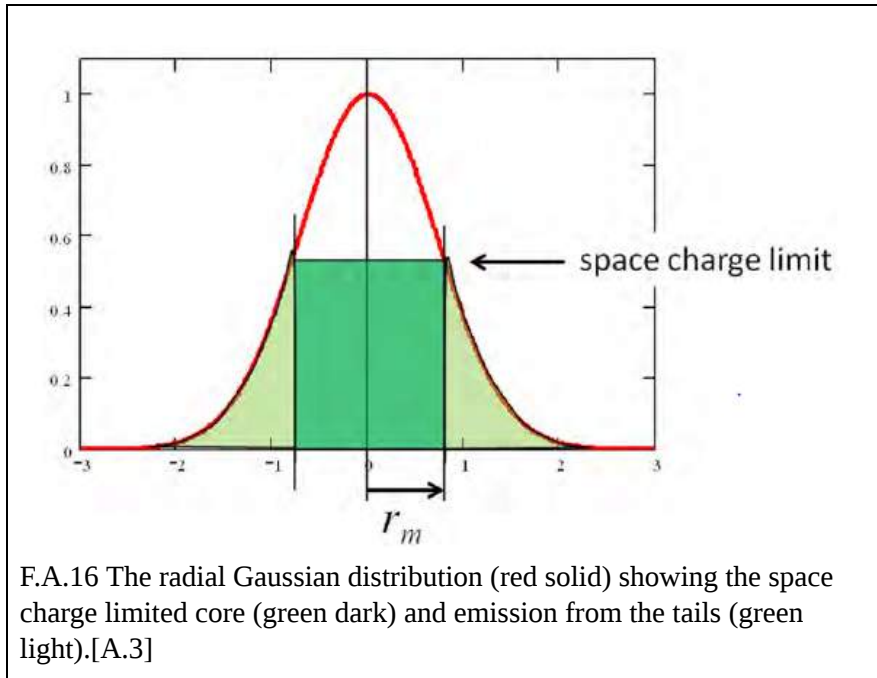
The emitted charge in this case is:

$$q_{emitted} = q_{core} + q_{tail} \quad (A.67)$$

$$q_{emitted} = \pi r_m^2 \varepsilon_0 E_0 \sin(\phi_0) + QE \frac{eE_{laser}}{\hbar\omega} \exp\left(\frac{-r_m^2}{2\sigma_r^2}\right) \quad (A.68)$$

where the radius of the saturated core, r_m , given by:

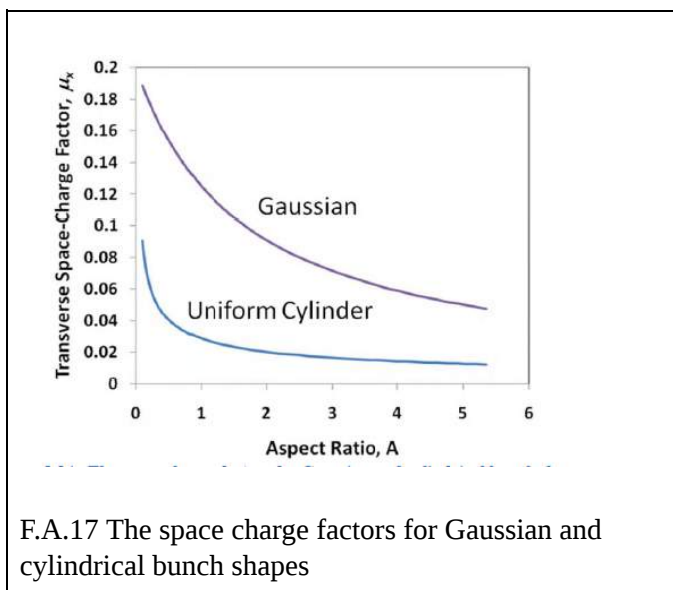
$$r_m = \sigma_r \sqrt{2 \ln\left(\frac{eE_{laser}QE}{2\pi\varepsilon_0\sigma_r^2\hbar\omega E_0 \sin(\phi_0)}\right)} \quad (A.69)$$



The case that was just discussed , leads to partial negation of the saturation with the second term of () and increase now is much lower due to the exponential term. Observations and simulations of such phenomena are discussed in [A.5], where a Gaussian and a flattop laser energy distribution are examined.

Emittance and bunch shape

Due to differences in the square root of the variance of the normalized transverse and longitudinal fields (induced by space charge) , it can be shown that the “pancake-like” bunch has much lower space charge emittance than do “cigar-like” shapes. Thus, the conclusions are the shorter the bunch the better and the shape should be a uniformly charged cylinder. This result explains the choice of the distribution made in simulations.



A.4 References

- [A.1] Wiedemann, Helmut. *Particle Accelerator Physics: with 264 Figures*. Springer, 2007
- [A.2] Ferrario, Massimo. "Space Charge Mitigation." *CERN Yellow Reports: School Proceedings*, dx.doi.org/10.23730/CYRSP-2018-001.177.
- [A.3] Rao, Triveni, and David H. Dowell. *An Engineering Guide to Photoinjectors*. CreateSpace Independent Publishing, 201A.
- [A.4] Wangler, Thomas P. *RF Linear Accelerators*. Wiley-VCH Verlag, 2017.
- [A.5] Hernandez-Garcia, C., et al. "Charge Production Studies from Cs₂Te Photocathodes in a Normal Conducting RF Gun." *Nuclear Instruments and Methods in Physics Research Section A: Accelerators, Spectrometers, Detectors and Associated Equipment*, vol. 871, 2017, pp. 97–104., [doi:10.1016/j.nima.2017.06.051](https://doi.org/10.1016/j.nima.2017.06.051).
- [A.6] Maurizio. "Linear Accelerators." *CERN Document Server*, CERN, 29 Mar. 2013, arxiv.org/ct?url=https://dx.doi.org/10.5170/CERN-2013-001.225&v=e1312714.

Appendix B. Photocathode Theory

B.1 Three-Step Model in Metals

Before presenting the model of photoemission, the Quantum Efficiency (QE) should be defined :

$$QE = \frac{n_e}{n_p} = \frac{h\nu[eV]}{E_{laser}[J]} q [C] \quad (B.1)$$

In other words, it is the ratio of the number of emitted electrons (n_e) to the number of incident photons (n_p).

The Three-Step model consists of the following steps:

1) Step 1 – Photon Absorption and Electron Excitation

A photon will either be reflected from the cathode or it will be absorbed. Making two assumptions:

- that the states lying below the Fermi energy, E_f , are filled and
- the states above are empty.

This is equivalent to treating the material as a conductor at zero temperature.

The probability of transmission into the material, $T(\nu)$, and absorption in an infinitely thick cathode, $A(\nu)$, is calculated from the reflectivity:

$$T(\nu) = A(\nu) = 1 - R(\nu) \quad (B.1)$$

The probability of exciting an electron to a given energy within the material is given by:

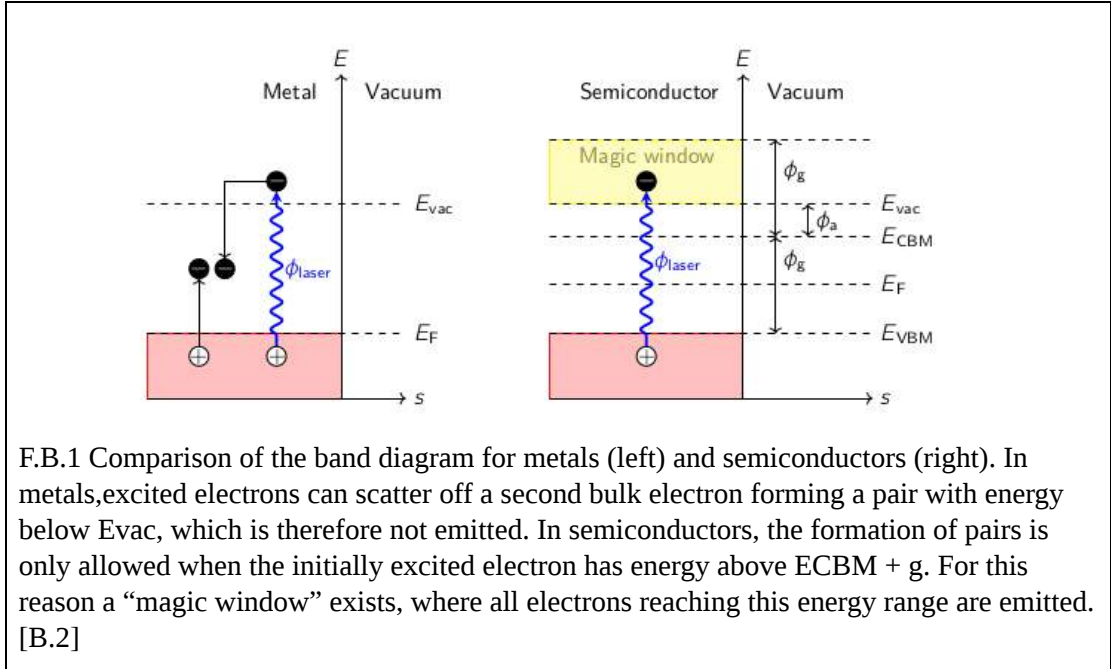
$$P(E, h\nu) = \frac{N(E)N(E - h\nu)}{\int_{E_f} dE' N(E')N(E' - h\nu)} \quad (B.2)$$

which shows that the probability is proportional to the number of initial states, $N(E_0)$, and the number of final states, $N(E)$. The denominator is the total number of states.[B.1]

2) Step 2 – Photon Absorption Length and Electron Transport

The second step refers to the probability of a hot (excited) electron to reach the cathode surface, which is equivalent to reaching the surface with energy above the work function. While moving inside the material the hot electrons might undergo several scatterings. In metallic cathodes, electron-electron (e-e) scattering limits the range of the hot electrons in the material, because such a scattering is likely to remove significant energy from the electron, thus such electrons are considered to be lost in cases where the energy given is near threshold for emission. In an e-p scattering the energy is considered invariant, while the momentum transfer is irrelevant assuming an isotropic initial momentum distribution.

In semiconductor photocathodes, if the photon energy used is less than double the band gap energy (Spicer's "magic window"), e-e scattering is forbidden. Therefore, electron-electron scattering, which is lowering the QE of metals, is not a dominant process in semiconductors since almost all of the electrons excited into the magic window are emitted. The result is a much higher QE for semiconductors. For example, a Cs₂Te photocathode has 1000 orders of magnitude higher QE than Cu.



3) Step 3 – Escape

The escape criteria is:

$$\frac{\hbar^2(k_{\perp})^2}{2m} \geq E_T \quad (\text{B.3})$$

where E_T is the energy required to escape ($E_T = \phi$ for a metal), k_{\perp} represents the component of the excited electron's momentum directed perpendicular to the surface of the cathode material resulting in an escape cone.

Only those electrons whose trajectory falls within the cone described by Equ. 5.14 will escape the surface. The excitation and scattering processes are assumed to produce electrons with an isotropic angular distribution of angle:

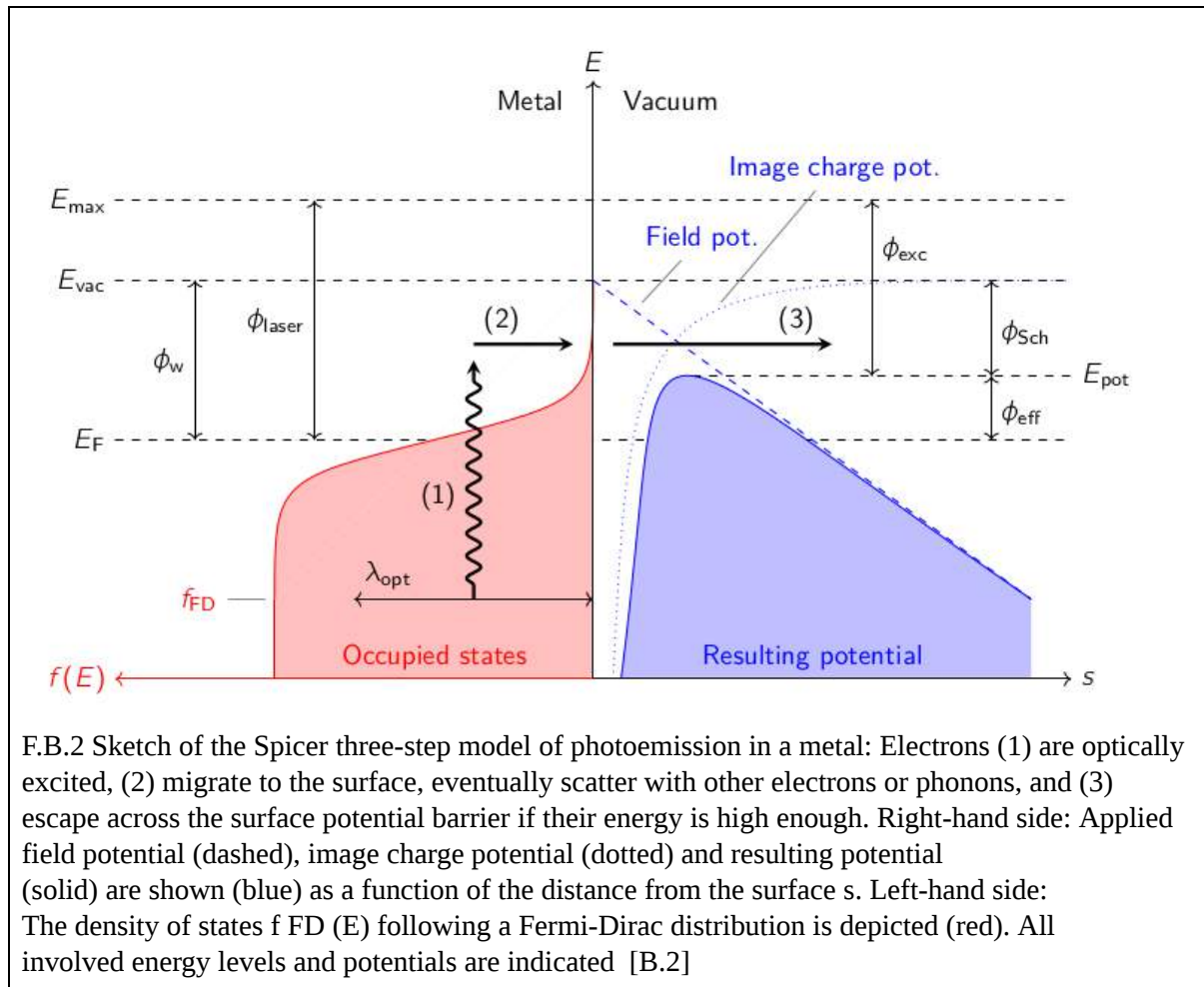
$$\cos(\theta) = \frac{k_{\perp min}}{|\vec{k}|} = \sqrt{\frac{E_T}{E - E_f}} \quad (\text{B.4})$$

The fraction of escaping electrons is given by integrating the solid angle of the cone [B.2]:

$$D(E) = \begin{cases} 1/2(1 - \sqrt{\frac{E_T}{E - E_f}}), & \text{if } E - E_f > E_T \\ 0 & \text{if } E < E_T \end{cases} \quad (\text{B.5})$$

The product of the probability densities from each of the three steps (prior to energy integration) provides the number of electrons emitted at a given energy from the material. This distribution is called the energy distribution curve (EDC).

$$EDC(E, \nu) = A(\nu) P(E) T(E, \nu) D(E) \quad (\text{B.6})$$



B.2 Transverse Emittance and Quantum Efficiency in the Three-Step Model for Metals

It can be shown that for small values of electron energy in excess of the threshold, the QE is expected to show quadratic dependence on the excess energy.

$$QE(\nu) \propto (h\nu - \phi)^2 \quad (\text{B.7})$$

We define as excessive energy the difference :

$$\varphi_{exc} = h\nu - \phi \quad (\text{B.8})$$

If the photon energy is close to the effective work function and the electron density of states near the Fermi energy can be considered a constant, then the following relations for momentum deviation and emittance hold:

$$\sigma_{p_x} = \sqrt{\frac{h\nu - \phi_{eff}}{3mc^2}} \quad (\text{B.9})$$

$$\varepsilon_n = \sigma_x \sqrt{\frac{h\nu - \phi_{eff}}{3mc^2}} \quad (\text{B.10})$$

where , $h\nu$ the photon energy, ϕ_{eff} the effective work function, m the electron mass. The effective work function is the energy required to excite an electron to the vacuum without kinetic energy.

An important detail is that the average kinetic energy of the electrons extracted from the metallic cathode is given by $E_{kin} = \varphi_{exc}/2$, due to the statistical averaging of the electrons' density of final states.

$$E_{kin} = \frac{(h\nu - \phi_0)}{2} \quad (\text{B.11})$$

B.3 The Schottky Effect

When a photocathode is subject to an external electrical field then the work function decreases. That is called the “*Schottky Effect*” . The change in the work function can be obtained by:

$$\Delta\phi_{Schottky} [\text{eV}] = \alpha \sqrt{E \left[\frac{\text{V}}{\text{m}} \right]} \quad (\text{B.11})$$

where

$$\alpha = e \sqrt{\frac{e}{4\pi\epsilon_0}} = 3.7947 \times 10^{-5} [e\sqrt{\text{Vm}}]$$

and E is the external electrical field on the cathode. So the work function and the kinetic energy in the moment of excitation will become:

$$\varphi_{eff} = \varphi_0 - \Delta\Phi_{Schottky} \quad (\text{B.12})$$

$$E_{kin} = h\nu - \varphi_0 - \Delta\Phi_{Schottky} \quad (\text{B.13})$$

Also, the QE parameter is proportional to :

$$QE(\nu) \propto (h\nu - \phi_0 + \alpha\sqrt{E})^2 \quad (\text{B.14})$$

B.4 Semiconductor Photocathodes

In a semiconductor the relations introduced above differ at some points because of the effect of the “*magic window*” introduced above. The first parameter is the much higher QE that enables greater charge production with less laser power.

The effective work function is defined by :

$$\phi_{eff} = \phi_g + \phi_a \quad (\text{B.15}),$$

where ϕ_a is denoted in F.B.1.

The next parameter is the kinetic energy. In contrast with metals, the kinetic energy in semiconductors equals to the excessive energy $E_{kin} = \phi_{exc} = h\nu - \phi_{eff}$, the alteration in the density of electron states. E_{kin} is often written as MTE, which is the mean transverse energy, defined as $MTE = \langle \frac{1}{2}m_0v_x^2 \rangle + \langle \frac{1}{2}m_0v_y^2 \rangle$, with x and y denoting the directions perpendicular to the cathode’s emission normal.

The normalised thermal emittance is estimated as:

$$\frac{\epsilon_{n,th}}{\sigma_x} = \sqrt{\frac{MTE}{3m_0c^2}} \quad , \quad \text{where } MTE = h\nu - (\phi_g - \phi_a) + \Delta\Phi_{Schottky} \quad (\text{B.16})$$

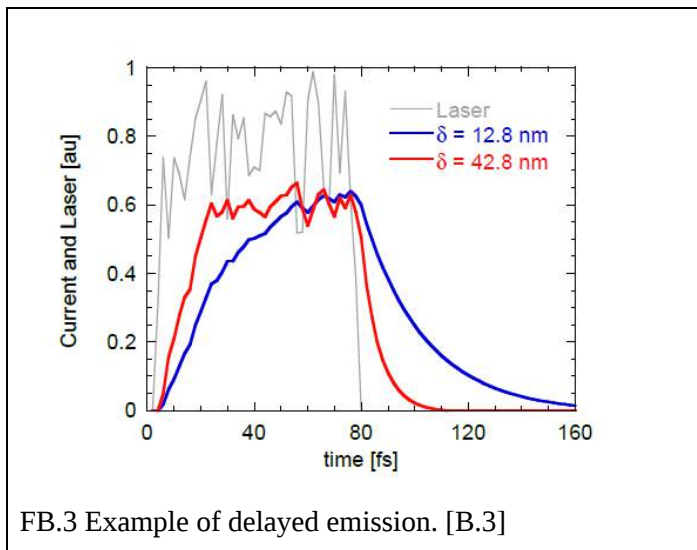
and $m_0c^2 = 0.511 \text{ MeV}$ is the electron’s rest energy.

Another very important parameter that cannot be ignored in semiconductors is the Emission Delay or Response Time (τ), which is the time between the electron excitation and its exit from the metallic surface. In metals it is very small , as shown in Table B.1, thus, is ignored. For semiconductors like Cs_2Te the time delay is non-negligible and in the order of $\Delta t = 0.1\text{--}1 \text{ ps}$. Specific Monte Carlo simulations for Cs_2Te predict a time response of $\Delta t = 0.4 \text{ ps}$ [B.2]

TABLE B.1: Expression of the response time (τ) , based on the Three-Step model for different classes of photoemitters, showing the range of value τ .

Material	Dominating mode of scattering	Equation for τ	Estimate range of τ (sec)	Typical yield (el/photon) 1 eV above threshold
Metals	Electron-electron	$\tau = \frac{L}{v_a} \quad (9)$	10^{-15} to 10^{-14}	8×10^{-5} to 4×10^{-4}
Semiconductors and insulators (Cs ₃ Sb or multialkali)	Electron-lattice	$\tau = \frac{E_k \cdot l_p}{\Delta E_p \cdot v_a} \quad (13)$	10^{-13} to 10^{-12}	0.05 to 0.25
Negative affinity	Electron-lattice (thermal diffusion of electrons in CBM)	$\tau = \frac{L_D^2}{\mu kT/q} \quad (14)$	2×10^{-10} to 7×10^{-9}	0.1 to 0.6

A very interesting effect of the delay is the smoothing of the laser longitudinal profile in emission. Such a smoothing can be observed in F.B.3 that shows a simulation of delayed emission current. δ represents the penetration depth.



B.5 Semiconductors and Cu Photocathode Parameters

In the following table [B.2], the most important parameters for the most common semiconductor materials used in photocathodes.

TABLE B.2: Commonly used Semiconductor photoemitters

Cathode Wavelength	λ [nm], E_{ph} [eV]	QE [%]	$E_a + E_{gap}$ [eV]	Thermal emittance $\left[\frac{\text{mm mrad}}{\text{mm rms}} \right]$	
				Theory (Equ. 7.6)	Experiment
Cs ₂ Te	262, 4.73	~10	3.5	0.9	1.2 ± 0.1
Cs ₃ Sb	532, 2.33	~4	1.6 + 0.45	0.42	0.56 ± 0.03
	473, 2.62	~7		0.62	0.66 ± 0.03
	405, 3.06	~9		0.82	0.80 ± 0.04
Na ₂ KSb	330, 3.76	~10	1 + 1	1.07	N/A
Na ₂ KSb:Cs	390, 3.18	~20	1 + 0.55	1.03	N/A
K ₂ CsSb	532, 2.33	~4	1 + 1.1	0.38	0.56 ± 0.03
	473, 2.62	~11		0.58	0.69 ± 0.03
	405, 3.06	~25		0.80	0.87 ± 0.04
GaAs(Cs,F)	532, 2.33	~10	1.4 ± 0.1	0.77	0.47 ± 0.03
GaN(Cs)	260, 4.77	~15	3.4 ± 0.1	0.94	1.35 ± 0.11

For Cu the respective parameters are :

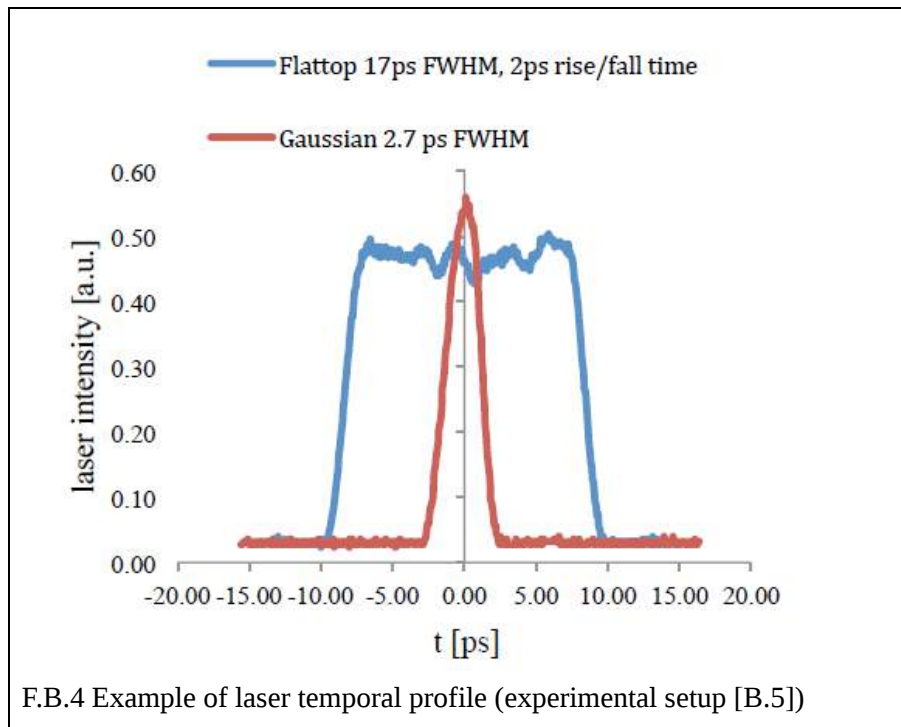
TABLE B.3		
QE[%]	ϕ_{eff} [eV]	Normalized Thermal Emittance [mm mrad /mm]
~10 ⁻⁵	4.65	0.23

The laser parameters for Cu are not strict the ones chosen in each case are presented before the simulations. In general the laser must be adjusted so that the excessive energy is low, so that the thermal emittance is small.

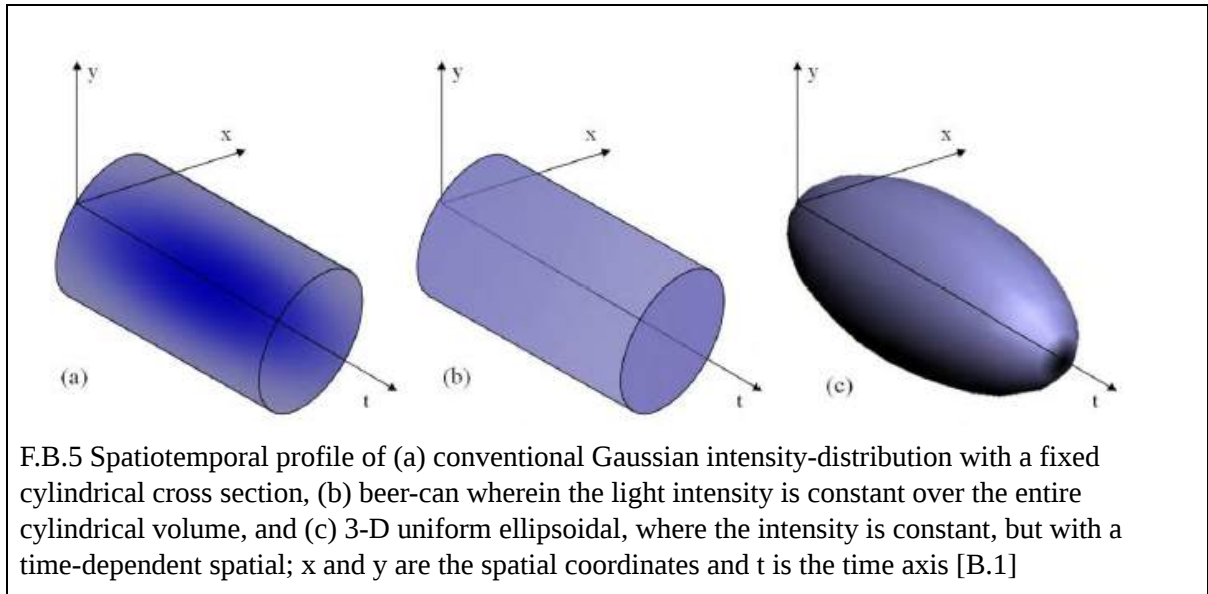
B.6 Laser Parameters

The laser parameters that will concern the simulations of this thesis are the photon wavelength and energy, the transverse and the longitudinal profile of the laser pulse. The photon energy, as mentioned already, is chosen in such a way that the excess energy of the electrons is low, thus the emittance.

The longitudinal/temporal profile of a laser usually either a Gaussian or a Flattop one. The Flattop profile can be created by stacking Gaussian pulses , as done in SwissFEL [B.2] . Recently the case of an ellipsoidal profile is tested as it shows better performance.



The temporal profile of the laser translates to beam temporal profile. The temporal profile affects the stability of the beam and the transverse emittance and the transverse size [see B.1 ch.9.6.1] as it affects the space charge fields and the stability of the beam. In [B.1] it is reported that in simulations an Ellipsoidal temporal distribution would result in the least emittance while a Flattop one gives smaller emittance than a Gaussian in simulations. In [B.7] specific simulations are also reported confirming the above. In the simulations of this thesis, a Flattop profile will be used as such a laser system is already in use in SwissFEL facilities and as it will be presented it can provide very good results.



The duration of the pulse can not be arbitrary, it is limited by the RF frequency. The bunch length, and hence the peak current from the injector depends upon the RF frequency of the main accelerator since the bunch length should be a small fraction of an RF period. A sensible guideline is less than 10° RF 1 for the full bunch length.[B.1] In the simulations below, the S-band and X-band are the frequencies that were used. The S-band frequencies that were used are 2.856 GHz (1.5 cells) , 2.998GHz (2.5 cells) and in the X-band 11.992GHz (4.6 cells). The upper limits in these cases are approximately the one presented in Table B.4.

TABLE B.4		
3GHz	<10 psec	The pulse duration can be computed by: $L_t = \frac{1}{f} \cdot \frac{10^\circ}{360^\circ}$
12GHz	<2.3 psec	

As for the laser transverse profile, the spot size needs to be determined. From equation (B.16) and the space charge limit (A.66) one can assume that the best choice is to choose the smaller size permitted. But, this does not work because the smaller the size , the greater the space charge forces and , as a result, the emittance increases. The ideal size depends on many parameters and is chosen with tests and optimisation algorithms. The transverse profile usually is Gaussian, Flattop or Uniform with the latter introducing the least non-linear space charge forces. The uniform distribution is often assumed.

B.8 The “Halo” Effect

In laser transverse profile there can be exponentially decaying extensions. This altering of the ideal transverse distribution can cause differences in charge production in two ways. The first is the altering of the desired profile in the beam and the introduction on non linear forces, either significant or not , and change in the beam emittance and size. The second is the production of extra space charge

and the cancellation of the saturation, which can cause miscalculations in space charge production in simulations and in experiment where the halo is not anticipated. Relevant studies can be found in [B.5]

B.7 References

- [B.1] Rao, Triveni, and David H. Dowell. *An Engineering Guide to Photoinjectors*. CreateSpace Independent Publishing, 2013.
- [B.2] Schaer, and Mattia. “RF Traveling-Wave Electron Gun for High Brightness Photoinjectors.” *RF Traveling-Wave Electron Gun for High Brightness Photoinjectors - Research Collection*, ETH Zürich, 1 Jan. 1970, doi.org/10.3929/ethz-a-010749949.
- [B.3] Jensen, Kevin L., et al. “Delayed Photo-Emission Model for Beam Optics Codes.” *Journal of Vacuum Science & Technology B, Nanotechnology and Microelectronics: Materials, Processing, Measurement, and Phenomena*, vol. 35, no. 2, 2017, doi:10.1116/1.4968511.
- [B.5] Hernandez-Garcia, C., et al. “Charge Production Studies from Cs₂Te Photocathodes in a Normal Conducting RF Gun.” *Nuclear Instruments and Methods in Physics Research Section A: Accelerators, Spectrometers, Detectors and Associated Equipment*, vol. 871, 2017, pp. 97–104., doi:10.1016/j.nima.2017.06.051.

Appendix C. Table of abbreviations

Cu	Copper
Cs ₂ Te	Cesium-Telluride
FEL	Free Electron Laser
X-FEL	X-Ray Free Electron Laser
FWP	Ferrario Working Point
TWS	Travelling Wave Structure
MTE	Mean Transverse Energy